# UNIVERSITY OF SOUTHAMPTON

FACULTY OF NATURAL AND ENVIRONMENTAL SCIENCES

School of Ocean and Earth Sciences


# Coccolithophores and Light:
# Photophysiology and Ecology amongst Different Species


by

**Lucie Rebecca Daniels**


Submitted in partial fulfilment for the degree of Doctor of Philosophy

August 2019

*For Chris*

**UNIVERSITY OF SOUTHAMPTON**

# ABSTRACT

FACULTY OF NATURAL AND ENVIRONMENTAL SCIENCES

SCHOOL OF OCEAN AND EARTH SCIENCE

Doctor of Philosophy

## Coccolithophores and Light: Photophysiology and Ecology amongst Different Species

Lucie Rebecca Daniels

The coccolithophores are a class of unicellular algae and are considered one of the key phytoplankton functional types. Regionally coccolithophores can contribute > 20 % of primary productivity and are major contributors to pelagic calcite production. Amongst the > 280 extant coccolithophore species there is remarkable diversity in morphology, and evidence that different species inhabit distinct ecological niches. Despite this, the current understanding of the biology and ecology of coccolithophores is largely based on the cosmopolitan and bloom-forming species *Emiliania huxleyi,* as its reflectance signature is easy to detect in field and it is easier to grow in the laboratory than most other species. Light is a key primary resource for the coccolithophores, and the coccolithophore niche is often considered to be characterised by high irradiance, based largely on observations of *E. huxleyi* ecology and physiology. In this thesis, I tackle this research bias by investigating the response to irradiance in 10 different species, spanning a broad taxonomic range. A detailed analysis of physiology, including pigment content, light absorption properties, and photophysiological parameters, in response to three growth irradiances (25, 100 and 200 μmol photons $m^{-2}$ $s^{-1}$) provide an unprecedented wealth of comparative data between species. The results reveal characteristics that are common amongst the coccolithophores as a group. For example, all species had high accessory pigment content (including fucoxanthin derivatives and chlorophyll *c*s) relative to chlorophyll *a* regardless of growth irradiance. The shape of spectral light absorption (with elevated absorption in the 440 - 470 nm region) was also conserved amongst all the coccolithophore species. Notable differences between the coccolithophore species were also revealed in, for example, the contribution of the 'biomarker pigment' (19'Hexanoyloxyfucoxanthin) to total pigment varied widely between species, and in the photoacclimation strategy. The size range (cell volumes ranging from 11 $\mu m^3$ to 2120 $\mu m^3$) of the species used allowed examination of interspecific size scaling with respect to light in the coccolithophores for the first time. Negative size scaling of maximum growth rate and pigment density (per unit cell volume) was found, consistent with previous findings in other phytoplankton groups. However, large coccolithophore cells (> 100 $\mu m^3$) did not experience a growth rate penalty under low light, which was an unexpected finding. An assessment of coccolithophore communities in the field found differences in the species composition between the contrasting hydrographic regimes of the stratified central shelf and shelf-break of the Celtic Sea. Patchiness in the community on the stratified shelf environment, and a lack of vertical differentiation of the community, underline the complexity of environmental drivers of coccolithophore distributions in the real world. The evidence presented in this thesis sheds light on the considerable physiological diversity within the coccolithophore group, and advocates continuing to examine a higher diversity of coccolithophore species in experimental work. Physiological studies using a variety of coccolithophore species can help to build on the solid foundation of pre-existing research on *E. huxleyi,* in order to advance our understanding of the coccolithophores as a group.

# Table of Contents

# List of Tables

# List of Figures

# Research Thesis: Declaration of Authorship

I, **Lucie Rebecca Daniels**, declare that this thesis entitled **Coccolithophores and Light: Photophysiology and ecology amongst different species** and the work presented in it are my own and has been generated by me as the result of my own original research.

I confirm that:

1. This work was done wholly or mainly while in candidature for a research degree at this University;
2. Where any part of this thesis has previously been submitted for a degree or any other qualification at this University or any other institution, this has been clearly stated;
3. Where I have consulted the published work of others, this is always clearly attributed;
4. Where I have quoted from the work of others, the source is always given. With the exception of such quotations, this thesis is entirely my own work;
5. I have acknowledged all main sources of help;
6. Where the thesis is based on work done by myself jointly with others, I have made clear exactly what was done by others and what I have contributed myself;
7. None of this work has been published before submission

| | | | |
|---|---|---|---|
| Signature: | | Date: | |

# Acknowledgements

So many people had a hand in helping me to get this thesis over the finish line, and heartfelt thanks goes out to every one of them, but I will keep this brief. Firstly, a huge thanks to my supervisors Anna Hickman and Alex Poulton, for their patient guidance throughout this journey. They have gone above and beyond to support me in so many ways, and I feel so grateful and lucky to have had them as advisors. Many other scientists at the NOC and further afield have also given valuable advice, assistance and inspiration, including Toby Tyrrell, Richard Pearce, Mark Moore, Sam Gibbs, Duncan Purdie, Heather Bouman in Oxford, Ruth Airs at PML, Kevin Oxborough from Chelsea Technologies and Ian Probert in Roscoff. Special thanks also to Mary Smith and the graduate school team, I know I created much more than my fair share of admin for them! I gratefully acknowledge funding from a NERC SPITFIRE studentship, and small grants from the British Phycological Society and the Challenger Society for Marine Science which allowed me to attend international conferences.

I need to also acknowledge the wonderful friends I have made through my time in Southampton, and thank them for never failing to make me smile on even the worst days. Kyle, for being the best partner in cocco-crime right from the start. Lissette, for the fun times, the stats advice, and for reminding me to exercise! Rosie & Lena, for always being there for me, even after moving halfway around the world. Victoria, for the veggie meals and board games. Manon, for all the giggles. Vlad, Chelsey and Amber, for being the best and daftest office mates a girl could ask for on the home stretch. There are so many lovely people that I have crossed paths with on this journey, too many to mention all by name, including the excellent humans I had the pleasure of attending conferences with, and cruising with. I am so grateful to have had the opportunity to meet them, and for the many ways in which they have enriched my life.

My wonderful family. I quite literally cannot imagine how I could have completed this PhD without you. Mum, Dad, Elena, and the Daniels', the love and support you have shown me is incomparable. Thank you all so much.

Lastly, and most importantly, Chris. You were my cheerleader, my critic, my sounding board, my mentor, my husband, my best friend. I promised you I would finish this, and though you are no longer here, this thesis is for you.

# Abbreviations and Notation

**Abbreviations**

| | |
|---|---|
| ATP | Adenosine Triphosphate |
| CTD | Conductivity Temperature Depth instrument |
| ETR | Electron Transport Rate |
| FRRf | Fast Repetition Rate fluorometry |
| HL | High Light growth conditions (200 μmol photons $m^{-2}{}^{-}s^{-1}$) |
| HPLC | High Performance Liquid Chromatography |
| LL | Low Light growth conditions (25 μmol photons $m^{-2}{}^{-}s^{-1}$) |
| LEZ | Lower Euphotic Zone |
| LED | Light-Emitting Diode |
| ML | Medium Light growth conditions (100 μmol photons $m^{-2}{}^{-}s^{-1}$) |
| NADPH | Nicotinamide Adenine Dinucleotide Phosphate |
| PAR | Photosynthetically Active Radiation (400 – 700 nm) |
| PSU | Photosynthetic Unit |
| PSII | Photosystem II |
| PSI | Photosystem I |
| RAM | Relative Atomic Mass |
| RC | Reaction Centre |
| RCII | Reaction Centre of Photosystem II |
| RuBisCo | Ribulose 1-5 Bisphosphate carboxylase/oxygenase |
| SCM | Sub-surface Chlorophyll *a* Maximum |
| SEM | Scanning Electron Microscopy |
| SEZ | Sub-Euphotic Zone |
| SI | Stratification Index |
| SML | Surface Mixed Layer |
| UEZ | Upper Euphotic Zone |
| 1N | Haploid |
| 2N | Diploid |

**Pigments**

| | |
|---|---|
| Accessory | All pigments except Chlorophyll *a* |
| BF | 19'Butanoyloxyfucoxanthin |
| β-car | B-carotene |
| Chl *a* | Chlorophyll *a* |
| Chl *c*3 | Chlorophyll *c*3 |
| Chl *c*2-M | Chlorophyll *c*2-monogalactosyl-diacylglyceride-ester |
| Chl *c*2 | Chlorophyll *c*2 |
| Chl *c*1 | Chlorophyll *c*1 |
| Dd | Diadinoxanthin |
| Dt | Diatoxanthin |
| F | Fucoxanthin |
| HF | 19'Hexanoyloxyfucoxanthin |
| HKF | 19'Hexanoyloxy-4-ketofucoxanthin |
| NPS | Non-Photosynthetic pigments |
| PS | Photosynthetic pigments |
| TP | Total Pigment |
| ΣFs | Sum of Fucoxanthin derivative pigments |
| Σ*c*s | Sum of Chlorophyll *c* pigments |

**Statistical**

| | |
|---|---|
| ANOSIM | Analysis of Similarity |
| ANOVA | Analysis of Variance |
| H' | Shannon's diversity index |
| J' | Pielou's evenness index |
| NMDS | Nonmetric Multidimensional Scaling |
| OLS | Ordinary Least Squares regression |
| PCA | Principal Component Analysis |
| RMA | Reduced Major Axis regression |
| SD | Standard Deviation |
| SIMPER | Similarity Percentages analysis |

**Notation for Physiological Parameters**

| | |
|---|---|
| $\alpha$ | Initial slope of photosynthesis-irradiance curve |
| $a^{chl}$ | Chl *a*-specific absorption coefficient |
| $a^{chl}_{sol}$ | Reconstruction of Chl *a*-specific absorption coefficient from reference spectra |
| $E_k$ | Photosynthesis-irradiance saturation parameter |
| $F_v/F_m$ | Maximum quantum yield of PSII |
| $K_d$ | Light attenuation coefficient |
| $K_E$ | Growth-irradiance saturation parameter |
| $\lambda$ | Wavelength |
| $\mu$ | Exponential growth rate |
| $P_{max}$ | Maximum photosynthetic rate |
| $\Phi$ | Quantum yield |
| $Q^*$ | Packaging factor relating measured and maximum absorption efficiencies |
| $\sigma_{PSII}$ | Absorption cross-section of PSII photochemistry |

# Chapter 1 Introduction

## 1.1 Phytoplankton: Photosynthesisers of the Ocean

Photosynthesis is the fundamental process that converts light energy from the sun into chemical energy that fuels almost all life on earth. Just under half of the primary production on our planet is done by microscopic algae living and photosynthesising in the sunlit surface layers of the ocean, known as phytoplankton (Field *et al.*, 1998; Falkowski and Raven, 2007). Phytoplankton produce oxygen and sequester carbon which can be transported and trapped in the deep sea, and as such have a key role in biogeochemical cycling of carbon and of other elements (Sanders *et al.*, 2014). Production by phytoplankton also forms the base of marine food chains, so they are critical in understanding marine biological systems (Falkowski and Raven, 2007).

Phytoplankton are restricted to the surface layers of the ocean where there is sufficient light to photosynthesise, in what is known as the photic zone. Light, therefore, determines the first order distribution of phytoplankton in the oceans and is commonly cited as a limiting factor for oceanic productivity (Kirk, 2011). However, the distributions and productivity of phytoplankton populations are affected by many interrelated factors. Physical factors such as light, temperature, salinity and the availability of essential elements (nutrients) can interact with biotic factors such as grazing pressure, and viral and bacterial pathogens. The variations in these driving factors, both spatially and temporally, result in a dynamic range of marine environments, to which a vast diversity of different phytoplankton are adapted to exploit.

There is thought to be over 5000 individual species of phytoplankton (Guiry, 2012), ranging in size from picoplankton (< 2 μm), through to nanoplankton (2 – 20 μm) and to microplankton (> 20 μm). The huge diversity of phytoplankton species can be classified into broad taxonomic groups, each sharing an evolutionary history and certain physical traits. Diatoms, for example, are a group of siliceous microplankton that can account for up to 40 % of primary production in marine environments where surface nutrients are replenished by winter mixing or upwelling (Field *et al.*, 1998; Tréguer *et al.*, 2018). In vast areas of the low latitude surface ocean where inorganic nutrients are in short supply, picoplankton like cyanobacteria dominate the phytoplankton community (Chisholm *et al.*, 1988; Partensky, Hess and Vaulot, 1999; Johnson *et al.*, 2006). Coccolithophores are another class of widespread unicellular nanoplankton. The 280 extant coccolithophore species (Young *et al.*, 2003) are a key component of marine primary production globally, constituting ~10 % of marine

phytoplankton biomass (Poulton *et al.*, 2006) and in some regions account for > 20 % of carbon fixation (Poulton *et al.*, 2007, 2013). Taxonomically, coccolithophores sit within the haptophyte algae, but are distinct in their ability to produce calcified scales called coccoliths. Coccolithophores are regarded as the main producers of biogenic calcite, particularly in the open ocean (Baumann, Boeckel and Frenz, 2004) and the most important taxa in calcite burial (Milliman, 1993). This thesis focuses on the ecology and physiology of coccolithophores, and they will be introduced in more detail in section 1.2. First, a general introduction to photosynthesis in phytoplankton is given.

### 1.1.1 Photosynthesis

Photosynthesis is a biochemical process that converts light energy into chemical energy in carbohydrate molecules, which are then used to fuel almost all other biological processes of living organisms (Nelson and Ben-Shem, 2004). The most common form of photosynthesis, and that used by coccolithophores, is oxygenic photosynthesis. Photosynthesis is a complex multi-stage process, but in summary uses carbon dioxide and water as substrate to produce carbohydrate and oxygen (Equation 1.1):

$$6CO_2 + 6H_2O + \text{light} \rightarrow C_6H_{12}O_6 + 6O_2 \quad (1.1)$$

The process of photosynthesis can be split into a light-dependent and a light-independent set of reactions. The light-dependent reactions occur at a membrane, typically inside an organelle called a chloroplast. Light energy is collected by pigments like Chlorophyll *a* (Chl *a*), and used to split water (Equation 1.2) and to drive a chain of electron transport which ends in the production of a molecule called NADPH (nicotinamide adenine dinucleotide phosphate). The electron transport chain creates a proton gradient across the membrane. The trans-membrane energy gradient is used to synthesise ATP (adenosine triphosphate), a molecular unit of energy currency, which is carried forward with NADPH to the light-independent reactions (Nelson and Ben-Shem, 2004).

$$2H_2O + \text{light} \rightarrow 4H^+ + 4e + O_2 \quad (1.2)$$

The light-independent step involves a cyclical sequence of reactions known as Calvin-Benson Cycle. Broadly, ATP and NADPH from the light dependent reactions are used to synthesise an organic substrate called ribulose 1,5-bisphosphate. An enzyme called RuBisCo (Ribulose 1-5 Bisphosphate carboxylase/oxygenase) combines this substrate with carbon dioxide and fixes it into a sugar (Herrmann, 1999).

The mechanisms of electron transport and carbon fixation are highly conserved amongst oxygenic photosynthesisers (Falkowski and Raven, 2007), with the cellular machinery and the enzymes used being similar from trees to single celled phytoplankton. However, the initial process of harvesting light energy is achieved in diverse ways amongst photosynthetic organisms, as different light acquisition techniques have evolved in response to the conditions in the organism's habitat.

### 1.1.2 Light in the Ocean

What is termed 'light' here is electromagnetic radiation of the wavelength range 400 to 700 nm. This wavelength range is also called photosynthetically active radiation (PAR), as this is the electromagnetic energy that can be used for photosynthesis (Kirk, 2011). The radiation spectra of the sun (Figure 1.1) includes light in the PAR range, from short wavelength blue light, to longer wavelength red light, and everything in between.

Light is a variable resource in the marine environment in every sense. Latitude (sun angle and day-length), and diurnal cycles (night and day) produce predictable patterns in the total irradiance that reaches the surface ocean in a given area. However, many other factors affect available light in the upper ocean, making light a dynamic resource. Local weather conditions such as cloud cover can radically alter incident light, with thick cloud cover reducing transmission of solar irradiance by up to 90 %, for example (Kirk, 2011). Wind speeds and the resulting effect on sea state also change the ratio of reflected to transmitted light at the sea surface (e.g. Fell and Fischer, 2001), and roughened sea surfaces also produces patterns of focussing and defocussing known as caustic networks (the patterns seen on the seabed in shallow, clear water).

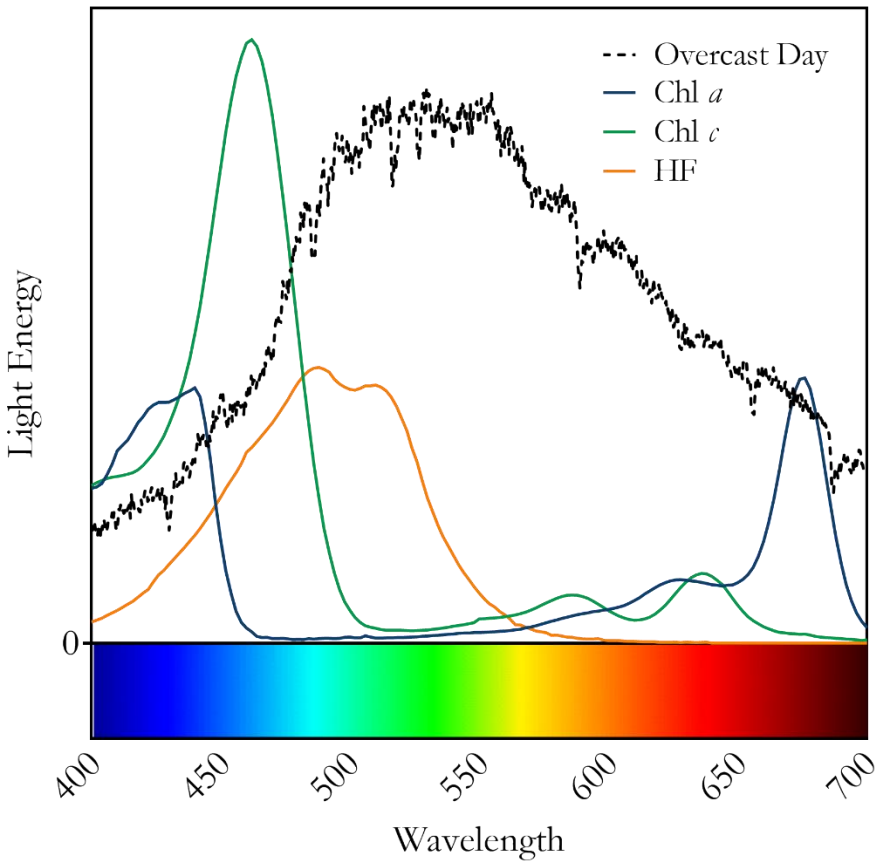


**Figure 1.1.** Shapes of pigment absorption spectra (Bricaud *et al.*, 2004). Chl *a* = Chlorophyll *a*, Chl *c* = Chlorophyll *c*, HF = 19'Hexanoyloxyfucoxanthin, and Overcast Day = An example light emission spectra from the sun on an overcast day at the National Oceanography Centre Southampton, UK, measured with a light sensor (Biophysical Instruments, QSL-2101). Colour bar indicates approximate colour of light in different regions of the spectrum.

Beneath the surface, light is attenuated with depth creating a vertical gradient of light intensity in the upper ocean. Light also changes in quality (or colour) with depth, as constituents of the water column preferentially absorb certain wavelengths. In the open ocean, longer wavelengths of light are attenuated faster by water molecules, resulting in progressively bluer light with depth (Figure 1.2). Any suspended material in the water column that absorbs or scatters light also affects the spectral quality of the light field. For example, phytoplankton themselves can alter the light environment in the photic zone as they absorb mostly red and blue light for photosynthesis, leaving a green coloured light field. Coastal waters typically contain higher quantities of suspended and dissolved organic and particular matter, leading to faster attenuation of blue light, and shallower photic zones (Figure 1.2).

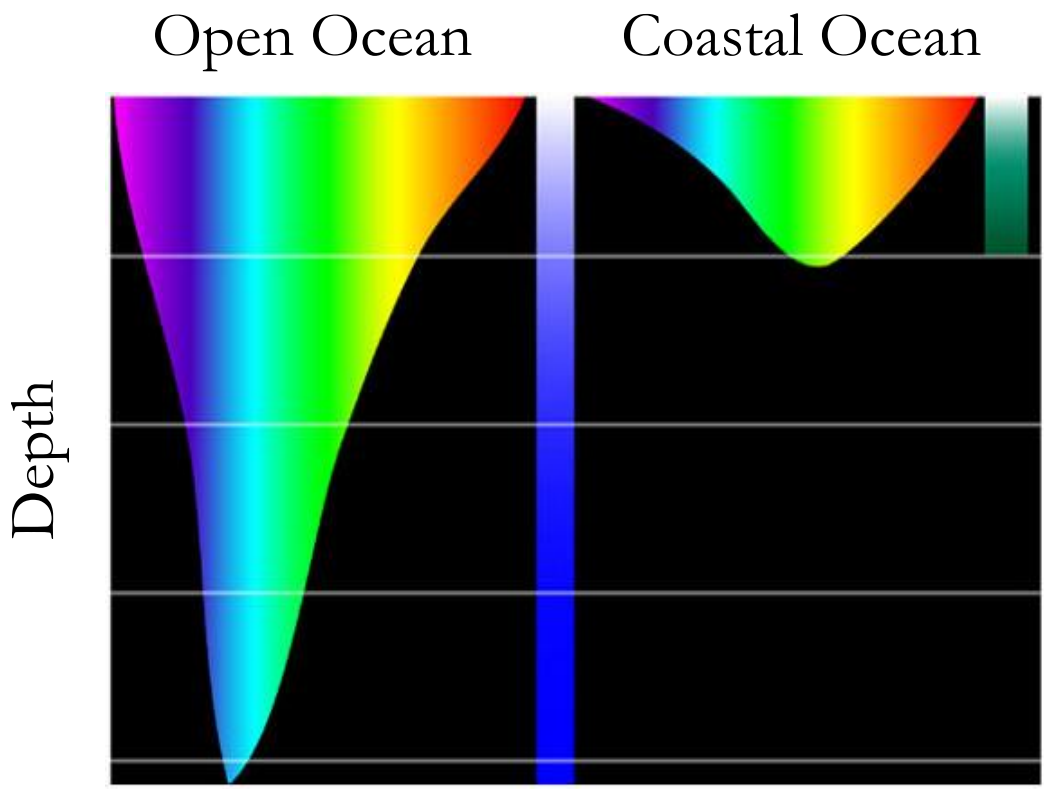


**Figure 1.2.** An illustration of the change in spectral quality (or colour) of visible light with depth in the typical open ocean and in the coastal ocean. (Diagram adapted from the 'Ocean Explorer' section of the National Oceanic and Atmospheric Administration website https://oceanexplorer.noaa.gov/ Image courtesy of Kyle Carothers).

Additionally, the planktonic nature of single celled algae such as coccolithophores means that their movement is subject to the circulation and turbulence of the water, in contrast to static photosynthesisers, such as anchored seaweeds, seagrasses or terrestrial plants. Turbulence and mixing, therefore, substantially increase the variability of light to which an individual cell can be exposed on relatively short (minutes to hours) timescales (Simpson and Sharples, 2012).

### 1.1.3 Pigments

Photosynthetic organisms absorb the light energy for photosynthesis using molecules called pigments. In photosynthetic eukaryotes, including coccolithophores, light harvesting pigments and the photosynthetic apparatus are housed in and around the thylakoid membrane in the chloroplasts (Figure 1.3). Photosynthetic units are embedded within the thylakoid, of which the pigment Chl *a* is an integral part. Two Chl *a* molecules are found at the RC of every photosystem, and act as primary electron donors for the electron transport chain (Nelson and Ben-Shem, 2004). The chlorophyll containing RCs are surrounded by pigment-protein complexes known as antenna (Neilson and Durnford, 2010), which contain Chl *a*, as well as

other pigments known as accessory pigments (Figure 1.3). Pigment molecules in the antenna contribute to light absorption and funnel energy to the RCs via excitation energy transfer, thereby increasing the absorption cross-section, often denoted 'σ', of photochemistry (Renger, May and Kühn, 2001).

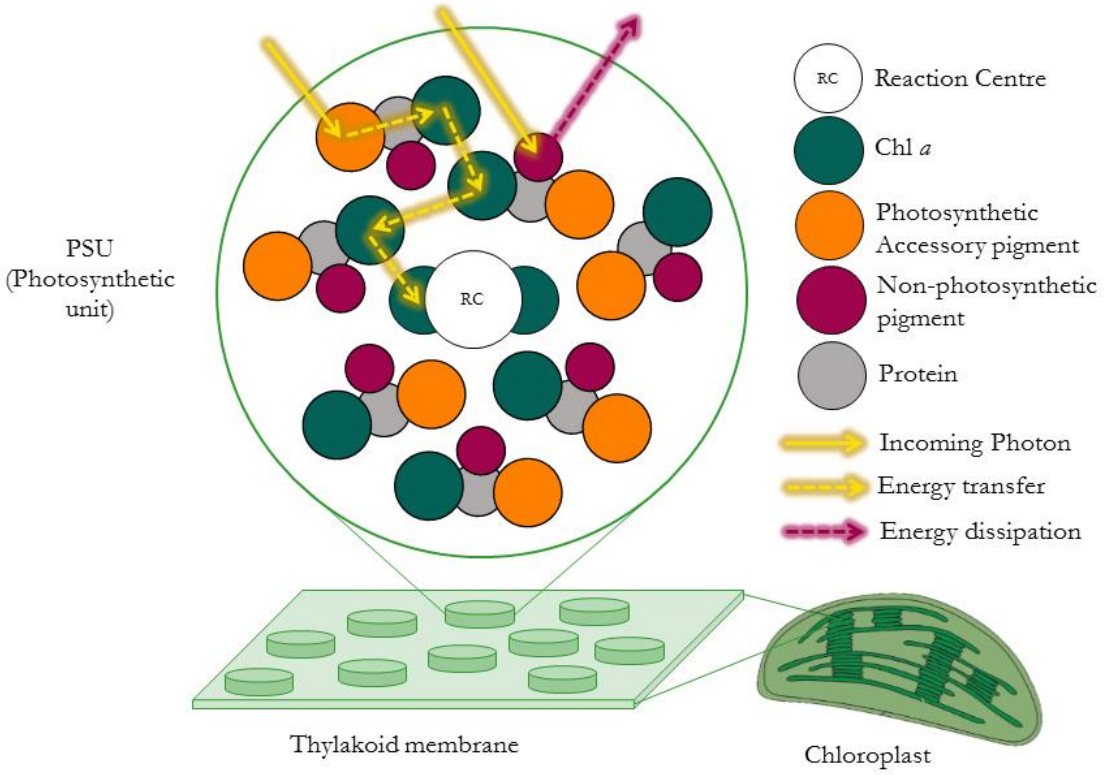


**Figure 1.3.** Schematic showing a simplified photosynthetic unit (PSU), sitting within the thylakoid membrane in the chloroplast of a eukaryote. Pigment protein complexes, containing different types of pigment, surround a chlorophyll containing reaction centre (RC) where the initial light-driven charge separation of photosynthetic reactions and oxygen evolution takes place. The funnelling of excitation energy from an incident photon towards the RC is shown, along with the dissipation of energy by a non-photosynthetic pigment

Each pigment has characteristic spectral absorption properties, which are driven by the molecular structure of the pigment. The diversity of pigments found amongst phytoplankton is much greater than that found in terrestrial plants (Jeffrey, Wright and Zapata, 2011) in response to the varying light environments of the marine photic zone. The absorption spectra of phytoplankton, which is determined by their constituent pigments, in natural populations are found to be adapted to match the spectrum of available light in their habitats (Bidigare, Marra, *et al.*, 1990; Hickman *et al.*, 2009). Chl *a* absorbs strongly in the red region of the light spectrum (Figure 1.1). This red absorption peak becomes less effective with depth in the

ocean, as the light field becomes more blue-green enriched, and accessory pigments have evolved to compensate by absorbing light energy in different regions of the visible spectrum to Chl *a* (Falkowski and Raven, 2007). Over evolutionary time, molecular modifications to Chl *a*, have produced accessories such as chlorophyll *b* in the green algae and chlorophyll *c* in the red algal lineages, in which the blue absorption peak is shifted to higher wavelengths (Figure 1.1). Accessory pigments, therefore, allow light to be efficiently harvested across the full spectrum. The other main group of accessory pigments found in eukaryotic algae are a group of hydrocarbons called the carotenoids, which exhibit an even wider range of spectral absorption characteristics (Jeffrey *et al.*, 2011). A diverse group of photosynthetically relevant carotenoids are the xanthophylls, including important pigments like fucoxanthin and its derivatives (Roy *et al.*, 2011). Some coccolithophores contain a pool of these fucoxanthin derivative pigments (van Lenning *et al.*, 2004; Roy *et al.*, 2011), but the range of coccolithophore species in which the contributions of accessory pigments has been quantified is limited.

The evolution of accessory pigments enables phytoplankton cells to absorb a wider spectrum of the available light than if they used Chl *a* alone (Figure 1.1), a phenomenon termed chromatic adaptation (e.g. Hickman *et al.*, 2010). The type of pigments in a phytoplankton cell are evolutionarily determined, meaning pigments can be a key tool in assessing phytoplankton community composition (Jeffrey, Mantoura and Wright, 1997; Roy *et al.*, 2011). One such widely used system that uses pigment identification, normally by High Performance Liquid Chromatography (HPLC) to identify phytoplankton groups in natural samples is CHEMTAX (Mackey *et al.*, 1996), its name referring to the chemo-taxonomic method employed. In such analyses, the fucoxanthin derivative pigment 19-Hexanoyloxyfucoxanthin (HF) is used as a chemo-taxonomic 'biomarker' for the haptophytes.

### 1.1.4 Photoacclimation

The variable marine light environment is a major challenge faced by phytoplankton. In order to survive and thrive, cells must be able to adjust their investment in light harvesting equipment such that the light energy collected for photosynthesis meets their metabolic energy demands. Under low light conditions cells may struggle to harvest enough light energy, but high light conditions can also present a challenge, as an excess of absorbed light energy can cause photodamage (Barber and Andersson, 1992). Over excitation of Chl *a* can lead to the formation of chlorophyll triplets, which in turn can form reactive oxygen species that are harmful, sometimes lethal, to photosynthetic cells. In contrast to chromatic adaptation, which occurs over evolutionary timescales, phytoplankton cells acclimate to ambient light conditions

on very short timescales (hours to days), by a process termed photoacclimation (Falkowski and La Roche, 1991).

Photoacclimation often involves producing more or less pigment molecules. The relative quantities of different pigments in phytoplankton cells is highly plastic depending on irradiance (MacIntyre *et al.*, 2002; Graff *et al.*, 2016). For example, cells growing under low light and nutrient replete conditions typically invest in high pigment concentrations in order to maximise acquisition of the limiting resource: light. Alternatively, under high light conditions where nutrients are limiting, cells may invest less in pigment production to avoid photodamage.

Differences in energy transfer efficiency between the various pigments means that photoacclimation of pigments not only causes changes in the amount and colour of light absorbed, but also in the energy transfer dynamics within the light harvesting antenna (Neilson and Durnford, 2010; Nelson and Junge, 2015). The primary role of most accessory pigments is to harvest light, but some carotenoids like β-carotene are not considered photosynthetic, as the light energy they absorb is not transferred to the photosystems at all. These non-photosynthetic (NPS) pigments help protect photosystems from oxidative damage by dissipating excess absorbed energy. The 'xanthophyll cycle' pigments (diadinoxanthin and diatoxanthin), which are present in diatoms and haptophytes (Lavaud *et al.*, 2002; Roy *et al.*, 2011), are another example of photoprotective (or NPS) pigments, as the de-epoxidation cycle dissipates excess energy in the antennas in a process known as non-photochemical quenching (Gilmore and Yamamoto, 1991).

Photoacclimation can be a complex process, as it also involves adjustment of the non-pigment components of photosynthetic units, and the photosynthetic machinery downstream of the light harvesting step (MacIntyre *et al.*, 2002, and references within). All steps in the photosynthetic process require investment in terms of the nutrients used to manufacture the necessary machinery, and cells invest differentially in these components depending on the availability of nutrient resources, as well as in response to irradiance.

### 1.1.5 Cell Size and Light Absorption

Cell size is a key determinant of metabolic rate and many other aspects of phytoplankton physiology (Marañón, 2015; Ward *et al.*, 2017). For example, growth rates typically scale negatively with cell size, and the surface area to volume ratio of single celled phytoplankton is a determining factor in the maximum rate of gas exchange or nutrient uptake a cell can achieve. Cell size also has important ramifications for absorption of light for photosynthesis

due to internal shading causing a reduction in absorption efficiency of pigments, a phenomenon known as 'package effect' (e.g. Bidigare, Ondrusek, *et al.*, 1990, Figure 1.4). Robust physical theory underpins the package effect phenomenon (Kirk, 1976; Morel and Bricaud, 1981) and demonstrates that larger or more highly pigmented cells absorb incident light with reduced efficiency. Limitations on light absorption efficiency placed on large cells can theoretically translate into limitations to photosynthetic rate and growth rate (Finkel and Irwin, 2000), and can thus help us to understand the differences in ecological preference between cells of different sizes, and to predict where and how fast certain species will grow. For example, the theory of packaging suggests that larger cells may not be able to use incident light as efficiently as smaller cells, and thus that smaller cell size may be competitively advantageous in low light environments (Finkel, 2001; Key *et al.*, 2010).

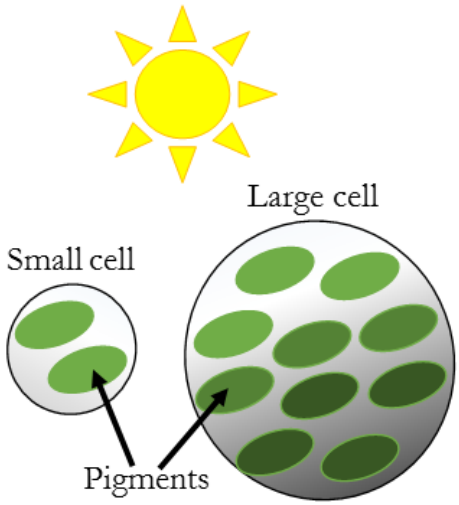


**Figure 1.4.** Schematic depicting package effects on pigments in algal cells. In the small cell there is not much internal shading and the pigments each absorb at maximum efficiency. In contrast, in the larger cell pigments shade each other, thereby reducing the absorption efficiency of each pigment molecule.

## 1.2 Coccolithophores

This thesis concerns photophysiology and response to light in coccolithophore algae. The coccolithophores are part of a division of eukaryotic algae called haptophytes. The ancestors of coccolithophores evolved as the result of an endosymbiosis of red algae and a heterotroph (McFadden, 2001). This line then diversified into several important phytoplankton lineages, such as the haptophytes (including coccolithophores), the heterokonts (including diatoms), and the alveolata (including dinoflagellates). Although there are non-calcifying haptophyte species, these are not termed coccolithophores, despite being closely related.

Coccolithophores have a dimorphic life cycle, with morphologically distinct haploid (1N) and diploid (2N) phases (Green, Course and Tarran, 1996). The haploid phase is usually flagellated

and has simplified coccoliths known as holococcoliths. The different life-cycle phases are hypothesised to occupy different niches in the natural environment (Houdan *et al.*, 2006; Silva *et al.*, 2013; von Dassow *et al.*, 2014; Frada *et al.*, 2018), but differences in the physiology and ecology between the life-cycle phases are not consistent across species (see review by Frada *et al.*, 2018).

### 1.2.1 Calcifying Phytoplankton

All coccolithophore species produce a form of calcite exoskeleton (coccoliths) at some phase of their life cycle. Although coccolithophores are relatively small (between 3–20 μm in diameter), they are a major pelagic calcite producer (Berelson *et al.*, 2007), and have a distinct role in export of both organic and inorganic carbon to the deep ocean. Calcified exoskeletons are more resilient to degradation and remineralisation than soft organic equivalents, and can also act as "ballast" enhancing the rate at which organic particles sink into the deep ocean (Armstrong *et al.*, 2002; Balch *et al.*, 2016). Coccolithophores thus have a unique influence on global carbon dynamics. The degradation-resistant coccoliths mean that coccolithophores also provide the best-preserved and most widespread fossil indicators of marine phytoplankton, dating back > 200 million years (Bown, Lees and Young, 2004). Coccolith geometry, isotopic signatures and biomarkers such as alkenones in their fossilised shells allow interpretation of environmental conditions in geological history (Henderiks and Pagani, 2007; Gibbs *et al.*, 2013). A good understanding of the ecology of modern coccolithophores is, therefore, valuable both for making paleontological inferences, and for predicting how they will respond to changes in the future in a changing ocean.

Coccoliths are produced in a vesicle inside the cell, where nucleation of calcite crystals forms the intricate patterns and varied morphologies of coccoliths, and are subsequently extruded onto the cell surface (Young, Henriksen and Probert, 2004; Taylor *et al.*, 2007). The process of coccolith production is a distinctive feature, and requires investment of energetic resources (Brownlee and Taylor, 2004). Although many theories have been postulated, definitive evidence of the adaptive function of coccoliths continues to elude scientists (Monteiro *et al.*, 2016; Taylor, Brownlee and Wheeler, 2017). Classically, the calcite exoskeleton is thought to provide protection from grazers (Young, 1994), in a similar fashion to the silicon frustules of diatoms (Sikes and Wilbur, 1982). Whilst some evidence suggests the coccosphere provides mechanical protection (Jaya *et al.*, 2016), it has been difficult to demonstrate that calcification lowers the rate of grazing (Sikes and Wilbur, 1982). In fact, microzooplankton grazing has been found to exert strong top-down control on coccolithophores in natural populations (Holligan *et al.*, 1993; Mayers *et al.*, 2018). Other commonly cited functions of coccoliths include protection from

viral/pathogen attack, buoyancy control, a form of carbon concentrating mechanism (as the calcification reaction produces $CO_2$), and as an extension of the cells microhabitat to provide buffering from external environmental conditions (Young, 1994; Monteiro *et al.*, 2016).

Coccoliths are colourless, but are highly efficient at scattering light, such that blooms of coccolithophores (high cell densities) turn the ocean a milky colour, and can be detected from space (Holligan *et al.*, 1983; see review by Balch, 2018). Some authors have suggested that this scattering could protect the cells from stress caused by high irradiance (e.g. Lohmann, 1913; Braarud and Nordli, 1952; Guan and Gao, 2010) but other studies present evidence to refute this 'sunshade' hypothesis, with a similar resistance to photoinhibition being present in both non-calcifying and calcifying cells (Nanninga and Tyrrell, 1996). Light absorption and transmission measurements have shown that coccoliths decrease the amount of light transmitted through a culture of coccolithophore cells (Harris, Scanlan and Geider, 2005; Gao *et al.*, 2009), and that coccoliths decrease transmittance of UV light by over 14 % (Xu *et al.*, 2016). However, difficulties remain in assessing how the scattering effect of coccoliths affect the amount of light that is absorbed by the internal cell for photosynthesis. Although the purpose of coccoliths is unclear, their potential effect on light acquisition by coccolithophore cells remains an interesting avenue of research.

### 1.2.2 Ecology and Biogeography of Coccolithophores

Our understanding of coccolithophore ecology is drawn from both observations in the field, and controlled laboratory experiments. For several reasons, our understanding of the biogeography and physiology of coccolithophores is biased to one particular species, *Emiliania huxleyi*, and this will be adressed in section 1.2.3. With this caveat in mind, an overview of the ecology and biogeography of coccolithophores is presented.

Published studies on the geographical distribution of coccolithophores show that they are a substantial component of tropical, sub-tropical and sub-polar plankton communities (Ziveri *et al.*, 2004; O'Brien *et al.*, 2013; Saavedra-Pellitero *et al.*, 2014). After the picoplankton (cyanobacteria like *Prochlorococcus* and *Synechococcus*) coccolithophores can be numerically abundant in 'blue-water' (oligotrophic) regions of the open ocean (Winter and Siesser, 1994), and their maximum contribution (~20 %) to total carbon fixation is thought to occur in the oligotrophic subtropical gyres (Poulton *et al.*, 2007). Studies utilising biomarker pigments to quantify phytoplankton groups find the contribution of 19'Hexanoyloxyfucoxanthin (a coccolithophore biomarker pigment) is also highest in subtropical gyres (Barlow *et al.*, 2002; Aiken *et al.*, 2009), and coccolithophore diversity is highest in the low latitudes (O'Brien, Vogt

and Gruber, 2016). Phytoplankton biomass overall is low in the subtropical gyres, however, so the areas of highest coccolithophore diversity and greatest contribution to the phytoplankton community do not necessarily coincide with where coccolithophore biomass is greatest. In fact, coccolithophore biomass peaks at mid-latitudes (O'Brien *et al.*, 2013) as coccolithophore 'blooms' (high cell numbers typically of one species) are more frequent in these temperate regions. Transiently, coccolithophores can comprise up to 40 % of local carbon fixation during large bloom events in temperate coastal waters (Poulton *et al.*, 2013, 2014; Mayers *et al.*, 2018).

In addition to these overall trends, it is clear that within the coccolithophores, different species exhibit different environmental preferences. Both horizontal (latitudinal) and vertical (depth zone) patterns in coccolithophore assemblage have been observed (Winter and Siesser, 1994; Hagino, Okada and Matsuoka, 2000; Boeckel and Baumann, 2008; Poulton *et al.*, 2017). For example, *Umbellosphaera sp.* are typical of oligotrophic environments (Kinkel, Baumann and Cepek, 2000), *Coccolithus pelagicus* prefers arctic/subarctic waters < 14 °C (McIntyre and Bé, 1967; Baumann, Andruleit and Samtleben, 2000), and species such as *Florisphaera profunda* are typical of the lower photic zone (Cortés, Bollmann and Thierstein, 2001). However, the importance of light in determining biogeography, and the extent to which different coccolithophore species are adapted to different light environments remains relatively unexplored.

### 1.2.3 *Emiliania huxleyi*: a model coccolithophore?

The most common coccolithophore species is considered to be *Emiliania huxleyi,* a species with a broad geographical range (Winter and Siesser, 1994), and which often numerically dominates the coccolithophore community (Paasche, 2002). It can form high density blooms (> 1000 cells $mL^{-1}$) which have attracted much attention as they can be seen with the naked eye, and detected from satellites (Holligan *et al.*, 1983, 1993). Uniquely, *E. huxleyi* cells can produce several layers of coccoliths when blooming, and shed outer coccoliths into the water column, a feature not seen in other coccolithophore species (Gibbs *et al.*, 2013; Sheward *et al.*, 2017). It is these detached coccoliths that most strongly scatter light and result in a milky appearance in the water. Therefore, satellite algorithms for coccolithophores are somewhat biased towards *E. huxleyi* blooms specifically, rather than coccolithophores in general (Hopkins *et al.*, 2015; Daniels *et al.*, 2018). Based on the prevalence of high light conditions during coccolithophore bloom events, it is suggested that coccolithophores are adapted to high light environments (Iglesias-Rodriguez *et al.*, 2002; Tyrrell and Merico, 2004). However, the vast majority of coccolithophore species are not bloom-forming, and it seems *E. huxleyi*

may inhabit a different niche to most other coccolithophore species (Balch, 2004). It is increasingly recognised, therefore, that care should be taken when using the distribution of *E. huxleyi* to make generalisations about the ecological preferences of coccolithophores as a group (Balch, 2018).

*E. huxleyi* has become a model species for laboratory-based studies on coccolithophores, and on phytoplankton in general. Being a robust cell with interlocking coccoliths (placoliths), it is relatively easy to isolate and grows well in the laboratory, in both natural and artificial seawater. Hundreds of *E. huxleyi* strains are now cultured around the world, and as such, an overwhelming majority of laboratory studies on coccolithophores feature *E. huxleyi.* It can achieve high exponential growth rates ($> 1.5\ d^{-1}$) when supplied with replete nutrients and light (see Paasche 2002), appears to tolerate high light intensity well (Balch, Holligan and Kilpatrick, 1992; Nanninga and Tyrrell, 1996; Suggett *et al.*, 2007), and can persist in 'stationary' phase for prolonged periods (Young, unpublished), all characteristics that help it to tolerate the artificial environment of laboratory incubation. However, these traits are not all representative of the physiology and ecology of the coccolithophores generally, meaning coccolithophores other than *E. huxleyi* are less frequently cultured (Winter and Siesser, 1994; Probert and Houdan, 2004).

Additionally, *E. huxleyi* is unusual in that its haploid life stage is non-calcifying (Klaveness, 1972), frequently even diploid (mutant) strains are non-calcifying (Paasche, 2002; Marsh, 2003), and it is genetically more closely related to some none-calcifying haptophytes than to most other coccolithophore species (Figure 1.5, see de Vargas *et al.*, 2007; Bendif *et al.*, 2015). *E. huxleyi* also appears to lack a silica requirement for coccolith formation that is seen in other coccolithophore species (Durak *et al.*, 2016). In summary, whilst much has been learned from using *E. huxleyi* as a model species, it has several physiological quirks, which suggest it may not be representative of the characteristics of coccolithophores as a whole. Evidence shows that coccolithophore species other than *E. huxleyi* are important, at least regionally. For example, heavily calcifying species are comparably important in terms of biomass and for the global calcification budget (Daniels, Sheward and Poulton, 2014; Daniels *et al.*, 2016). Caution should be exercised, therefore, when extrapolating what is known about *E. huxleyi* to other species, and exploring the traits of a range of coccolithophore species is a valuable research avenue when attempting to understand the fundamental physiology and ecology of the coccolithophores.

### 1.2.4 Revealing diversity within the Coccolithophores: A Challenge

Although the coccolithophores are commonly considered as a functional group of phytoplankton, it is increasingly acknowledged that the paradigms regarding this group need to be revised, as they inhabit a variety of marine environments, and likely fill a wide range of ecological niches (Balch, 2018). There are ~ 280 extant coccolithophore species, ranging in size from 2 – 20 μm in diameter, and with vastly diverse coccolith morphologies and habits, including some species which are motile. There is evidence that some coccolithophores, particularly those possessing flagella and/or haptonema (an organelle known to facilitate phagotrophy in prymnesiophytes, Kawachi *et al.*, 1991) are able to utilise dissolved or particulate organic nutrients (Parke and Adams, 1960; Houdan *et al.*, 2006). Phylogenetic and paleontological data suggest the coccolithophores evolved from mixotrophic or heterotrophic ancestors that occupied coastal or neritic environments (de Vargas *et al.*, 2007), so it is plausible that some coccolithophore species have retained a mixotrophic nutritional strategy. Indeed some coccolithophores (e.g. Papposphaeraceae) appear to lack chloroplasts (Marchant and Thomsen, 1994) and thus may be completely heterotrophic.

As mentioned, patterns in coccolithophore community structure in the field (e.g. Charalampopoulou *et al.*, 2011; Poulton *et al.*, 2017) show that coccolithophore species have different environmental preferences for light, nutrient and temperature conditions. However, it is challenging to explore these differential ecologies experimentally as there are far fewer coccolithophore species in culture in comparison to the diversity observed in the field. Amongst the coccolithophore species in culture, structurally robust placolith taxa (species with interlocking coccoliths e.g. *E. huxleyi*) are better represented than delicately calcified murolith species (without interlocking coccoliths e.g. *Syracosphaera* species), presumably as they are better able to survive the rough process of single cell isolation. Once isolated, a coccolithophore species must be able to grow well under culture conditions (high inorganic nutrients, stable and high light, constant temperature), which discriminates against certain ecological strategies, including those with slow growth rates such as species adapted to lower irradiance conditions. Classic algal culturing methods are also not designed to support mixotrophic strategies, as culture media is typically sterile and does not include organic substrate, leading to an exacerbation of the bias towards photoautotrophic coccolithophores.

However, over recent decades the number of species and strains of coccolithophore successfully cultivated in laboratory settings has grown, meaning comparative studies have an increasing diversity with which to work. This thesis tackles the research bias towards *E. huxleyi* in culturing studies by utilising the broadest range possible within the coccolithophore species

that are available in culture (Table 1.1). For example, although the majority of species used in this study have placolith-type coccoliths, *Syracosphaera pulchra*: (one of the only murolith-type species to be cultured successfully) is included in my experimental work (Figure 1.6). Two of the species included are flagellated motile species (*Helicosphaera carteri* and *Syracosphaera pulchra*), and each of the five major divisions of coccolithophores are represented by at least one species (Figure 1.5). Both a haploid and diploid life phase of *E. huxleyi* were cultured, and these are referred to in the text as *E. huxleyi* (1N) and *E. huxleyi* (2N) respectively.

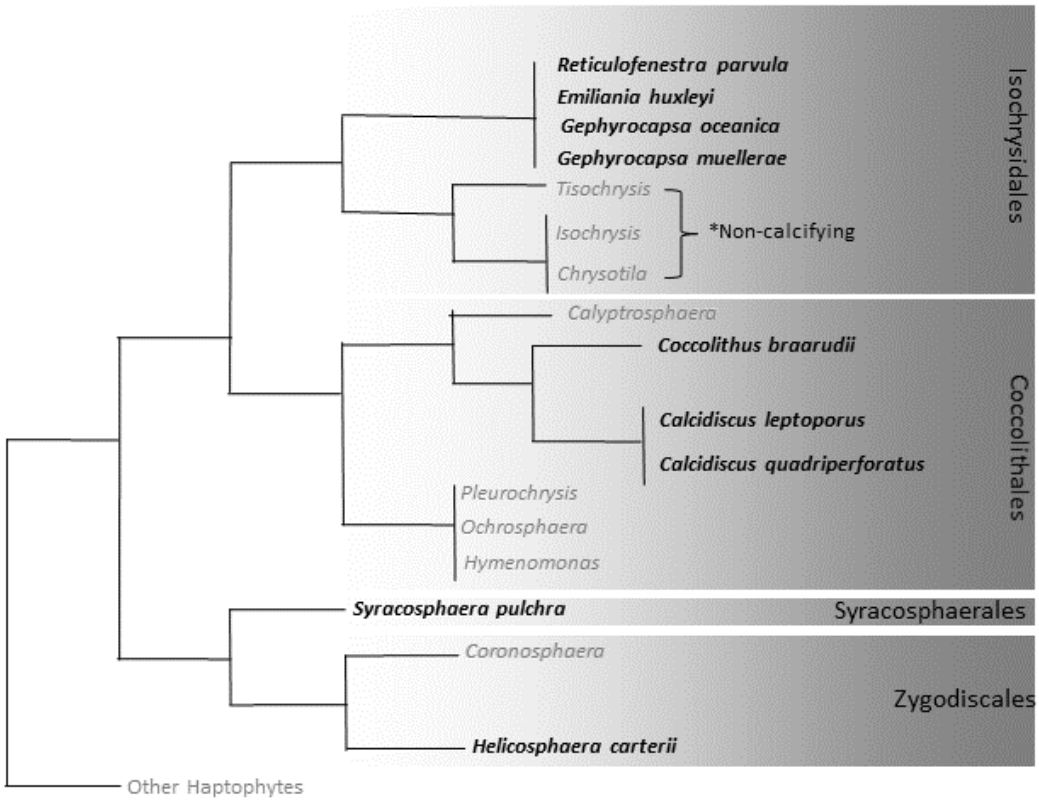


**Figure 1.5.** Coccolithophore phylogeny adapted from Bendif *et al.*, 2015, using 18 S Nuclear rDNA. Species in bold used in laboratory experiments in this thesis.

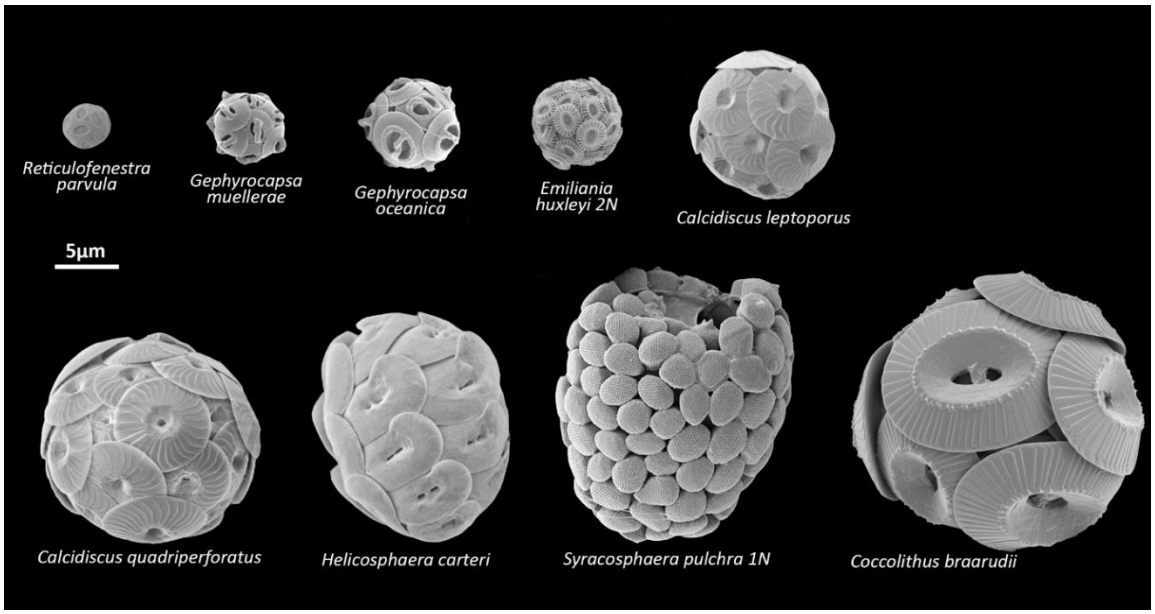


**Figure 1.6.** To scale Scanning Electron Microscope (SEM) images of all calcifying species used in this study. Images are from Nannotax 3 (Young *et al.,* 2014), or taken at the National Oceanography Centre, Southampton with the assistance of Richard Pearce.

**Table 1.1.** Details of coccolithophore culture strains selected for this thesis. All strains provided by Roscoff Culture Collection (RCC), Station Biologique de Roscoff.

| RCC Code | Species | Isolation | Haploid/ Diploid | Calcifying/ Non-calcifying | Motile/ Non-motile |
|---|---|---|---|---|---|
| 4036 | *Reticulofenestra parvula* | Chilean Coast P. Von Dassow | Diploid | Calcifying | Non-motile |
| 3370 | *Gephyrocapsa muellerae* | Chile, 2011, P. Von Dassow | Diploid | Calcifying | Non-motile |
| 1314 | *Gephyrocapsa oceanica* | French Coast, 1998 | Diploid | Calcifying | Non-motile |
| 1217 | *Emiliania huxleyi* | Tasman Sea, 1998. I. Probert | Haploid | Non-calcifying | Motile |
| 1731 | *Emiliania huxleyi* | South Atlantic (S.Africa), 2000. I. Probert | Diploid | Calcifying | Non-motile |
| 1130 | *Calcidiscus leptoporus* | South Atlantic (S.Africa), 2000. I. Probert | Diploid | Calcifying | Non-motile |
| 1135 | *Calcidiscus quadriperforatus* | South Atlantic (S.Africa), 2000. I. Probert | Diploid | Calcifying | Non-motile |
| 1323 | *Helicosphaera carteri* | South Atlantic (S.Africa), 2000 I.Probert | Diploid | Calcifying | Motile |
| 1461 | *Syracosphaera pulchra* | Italian coast, 2000. I. Probert | Haploid | Calcifying | Motile |
| 1197 | *Coccolithus braarudii* | English Channel. M.Parke | Diploid | Calcifying | Non-motile |

## 1.3 Aims and Objectives

The overarching aim of this thesis is to explore the diversity of photophysiology and ecology amongst different coccolithophore species, both through laboratory experiments, and by examining coccolithophore communities in the field. The results enhance current understanding of how coccolithophores use light, reveal patterns, similarities and differences within the group, and help to address whether the model coccolithophore species *E. huxleyi* is representative of the coccolithophores as a whole.

Specific objectives are:

- To generate a suite of comparative physiological data between a greater range of coccolithophore species ($n$ = 10) than has previously been attempted in a single experimental setup.

- To quantify photosynthetic parameters amongst these coccolithophore species (including pigment content, light absorption efficiency, and fluorescence dynamics of PSII), and how these parameters change when the cells photoacclimate to different growth irradiances.

- To consider the influence of cell size (ranging from 11 $\mu m^3$ to 2120 $\mu m^3$ in the species examined) on light absorption and photosynthesis amongst the coccolithophores.

- To examine the coccolithophore community (to a high level of taxonomic detail) in the natural environment of a summer temperate shelf sea, and to identify patterns and drivers determining the coccolithophore distributions.

## 1.4 Thesis Outline

**Chapter 2** quantifies the photoacclimation response to three different growth irradiances amongst a wide range of coccolithophore species (Table 1.1), in order that direct interspecies comparisons can be made. Measurements of pigment, light absorption and photosynthesis (using a variable fluorescence method) are integrated to identify the acclimation strategies employed by the different species of coccolithophores.

**Chapter 3** examines the size scaling of light absorption, photosynthetic rates and growth rates in coccolithophores, spanning two orders of magnitude in cell volume. The work tests whether maximum growth rates ($\mu_{max}$) scaled negatively with cell volume, and whether the size scaling exponent of growth rate decreased under low light conditions, in line with the current understanding of size-dependent light acquisition in other phytoplankton (e.g. Finkel, 2001; Finkel, Irwin and Schofield, 2004). The results presented provide novel information on the inter-specific size scaling relationships in the coccolithophore group.

**Chapter 4** is an investigation into coccolithophore community composition in a summer temperate shelf sea, across a horizontal gradient from the shelf to the dynamic shelf-break region. High-resolution depth profiles of the taxonomically detailed coccolithophore community composition is used alongside ancillary physical, chemical and biological measurements, to identify patterns and drivers determining distributions of coccolithophore populations in this region.

**Chapter 5** synthesises the findings of chapters 2, 3 and 4, and integrates the results with current knowledge. The contribution of the results presented in the thesis to the understanding of the ecological niche of the coccolithophores in discussed, and avenues for future research are highlighted.

# Chapter 2 Pigments and Photoacclimation Strategies in Coccolithophores

## Abstract

Photoacclimation is a key concept in phytoplankton biology and ecology. Parameterising pigment content and photosynthetic parameters, and how these vary with irradiance, is essential for understanding phytoplankton dynamics. The coccolithophores are an important group of phytoplankton, contributing substantially to primary production and pelagic calcite production, but thus far research into the photophysiology of this group has focussed primarily on one species, *Emiliania huxleyi*. This chapter broadens the present knowledge base significantly by quantifying pigment content, absorption properties and photophysiology amongst 10 different species, and assessing how these different species photoacclimate to three different irradiances (25, 100 and 200 μmol photons $m^{-2}$ $s^{-1}$). Several striking similarities amongst the coccolithophore species were noted. All species had a high abundance of accessory pigments, including fucoxanthin-derivatives and chlorophyll *c*'s (Chl *a* : Accessory pigment ratio < 1 : 1), which was conserved under all three irradiances. High accessory pigment content and high absorption-cross section of PSII ($\sigma_{PSII}$) suggest that the photosynthetic unit size is large in coccolithophores. High accessory pigment content directly resulted in high light absorption in the 440 - 470 nm region in all the coccolithophore species examined. The characteristic spectral shape clearly distinguished the coccolithophores from a diatom species (*Thalassiosira weissflogii*) grown in parallel, which had less accessory pigment (Chl *a* : Accessory pigment ratio > 2 : 1) and lower absorption in the 440 - 470 nm region. Whilst the total accessory pigment content was conserved across coccolithophore species, notable diversity amongst the different coccolithophore species was revealed in terms of the contribution to the accessory pigment pool. For example, a commonly used coccolithophore 'biomarker' pigment (19-Hexanoyloxyfucoxanthin) varied between species from 0.5 % to 38.4 % of total pigment content in *Coccolithus braarudii* and *Calcidiscus quadriperforatus,* respectively. Considerable diversity was also revealed in the photoacclimation response amongst species, with some species exhibiting strong 'n-type' acclimation (an estimated 4-fold increase in the density of photosynthetic units) whereas the response was comparatively modest in other species (e.g. *Syracosphaera pulchra*). Implications of these results for assessment of coccolithophores in the field and for our understanding of coccolithophore niches are discussed.

## 2.1 Introduction

### Coccolithophores and Light

Coccolithophores are a class of widespread unicellular haptophyte phytoplankton. The > 280 extant species are a key component of marine phytoplankton and primary production globally, constituting ~ 10 % of marine phytoplankton biomass (Poulton *et al.*, 2006) and in some regions accounting for > 20 % of carbon fixation (Poulton *et al.*, 2007, 2013). Coccolithophores are often considered one of the key phytoplankton functional types, as they are the most numerically abundant calcifying phytoplankton, and hence have an important role in the global carbon cycle. Current understanding of the ecological niche of coccolithophores is largely based on the biology of one species, the cosmopolitan and often bloom-forming *Emiliania huxleyi*. This bias occurs because cultures of *E. huxleyi* grow very well in laboratory conditions and blooms of *E. huxleyi* are relatively easy to detect in the environment (as the scattering signature of high densities of detached coccoliths can be detected by satellites). Blooms of *E. huxleyi* have often been detected in areas with shallow mixed layers, corresponding to a high light environment (Nanninga and Tyrrell, 1996), which has led to the perception that coccolithophores in general are adapted to high light environments. However, the coccolithophores are a group with diverse morphologies, and differential environmental distributions (e.g. Charalampopoulou *et al.*, 2011; Poulton *et al.*, 2017), with some species showing a preference for the low light environment of the lower photic zone. Additionally, where the physiology of coccolithophore species other than *E. huxleyi* have been studied, notable diversity has been revealed, for example differences in requirements for calcification (Walker *et al.*, 2018), nutrient demands (Durak *et al.*, 2016), differences in inorganic carbon to organic carbon ratios, motility and apparent mixotrophy (Houdan *et al.*, 2006). This study provides insights into photoacclimation strategy of a wide range of coccolithophore species, in order to help indicate whether knowledge of *E. huxleyi* can be extrapolated to the rest of the coccolithophore group.

Phytoplankton generally are restricted to the surface layers of the ocean where there is sufficient light to photosynthesise, in what is termed the photic zone. Light, therefore, determines the first order distribution of phytoplankton in the oceans and is commonly cited as a limiting factor for oceanic productivity (Kirk, 2011). Light is also highly variable in intensity and quality in the marine environment. As light is attenuated with depth, there is both a vertical gradient of intensity and of spectral quality (colour), with longer wavelengths of light being attenuated faster by water (see Figure 1.2). Phytoplankton use various strategies to acclimate to different light environments, to maximise photosynthetic rate, whilst minimising

the cost to the cell. Differential investment of pigments and other photosynthetic components in response to environmental conditions is termed photoacclimation. A comprehensive understanding of the mechanisms of photoacclimation in the different phytoplankton groups will help to understand the differential niches of the groups, as well as improving our interpretation of commonly measured parameters such as Chlorophyll *a* (Chl *a*) concentrations. Estimating primary productivity in models also relies on the accurate parameterisation of photoacclimation (e.g. Behrenfeld *et al.*, 2002; Westberry *et al.*, 2008).

This study addresses a gap in current knowledge regarding light harvesting and photosynthetic strategies in coccolithophores other than *E. huxleyi*. The pigment contents, spectral absorption efficiencies, and photophysiology (as probed by variable fluorescence measurements, Kolber, Prášil and Falkowski, 1998) of 10 coccolithophores are examined (see Figure 1.6 and Table 1.1, Chapter 1), in response to three different growth irradiances. The species selected represent the four orders of the coccolithophores (Prymnesiophyceae), including five representatives from the Isochrysidales (*Reticulofenestra parvula*, *Gephyrocapsa muellerae, Gephyrocapsa oceanica,* a haploid (1N) and diploid (2N) *Emiliania huxleyi*), three from the Coccolithales (*Coccolithus braarudii, Calcidiscus leptoporus* and *Calcidiscus quadriperforatus*), one Syracosphaerale (a haploid *Syracosphaera pulchra*) and a Zygodiscale (*Helicosphaera carteri*). Results are compared to the diatom species *Thalassiosira weissflogii,* which is a small-celled coastal bloom species often used in ecophysiological studies of diatoms. The data provides novel insights into photoacclimation strategies in the coccolithophores, revealing both characteristics that are conserved amongst the coccolithophores and others that are different between species.

**Optical signatures for identifying phytoplankton groups**

Pigments are the molecules responsible for harvesting light energy for photosynthesis, and each have characteristic spectral absorption properties (Figure 2.1). Chl *a* is common to all oxygenic photosynthesisers, but phytoplankton also contain a range of accessory pigments, vastly more diverse than those found in terrestrial plants (Roy *et al.*, 2011). The diversity of accessory pigments in phytoplankton groups are thought to have evolved due to the red absorption peak of Chl *a* (Figure 2.1) becoming less effective with depth underwater (Falkowski and Raven, 2007). Accessory pigments compensate by absorbing light energy in different regions of the visible spectrum to Chl *a* (Figure 2.1), allowing phytoplankton to efficiently utilise the blue-green enriched underwater light field (Bidigare, Ondrusek, *et al.*, 1990; Hickman *et al.*, 2009).

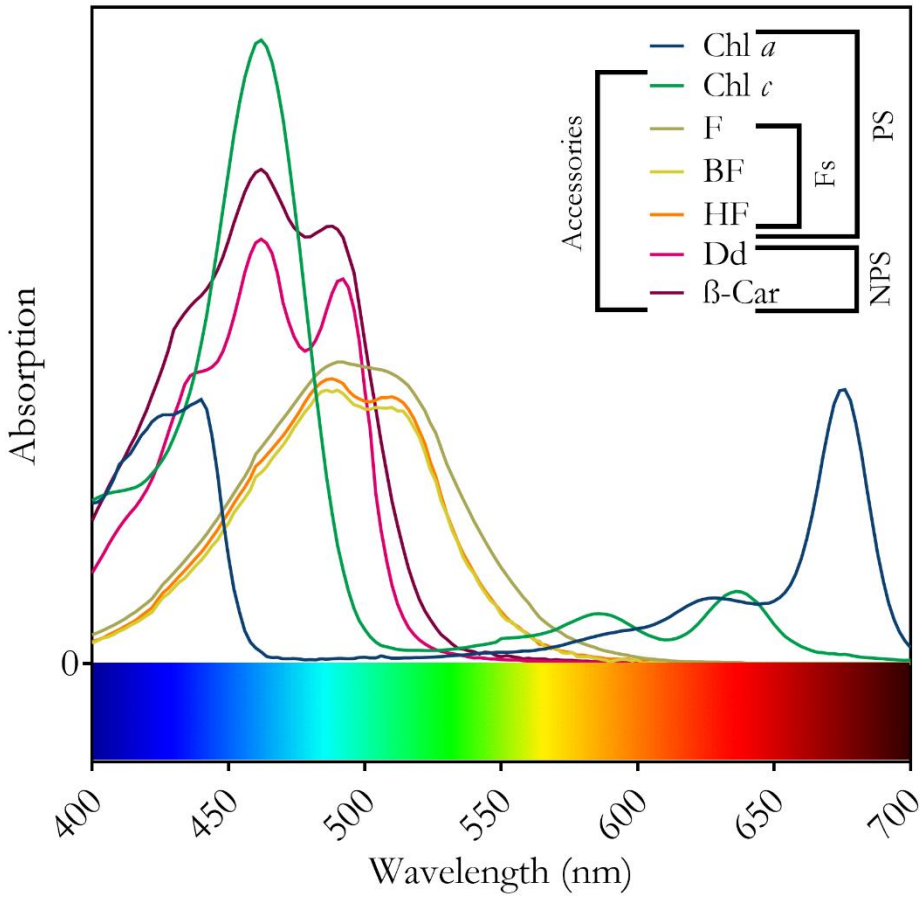


**Figure 2.1.** Shapes of absorption spectra of extracted pigments commonly found in coccolithophores and diatoms. Chl *a* = Chlorophyll *a*, Chl *c* = Chlorophyll *c1* / *c2*, F = Fucoxanthin, BF = 19'Butanoyloxyfucoxanthin, HF = 19'Hexanoyloxyfucoxanthin, Dd = Diadinoxanthin, β-Car = Beta carotene. Pigment groupings into Photosynthetic (PS), Non-photosynthetic (NPS), Fucoxanthin derivative (Fs) and Accessories are shown. Colour bar indicates approximate colour of light in different regions of the spectrum.

The type of pigments in a phytoplankton species are evolutionarily determined. For example, both coccolithophores and diatoms are descendants of the red-algal lineage, and as such, both contain similar accessory pigments: Chlorophyll *c*s (Chl *c*) and fucoxanthin derivatives (Fs). Pigments can thus be a key tool in assessing phytoplankton community composition (Jeffrey et al. 1997; Roy et al. 2011). One such widely used technique is CHEMTAX, in which a fucoxanthin derivative called 19-Hexanoyloxyfucoxanthin (HF) is used as a biomarker pigment for the haptophytes (Letelier *et al.*, 1993; Mackey *et al.*, 1996). However, the proportional contribution of HF to total pigment has been found to vary between different haptophyte species (e.g. between *E. huxleyi* and the *Pleurochrysis* and *Ochrosphaera* genera; Zapata *et al.*, 2004), between strains of the same species, (of *E. huxleyi*; Stolte *et al.*, 2000; Leonardos and Harris, 2006), and in response to growth irradiance (Schlüter *et al.*, 2000; Stolte *et al.*, 2000;

Seoane, Zapata and Orive, 2009; Lefebvre *et al.*, 2010; Garrido, Brunet and Rodríguez, 2016). This variability in proportional contribution of HF to total pigment renders quantification of haptophytes by chemotaxonomic methods particularly susceptible to error, as demonstrated by sensitivity analyses (Schlüter *et al.*, 2000). This study helps to address this issue by greatly increasing the number of coccolithophore species in which proportional pigment contributions under different irradiances are compared.

This study also examines the effect of different pigment proportions on the spectral absorption properties of coccolithophore cells. The binding of pigments to proteins within the cells 'tunes' the absorption wavelengths and the width of absorption bands (Croce and van Amerongen, 2014), meaning absorption of pigments in vivo is not the same as absorption by pigments in solution. Quantifying differences in shape of absorption spectra between cells with different proportional contributions of pigments with similar absorption properties (e.g. the Fs, Figure 2.1) can help to shed light on the functional differences between closely related pigments. New technologies are beginning to use templates of absorption properties of different phytoplankton cells to successfully identify phytoplankton groups (Bracher et al. 2008), including coccolithophore blooms (Sadeghi et al. 2012). Template spectra used in these studies for the coccolithophores are currently drawn from *E. huxleyi* alone. Therefore, spectral absorption properties of a range of coccolithophores will indicate whether such templates are representative of the coccolithophore group as a whole.

**Structure of the photosynthetic unit (PSU)**

In addition to pigments providing the means to identify phytoplankton in the field, the relative abundance of pigments provides valuable insight into the structure of the photosynthetic equipment within cells, as pigments form an integral part of the photosynthetic unit (PSU). PSUs are the basic building block of the photosynthetic machinery, embedded within the thylakoid membrane in the chloroplast (see Figure 1.3, Chapter 1). A PSU consists of protein bound Chl *a* and accessory pigments (Neilson and Durnford, 2010) arranged into light harvesting complexes. The light harvesting complexes funnel light energy to Chl *a* at the RC, where the energy 'closes' the reaction centre (RC), and photosynthetic electron transport begins (Falkowski and Raven, 2007). The PSU includes all the proteins and cellular equipment at the RC which are required for linear electron transport and oxygen evolution during the first stages of photosynthesis.

The structure of light harvesting complexes in higher plants is well studied and characterised (e.g. Liu *et al.*, 2004), but less is known about light harvesting complexes in phytoplankton (Neilson and Durnford, 2010), including the coccolithophores. Recent work is improving the

resolution of diatom thylakoids (e.g. Lepetit *et al.*, 2012), and such work is beginning to inform our understanding of thylakoid structure in *E. huxleyi*, in which similar genes coding for proteins in the diatom light harvesting complexes have been identified (McKew, Lefebvre, *et al.*, 2013). Light harvesting complexes of the diatoms are thought to bind a much higher ratio of accessory pigments to Chl *a* than higher plants(4 : 14 in higher plants light harvesting complex II; Liu *et al.*, 2004, compared to 4 : 4 in the diatom fucoxanthin-chlorophyll protein complex; Papagiannakis *et al.*, 2005; Premvardhan *et al.*, 2010). Whilst little has been explicitly resolved regarding the structure of light harvesting complexes in *E. huxleyi*, the typically high quota of accessory pigments (including the marker pigment HF, other Fs and Chl *c*s, Van Lenning et al. 2004; Roy et al. 2011), has led to the suggestion that *E. huxleyi* could have an even higher accessory binding ratio than the diatoms. Quantification of pigment ratios in a range of coccolithophore species will help to determine whether the high accessory binding ratios proposed for *E. huxleyi* are common to the coccolithophores as a group, or unique to *E. huxleyi* alone.

Elucidation of the pigment binding ratios within PSUs provides insights into the functional differences between the photosynthetic equipment in different phytoplankton. Differences in energy transfer efficiency between the various pigments means that differences in pigment composition not only causes changes in the amount and colour of light absorbed, but also in the energy transfer dynamics within light harvesting antenna. For example, some accessory pigments (e.g. carotenoids) may have reduced photosynthetic energy transfer efficiencies in comparison to the chlorophylls (Croce and van Amerongen, 2014) and can have enhanced energy dissipation capacities (Sandmann, Kuhn and Böger, 1993; Polívka and Frank, 2010; Blankenship, 2014) offering protection from the damage caused by an excess of absorbed light energy. Indeed, some carotenoids, such as β-carotene and the xanthophyll cycle pigments are not considered photosynthetic at all, as their primary function is safe dissipation of absorbed energy (see Figure 1.3, Chapter 1). Therefore, proportional abundance of different pigment types within the light harvesting complexes can be crucial for the optimal functioning of the photosynthetic machinery under different light conditions (Croce and van Amerongen, 2014).

The number and arrangement of pigment molecules associated with each PSU has important implications for photophysiology. PSU size (the number of pigments serving each RC) influences the absorption cross-section of photochemistry (σ, see section 1.1.3, Chapter 1). For example, a large PSU with many associated pigments may have a higher σ, as the probability of photons being absorbed is higher. However, at any given time the RC of a large PSU is more likely to be in the closed state than the RC of a small PSU (Wientjes, Van Amerongen and Croce, 2013; Croce and van Amerongen, 2014). Large PSUs can thus have

lower photosynthetic efficiency, and carry a higher risk of suffering photodamage. Absorption cross-section of PSII photochemistry ($\sigma_{PSII}$) and the maximum quantum yield of PSII ($F_v/F_m$) can be obtained using variable fluorescence techniques, such as Fast Repetition Rate fluorometry (FRRf; Kolber, Prášil and Falkowski, 1998). In this study, these photophysiology parameters are integrated with pigment and absorption data, in order to increase our understanding of the structure and functioning of photosynthetic light harvesting in the coccolithophores.

**Photoacclimation**

Photoacclimation can be complex (see also section 1.1.4, Chapter 1), but acclimation to low light usually involves increasing the light absorption capacity of the cell by increasing pigment concentrations. Photoacclimation can be classified into two general strategies (Figure 2.2) relating to how extra pigment is incorporated into the photosynthetic equipment, either involving increasing the number of PSUs (i.e. number of RCs, here termed 'n' type), or involving a change in the size of PSUs (or absorption cross-section of photochemistry, here termed 'σ' type) (Moore *et al.*, 2006; Suggett *et al.*, 2007). For example, in acclimation to low irradiance, an n-strategy would involve increasing the number of RCs and their corresponding pigment antennas, whilst a σ-strategy would involve increasing the size of the antenna bed delivering excitation energy to each RC, increasing the absorption cross-section (σ) of photochemistry (Figure 2.2). Acclimation by n-strategy can be considered expensive, as the protein-rich RCs are costly to produce and maintain, whilst acclimation by σ-strategy is considered cheaper, as the pigment-rich antennas are less costly (Croce and van Amerongen, 2014). These differences in costs (in terms of nutrient resources) mean that nutrient availability is likely to be an important factor affecting the acclimation strategy adopted by a cell, and that n-strategy acclimation may be less favourable under nutrient limited conditions. Drawbacks of σ-strategy acclimation (large PSUs) include a potential decrease in quantum efficiency and higher vulnerability to over-excitation and photodamage. In reality, a common photoacclimation strategy in phytoplankton involves a mix of 'n' and 'σ' strategies, with big changes in 'n' coupled with smaller changes in 'σ' (e.g. Dubinsky et al. 1986, Moore et al. 2006). Quantitative data on photoacclimation to different irradiances in the coccolithophores is limited to *E. huxleyi*, and has identified differences in strategy even within different strains of this species (Harris, Scanlan and Geider, 2005; Suggett *et al.*, 2007). In acclimation to low irradiance, one *E. huxleyi* strain (PML-B11) was found to acclimate using 'n' and 'σ' strategies to a similar extent (increasing both the size and number of PSUs), whilst another strain (PML-B92A) preferentially used 'σ' strategy (increasing the size of PSUs over increasing the number). There is, therefore, good reason to suspect that the diversity of photoacclimation strategies

between different coccolithophore species (or strains) could be high, and warrants further exploration.

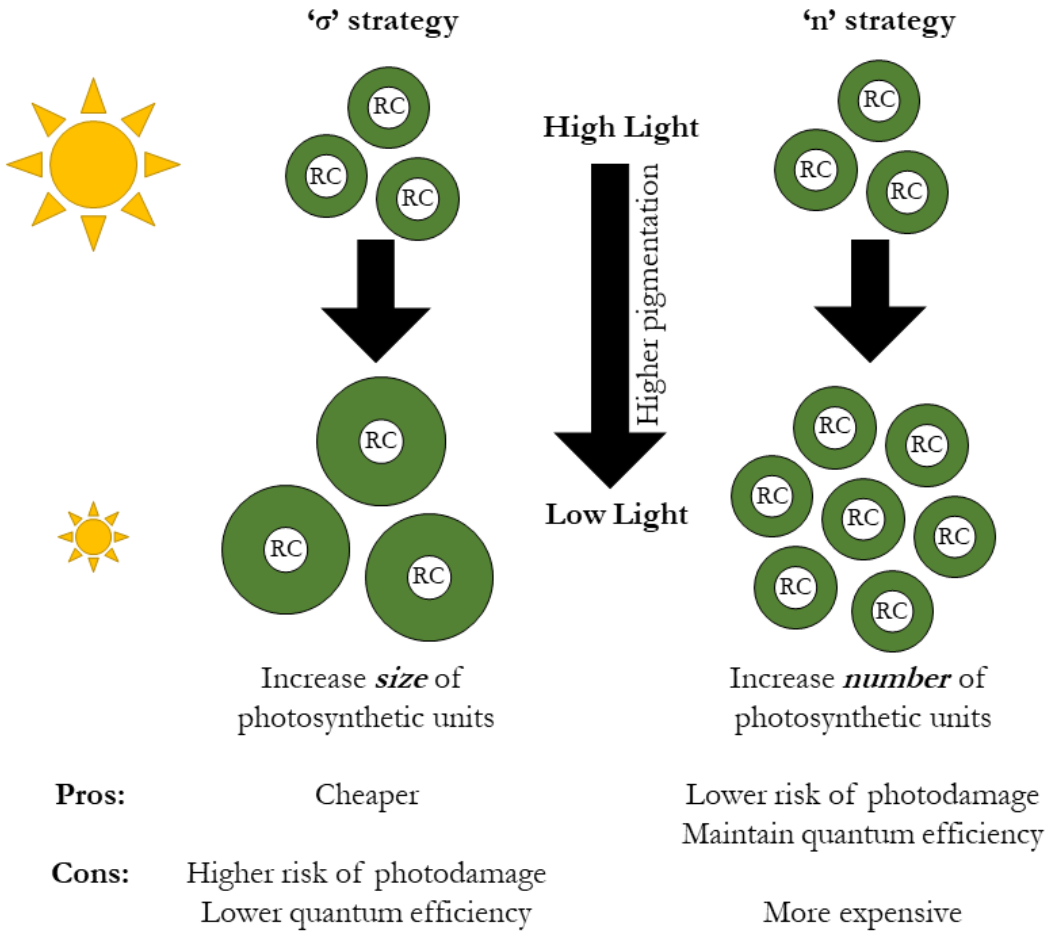


**Figure 2.2.** Schematic summarising two contrasting strategies for photoacclimation to low light: 'σ' and 'n' type. Both involve an increase in pigment content. The σ strategy incorporates this extra pigment by increasing the size of PSUs (an increase in the amount of pigment around each RC), whilst the n strategy increases the number of PSUs (an increase in the number of RCs, without changing the amount of pigment around each).

**Aims**

The aim of this work is to quantify pigment content, absorption properties, and photophysiology of PSII amongst 10 coccolithophores (see Figure 1.6 and Table 1.1, Chapter 1). Specifically, this study aims to use these physiological measurements to:

1) **Identify similarities and/or differences between coccolithophore species (contextualised by comparison to a diatom species, *Thalassiosira weissflogii*).**

2) **Quantify how these species acclimate to different growth irradiances.**

The physiological parameters measured are interdependent (Figure 2.3). The types and relative proportions of pigments in the cell influences the shape of the absorption efficiency spectra, whilst the size of PSII (i.e. the amount of pigment around PSII) influences the absorption cross-section of PSII photochemistry ($\sigma_{PSII}$). Therefore, measurements of pigment, light absorption and variable fluorescence measurements can be integrated (Suggett, MacIntyre and Geider, 2004) to shed light on the acclimation strategies employed by the coccolithophores.

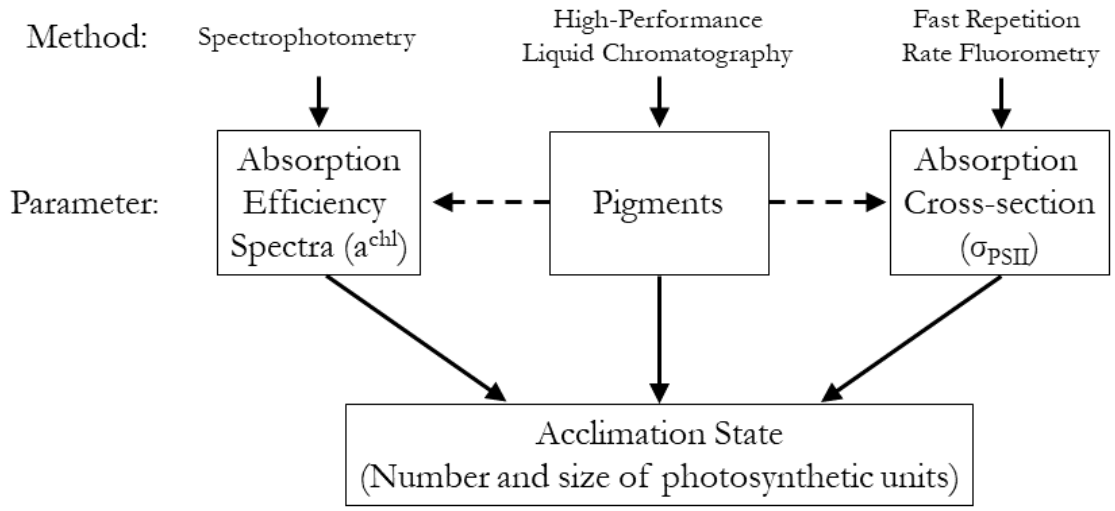


**Figure 2.3.** Schematic showing the methods used in this study, the parameters measured, and how the data interelate to provide information on photoacclimation strategy.

## 2.2 Methods

### 2.2.1 Experiment Overview

Monoclonal cultures of 10 species of coccolithophore (Table 1.1, Chapter 1) were obtained from the Roscoff Culture Collection (RCC), Station Biologique de Roscoff, along with a diatom (*Thalassiosira weissflogii*). Each strain was grown in duplicate batch culture at three light levels (25, 100 and 200 μmol photons $m^{-2}$ $s^{-1}$). When in exponential growth phase, cultures were sampled for pigment content, spectral absorption properties, and variable fluorescence measurements.

### 2.2.2 Culturing

Coccolithophore cultures were grown in 0.2 μm sterile-filtered K/10 culture media. Seawater collected from the Celtic Sea during the Shelf Seas Biogeochemistry cruise in August 2014 was aged in the dark for > 12 months, filtered and enriched with nutrients, vitamin and trace metals, following a method modified from (Keller *et al.*, 2007). The diatom *T. weissflogii* was grown in identical media with additional silica enrichment (1 mL of 0.33 mM sodium metasilicate solution $L^{-1}$). All cultures were grown at 17 °C in dilute batch culture in ventilated flasks, in incubators fitted with LED panels providing light of known spectral quality on a 14:10 Light:Dark cycle. Three different average irradiance environments were created by covering LED panels with 0.15, 0.3 and 0.6 neutral density filters (Lee Filters™, Andover, Hampshire,UK). Average irradiances were 25, 100, and 200 μmol photons $m^2$ $s^{-1}$ as measured by a Biospherical light sensor (Biospherical Instruments, QSL-2101) placed in the culture vessel filled with media. Growth irradiances equated to daily photon fluxes of 1.25, 5.0 and 10.0 mol photons $m^{-2}$ $d^{-1}$ respectively, and are hereafter referred to as low light (LL), medium light (ML) and high light (HL) treatments. Cultures were acclimated to each experimental condition for approximately 10 generations before commencing experiments. The 33 culture experiments (11 species each under three irradiance levels) were each conducted in duplicate. Culture work on each species was carried out sequentially between February and May 2016, with the three light treatments for a given species run in parallel.

Each experiment followed a batch culture procedure. To initiate each experiment, duplicate flasks of 485 mL of K/10 culture media were spiked with equal quantities of acclimated cells such that the initial cell concentration was approx. 300 cells $mL^{-1}$. During experiments, cultures were manually agitated once per day. Cell density was determined daily, or every other day, in triplicate either using a Sedgwick rafter cell (Langer *et al.*, 2006) for large

coccolithophores (*C. braarudii, C. quadriperforatus, C. leptoporus, S. pulchra* and *H. carteri*) or a Multisizer™3 Coulter Counter® (Langer *et al.*, 2009) for small coccolithophores (*E. huxleyi, G. oceanica, G. muellerae, R .parvula*) and the diatom (*T. weissflogii*). Motile species (*H. carteri* and *S. pulchra*) were immobilised by adding 40 µL of 10 % formaldehyde solution $mL^{-1}$ of culture before counting, with correction for the volume difference. Exponential growth rate (µ) was calculated using GraphPad Prism 6.03 software from exponential regressions (Langer *et al.*, 2006). Cultures were harvested for subsequent analyses in mid-exponential growth phase, well before approaching maximal cell densities (as determined by preliminary growth experiments), to avoid nutrient limitation or biological effects on the carbonate system (Langer *et al.*, 2009; Hoffmann *et al.*, 2015). Exponential growth was not achieved by *C. braarudii* or *H. carteri* under the HL treatment, so these experiments were excluded from subsequent analysis. For each species, harvesting of cells was done before 12.00 h midday (local time), and involved preservation of filtered samples for cell volume, light absorption and pigment analysis. Remaining cell culture was placed back into the incubator until variable fluorescence analysis between 14.00 and 17.00 h.

### 2.2.3 Cell volume

Cell volumes were calculated using biometric measurements made on samples collected on cellulose nitrate filter (0.8 µm) and prepared following Poulton *et al.,* (2010) and Sheward *et al.,* (2017). Cross polarized light microscopy and CellD software supported by Olympus (Gibbs *et al.*, 2013) was used to measure internal cell diameter of at least 50 cells per sample, except haploid *E. huxleyi* for which cell diameter was approximated from Multisizer™3 Coulter Counter. Estimates of cell volumes were calculated assuming all species were spherical except *H. carteri* and *T. weissflogii* which were assumed to be cylindrical, and *S. pulchra* which was assumed to be a 'cone + half sphere' shape (shapes were approximated in a similar way to the volume calculations of Sun and Liu, 2003).

### 2.2.4 Pigment analysis

Duplicate 120 mL samples for HPLC analysis were filtered onto Whatman GF/F filters, frozen immediately and stored at - 80 °C until analysis. Pigments were extracted and analysed following Steele *et al.*, (2015). Briefly, pigments were extracted by soaking filters in 5 mL chilled 90 % acetone and sonicated (Sonics Vibracell probe, 35 s 40 W) under low light (total extraction time = 1 h). Centrifugation (Centaur 2, 4000 rpm, 5 min) and filtration (0.2 µm, 17 mm Teflon syringe filters, DHI, Denmark) were used to clarify extracts. Samples were maintained at 4 °C in the dark in the autosampler and were analysed within 24 h of extraction.

Extracts were analysed on an Accela HPLC instrument (ThermoScientific, UK), comprising an Accela quarternary pump, thermostated autosampler, thermostated column compartment and photodiode array detector using a method and mobile phase based on Zapata *et al.*, (2000). A Waters C8 Symmetry column (150 × 2.1 mm; 3.5 μm particle size) was used at a flow rate of 200 μL $min^{-1}$. Quality assurance protocols described in Steele *et al.*, (2015) were adhered to for pigment analysis. These included daily analysis of a mixed pigment standard (DHI, Denmark) to check resolution of pigment critical pairs and consistency of retention times, and triplicate injections of Chl *a* standard to check response factors. Multipoint calibration of response factors for 19 pigments is performed annually on the system using pigment standards (DHI, Denmark). Pigments identified are listed in Table 2.1, along with their properties and classification. Trace amounts of what is thought to be gyroxanthin-dodecanoate-ethanoate (Gd) and magnesium-2,4-divinylpheoporphyrin-$a_5$-monomethyl-ester (MgDVP) were identified in some species (R. Airs, pers. comm.). These two pigments together contributed < 1 % of total pigment and are grouped as 'other' in the subsequent discussion. Pigment ratios are expressed as molar ratios.

Pigment concentrations measured in the culture samples were corrected to pigment densities within the cell, in units of fg $\mu m^{-3}$, as pigment abundances are commonly reported in terms of mass, as follows:

$$\text{Pigment density } (\text{fg } \mu m^{-3}) = \frac{\text{Pigment concentration in culture } (\text{fg } L^{-1})}{\text{Cell number (cells } L^{-1}) \times \text{Cell Volume } (\mu m^3 \text{ cell}^{-1})} \quad (2.1)$$

**Table 2.1.** Properties of pigments identified in HPLC analysis.

RAM = Relative atomic mass.

| Pigment | Abbrev. | Approx. Retention Time (min) | Response Factor x$10^{-6}$ | Molecular Formula | RAM | Classification |
|---|---|---|---|---|---|---|
| Chlorophyll $c_3$ | Chl $c_3$ | 7.51 | 4.45 | $C_{36}H_{28}N_4O_7Mg$ | 652.94 | PS Accessory |
| magnesium-2,4-divinylpheoporphyrin-$a_5$-monomethyl-ester | 'Other' | 10.38 | 2.86 | $C_{35}H_{30}N_4O_5Mg$ | 610.94 | PS Accessory |
| Chlorophyll $c_2$ | Chl $c_2$ | 11.03 | 2.86 | $C_{35}H_{28}N_4O_5Mg$ | 608.93 | PS Accessory |
| Chlorophyll $c_1$ | Chl $c_1$ | 11.70 | 2.86 | $C_{35}H_{30}N_4O_5Mg$ | 610.94 | PS Accessory |
| 19'Butanoyloxy-fucoxanthin | BF | 17.28 | 4.77 | $C_{46}H_{64}O_8$ | 745.00 | PS Accessory, Fucoxanthin derivative |
| Fucoxanthin | F | 18.18 | 4.96 | $C_{42}H_{58}O_6$ | 658.91 | PS Accessory, Fucoxanthin derivative |
| 19'Hexanoyloxy-4-ketofucoxanthin | HKF | 20.29 | 4.89 | $C_{48}H_{66}O_9$ | 787.03 | PS Accessory, Fucoxanthin derivative |
| 19'Hexanoyloxy-fucoxanthin | HF | 21.05 | 4.89 | $C_{48}H_{68}O_8$ | 773.05 | PS Accessory, Fucoxanthin derivative |
| Diadinoxanthin | Dd | 23.19 | 3.49 | $C_{40}H_{54}O_3$ | 582.85 | NPS Accessory |
| Diatoxanthin | Dt | 26.54 | 3.77 | $C_{40}H_{54}O_2$ | 566.86 | NPS Accessory |
| Gyroxanthin dodecanoate ethanoate | 'Other' | 28.73 | 3.49 | $C_{54}H_{78}O_7$ | 839.19 | PS Accessory |
| Chlorophyll $c_2$-monogalactosyl-diacylglyceride-ester | Chl $c_2$-M | 32.81 | 3.01 | $C_{76}H_{96}N_4O_{14}Mg$ | 1313.9 | PS Accessory |
| Chlorophyll *a* | Chl *a* | 33.59 | 11.29 | $C_{55}H_{72}N_4O_5Mg$ | 893.49 | PS Chl *a* |
| β-carotene | β-car | 36.58 | 3.98 | $C_{40}H_{56}$ | 536.87 | NPS Accessory |

### 2.2.5 Chlorophyll a specific light absorption coefficient ($a^{chl}$)

The chlorophyll *a* specific absorption coefficient of phytoplankton ($a^{chl}$) was measured using the filter pad technique (Tassan and Ferrari, 1995a; Bouman *et al.*, 2003), using a Shimadzu UV-2550 UV-VIS dual beam spectrophotometer fitted with an ISR-240A Integrating Sphere Attachment. Duplicate culture samples were filtered onto 25 mm diameter Whatman GF/F filters, rapidly protected from ambient light and stored at -80 °C. Analysis was carried out under low light conditions. Frozen filters were defrosted for 3-6 minutes with 5 drops of sterile filtered K/10 media. Absorbance spectra (spectral resolution = 1 nm) were normalised by subtracting the absorbance spectra of a blank filter moistened with K/10 culture media. Negligible absorption by detritus in samples was confirmed by no significant differences being found between several bleached samples (oxidation with 5 drops of 1.5 % NaClO solution, following Ferrari & Tassan, 1999) and blank filters. Absorbance ($OD_{phy}$) at wavelength ($\lambda$) was transformed into an absorption coefficient of phytoplankton following Bouman et al. (2003) using S, the clearance area of the filter ($m^2$), V, the volume of culture filtered ($m^3$) and a wavelength dependent correction factor $\beta(\lambda)$ to account for the increase in path-length due to multiple internal scattering from Bricaud & Stramski (1990). Spectra were normalised to corresponding Chl *a* concentrations [Chl *a*] (mg $L^{-1}$) as measured by HPLC, to produce a Chl *a* specific absorption coefficient, $a^{chl}$ ($m^2$ $g^{-1}$ Chl *a*) at wavelength $\lambda$:

$$a^{chl}(\lambda) = \frac{2.303 \times S \times OD_{phy}(\lambda)}{\beta(\lambda) \times V \times [\text{Chl } a]} \qquad (2.2)$$

Reference weight-specific absorption coefficient spectra (a*) from Bricaud et al. (2004) and densities (C) of the constituent pigments (i) were used to reconstruct absorption spectra, again normalised to corresponding Chl *a* concentrations, $a_{sol}^{chl}$ ($m^2$ $g^{-1}$ Chl *a*) (Equation 2.3). Such a reconstruction is dependent on the assumption that the absorption spectra of all the chlorophyll *c*'s and 19'Hexanoyloxy-4-ketofucoxanthin are well represented by the spectra of Chl *c*1,*c*2 and 19'Hexanoyloxyfucoxanthin, respectively.

$$a_{sol}^{chl}(\lambda) = \frac{\sum C_i \times a_i^*}{[\text{Chl } a]} \qquad (2.3)$$

### 2.2.6 Single turnover variable fluorescence measurements

Variable fluorescence parameters were measured using Fast Repetition Rate Fluorometry (FRRf). Single turnover measurements were made and processed using an Act2 system and Act2Run software (Chelsea Technologies Group Ltd, UK). Duplicate 5 mL samples were dark adapted for 30 min prior to analysis. During a single turnover measurement, a blue LED (450

nm) rapidly delivered a chain of saturating flashes (100 x 1 μs flashlets on a 2 μs pitch) which rapidly closed the majority of RCIIs (over ~200 μs). Act2Run software then fitted an induction curve to the resulting fluorescence transient using the Kolber-Falkowski-Prasil model (Kolber, Prášil and Falkowski, 1998). An example fluorescence transient for *E. huxleyi* (2N) is shown in Figure 2.4; fluorescence rises from initial minimum fluorescence ($F_o$) to maximum fluorescence ($F_m$) during the saturation phase, and the slope of the initial increase is used to calculate $\sigma_{PSII}$, the absorption cross section of PSII photochemistry (nm$^2$ PSII$^{-1}$). Variable fluorescence ($F_v$) is the difference between $F_o$ and $F_m$, and the maximum quantum yield of PSII is described by $F_v/F_m$. Optimisation protocols described in Oxborough (2015) were followed. Signal to noise ratio of the fluorescence was optimised by using the auto PMT function, which adjusts the voltage of the analogue output. The $R\sigma_{PSII}$ parameter (indicating the speed of saturation) and was optimised to a value ~ 0.04-0.06 by adjusting the LED flashlet intensity.

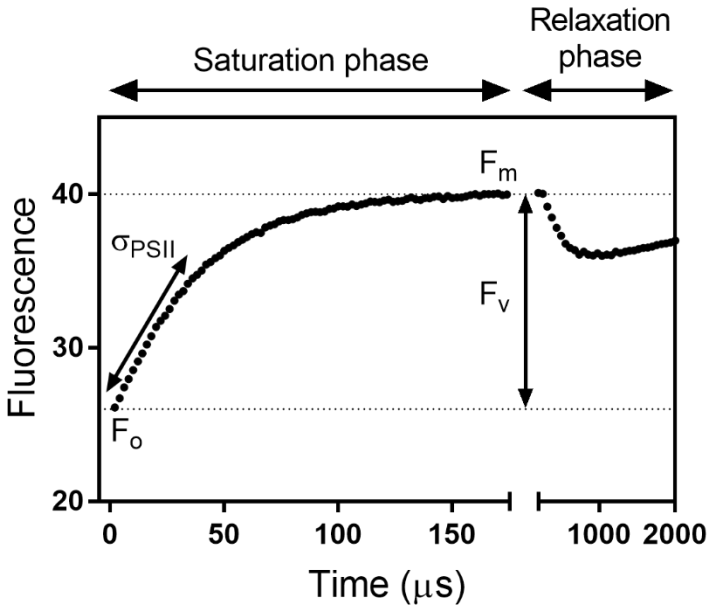


**Figure 2.4.** An example of a single turnover fluorescence induction curve of *E. huxleyi* 1N grown under LL (25 μmol photons m$^{-2}$ s$^{-1}$) as measured by Fast Repetition Rate fluorometry (FRRf).

### 2.2.7 Estimation of PSU density and PSU size

A method was used to derive PSU density and PSU size, expressed as number of PSII reaction centres (RCII) μm$^{-3}$ and mol Chl *a* (mol RCII)$^{-1}$ respectively (Suggett, MacIntyre and Geider, 2004). Briefly, the method corrects the Chl *a* specific absorption coefficient ($a^{chl}$) to account for the proportion of absorbed LED flashlet light that contributes to the excitation of RCIIs, resulting in a Chl *a* specific absorption coefficient for PSII ($a_{PSII}^{chl}$, m$^2$ g$^{-1}$ Chl *a*). It was

assumed that only light absorbed by photosynthetic pigments contributes to PSII excitation (Suggett, MacIntyre and Geider, 2004). All absorbed light was assumed to be divided equally between PSI and PSII following the findings that the proportion of light absorbed by PSII was 0.55-0.56 in *E. huxleyi* and 0.51-0.52 in *T. weissflogii* (Suggett, MacIntyre and Geider, 2004). Absorption was also spectrally corrected for the emission spectrum of the blue LEDs in the Act2 system. PSU size, conventionally expressed as moles of Chl *a* $RCII^{-1}$ , was then estimated:

$$\text{PSU size} = \frac{\sigma_{PSII}}{a_{PSII}^{chl}} \tag{2.4}$$

The density of PSU within the cell (PSU $\mu m^{-3}$) is then calculated by dividing Chl *a* density (mol Chl *a* $\mu m^{-3}$) by PSU size:

$$\text{PSU density} = \frac{[\text{Chl } a]}{\text{PSU size}} \tag{2.5}$$

Total PSU size (mols of total pigment $RCII^{-1}$) is then calculated by multiplying chlorophyll specific PSU size by the ratio of total pigment to Chl *a*:

$$\text{Total PSU size} = \text{PSU size} \times \frac{[\text{Total Pigment}]}{[\text{Chl } a]} \tag{2.6}$$

### 2.2.8 Statistical tests

Within species, one-way ANOVA tests were used to assess whether parameters were significantly different between the three light levels, using GraphPad Prism (v 7.04, GraphPad Software Inc.). When significant differences were identified (at the 95 % significance level, $p < 0.05$), subsequent Tukey's tests were performed to identify significantly different data groupings. For species in which data was only available for two light levels, a simple unpaired t-test (at the 95 % significance level, $p < 0.05$) was used to compare parameters between the two light levels.

## 2.3 Results

### 2.3.1 Pigments

Pigment profiles between species under the LL treatment are first compared as an example (Figure 2.5) to highlight the key interspecies similarities and differences. Changes in pigment abundance with growth irradiance are then presented (Figures 2.6 & 2.7).

Analysis of pigment content by HPLC showed a similar suite of pigments in all the coccolithophore species examined. Figure 2.5 shows pigment composition as percentage of total pigment (TP) by weight, across the different species, when grown under LL (25 μmol photons $m^{-1}$ $s^{-1}$). The most abundant chlorophyll pigment in all coccolithophore species was Chl *a*, ranging from 34.5 % of TP in *E. huxleyi* 2N to 42.9 % of TP in *H. carteri*. Chl *a* contributed a higher percentage of TP in the diatom *T. weissflogii* (64.4 %) than in any of the coccolithophores (Figure 2.5). The much higher Chl *a* content in the diatom results in ratios of Chl *a* to the other pigments being consistently much lower in the coccolithophores compared to the diatom. Substantial amounts of chlorophyll c's were also present in the coccolithophores, mainly chlorophyll *c*2, chlorophyll *c*3 and chlorophyll *c*2-MGDG1 (Figure 2.5). Together, the Chl *c*'s totalled between 15.3 % in *C. leptoporus* and 23.9 % in *E. huxleyi* 2N. In contrast, the diatom *T. weissflogii* had a much smaller pool of Chl *c*'s (5.6 % of TP, Figure 2.5) which was dominated by chlorophyll *c*1.

A large pool of fucoxanthin derived pigments (Fs) was present in all coccolithophore species, including Fucoxanthin (F), 19'Hexanoyloxyfucoxanthin (HF), 19'Hexanoyloxy-4-ketofucoxanthin (HKF) and 19'Butanoyloxyfucoxanthin (BF) (Figure 2.5). Together the sum of the fucoxanthin derivative pool (ΣFs) comprised just over a third of total pigment in the coccolithophores (34.7 % to 38.8 %), however, the abundances of the different pigments within the Fs pool varied considerably. Commonly used as a biomarker pigment for haptophytes, HF was present in all the coccolithophores examined, yet varied widely in abundance between species, from 0.5 % of total pigment in *C. braarudii* to 38.4 % of TP content in *C. quadriperforatus* (Figure 2.5). Coccolithophore species with low abundances of HF had higher abundances of F, in what seems to be an inverse relationship ($r^2 = 0.97$, $p < 0.0001$, $n = 27$). For example, *C. braarudii* had a very low HF content of just 0.5 % whilst F comprised 33.0 % of its total pigment content (Figure 2.5). The dominance of either HF or F in the fucoxanthin derivative pool did not appear to be driven by taxonomy (i.e. evolutionary relatedness), as there were marked differences between species within the same genus, for example the *Gephyrocapsa* species (Figure 2.5). In *G. oceanica,* the major fucoxanthin derivative

pigment under low light was F (F = 62.2 % and HF = 21.5 %), whilst in *G. muellerae* HF was more abundant (F = 3.3 % and HF = 95.1 %). When present, HKF and BF were low in abundance, with HKF < 5.8 % of total pigment content and BF < 1.5 % of total pigment (Figure 2.5). The diatom *T. weissflogii* did not contain any HF, BF or HKF, but did have a substantial quantity of F (23.8 % of TP).

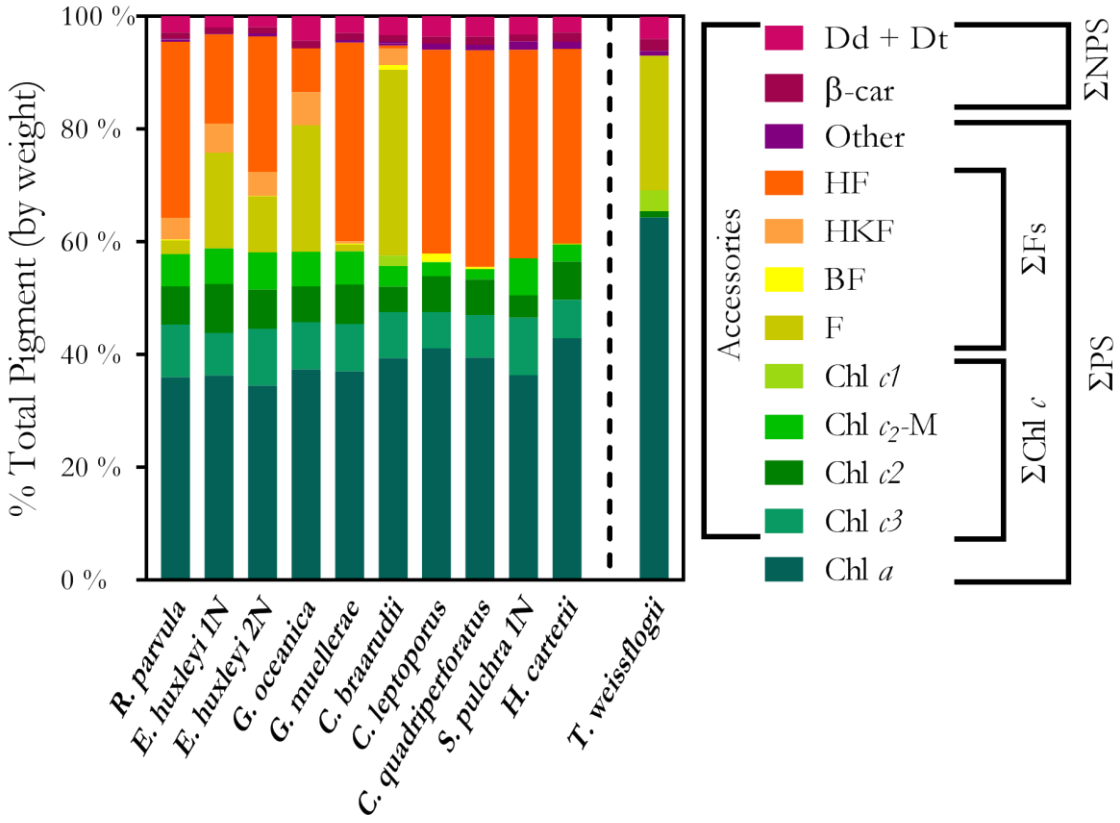


**Figure 2.5.** Percentage of total pigment (by weight) across 10 coccolithophore species, and a diatom, grown under low irradiance (25 µmol photons $m^{-2}$ $s^{-1}$). Classification of pigments into groups is also indicated; PS = photosynthetic, NPS = Non-photosynthetic, Fs = Fucoxanthin derived carotenoids, Chl *c* = Chlorophyll *c* pigments. All pigments except Chl *a* are considered accessory

Within each species, the suite of pigments identified were constant regardless of ambient irradiance. However, the overall concentrations and relative contributions of these pigments did change. All species showed evidence of photoacclimation of their pigment content, but the extent of photoacclimation differed between species. Total pigment density within the cell was significantly higher under LL in all species (Figure 2.6a, one-way ANOVA, $p < 0.05$). At the lowest irradiance, pigment density was on average 2.17 times greater than that at the highest irradiance. The extent of photoacclimation of PS pigments varied between species, with the pigment density under LL ranging from 1.37 (*S. pulchra*) to 3.37 (*C. leptoporus*) times

greater than respective HL pigment densities (Figure 2.6a). The diatom *T. weissflogii* also had higher PS pigment density under LL (Figure 2.6a).

Non-photosynthetic pigments (NPS, including β-carotene, diadinoxanthin and diatoxanthin) were a minority, ranging from 3.0 % to 15.8 % of the total pigment pool (Figure 2.6b). The relative contribution of the NPS pigments to the total pigment pool was significantly greater under HL in all the coccolithophore species and the diatom (Figure 2.6b, one-way ANOVA, $p < 0.05$). For example, in *C. quadriperforatus* NPS pigments accounted for 5.0 % of total pigment under low irradiance but trebled to 15.8 % under high irradiance.

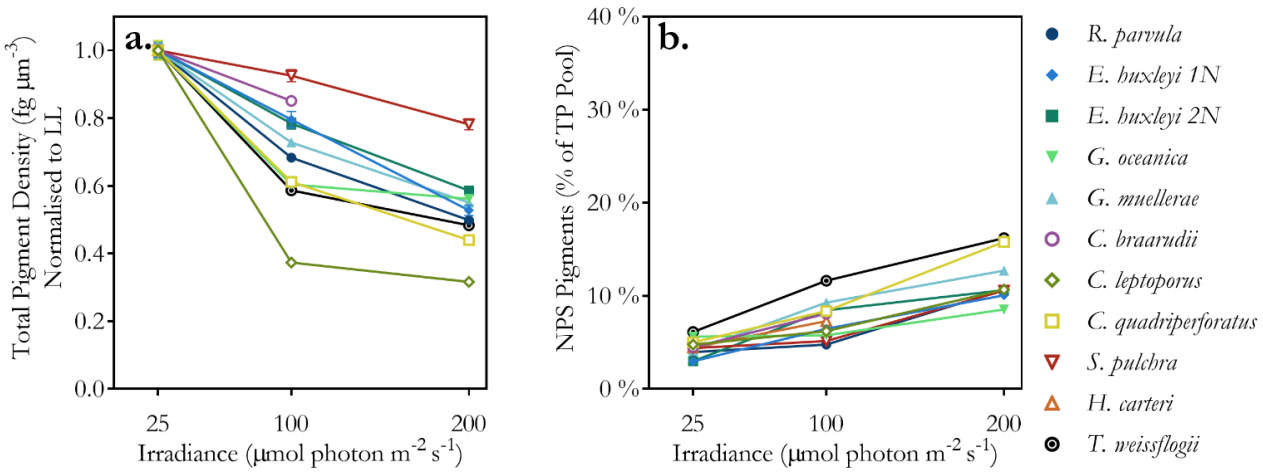


**Figure 2.6.** Changes in pigment composition plotted against growth irradiance in 10 coccolithophore species and a diatom (see key on right for species identities). a) Total pigment density, normalised to LL. b) Non-photosynthetic pigments as a % weight of total pigment pool.

Photoacclimation involved concurrent regulation of both Chl *a* and the photosynthetic accessory pigments, as shown by assessment of Chl *a* to pigment ratios (Figure 2.7). Key differences between the coccolithophores and the diatom were revealed. The ratio of Chl *a* to total photosynthetic accessory pigments (Chl *a* : ΣPS) was < 1 in all coccolithophore species, under all irradiances, meaning photosynthetic accessory pigments outweighed Chl *a* (Figure 2.7a). In the diatom *T. weissflogii,* on the other hand Chl *a*. dominated the PS pigment pool: the Chl *a* : ΣPS ratio was > 2, under all irradiances examined, higher than in all the coccolithophores. Within each species there were small changes (< 10 %) in the Chl *a* : ΣPS with growth irradiance, but no consistent increase or decrease with irradiance was observed (Figure 2.7a). The photosynthetic accessory pigments are comprised of Chl *c*s and Fs, and the ratios Chl *a* : ΣChl *c* and Chl *a* : ΣFs were both lower in the coccolithophore species than in the diatom (Figure 2.7b & c). High proportions of both Chl *c* and fucoxanthin derivatives,

therefore, contributed to the low Chl *a* : ΣPS in all species of coccolithophore examined. Within each species, Chl *a* : ΣChl *c* ratios were significantly higher under the highest growth irradiance (Figure 2.7b, one-way ANOVAs, $p < 0.05$), but the differences between light levels were < 20 %. No consistent increase or decrease in Chl *a* : ΣFs with irradiance was observed (Figure 2.7c).

In some species, the proportional composition of the Fs pool, most notably proportions of F and HF, varied with irradiance (Figure 2.7d). In *G. oceanica, G. muellerae, C. braarudii,* and both *E. huxleyi* 1N and 2N, the Fs pool became more dominated by HF under higher irradiance (Figure 2.7d). For example, in *E. huxleyi* 2N, HF comprised 60.1 % of the Fs pool at LL, rising to 86.3 % of the Fs pool at HL. In the other species, the fucoxanthin-derived pigment pool was almost completely dominated by HF (> 95 %) under all irradiances (Figure 2.7d).

Despite differences in the contribution of the Fs to the total pool between species and between irradiance levels, the ratio of ΣFs : Chl *a* was strikingly constant at around 1 (± 0.08) : 1 in all coccolithophore species, at all irradiance levels. Whether the Fs pool was mainly HF, or made up of a mixture of HF, F and other pigments, it consistently comprised around a third of TP in the coccolithophores (31.5 % to 41.4 %). In contrast, the Fs made a smaller contribution (22.9 % to 28.4 % of TP) in the diatom *T. weissflogii*.

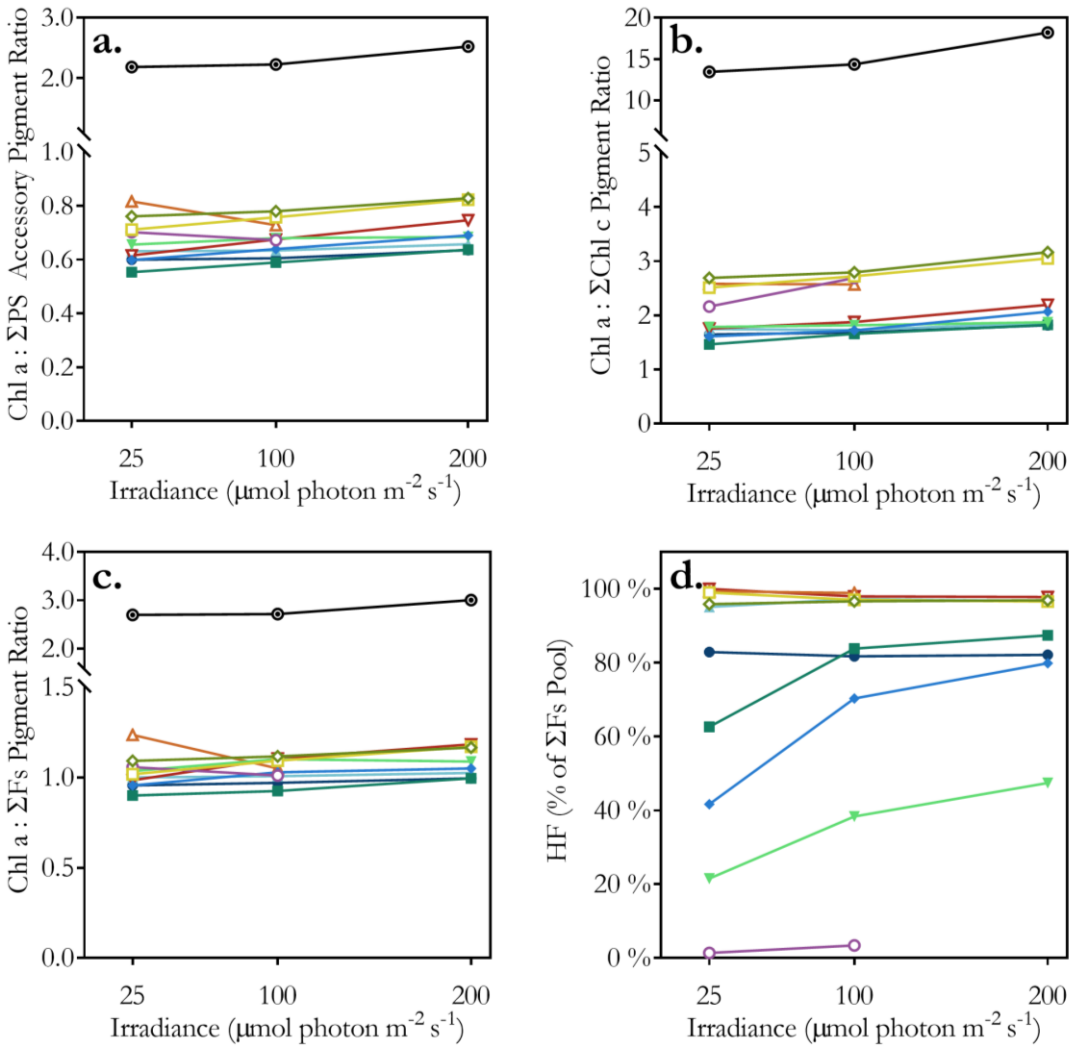


**Figure 2.7.** Changes in molar pigment ratios plotted against growth irradiance in 10 coccolithophore species and a diatom. a) Ratio of Chlorophyll *a* : Sum of photosynthetic accessory pigment. b) Ratio of Chlorophyll *a* : Sum Chlorophyll *c* pigments. c) Ratio of Chlorophyll *a* : Sum of fucoxanthin derivatives. d) HF as a % of fucoxanthin derivative pigments. Colours and symbols correspond to the different species, as in Figure 2.6.

### 2.3.2 Chlorophyll *a*-specific absorption efficiency spectra

The shapes and magnitudes of absorption efficiency spectra are first compared between species under the LL treatment, to highlight the key interspecies similarities and differences, before the changes with growth irradiance are considered.

The shapes of absorption spectra ($a^{chl}$, normalised to 440 nm) of all the coccolithophore species examined were similar, with absorption peaks at 440, 470 and 675 nm (Figure 2.8a). The same main absorption peaks feature in both $a^{chl}$ and $a_{sol}{}^{chl}$ spectra (Figure 2.8a & b), demonstrating that the types and abundances of pigments present drive the shape of the absorption spectra. Absorption by Chl *a* leads to characteristic peaks around 440 nm and 675

nm, whilst the Fs have high absorption between 440 nm and 470 nm (Figure 2.1). The high proportion of Fs in the coccolithophores thus resulted in characteristically high $a^{chl}$ around 470 nm, in contrast to the diatom *T. weissflogii*, which had a much lower proportion of Fs, and concomitant lower absorption at 470 nm (Figure 2.8). The differences between shapes of $a_{sol}^{chl}$ and $a^{chl}$, occur primarily because absorption spectra are different in solution to that packaged within the cell, a phenomena which is discussed further in Chapter 3.

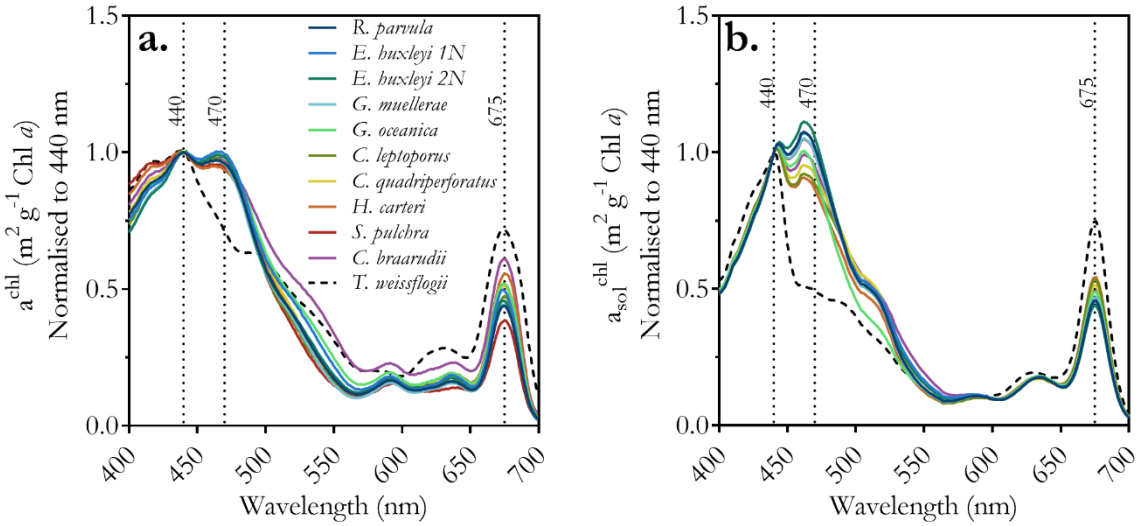


**Figure 2.8.** a) Chl *a*-specific absorption efficiency spectra ($a^{chl}$) and b) reconstructed absorption spectra from constituent pigments ($a_{sol}^{chl}$) of 10 coccolithophore species and a diatom (normalised to 440 nm) grown under LL (25 µmol photons $m^{-2}$ $s^{-1}$). See key for species identities.

Whilst the shapes of absorption spectra were similar amongst the coccolithophore species, the magnitude of spectrally averaged absorption ($\bar{a}^{chl}$) ranged more than two fold at LL, from 8.06 $m^2$ (g Chl *a*)$^{-1}$ in *C. leptoporus* to 20.14 $m^2$ (g Chl *a*)$^{-1}$ in *S. pulchra* (Figure 2.9a). In the diatom, $\bar{a}^{chl}$ was at the lower end of this range (6.39 – 10.35 $m^2$ (g Chl *a*)$^{-1}$).

Spectral shape of absorption in the 440 – 470 nm region, wherein absorption of the key photosynthetic accessory pigments is high, is quantified by the 440 : 470 nm ratio. The 440 : 470 nm ratio was largely conserved (ranging from 1.01 to 1.07 under LL) amongst the coccolithophores (Figure 2.9b). Therefore, the widely disparate contributions of the marker pigment HF to the Fs pool (ranging from 0.5 % in *C. braarudii* to 99.0 % in *C. quadriperforatus*, Figure 2.5) had little impact on spectral shape in the 440 – 470 nm region. In contrast, the 440 : 470 nm absorption ratio was 1.40 in the diatom, markedly higher than in all the coccolithophore species (Figure 2.9b), due to a lower overall proportional contribution of accessory pigments to the total pigment pool in the diatom (Figure 2.5). Under LL, the 440 : 675 nm $a^{chl}$ ratio ranged between 1.64 (*C. braarudii*) and 2.60 (*S. puclhra*) in the

coccolithophores, but was low in the diatom (1.40). The 440 : 675 nm $a_{sol}^{chl}$ ratio was also lowest in the diatom (Figure 2.9c), indicating that the high proportion of Chl *a* in the diatom contributes to this difference in spectral shape between the diatom and the coccolithophore species.

Irradiance dependent changes in the shape and magnitude of Chl *a*-specific absorption efficiency spectra are summarised by comparing the spectrally averaged absorption ($\bar{a}^{chl}$) and diagnostic absorption ratios between different light treatments (Figure 2.9). Within species, $\bar{a}^{chl}$ varied with growth irradiance, but not in a way that was consistent across the different species (Figure 2.9a). In *E. huxleyi* 2N, *G. muellerae, R. parvula* and the diatom *T. weissflogii,* $\bar{a}^{chl}$ was significantly higher at HL (one-way ANOVAs, $p < 0.05$), whilst in the other species no significant differences between irradiances were identified. Generally, differences between species were greater than differences within a species at the different growth irradiances. The 440 : 470 nm absorption ratio of each coccolithophore species was significantly lower at LL compared to HL (one-way ANOVAs, $p < 0.05$) by between 1.7 and 7.6 %. The irradiance related differences within species were small in comparison to the overall difference between the coccolithophores and the diatom (Figure 2.9b). The 440 : 675 nm absorption ratio was also significantly lower at LL compared to HL in all coccolithophore species except *S. pulchra* (Figure 2.9c, one-way ANOVAs, $p < 0.05$). Amongst the coccolithophores, the 440 : 675 nm absorption ratio was an average of 16.25 % lower under LL than HL, whilst in the diatom it was 20.21 % lower. This flattening of the absorption spectra is typical of increasing package effects as the cells become more highly pigmented under low irradiance (Duysens, 1956; Bidigare, Ondrusek, *et al.*, 1990; Fujiki and Taguchi, 2002), and the importance of these package effects on acquisition of light by the cells is further explored in Chapter 3.

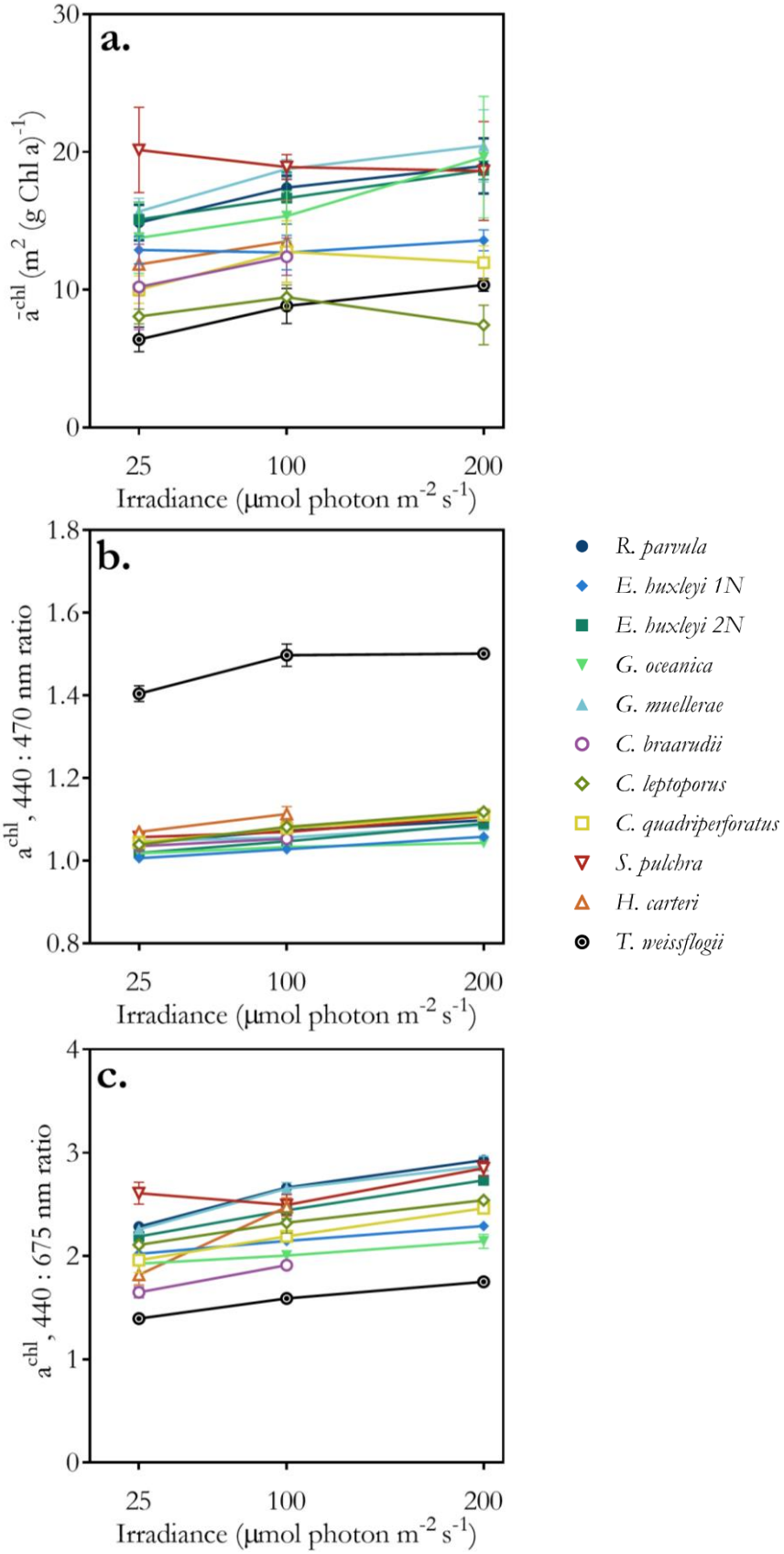


**Figure 2.9.** a) Spectrally averaged Chl *a*-specific absorption ($\bar{a}^{chl}$), b) 440 : 470 nm $a^{chl}$ absorption ratios and c) 440 : 675 nm $a^{chl}$ absorption ratios plotted against growth irradiance, in 10 coccolithophores and a diatom (see key on right for species identities).

### 2.3.3 Absorption cross-section of PSII photochemistry ($\sigma_{PSII}$) and quantum yield of PSII photochemistry ($F_v/F_m$)

Absorption cross-section of PSII photochemistry ($\sigma_{PSII}$) varied between the coccolithophore species (Figure 2.10a). For example, under LL $\sigma_{PSII}$ ranged from 5.44 $nm^2$ $PSII^{-1}$ in *C. quadriperforatus* to 9.50 $nm^2$ $PSII^{-1}$ in *R. parvula*. Quantum yield of PSII photochemistry ($F_v/F_m$) also varied between species, between 0.51 in *G. oceanica* and 0.31 in *C. braarudii* (Figure 2.10b). All coccolithophore species had higher $\sigma_{PSII}$ than the diatom, in which $\sigma_{PSII}$ = 3.96 $nm^2$ $PSII^{-1}$ under the same light conditions. Correspondingly, all coccolithophore species had lower $F_v/F_m$ than the diatom, in which $F_v/F_m > 0.51$ under all irradiances.

Under all growth irradiances, $\sigma_{PSII}$ of all the coccolithophores was higher than that of the diatom (Figure 2.10a). Within coccolithophore species, $\sigma_{PSII}$ varied with growth irradiance, but not in a way that was consistent across the different species, with some species having a higher $\sigma_{PSII}$ under HL (e.g. *C. quadriperforatus, G. muellerae*) whilst in *S. pulchra* $\sigma_{PSII}$ was lowest under HL (Figure 2.10c). In most species, $F_v/F_m$ was slightly higher at LL though these differences were not statistically significant (Figure 2.10d, one-way ANOVA, $p > 0.05$). An exception was *S. pulchra,* in which $F_v/F_m$ was significantly lower at LL (0.33) compared to HL (0.46).

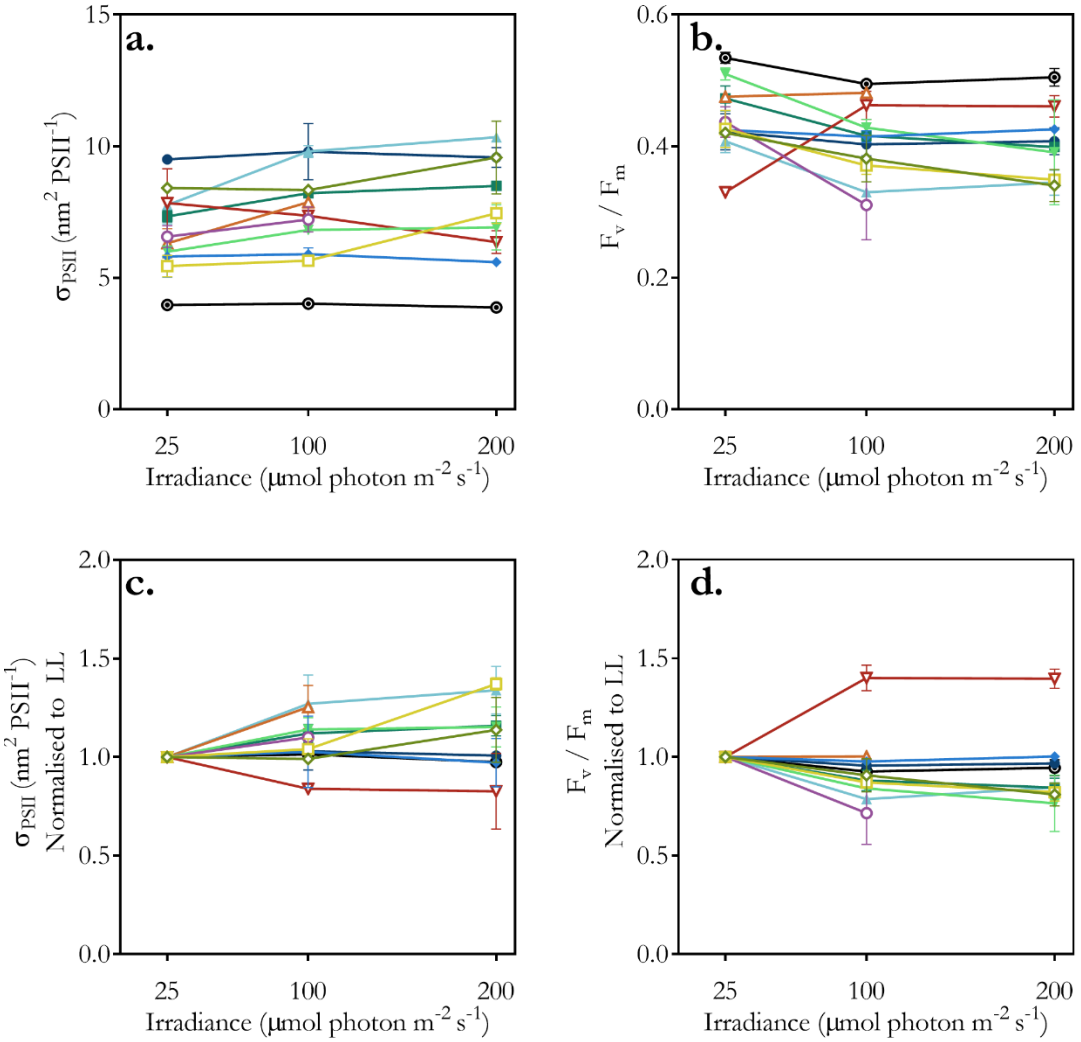


**Figure 2.10.** a) Absorption cross section of PSII photochemistry ($\sigma_{PSII}$), and b) quantum yield of PSII photochemistry ($F_v/F_m$), in 10 coccolithophores and a diatom. c & d) $\sigma_{PSII}$ and $F_v/F_m$ normalised to low growth irradiance (25 µmol photons $m^{-2}$ $s^{-1}$) respectively. Colours and symbols correspond to species as in Figure 2.6.

### 2.3.4 Photosynthetic unit size and density

Measurements of pigment density, $a^{chl}$ and $\sigma_{PSII}$ were integrated in order to derive an estimate of the size of the photosynthetic unit (PSU), and the density of PSU units within the cell (Suggett, MacIntyre and Geider, 2004), which are metrics for quantifying the mode of photoacclimation (Moore *et al.*, 2006; Suggett *et al.*, 2007). PSU size and density values are first compared between species under the LL treatment, to highlight the key interspecies similarities and differences, before the changes with growth irradiance are considered.

PSU size varied by over two-fold between coccolithophore species (Figure 2.11a), ranging from 875 mol pigment (mol RCII)$^{-1}$ in *S. pulchra* to 1,925 mol pigment (mol RCII)$^{-1}$ in *C. leptoporus*, at LL. The size of PSU in the diatom *T. weissflogii*, fell within the lower part of this

range, at 928 mol pigment (mol RCII)$^{-1}$ at LL. Cellular densities of PSU, conventionally expressed as RCII (μm)$^{-3}$, varied more than eight fold between coccolithophore species (Figure 2.11b). Under LL, PSU density ranged from 1,293 RCII (μm)$^{-3}$ in *S. pulchra* to 16,681 in *E. huxleyi* 1N. In the diatom *T. weissflogii,* PSU density was intermediate within this range, at 5,297 RCII (μm)$^{-3}$ at LL.

The PSU size did not change in a consistent way under the different growth irradiances across the coccolithophore species examined (Figure 2.11c). Some species had larger PSUs under HL (e.g. *C. leptoporus* and *C. quadriperforatus*), whilst most species had slightly smaller PSU size under HL. All irradiance driven changes in PSU size amongst the coccolithophores were within ± 29 % relative to that at LL (Figure 2.11c)). The diatom displayed a greater decrease in PSU size with increasing irradiance than any of the coccolithophores (33 % smaller under HL). In all coccolithophores, except *S. pulchra*, lowest PSU density was found under the highest growth irradiance (Figure 2.11d). PSU density was between 1.41 (*G. oceanica*) and 3.82 (*C. leptoporus*) times greater at LL than HL. In the diatom PSU density was 1.34 times greater at LL than at HL.

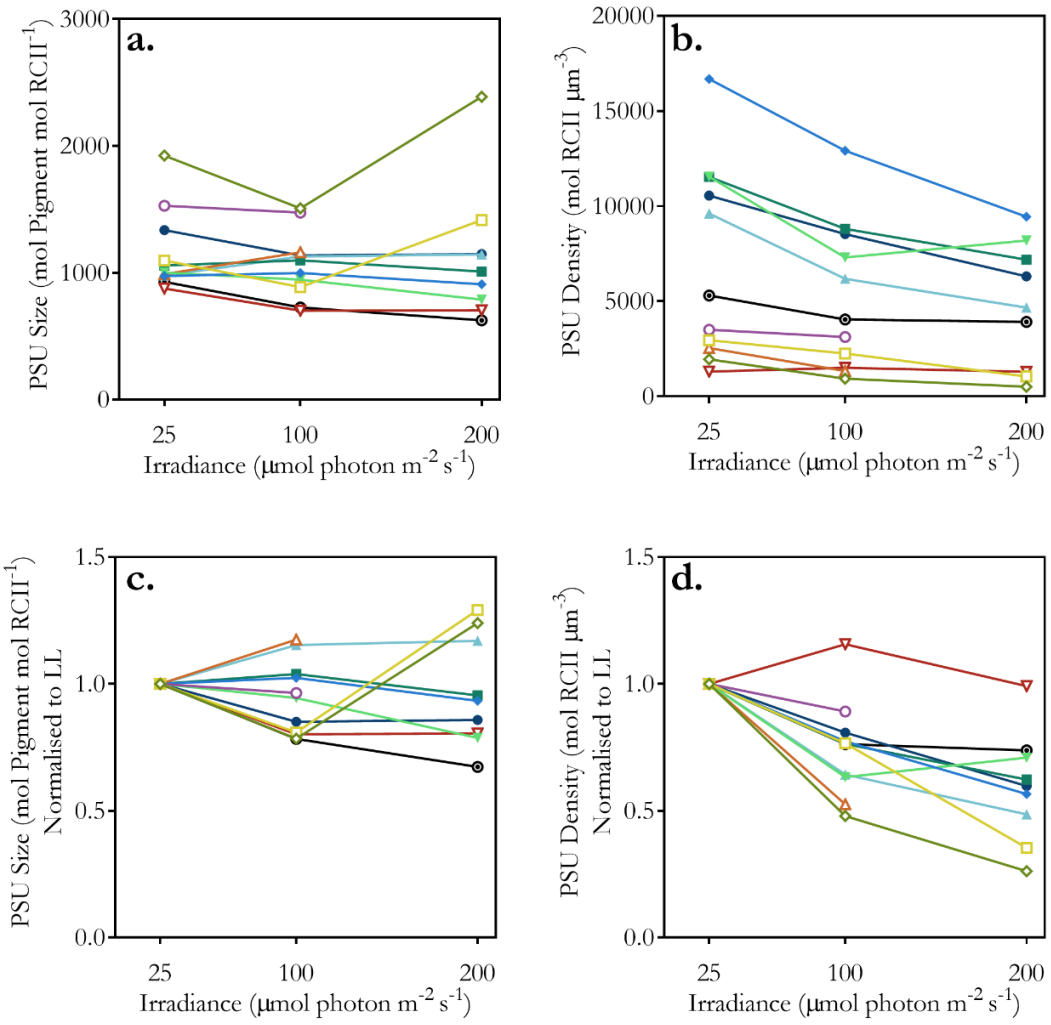


**Figure 2.11.** a) Estimated pigment-specific photosynthetic unit size (PSU Size, mol pigment (mol RC)$^{-1}$), and b) Photosynthetic unit density, expressed as moles of RCII per µm$^3$ (RCII µm$^{-3}$), in 10 coccolithophores and a diatom. c & d) PSU size and PSU density normalised to LL (25 µmol photons m$^{-2}$ s$^{-1}$), respectively. Colours and symbols correspond to species as in Figure 2.6.

## 2.4 Discussion

### 2.4.1 High accessory pigment content amongst the coccolithophores

The coccolithophore species cultured in this study were found to contain a suite of 14 different pigments, in agreement with previous studies on pigment presence/absence in coccolithophore species ($n$ = 36, van Lenning *et al.*, 2004). The quantification of these constituent pigments in this study broadens this knowledge base, by detailing the proportional contributions of pigments in a range of coccolithophores ($n$ = 10). All the coccolithophore species examined had a large pool of fucoxanthin derived (Fs) pigments, and all had a conserved stoichiometry between Chl *a* and Fs of around 1 : 1, regardless of growth irradiance (Figure 2.7c). Evidence of a conserved Chl *a* : **Σ**Fs ratio in *E. huxleyi* is found amongst existing literature (Schofield, Bidigare and Prézelin, 1990; Llewellyn and Gibb, 2000; Stolte *et al.*, 2000; Houdan *et al.*, 2005; Garrido, Brunet and Rodríguez, 2016), with these studies reporting an average molar ratio of 1.03 ± 0.16 : 1 ($n$ = 29) in various strains of *E. huxleyi* grown under a range of irradiances (18 – 600 μmol photons $m^{-2}$ $s^{-1}$). Data presented in the present work suggests a ~ 1 : 1 ratio of Chl *a* to fucoxanthin derived accessory pigments is not exclusive to *E. huxleyi*, but is common across a range of coccolithophore species, and prevails under a range of growth irradiances. Whilst all haptophytes have Fs pigments, non-coccolithophore haptophytes such as *Phaeocystis* generally do not have such consistent proportions of Fs, with Chl *a* : **Σ**Fs ratios ranging from 0.67 to 5.56 (Schlüter *et al.*, 2000; Seoane, Zapata and Orive, 2009; Leeuwe, Visser and Stefels, 2014). The ~ 1:1 stoichiometry between Chl *a* and the Fs seems to be a signature of calcifying coccolithophores.

In addition, all the coccolithophores examined had a large pool of Chl *c* pigments (Figure 2.5) in comparison to the diatom. Overall, this means that the coccolithophores had a high accessory pigment contribution to total pigments (Figure 2.7a). A high contribution of accessory pigments gives insight into the structure of the light harvesting pigment-protein complexes in coccolithophores, about which very little is currently known. The consistently high accessory pigment ratios observed in the current study, across several coccolithophore species and under different irradiances, indicate that the majority of pigment in coccolithophore light harvesting complexes are accessory pigments. The data, therefore, strongly support the previous suggestion that accessory pigments outnumber Chl *a* in *E. huxleyi* antenna pigment-protein complexes (McKew, Lefebvre, *et al.*, 2013), and furthermore that this is common amongst coccolithophore species. Amongst all photosynthetic organisms, it is rare for accessory pigments to outnumber Chl *a* in the light harvesting complexes, and

currently, the dinoflagellate peridinin-Chl*a*-protein is the only structurally resolved light harvesting complex which is enriched in carotenoid compared to Chl *a* (Polívka and Frank, 2010). This dinoflagellate peridinin-Chl*a*-protein complex is atypical in that it is thought to reside in the lumen, as opposed to being integral to the thylakoid membrane (Blankenship, 2014). Thus, the coccolithophores are unusual, possibly even unique, in having light harvesting complexes highly enriched in accessory pigments embedded within the thylakoid. Explicitly resolving the unusual structure of coccolithophore pigment-protein complexes, therefore, is an exciting avenue for further research.

Absorption properties of the coccolithophores in this study reveal part of the functional significance of having a large pool of accessory pigments for light harvesting. High proportions of Fs pigments in coccolithophores directly results in higher light absorption in the blue region (Figure 2.8), in which the underwater light field is relatively enriched (Figure 1.2). The shapes of the absorption spectra (normalised to 440 nm) are such that absorption in the 440 – 500 nm region is 16.6 – 22.1 % higher in the accessory-rich coccolithophores, in comparison to the Chl *a*-rich diatom (Figure 2.8). The high proportion of carotenoids could give the coccolithophores an adaptive edge over the diatoms, for example, in environments where the available light is blue in quality, such as the lower photic zone in oligotrophic gyres.

The data presented here helps to address the prevailing uncertainty over the function (e.g. photosynthetic or non-photosynthetic) of the various accessory pigments. Under low irradiance, the coccolithophore species in this study increased both Chl *a* and Fs concentrations, indicating that the primary function of the Fs is light harvesting. Whilst some carotenoids can provide a degree of photoprotection as they are efficient quenchers of excited Chl *a* triplets (Polívka and Frank, 2010; Blankenship, 2014), the Fs were not upregulated under high irradiance like the NPS pigments (β-car and Dd + Dt). However, a potential role for the Fs in protection from photodamage should not be ruled out, as the different energy transfer properties of different pigments (Sandmann, Kuhn and Böger, 1993; Polívka and Frank, 2010; Blankenship, 2014) can have implications for the light harvesting dynamics, particularly considering differences in the size of the PSUs.

### 2.4.2 Evidence that the coccolithophores have large photosynthetic units

The coccolithophores had high accessory pigment content (Figures 2.5 & 2.7) and high $\sigma_{PSII}$ (Figure 2.10a) in comparison to the diatom. Both measures indicate that coccolithophore RCs are served by a relatively high number of pigments, and indeed most species were estimated to have larger PSUs than the diatom (Figure 2.11) following a method which compares $\sigma_{PSII}$ with

absorption efficiency of the cell overall (Suggett, MacIntyre and Geider, 2004). These data provide an indication of PSU size, but as RCs have not been directly quantified, it is important to be aware of the limitations associated with interpretation of this data. The ratio between Chl *a* and accessory pigments have previously been used to assess PSU size in higher plants and green algae; higher proportions of accessory pigments indicates large antenna systems. However, Chl *a* : accessory pigment ratios are somewhat a crude measure, and may not give a good indication of PSU size in groups such as the coccolithophores. For example, protein quantification in *E. huxleyi* has shown that large differences in the ratio of antenna proteins to RC proteins are not accompanied by large changes in Chl *a* : accessory pigment ratios (McKew, Davey, *et al.*, 2013). Pigment ratios alone are, therefore, not necessarily indicative of PSU size.

The absorption cross-section of PSII photochemistry ($\sigma_{PSII}$) is proportional to the amount of excitation energy received by a RCII, and as such, gives an independent indication of PSU size. The higher $\sigma_{PSII}$ in all of the coccolithophore species in comparison to the diatom, alongside the higher Chl *a* : accessory pigment ratio in the diatom taken together suggest that PSU size *is* generally large in the coccolithophores. However, there are substantial differences in $\sigma_{PSII}$ between coccolithophore species (Figure 2.10) whilst pigment ratios are very similar between species (Figure 2.7), again indicating that neither measure reveals the whole story. It is important to note that my measurements of $\sigma_{PSII}$ and subsequent calculation of PSU density and size are representative only of changes in PSII, as PSI does not exhibit variable fluorescence. In this interpretation, the PSI : PSII is assumed to be 1 : 1, and the pigment is assumed to be distributed evenly between them. However, PSI : PSII ratios are known to vary between strains of *E. huxleyi* (Suggett *et al.*, 2007), indicating that the simplistic 1 : 1 assumption for all the coccolithophore species in this study could mask important information about the structure of the light harvesting equipment. To provide more robust evidence for large PSUs in the coccolithophores future work should aim to explicitly measure pigment to RC ratios, by directly quantifying RCs (e.g. using oxygen flashlet yields and/or protein quantification; Suggett *et al.*, 2007, Six *et al.*, 2008; McKew, Davey, *et al.*, 2013). Such work would also shed light on the drivers behind the interspecific differences in $\sigma_{PSII}$ and derived PSU size estimates in this study.

High accessory pigment content could be crucial to the effective functioning of large PSUs in the coccolithophores. A high proportion of Fs accessory pigments, interspersed with Chl *a,* may allow the coccolithophores to build larger PSUs, whilst minimising the risk of photodamage that may occur if the pigment was primarily Chl *a*. The diatom examined in this study had a lower proportion of Fs than in the coccolithophores, and a low $\sigma_{PSII}$, suggesting

that each diatom RC was served by less pigment. It is possible that photodamage-related risks associated with high Chl *a* content effectively limit PSU size in the Chl *a* –rich diatom.

Production of large PSUs in the coccolithophores could have evolved as an economic strategy under nutrient limited growth conditions, as larger PSUs allow a high capacity for light harvesting whilst minimising the costs of expensive RC machinery. Additionally, chlorophyll pigments contains nitrogen, a nutrient often assumed to be limiting in oceanic environments (Moore *et al.*, 2013), whilst the Fs pigments do not contain nitrogen (Table 2.1). Therefore, high accessory pigment content could also be more economical in environments where nitrogen is limiting (i.e. the oligotrophic gyres where coccolithophore exhibit their highest diversity).

### 2.4.3 Light mediated interconversion in the fucoxanthin pool

In some coccolithophore species the pool of Fs pigments was dominated by HF, whilst in others it was dominated by F (Figure 2.5). Interspecific variability in the proportional contributions of pigments to the Fs pool is in agreement with other studies, which report that the components of the Fs pool vary between species of haptophyte (Zapata *et al.*, 2004) and even between strains of the same species (*E. huxleyi;* Stolte *et al.*, 2000; Leonardos and Harris, 2006). In addition to interspecific differences, the pigments within the Fs pool appear to be plastic within species in response to growth irradiance (Figure 2.7d), specifically an increase in the contribution of HF with increasing irradiance. Numerous other studies have documented irradiance-mediated transformations within the Fs pool in haptophytes (Schlüter *et al.*, 2000; Stolte *et al.*, 2000; Seoane, Zapata and Orive, 2009; Lefebvre *et al.*, 2010; Garrido, Brunet and Rodríguez, 2016) and also in other micro-algal groups such as diatoms and dinoflagellates (Millie, Kirkpatrick and Vinyard, 1995; Alami, Lazar and Green, 2012). The functional significance of these changes remains unclear, particularly as differences in spectral absorption properties between the Fs pigments are minimal both in solution (Figure 2.1) and *in vivo* in these coccolithophores (Figure 2.8). However, the molecular differences between Fs pigments (addition of an acycloxy group to F to make BF and HF; Table 2.1) can alter their chemical binding affinities (Croce and van Amerongen, 2014) causing changes in the positioning and orientation within the light harvesting equipment. Space filling models suggest that the increased 'bulkiness' of HF compared to F could increase distances between adjacent pigments (Alami, Lazar and Green, 2012), potentially decreasing the efficiency of energy transfer and providing protection from photodamage. Increased HF : F under high irradiance in the coccolithophores in this study could represent 'fine tuning' of energy transfer dynamics between pigments to avoid photodamage under high irradiance.

### 2.4.4 Diverse photoacclimation strategies amongst the coccolithophores

Photoacclimation to LL involved an increase in the concentration of PS pigments in all coccolithophore species, and a decrease in the contribution of NPS pigments (Figure 2.7). The extent of this pigment acclimation, however, differed between species, for example with species like *C. leptoporus* increasing pigment density by a much greater margin than others like *S. pulchra* (Figure 2.6). The acclimation strategy (in terms of the estimated number and size of PSUs) also differed between coccolithophore species (Figure 2.11), indicating that there could be diversity of photoacclimation strategies within the coccolithophores.

Whilst the Chl *a* : accessory pigment ratios in the current study were approximately constant in all coccolithophore species under a range of growth irradiances, there were species differences in acclimation of $\sigma_{PSII}$ between LL and HL (Figure 2.10). This is consistent with previous work on *E. huxleyi* in which acclimation of $\sigma_{PSII}$ was accompanied by only a small change in Chl *a* : accessory pigment ratios (McKew, Davey, *et al.*, 2013). However, whilst in the present study there were no significant light-mediated changes in *E. huxleyi* $\sigma_{PSII}$, McKew *et al.*, (2013) reported increased $\sigma_{PSII}$ under low irradiance in *E. huxleyi*. Reasons for this discrepancy in results could be due to the irradiance levels used. Whilst LL levels are comparable between the studies (30 compared with 25 μmol photons $m^{-2}$ $s^{-1}$ in this work), McKew *et al.*, (2013) used a HL 5-fold higher (1000 μmol photons $m^{-2}$ $s^{-1}$) than used in the current work (200 μmol photons $m^{-2}$ $s^{-1}$) and a longer light period (16 h compared to 14 h in this work). In another *E. huxleyi* study using more comparable light levels, only a 5-10 % increase in $\sigma_{PSII}$ was observed between HL and LL (Suggett *et al.*, 2007), a range possibly within the measurement error of the $\sigma_{PSII}$ in the present work.

Estimates of PSU size in this study suggests that light-mediated changes in antenna size are modest (Figure 2.11) in comparison to the high flexibility in pigment density (Figure 2.6). These observations can be reconciled if coccolithophore species are predominantly using an 'n' type acclimation strategy (producing more PSUs). The estimated number of PSUs appears to generally be more plastic than PSU size under the different irradiances (Figure 2.11), supporting the dominance of 'n' strategy acclimation. Note that cultures were nutrient replete in this experimental setup, meaning that nutrient limitation stress on the cells was minimised in an artificial way. It is important to, therefore, be aware that a less heavy dominance of the 'n' type acclimation (expensive in terms of resources, see Figure 2.2) may be seen under low nutrient conditions that are more representative of the natural environment. However, in natural systems, a common photoacclimation strategy does appear to involve large changes in PSU density and smaller changes in $\sigma_{PSII}$ (Moore *et al.*, 2006). However, there is interspecific

variation within this general 'n' strategy theme: *S. pulchra* displayed a markedly different photoacclimation strategy to all the other species.

The increase in *S. pulchra* pigment density under LL was modest in comparison to the other coccolithophores. Additionally, in sharp contrast to all other species, the maximum quantum yield ($F_v/F_m$) of *S. pulchra* was lower under LL (Figure 2.10) indicating that absorbed photons were actually *less* likely to drive PSII photochemistry in LL adapted *S. pulchra* cells. Estimates of PSU density under LL suggest that there was no significant increase compared to HL, also in sharp contrast to all the other coccolithophore species (Figure 2.11d). This discrepancy may link to the nutritional strategies hypothesised to be adopted by some light-limited deep-dwelling coccolithophores, namely mixotrophy (Poulton *et al.*, 2017). A growing body of evidence shows that some haptophytes use other nutritional strategies like mixotrophy and phagotrophy (Kawachi *et al.*, 1991; Tillmann, 1998; Houdan *et al.*, 2006; Rokitta *et al.*, 2011) and anecdotal evidence suggests *S. pulchra* grows faster in media enriched in organics (preliminary experiments, and I. Probert, pers. comm.). If species like *S. pulchra* make a facultative switch to mixotrophy under LL, a complete re-evaluation of how photoacclimation occurs in such coccolithophores could be required.

Comparison with the diatom species grown in parallel helps to contextualise these differences in photoacclimation strategy amongst the coccolithophores. Differences within the coccolithophore species are as big, if not bigger, than differences between the coccolithophores as a group and the diatom (Figure 2.11). In the diatom, a similar magnitude of change in both PSU density and size was reported, in agreement with previous reports of co-regulation of antennas and RCs during diatom photoacclimation (Dubinsky, Falkowski and Wyman, 1986; Lepetit *et al.*, 2012).

In summary, this data set suggests that *E. huxleyi* may not be representative of photoacclimation strategies in the coccolithophores as a group. Furthermore, acclimation of the machinery of downstream electron transfer steps are likely to be of equal or more importance relative to the acclimation of the light harvesting equipment explored here. Field studies suggest that within taxa, plasticity in size of PSII antennas is limited, whilst parameters downstream of PSII are able to acclimate to a greater extent (Moore *et al.*, 2006). Future work explicitly measuring photoacclimation of the photosynthetic equipment will help shed further light on photoacclimation strategies in the coccolithophores.

### 2.4.5 Implications for quantifying coccolithophores in the field

The results presented have some important implications for techniques used to identify and quantify the coccolithophores as a group in the field. The highly variable contribution of HF to total pigment amongst the coccolithophores (Figure 2.5), and the fact that it is influenced by the light environment (Figure 2.7d), has implications for chemotaxonomic methods. Whilst HF is unquestionably a useful diagnostic biomarker, as it is unique to the haptophytes, and present in all coccolithophore species examined so far (this study, van Lenning *et al.*, 2004), caution should be used when using it to infer quantitative changes in the haptophyte group with chemotaxonomic methods. For example, the genus *Coccolithus* can comprise an important part of the community in high latitude regions (Daniels *et al.*, 2016) and contains < 0.5 % HF (Figure 2.5). Chemotaxonomic methods could therefore profoundly underestimate populations of *Coccolithus* in such regions, or misidentify them as diatoms due to their high F content (~ 33 %).

The consistency of shape of the absorption spectra of the 10 coccolithophores in this study could also have implications for satellite remote sensing techniques. The distinct shape of the absorption spectra appears to be a robust signature in a wide range of coccolithophores, including a non-calcifying haploid *E. huxleyi* strain (Figure 2.8). This characteristic spectral shape could be used as a reference spectrum in hyper-spectral sensing methods (e.g. Bracher *et al.*, 2008; Sadeghi *et al.*, 2012), with confidence that it is representative of the coccolithophores as a whole. Such techniques could be used in conjunction with the well-developed PIC algorithms that exploit backscatter to detect coccolithophores (Holligan *et al.*, 1983; Iglesias-Rodriguez *et al.*, 2002; Balch *et al.*, 2005) to reduce their bias towards *E. huxleyi* blooms (Paasche, 2002; Gordon *et al.*, 2009).

# Chapter 3 Size scaling of Irradiance Dependent Physiology in Coccolithophores

## Abstract

Cell volume affects ecologically important aspects of phytoplankton physiology such as photosynthetic and growth rates, and size scaling relationships can be described with a size scaling exponent 'b' derived from a simple power-law function. Under optimum conditions, growth rates typically follow the '¾ law' of metabolic theory, and scale negatively with cell volume with an exponent of -0.25. However, under low light, acquisition of energy to drive photosynthesis is more challenging for large cells, due to increased self-shading (termed package effects), and the size scaling exponent of growth is expected to decrease ($b < -0.25$). Size scaling of growth rates under varying irradiance is here examined for the first time amongst coccolithophores, a biogeochemically important phytoplankton group. Growth rates were measured in cultures of 10 species of coccolithophore with cell volumes spanning two orders of magnitude (from 11 $\mu m^3$ to 2120 $\mu m^3$) under three light intensities (25, 100 and 200 $\mu$mol photons $m^{-2}$ $s^{-1}$). Maximum growth rate scaled negatively with cell volume, with an exponent of -0.22 ± 0.04, statistically similar to the -0.25 predicted by metabolic theory (extra sum-of-squares F test, $p < 0.05$). However, under low light conditions, the size scaling exponent of growth rate *increased* to -0.12 ± 0.03, in direct contrast to the predicted decrease.

Physiology of coccolithophore cells, including pigment content, light absorption efficiency and photosynthesis (estimated from electron transport rates at photosystem II) are investigated to determine how the large coccolithophores in this study maintained growth rates near maximum in low light conditions, whilst small cells suffered growth rate limitation. Pigment density scaled negatively with cell volume with exponents of between -0.37 ± 0.08 under low light to -0.46 ± 0.09 under high light, likely in response to the pressures of size-dependent package effects, entirely in keeping with expectations. No size dependence was identified in either chlorophyll *a*-specific absorption efficiency or electron transport rate at photosystem II, and therefore, neither of these parameters explains the unusual resilience to light limitation in the large-celled coccolithophore species. However, the large-celled coccolithophores in this study had lower volume-specific photosynthetic requirements to reach maximum growth rates, and the quantum yield of growth (an indicator of the efficiency with which electron transport drives biomass production) scaled positively with cell volume under the low light treatment, with an exponent of 0.33 ± 0.08. The results indicate that the coccolithophore species studied here do not conform to the existing theoretical framework regarding size scaling of growth rates under low light conditions.

## 3.1 Introduction

### Size scaling

Size is a key determinant of metabolic rate in all organisms (Peters, 1983; Brown, 1995). Single celled phytoplankton are no exception, and cell volume is found to affect most aspects of phytoplankton physiology (Marañón, 2015; Ward *et al.*, 2017). Relationships between cell size and ecologically important rates like photosynthesis and growth are useful for understanding the dynamics of phytoplankton communities in the field, and for predicting how these communities might respond to environmental change. The size dependence of phytoplankton traits can be incorporated into biogeochemical models, which require parameters to be described in simple but effective terms (Cullen *et al.*, 1993; Le Quere *et al.*, 2005; Brewin *et al.*, 2010; Ward *et al.*, 2012). Size scaling of most metabolic rates or cellular properties (Y) can be described as varying with cell volume (V) with a simple power-law function:

$$Y = a \times V^b \tag{3.1}$$

where 'a' is a group specific constant, and 'b' is the size scaling exponent. Biomass-specific parameters which scale in direct proportion to cell volume (i.e. isometric) have an exponent b = 0, whilst relative increases or decreases with cell volume result in an exponent of greater or less than 0, respectively. The size scaling exponent 'b' is estimated by the slope of a linear regression through a log-log plot of the biomass-specific parameter in question on the y axis, and cell volume on the x axis (Finkel, 2001; Finkel, Irwin and Schofield, 2004; Key *et al.*, 2010; Ward *et al.*, 2017; Malerba *et al.*, 2018).

Biomass-specific metabolic rates under optimal growth conditions are commonly lower in large cells, following a general scaling pattern (sometimes known as the '¾ rule'; Peters, 1983; West, 1997; Finkel, Irwin and Schofield, 2004), which is thought to be driven by fundamental metabolic limits imposed by geometric scaling of cellular transport networks (West, 1997; Banavar *et al.*, 2002). However, as more laboratory and field studies continue to explore size scaling in phytoplankton, exceptions to general size scaling rules are found (Bec *et al.*, 2008; Maranon *et al.*, 2013), especially, as will be discussed, under suboptimal growth conditions. Therefore, it is crucial to observe, and mechanistically understand, size scaling relationships in different phytoplankton groups and under different environmental conditions.

The coccolithophores are a biogeochemically important group (Berelson *et al.*, 2007; Broecker and Clark, 2009), the traits of which are mostly inferred from knowledge about one species in particular, *Emiliania huxleyi*. However, there are over 280 known extant coccolithophore species (Young *et al.*, 2003), varying in size, morphology, physiology and environmental

distribution (Thierstein and Young, 2004; Houdan *et al.*, 2006; Monteiro *et al.*, 2016; Poulton *et al.*, 2017; Walker *et al.*, 2018). The number of coccolithophore species in which physiology has been examined is considerably limited, yet cell volume of cultured species spans two orders of magnitude. Thus, the coccolithophores present an opportunity for exploring size scaling in a heretofore relatively unexplored phytoplankton group.

Growth rate ($\mu$) is a key phytoplankton trait, as it affects both the relative fitness of individual species and the functional properties of overall communities. Maximum growth rate ($\mu_{max}$) is achieved when environmental conditions and resource availability are optimal. Interspecifically, $\mu_{max}$ is often found to scale negatively with cell volume, with an exponent of -0.25, following the '¾ rule' of metabolic theory of ecology (Peters, 1983; West, 1997). However, when availability of key resources for growth, such as nutrients and light, is suboptimal, the size scaling of growth rates can deviate from the metabolic theory (Sommer, 1989; Finkel, 2001; Gillooly *et al.*, 2001). In this study, the effect of availability of light on size scaling of growth rates in the coccolithophores is explored for the first time.

Light energy drives photosynthesis and is a crucial (energetic) resource for phytoplankton. Suboptimal irradiance limits productivity of the cell by limiting photosynthetic rate. The efficiency of light absorption by phytoplankton cells is influenced by 'package effects', a term given to describe the reduction in a pigments absorption efficiency due to internal shading (Kirk, 2011). Robust physical theory underpins the package effect phenomenon (Kirk, 1976; Morel and Bricaud, 1981) and demonstrates that large or more highly pigmented cells absorb incident light with reduced efficiency (See Figure 1.4, Chapter 1). Package effects, therefore, are commonly quantified by measuring or estimating the Chl *a*-specific absorption efficiency ($a^{chl}$) by physically measuring light absorption of a sample with a spectrophotometer. High levels of package effects result in low values of $a^{chl}$, whilst a low level of package effects results in $a^{chl}$ approaching a maximum value, equal to the absorption efficiency of the pigment isolated in solution (i.e. not packaged within a chloroplast or cell). As package effects can have a large effect on the efficiency of absorption of light energy for photosynthesis, understanding the magnitude of package effects experienced by cells is crucial in any interpretation of photosynthetic or growth responses under different irradiances. Where absorption efficiency has not been directly quantified, mechanistic models (e.g. Morel and Bricaud, 1981) that incorporate measurements of cell volume and pigmentation can be used to estimate absorption efficiency (e.g. Moore *et al.*, 2005).

The impact of the size-dependence of light absorption on growth rate is complicated by photoacclimation, the process by which cells alter concentrations of their photosynthetic

equipment in order to optimise energetics under given environmental conditions (Falkowski and Raven, 2007). Pigment density is particularly plastic within species, and also varies greatly between different species. Pigments are an investment as they carry a cost to produce and maintain, and deliver benefits in the form of light harvesting. Package effects mean that the benefits of producing more pigment diminish with increasing cell size (Kirk, 2011). An analysis of the cost-benefit trade off in cells of different sizes found that under low light intensities, the most energetically economical outcome is reached when pigment density scales negatively with cell volume, with an exponent of -0.33 (Finkel, Irwin and Schofield, 2004). The theoretical predictions of negative size scaling of pigment densities are supported by experimental data from diatoms and a few other taxa (Finkel, 2001; Fujiki and Taguchi, 2002), but as yet not in coccolithophores. Size dependent packaging effects appear to limit pigment densities and absorption efficiencies in large cells, limiting the amount of light energy harvested for photosynthesis per unit cell volume. Large cells are, therefore, thought to become light limited at higher irradiances than their smaller counterparts (Finkel, 2001; Finkel, Irwin and Schofield, 2004). A summary of the theory underpinning the expectation that large cells experience a higher degree of growth rate limitation (i.e. are relatively worse off) under low light growth conditions is shown in Table 3.1 below (further detailed in Finkel *et al.*, 2004). The expected relative differences in physiology of large and small cells resulting from this theory are also shown.

**Table 3.1.** Theoretical framework (based on Finkel, 2001; Finkel, Irwin and Schofield, 2004) summarizing the effects of size dependent packaging on pigment content, photosynthetic rate and growth rate. The relative consequences for large and small cells (in relative size) in light limiting conditions are summarized.

| Theory | Large Cell | Small Cell |
|---|---|---|
| 1 Size-dependent package effects govern pigment densities in the cell | Lots of self-shading (High package effects); Low benefit from producing more pigment results in low pigment density | Not much self-shading (Low package effects); High benefit from producing more pigment results in high pigment density |
| 2 Biomass-specific photosynthetic rates are governed by light absorption rates | Lower light absorption rate, and lower photosynthetic rate (per unit volume) | Higher light absorption rate, and higher photosynthetic rate (per unit volume) |
| 3 Growth rates are governed by biomass-specific photosynthesis rates | Lower growth rate. Growth rate saturates at a relatively high irradiance | Higher growth rate. Growth rate saturates at a relatively low irradiance |

The size dependence of photophysiological characteristics, and the consequential impact on growth rates, can be used to explain the relative competitive advantages of small and large cells under different light conditions (Key *et al.*, 2010). As discussed earlier, maximum growth rates (under optimal conditions) are expected to be lower in large cells due to metabolic limitations, often resulting in a size scaling exponent for growth rate of -0.25. When availability of light energy is limited, the growth rate disparity between small and large cells is expected to increase, and thus the size scaling exponent of growth rate is predicted to decrease (i.e. $b < -0.25$) in low light conditions (Finkel, Irwin and Schofield, 2004). The growth response to irradiance can be visualised by plotting the relationship between available irradiance and growth rate for a hypothetical small and large cell (Figure 3.1). Package effects mean acquisition of light is more challenging for large cells, and thus their growth rates are expected to be relatively more restricted under low light. As such, when low light growth rates are plotted against cell volume (Figure 3.1b) the difference between the growth rates of the small and large cells increases (i.e. the gradient 'b' of the line becomes steeper) relative to optimum conditions. Conventionally, the growth rate-irradiance relationship is approximated

by a Poisson function, where the saturating parameter ($K_E$) indicates the irradiance at which growth rate begins to saturate (MacIntyre *et al.*, 2002). The Poisson fits are included in Figure 3.1a, and $K_E$ parameters marked with red crosses. The greater growth rate limitation experienced by the large cell under low light results in a higher $K_E$ (Figure 3.1c), indicating that the cell requires a relatively high irradiance to reach growth rate saturation.

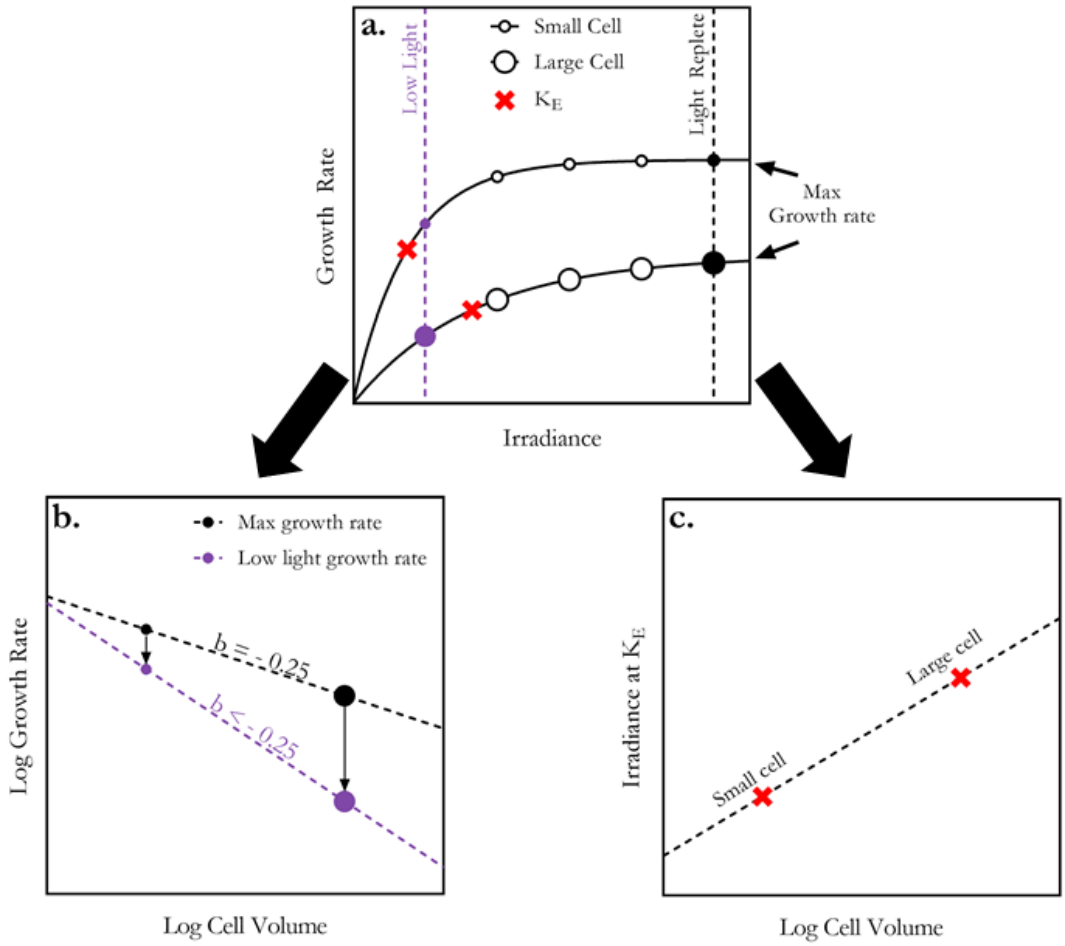


**Figure 3.1.** a) Hypothetical growth-rate irradiance curves for a large and small cell, based on the theoretical framework outlined in the text and in Table 3.1. Maximum growth rate (filled black circles), growth rate under low light (purple circles), and the growth saturation parameter ($K_E$, red crosses) indicated. b) The resulting size scaling of growth rate under optimum (black) vs low light (purple) conditions and c) of the growth saturation parameter.

Growth rates at certain irradiances are measured by quantifying the exponential rate of increase of cell numbers in a culture that is acclimated to a constant growth irradiance, usually for a matter of days or weeks. As mentioned, phytoplankton cells are highly plastic with respect to their photosynthetic machinery. Acclimation to a certain irradiance typically involves changing pigment concentrations, in order to increase or decrease the amount of light energy absorbed, but also includes myriad other changes including changes in the size or

number of photosystems, or changes in the abundance and functioning of any of the downstream steps of photosynthesis (Blankenship, 2014). Photosynthesis-irradiance curves are used to examine how acclimation contributes to photosynthetic rate response at a given growth irradiance (Jassby and Platt, 1976; Geider, MacIntyre and Kana, 1997; MacIntyre *et al.*, 2002). Variable fluorescence techniques, such as Fast Repetition Rate fluorometry (FRRf) measure electron transfer rates at PSII, which can be used as a proxy for photosynthetic rate (Kolber, Prášil and Falkowski, 1998). FRRf allows us to quantify the instantaneous photosynthetic response of a cell to different irradiances over a short time period (~30 minutes), capturing the response of a cell in a specific acclimation state. Photosynthesis-irradiance curves are similar in shape to growth rate-irradiance curves, and are also approximated by saturating curve fits (e.g. Jassby and Platt, 1976). The parameters of photosynthesis-irradiance curves from cells grown under different irradiance conditions represent how acclimation to a certain irradiance affects photosynthetic response. For example, the initial slope ($\alpha$) describes the efficiency with which available light energy is used for photosynthesis in the light-limited portion of the curve (Kirk, 2011). Following the theory set out in Table 3.1, large, more packaged cells are expected to have a lower efficiency under light-limited conditions (i.e. lower $\alpha$) than small cells. However, the currency used is of critical importance when interpreting the relative parameters of photosynthesis-irradiance curves (MacIntyre *et al.*, 2002). Namely, the units of photosynthesis must be relevant to the question addressed. In this case, as deviations of photosynthetic rates from isometry are being explored, it is important that photosynthesis be assessed in a volume-specific currency.

**Study Outline**

This study examines size scaling of growth rates in relation to irradiance in an unprecedented diversity of coccolithophores, spanning two orders of magnitude in cell volume. The work tests whether maximum growth rates ($\mu_{max}$) scale negatively with cell volume, with an exponent of -0.25 (following the ¾ rule), and whether the size scaling exponent of growth rate decreased under low light conditions, in line with the current understanding of size-dependent light acquisition.

Initial results showed that $\mu_{max}$ scaled negatively with cell volume as expected, but under low light conditions, the size scaling exponent of growth rate did not decrease, deviating from expectations. To understand this unexpected result, the theory detailed in Table 3.1 is tested, in order to identify where the physiology of coccolithophores deviates from this theoretical framework. Discrepancies between the hypotheses and the quantifiable physiology of coccolithophores are tested as in Table 3.2:

**Table 3.2.** Summary of how the theoretical framework (regarding the effects of size-dependent packaging on pigment content, photosynthetic rate and growth rate, Table 3.1) is tested in this study.

| | Hypothesis | How Hypothesis is Tested |
|---|---|---|
| **1** | Size-dependent package effects govern pigment densities in the cell | Quantify the size scaling of volume-specific pigment density, and quantify packaging effects experienced by cells. |
| **2** | Biovolume-specific photosynthetic rates are governed by light absorption rates | Calculate rates of light absorption for photosynthesis, and volume-specific electron transport rates (a proxy for photosynthetic rates). Examine the efficiency with which photons drive electron transport. |
| **3** | Growth rates are governed by biovolume-specific photosynthesis rates | Examine the efficiency with which volume-specific photosynthesis drives growth. |

Note that in this framework cell volume is used to represent biomass, as biomass in terms of organic content is not explicitly measured. For clarity, the terminology used is 'biovolume' to more accurately describe the measure of biomass. The results presented here provide novel information on the inter-specific size scaling relationships in coccolithophores. More generally, the analysis scrutinises the common underlying assumptions about the expected relative growth rates of different sized cells under low irradiance conditions.

## 3.2 Methods

### 3.2.1 Experimental Setup and Growth Rate – Irradiance Relationships

Batch culture experiments were used to quantify growth rates and photophysiology of 10 species of coccolithophore spanning two orders of magnitude in cell volume. Details of the strains used and experimental setup can be found in Chapter 2. Briefly, each strain was grown in duplicate at three light levels (25, 100 and 200 μmol photons $m^{-2}$ $s^{-1}$). Growth rate was monitored by daily cell counts. Whilst cultures were still in exponential growth phase (i.e. not yet nutrient limited) aliquots were taken for variable fluorescence measurements using FRRf that day, and other cell samples were harvested and stored for quantification of cell volume, pigment content and light absorption efficiency at a later date.

In order to examine the growth rate response to irradiance in the different coccolithophores, exponential growth rates (μ) under the three irradiance conditions were calculated using daily cell count data. Exponential regressions were performed using GraphPad Prism 6.03 software (Langer *et al.*, 2006). Growth rate – Irradiance relationships for each species were described using a Poisson function, to determine maximum growth rate ($\mu_{max}$) and the growth saturation parameter ($K_E$) (MacIntyre *et al.*, 2002):

$$\mu=\mu_{max}\left(1-e^{(-E/K_E)}\right) \quad (3.2)$$

When growth rates were inhibited at high irradiance, these high irradiance growth rate data points were excluded from the Poisson fit.

### 3.2.2 Testing Hypothesis 1: Size-dependent package effects govern pigment densities in the cell

In order to test whether size-dependent package effects govern pigment densities within the cell in the different coccolithophores, it was necessary to quantify both the pigment densities of the cells and the package effects experienced by the cells. Pigment densities within the cells were quantified by High Performance Liquid Chromatography (HPLC), whilst package effects were investigated by measuring light absorption efficiencies using the filter pad method (Tassan and Ferrari, 1995b). Measured absorption efficiencies were compared to efficiencies predicted by a commonly used model (Morel and Bricaud, 1981) in order to interrogate the package effects experienced by the coccolithophores.

### Pigment Analysis

Pigment concentrations in each culture were measured using HPLC, details of which can be found in Chapter 2. Briefly, duplicate 120 mL samples from each culture were filtered onto Whatman GF/F filters and immediately frozen at -80 °C, before being extracted in 90 % acetone, sonicated and analysed following Steele et al. (2015) on an Accela HPLC instrument (ThermoScientific, UK), with quality assurance protocols. Concentrations of pigments (i) measured in the culture samples were corrected to pigment densities within the cell ($C_C$) as follows:

$$C_c(i) = \frac{C_s(i)}{N \times V_c} \tag{3.3}$$

where $C_c$ is the density of a pigment inside the cell (fg $\mu m^{-3}$), $C_s$ is the density of a pigment in the culture sample (fg $L^{-1}$), N is the number of cells in the culture sample (cells $L^{-1}$), and $V_C$ is the volume of the cell ($\mu m^3$ $cell^{-1}$ ).

### Light Absorption Coefficients ($a^{chl}$)

The light absorption efficiency of the different coccolithophore cultures was quantified by measuring the Chl *a*-specific light absorption coefficient ($a^{chl}$) using the filterpad technique (Tassan and Ferrari, 1995a; Bouman *et al.*, 2003). The $a^{chl}$ measurement quantifies the efficiency with which pigment molecules are absorbing light, and as such helps us to explore package effects. Details of the light absorption efficiency measurement can be found in Chapter 2. Briefly, duplicate 50 mL samples from each culture were filtered onto Whatman GF/F filters and immediately frozen at -80 °C. When analysed, absorbance spectra of each filter was measured using a Shimadzu UV-2550 UV-VIS dual beam spectrophotometer fitted with an ISR-240A Integrating Sphere Attachment, and normalised by subtracting the absorbance spectra of a blank filter. Absorbance ($OD_s$) at wavelength ($\lambda$) was transformed into a Chl *a*-specific absorption coefficient of phytoplankton, $a^{chl}$ ($m^2$ $g^{-1}$ Chl *a*) following Bouman et al. (2003):

$$a^{chl}(\lambda) = \frac{2.303 \times M \times OD_s(\lambda)}{\beta(\lambda) \times V_s \times [\text{Chl } a]_s} \tag{3.4}$$

using M, the clearance area of the filter ($m^2$), $V_s$, the volume of culture sample filtered ($m^3$), $\beta(\lambda)$, a wavelength dependent correction factor to account for the increase in path-length due to multiple internal scattering from Bricaud & Stramski (1990), and Chl *a* concentrations of the culture sample, $[\text{Chl } a]_s$ (g $m^{-3}$).

Chl *a*-specific absorption coefficient were spectrally averaged as follows:

$$\bar{a}^{chl} = \frac{\sum_{400}^{700} a^{chl}(\lambda)}{(700 - 400)} \quad (3.5)$$

Chl *a*-specific absorption efficiencies were converted to cell volume-specific absorption efficiencies as follows:

$$\bar{a}^{vol} = \bar{a}^{chl} \times [\text{Chl } a]_c \quad (3.6)$$

where $\bar{a}^{vol}$ is volume-specific absorption efficiency ($m^2\ \mu m^{-3}$) and $[\text{Chl } a]_c$ is Chl *a* densities within the cell (g Chl *a* $(\mu m)^{-3}$).

**Quantifying Package Effects**

Light absorption efficiencies were used to explore package effects experienced by the cells in two ways. Firstly, Chl *a*-specific absorption efficiencies ($a^{chl}(\lambda)$) were compared to the maximum absorption efficiency given the constituent pigments in solution ($a_{sol}^{chl}(\lambda)$). Pigment concentrations of the constituent pigments ($C_i$), and their respective weight-specific absorption coefficient spectra ($a_i^*(\lambda)$) (Bricaud *et al.*, 2004), were used to reconstruct absorption spectra, again normalised to corresponding Chl *a* concentrations (Bidigare, Ondrusek, *et al.*, 1990; Marra *et al.*, 2000):

$$a_{sol}^{chl}(\lambda) = \frac{\sum C_i \times a_i^*(\lambda)}{[\text{Chl } a]_c} \quad (3.7)$$

and spectrally averaged:

$$\bar{a}_{sol}^{chl} = \frac{\sum_{400}^{700} a_{sol}^{chl}(\lambda)}{(700\text{-}400)} \quad (3.8)$$

The decrease in absorption efficiency due to package effects is quantified by a factor conventionally called Q* relating measured absorption efficiencies ($\bar{a}^{chl}$) with maximum values ($\bar{a}_{sol}^{chl}$). The factor describes what proportion of maximum absorption efficiencies the cells are achieving.

$$Q^* = \frac{\bar{a}^{chl}}{\bar{a}_{sol}^{chl}} \quad (3.9)$$

Low values of Q* indicate absorption efficiencies that are much lower than maximal possible values and indicate that packaging effects are large, whilst Q* values approaching 1 indicate that absorption efficiencies are near maximal, and thus that packaging effects are small.

Secondly, the measured absorption efficiencies of cells were compared to that predicted by a simple model (Morel and Bricaud, 1981; Moore *et al.*, 2005), denoted $\bar{a}_{model}^{chl}$ . Package effects

are known to increase with both the size and pigmentation of a cell, and the model incorporates both of these parameters. The comparison between $a_{phy}^{chl}$ and $a_{model}^{chl}$ therefore allows absorption efficiencies to be considered in the context of the most important factors driving the packaging phenomenon. The model uses Mie theory, a description of light absorption by homogenous spheres, and incorporates the impact of cell size (d, equivalent spherical diameter) and pigment density within the cell on Chl *a*-specific absorption efficiency as follows:

$$a_{model}^{chl}(\lambda) = a_{sol}^{chl}(\lambda) \times \left(\frac{3}{2} \times \frac{Q_{\rho(\lambda)}}{\rho(\lambda)}\right) \quad (3.10)$$

where

$$Q_{\rho(\lambda)} = 1 + \frac{2e^{-\rho(\lambda)}}{\rho(\lambda)} + 2\frac{e^{-\rho(\lambda)} - 1}{\rho(\lambda)^2} \quad (3.11)$$

and

$$\rho(\lambda) = a_{sol}(\lambda) \times d \quad (3.12)$$

and spectrally averaged:

$$\bar{a}_{model}^{chl} = \frac{\sum_{400}^{700} a_{model}^{chl}(\lambda)}{(700\text{-}400)} \quad (3.13)$$

### 3.2.3 Testing Hypothesis 2: Biovolume-specific photosynthetic rates are governed by light absorption rates

In order to explore how pigment densities and absorption efficiencies are related to biovolume-specific photosynthetic rates in the different coccolithophores, photosynthetic rate was quantified by measuring electron transport rates, and compared to biovolume-specific rates of light absorption. The parameter 'α' from photosynthesis-irradiance curves measures the efficiency of the use of *available* photons for photosynthesis. However, as pigment content and absorption efficiency affect how much available light is absorbed, an efficiency of the use of *absorbed* photons for photosynthesis was also calculated, by integrating independently acquired measurements of photon absorption rates and electron transport rates.

**Calculating Photosynthetic Photon Absorption Rates**

To explore the efficiency with which photons absorbed translate to electron transfer, it is necessary to first convert absorption efficiencies into absorption rates. The rate of photosynthetic photon absorption (Ā) depends on the available irradiance, the efficiency with which available light is absorbed, and how much of the absorbed light goes towards driving electron transport rather than being dissipated. Volume-specific photosynthetic photon absorption rates were thus calculated as follows:

$$\bar{A}_{PS}^{vol} = \left( \sum a^{vol}(\lambda) \times E_{inc}(\lambda) \right) \times PS_{inc} \quad (3.14)$$

where $\bar{A}_{PS}^{vol}$ is the volume-specific rate of absorption of photons for photosynthesis (photons $\mu m^{-3}$ $s^{-s}$), $\bar{a}^{vol}$ is volume-specific absorption efficiency ($m^2$ $\mu m^{-3}$), $E_{inc}(\lambda)$ is the spectral irradiance available in the growth incubator (photons $m^{-2}$ $s^{-1}$), and $PS_{inc}$ is the fraction of light absorbed by photosynthetic pigments only (all pigments except diadinoxanthin, diatoxanthin and β-carotene):

$$PS_{inc} = \frac{\sum a_{sol(PS)}^{chl}(\lambda) \times E_{inc}(\lambda)}{\sum a_{sol}^{chl}(\lambda) \times E_{inc}(\lambda)} \quad (3.15)$$

Note that spectra of absorption rates (Ā) are very different in shape to absorption efficiency spectra (a), as they depend on the spectra of available light (E).

**Fluorescence-Light Curves**

Rates of photosynthetic electron transfer at a given irradiance were quantified using Fast Repetition Rate fluorometry (FRRf), measured and processed using an Act2 system and Act2Run software (Chelsea Technologies, UK). Details of sample preparation, optimisation and single turnover measurement protocol are detailed in Chapter 2. A fluorescence light curve protocol was used to continuously make single turnover variable fluorescence measurements as background irradiance (I) was increased from 0 to 1320 μmol photons $m^{-2}$ $s^{-1}$ in 15 sequential steps (0, 23, 51, 84, 124, 171, 228, 296, 376, 473, 588, 726, 890, 1086, 1320). Each light step was maintained for 90 s. Acquisitions from the last 20 s of each light step were averaged. Electron transport rates at PSII were calculated at each light step (I) as follows (Suggett *et al.*, 2006):

$$ETR_I^{PSII} = \sigma_{PSII} \times \frac{F_q' \div F_m'}{F_v \div F_m} \times I \quad (3.16)$$

where $ETR_I^{PSII}$ is Electron transport rate at PSII (electron $PSII^{-1}$ $s^{-1}$), $F_v/F_m$ and $F_q'/F_m'$ are the potential photochemical efficiency RCIIs in the dark and under actinic light (I) respectively, and $\sigma_{PSII}$ is the absorption cross section of PSII photochemistry.

Hyperbolic tangent curves were fit through ETR – irradiance data for each fluorescence light curve (Jassby and Platt, 1976) in GraphPad Prism (v 7.04, GraphPad Software Inc.) in order to estimate parameters $P_{max}$ and $\alpha$ as follows:

$$ETR_I^{PSII} = P_{max} \times \tanh\left(\alpha \times \frac{I}{P_{max}}\right) \quad (3.17)$$

where $\alpha$ is equal to the initial slope of the curve, and is a measure of the efficiency of utilistation of incident light, whilst $P_{max}$ represents the maximum rate of photosynthetic electron transport (Kirk, 2011).

**Estimating Volume-specific Electron Transport Rates**

In this investigation, electron transport rates are expressed in biovolume-specific units in order that they can be compared to photon absorption rates and growth rates. In order to convert PSII-specific rates into a biovolume-specific currency, it is necessary to know the concentration of RCII inside the cell. PSII-specific electron transport rates ($ETR_I^{PSII}$, electrons $PSII^{-1}$ $s^{-1}$) were thus transformed into volume-specific electron transport rates ($ETR_I^{vol}$, electrons $\mu m^{-3}$ $s^{-1}$) by multiplying by the cellular density of RCIIs ([PSII], PSII $\mu m^{-3}$).

$$ETR_I^{vol} = ETR_I^{PSII} \times [PSII] \quad (3.18)$$

Density of RCIIs [PSII] was calculated following the optical method described by Suggett, MacIntyre and Geider (2004). This methods divides volume-specific absorption efficiency of PSII ($a_{PSII}^{vol}$, $m^2$ $\mu m^{-3}$) by PSII effective cross-section ($\sigma_{PSII}$, $m^2$ $PSII^{-1}$), as derived from FRRf measurements.

$$[PSII] = \frac{a_{PSII}^{vol}}{\sigma_{PSII}} \quad (3.19)$$

Volume-specific absorption efficiency of PSII ($a_{PSII}^{vol}$) is calculated by adjusting measured Chl *a*-specific absorption efficiencies ($a^{chl}(\lambda)$, $m^2$ (g Chl *a*)$^{-1}$) in order that they can be compared directly with the PSII effective cross-section ($\sigma_{PSII}$, $m^2$ $PSII^{-1}$) measured by FRRf. Chl *a*-specific absorption efficiency ($a^{chl}(\lambda)$) was spectrally corrected, to account for the spectrum of light delivered by the FRRf LED ($E_{Frrf}(\lambda)$), and converted to a volume-specific efficiency by multiplying by Chl *a* density ($[Chl\ a]_c$, g Chl *a* $\mu m^{-3}$). Absorption due to photosynthetic pigments only was accounted for by the factor $PS_{FRRf}$, a ratio describing the contribution of

photosynthetic pigments to the total absorption of the light emitted by the FRRf LED. It was also assumed that light absorbed by photosynthetic pigments was split equally between PSI and PSII, and thus absorption efficiency was multiplied by 0.5 to estimate absorption efficiency of PSII only.

$$a_{PSII}^{vol} = \left( \frac{\sum a^{chl}(\lambda) \times E_{FRRf}(\lambda)}{\sum E_{FRRf}(\lambda)} \right) \times [\text{Chl } a]_c \times PS_{FRRf} \times 0.5 \quad (3.20)$$

where

$$PS_{FRRf} = \frac{\sum a_{sol(PS)}^{chl}(\lambda) \times E_{FRRf}(\lambda)}{\sum a_{sol}^{chl}(\lambda) \times E_{FRRf}(\lambda)} \quad (3.21)$$

**Quantum Yield of Electron Transport Rate**

To examine how light absorption rates govern electron transport rates, the quantum yield of electron transport rate ($\phi_{ETR}$) is calculated:

$$\phi_{ETR} = \frac{ETR_I^{vol}}{\bar{A}_{PS}^{vol}} \quad (3.22)$$

Where $ETR_I^{vol}$ is volume-specific electron transport rate (electrons $\mu m^{-3}$ $s^{-1}$), and $\bar{A}_{PS}^{vol}$ is volume-specific absorption rate by photosynthetic pigments (photons $\mu m^{-3}$ $s^{-1}$), and $\phi_{ETR}$ is the quantum yield of electron transport rate, and describes the efficiency with which absorbed photons drive electron transport (electrons $photon^{-1}$).

### 3.2.4 Testing Hypothesis 3: Growth rates are governed by biovolume-specific photosynthesis rates

The efficiency with which photosynthetic rates translate into growth rates is examined in the following two ways:

**Photosynthetic Rate at Growth Saturating Irradiance**

Volume-specific electron transport rates when irradiance equalled the growth saturation parameter ($K_E$) were compared between species. The growth saturation parameter ($K_E$) indicates the irradiance at which growth rates start to become saturated in each species. Estimates of volume-specific electron transport rates ($ETR_I^{vol}$) from the photosynthesis-irradiance curves can be used to estimate photosynthetic rates when irradiance is equal to the growth saturation parameter (i.e. $I = K_E$) for each experimental condition. Comparing $ETR_I^{vol}$ when $I = K_E$ between species indicates each species' volume-specific photosynthetic

requirement for growth rate to start to become saturated. Note that photoacclimation of the photosynthetic machinery means that within a species, electron transport rates when $I = K_E$ may be different depending on the growth irradiance. Therefore, interspecific comparisons are made for each of the three growth irradiance conditions.

**Quantum Yield of Growth**

Quantum yield of growth rate ($\phi_\mu$) was calculated to quantify the efficiency with which absorbed photons are translated into growth using equations adapted from Finkel (2001).

$$\phi_\mu = \frac{\mu}{ETR_I^{vol}} \quad (3.23)$$

Where $\phi_\mu$ is the quantum yield of growth ($\mu m^3$ $electron^{-1}$), $\mu$ is exponential growth rate ($s^{-1}$) and $ETR_I^{vol}$ is volume-specific electron transport rate at growth irradiance (electrons $\mu m^{-3}$ $s^{-1}$). In this case, quantum yield of growth is measured as production of biomass (measured in terms of volume) per electron transported.

### 3.2.5 Statistical Analysis

The allometric power law states that biomass-specific variables (Y) can be described as varying with volume (V) with a constant 'a' and an exponent 'b' (Equation 3.1). The power law applies to biomass-specific rates, therefore where appropriate, parameters were normalised to cell volume, as a proxy for biomass. As described above, the following parameters were normalised to cell volume: pigment content, absorption efficiency and electron transport rates. Biomass-specific parameters scaling in direct proportion with cell volume will have an exponent $b = 0$, and deviations ($b \neq 0$) indicates scaling with size (i.e. deviations from isometry). A size scaling exponent of $b < 0$, indicates a negative scaling of the parameter with cell volume, whilst $b > 0$ indicates positive scaling. Size scaling relationships were thus investigated by log transforming data as follows:

$$\log(Y) = \log(a) + b\log(V) \quad (3.24)$$

The size scaling exponent 'b' can then be estimated by the slope of a linear regression. Estimation of the slope (b) of log-log allometric relationships in phytoplankton have variously utilised either Ordinary Least Squares (OLS) regression (Finkel, 2001; Key *et al.*, 2010; Malerba *et al.*, 2018) or Reduced Major Axis (RMA) regression (Finkel, Irwin and Schofield, 2004; Ward *et al.*, 2017). RMA can be considered a suitable regression model in this study as it is recommended where there is error in the 'x' variable (cell volume) as well as in the 'y' variable, and where the units of 'x' and 'y' are not the same (Legendre and Legendre, 2012). However, it

is not possible to use regular permutation tests to assess significance of RMA slope values (Legendre and Legendre, 2012), and it is therefore difficult to statistically compare slope values between experimental conditions (e.g. light levels), or with a theoretical value (e.g. with metabolic theory). Instead, RMA slopes are generally considered significantly non-zero based on significance of their correlation coefficient alone (McArdle, 1988). Whilst OLS is typically not recommended where there is error in the x variable, its significance can be assessed with permutation tests, and thus allows statistical comparison between experimental conditions or with theoretical values. OLS has been the regression of choice in some allometry studies, and some authors argue that it is justified where the magnitude of measurement error in 'x' has been minimised (Kilmer and Rodríguez, 2017). However, as each sample in this study is a population of individual cells within a monoculture, substantial variance in cell volume measurements is unavoidable as there is a genuine range of size of individual cells within each sample around the mean. Therefore, for completeness and ease of comparison to other studies, significant slope values calculated by both regression methods (OLS and RMA) are presented in tabular form (Table 3.5). For consistency and simplicity, OLS regressions only are plotted and reported throughout the text. It is worth noting that the type of regression used did not change the nature of the major results in this study, but it is nevertheless important to consider the regression model used, as OLS slopes are consistently attenuated in comparison to RMA slopes due to their exclusion of error consideration in the x variable.

Pearson correlation coefficients between cell volume and parameters were deemed significant at the 95 % significance level ($p < 0.05$) using GraphPad Prism (v 7.04, GraphPad Software Inc.). For significant correlations, OLS and RMA regressions were fitted with MATLAB™. Parameters with non-significant correlations with cell volume ($p > 0.05$) were considered non size scaling, as 'b' was not significantly different from 0. When OLS slope values 'b' were statistically compared between environmental conditions or to hypothetical values, an extra sum-of-squares F test (GraphPad Prism) was used, with a 95 % significance level.

**Table 3.3.** Details of the parameters calculated and plotted in subsequent Figures, with respective symbols, and units where appropriate

| Symbol | Parameter | Unit |
|---|---|---|
| $\mu_{max}$ | Maximum exponential growth rate | $d^{-1}$ |
| $\mu_{LL}$ | Exponential growth rate under low light | $d^{-1}$ |
| $K_E$ | Saturation parameter of growth-irradiance curve | μmol photons $m^{-2}$ $s^{-1}$ |
| $a^{chl}(\lambda)$ | Chl *a*-specific absorption efficiency at wavelength λ | $m^2$ (g Chl *a*)$^{-1}$ |
| $a_{sol}^{chl}(\lambda)$ | Chl *a*-specific sum of maximum absorption efficiencies of constituent pigments in solution at wavelength λ | $m^2$ (g Chl *a*)$^{-1}$ |
| $a_{model}^{chl}(\lambda)$ | Model derived Chl *a*-specific absorption efficiency at wavelength λ (based on package effect model, Morel and Bricaud, 1981) | $m^2$ (g Chl *a*)$^{-1}$ |
| $\bar{a}^{chl}$ | Spectrally averaged Chl *a*-specific absorption efficiency | $m^2$ (g Chl *a*)$^{-1}$ |
| $\bar{a}^{vol}$ | Spectrally averaged volume-specific absorption efficiency | $m^2$ $\mu m^{-3}$ |
| $\bar{a}_{model}^{chl}$ | Spectrally averaged model derived Chl *a*-specific absorption efficiency | $m^2$ (g Chl *a*)$^{-1}$ |
| Q* | Spectrally averaged ratio of $a^{chl}$ to a $a_{sol}^{chl}$ | - |
| $ETR^{PSII}$ | PSII electron transport rate | Electrons $PSII^{-1}$ $s^{-1}$ |
| $ETR_I^{vol}$ | Volume specific electron transport rate at irradiance, I | Electrons $\mu m^{-3}$ $s^{-1}$ |
| $\alpha^{PSII}$ | Initial slope of PSII ETR-irradiance curve | - |
| $\alpha^{vol}$ | Volume-specific initial slope of ETR-irradiance curve | - |
| $E_K$ | Saturation parameter of ETR-irradiance curve | μmol photons $m^{-2}$ $s^{-1}$ |
| $\bar{A}_{PS}^{vol}$ | Volume-specific photosynthetic photon absorption rate | photons $\mu m^{-3}$ $s^{-1}$ |
| $\Phi_{ETR}$ | Quantum yield of electron transport rate | Electrons $photon^{-1}$ |
| $\Phi_\mu$ | Quantum yield of growth rate | $\mu m^3$ $photon^{-1}$ |

## 3.3 Results and Discussion

Mean cell volumes (± SD) of the 10 coccolithophore strains, grown at each light intensity (25, 100 and 200 μmol photons $m^{-2}$ $s^{-1}$) spanned two orders of magnitude, from 11 $\mu m^3$ (*R. parvula*) to 2120 $\mu m^3$ (*C. braarudii*) (Figure 3.2). In 6 of the 10 strains, average cell volume was significantly smaller when grown under LL compared to ML and HL (t-test, $p < 0.05$, indicated with asterisks in Figure 3.2). Note that due to these irradiance-dependent differences in cell volume, the subsequent analyses always pairs irradiance-specific parameters with corresponding cell volumes, for volume normalisation and size scaling regression plots.

### 3.3.1 Size scaling of growth rates under optimum and low light

Exponential growth rates over all experiments ranged between 0.26 $d^{-1}$ (*H. carteri* under LL) to 1.10 $d^{-1}$ (*E. huxleyi* 1N under HL). Examples of growth-irradiance curves, used to examine the dependence of growth rate on growth irradiance, are presented for three species, including a small species (*E. huxleyi* 2N), a large species (*C. quadriperforatus*), and a species of intermediate size, which reached peak growth rate at ML (*G. oceanica*) (Figure 3.3a). When compared between species, the saturation parameter ($K_E$) of growth-irradiance curves showed no significant scaling with cell volume (Figure 3.3b), indicating that whilst there is interspecific variation in the irradiance required to reach growth saturation, it is *not* related to cell size.

There was a significant negative correlation between maximum growth rate ($\mu_{max}$) and cell volume (Figure 3.3c), consistent with that reported in other phytoplankton groups (Tang 1995; Finkel et al. 2010; Sarthou et al. 2005). The size scaling exponent ($b = -0.22 \pm 0.04$) of $\mu_{max}$ was not significantly different to the -0.25 predicted by metabolic theory (extra sum-of-squares F test, $p > 0.05$), meaning the steepness of the scaling relationship is also consistent with the value expected for optimal growth conditions (Banavar et al. 2002b; West et al. 1999; West 1997).

Growth rate under LL ($\mu_{LL}$) also correlated negatively with cell volume (Figure 3.3d) but the exponent of the relationship was higher ($-0.12 \pm 0.03$) compared to optimal conditions, and was significantly different from the -0.25 predicted by metabolic theory (extra sum-of-squares F test, $p < 0.05$). The increase in size scaling exponent under LL was unexpected, and sits in contrast to an expected decrease in exponent predicted by both theory and experimental evidence from other phytoplankton groups (Finkel 2001; Finkel et al. 2004; Mei et al. 2009). Deviation from a scaling exponent of -0.25 is often observed under sub-optimal growth conditions, where acquisition of the limiting resource is size dependent. In this case, acquisition of the resource (light energy) is expected to be more challenging for large cells, due

to increasing package effects with cell size, and thus the size scaling exponent is expected to decrease (i.e. $b < -0.25$). In contrast to these expectations, the large coccolithophore cells in this study maintained growth rates near maximal under low light, whilst small cells experienced marked reduction in growth rates under low light. For these coccolithophore species, there was an increase in size scaling exponent of growth rate under LL, in contrast to expectation. To explore this unexpected result, a detailed analysis of the size dependence of light harvesting, package effects, and photosynthetic efficiency is used to determine where the physiology of coccolithophores deviates from the theoretical framework.

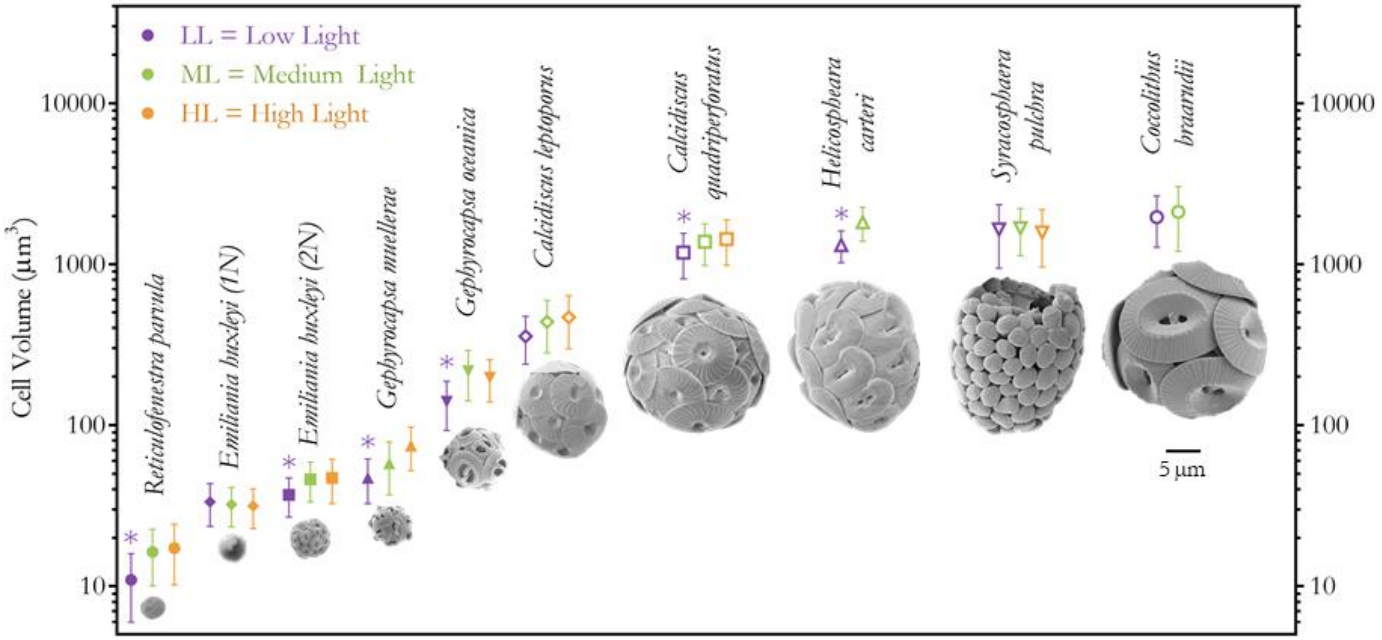


**Figure 3.2.** Mean cell volumes (± SD) of the 10 coccolithophore strains, sampled during exponential growth phase, grown at LL, ML and HL (25, 100 and 200 µmol photons $m^{-2}$ $s^{-1}$, respectively). Purple asterisks indicate where cell volume for a particular species was statistically significantly smaller under low light, compared to both medium and high light (t-test, $p < 0.05$). Accompanying SEM images (credit Jeremy Young, UCL) scaled according to coccosphere diameter grown at low light.

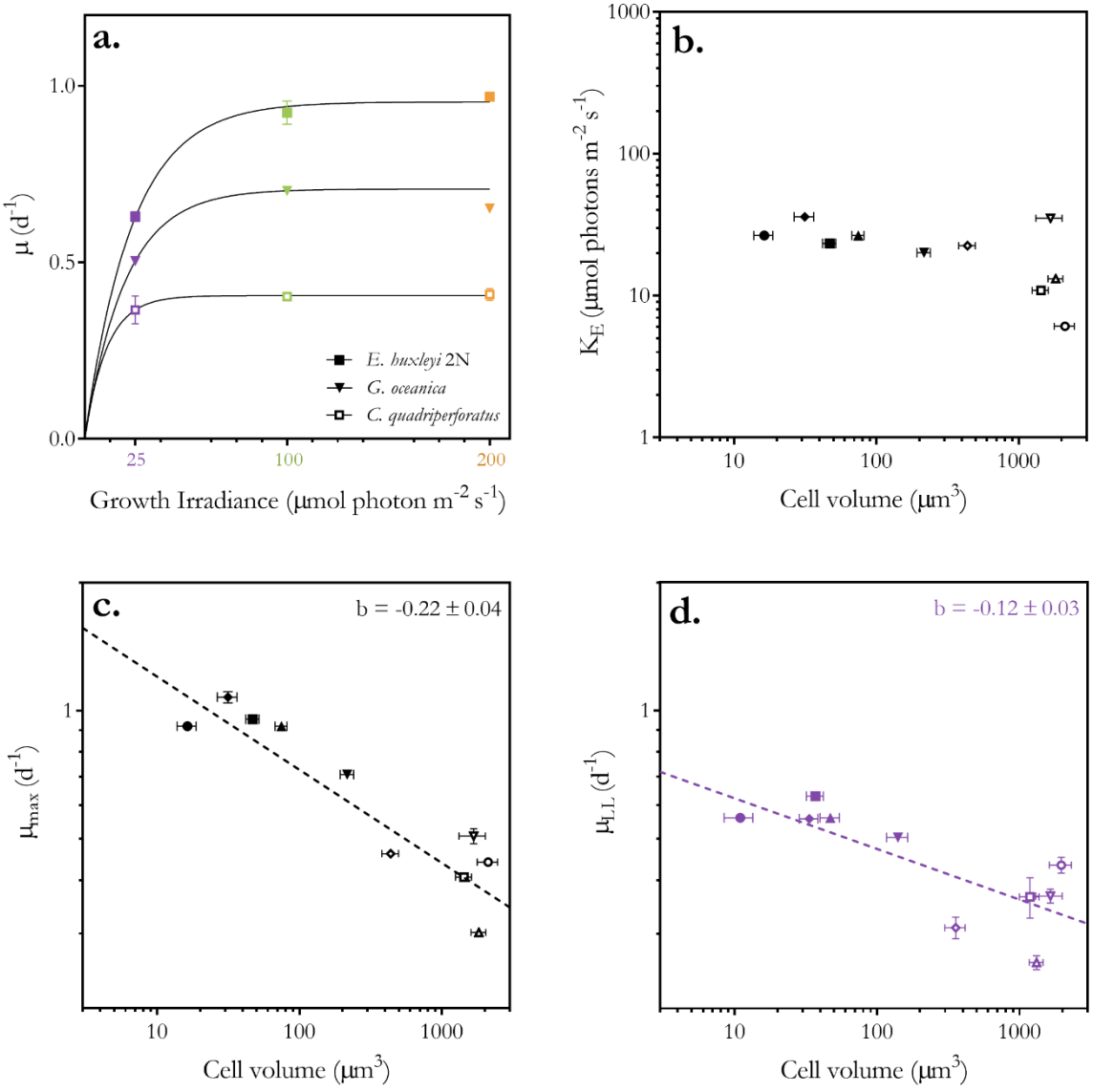


**Figure 3.3.** a) Growth rate-irradiance relationships for a small species (*E. huxleyi*, filled square) a large species (*C. quadriperforatus*, unfilled square), and an intermediate size species, that reaches peak growth rate at ML (*G. oceanica*, triangle), with Poisson fits. Data coloured according to growth irradiance as in Figure 3.2 (LL = purple, ML = green, HL = orange). b) Saturation coefficient ($K_E$) of the growth rate-irradiance relationships for all 10 coccolithophore species plotted against cell volume. c & d) Size scaling relationships for maximum growth rate ($\mu_{max}$, black) and growth rate under low light ($\mu_{LL}$, purple), both with OLS linear regression (dashed line), and size scaling exponent 'b' (± SD) indicated. Symbol shapes correspond to species as in Figure 3.2.

### 3.3.1 Hypothesis 1:

**Do size-dependent package effects govern pigment densities in the cell?**

All species showed evidence of photoacclimation, with highest pigment densities in all species occurring when grown under the lowest irradiance (Figure 3.4). A detailed analysis of the changes in pigment complement involved in photoacclimation to different irradiances is found in Chapter 2. All species contained large quantities of accessory pigments (more than half of total pigment), but crucially, the ratio of Chl *a* to photosynthetic accessory pigments was relatively conserved in all species and growth conditions (see Chapter 2). Normalisation of subsequent analyses to Chl *a* concentrations is, therefore, both reasonable (as a good indicator of relative pigment content) and consistent with existing literature.

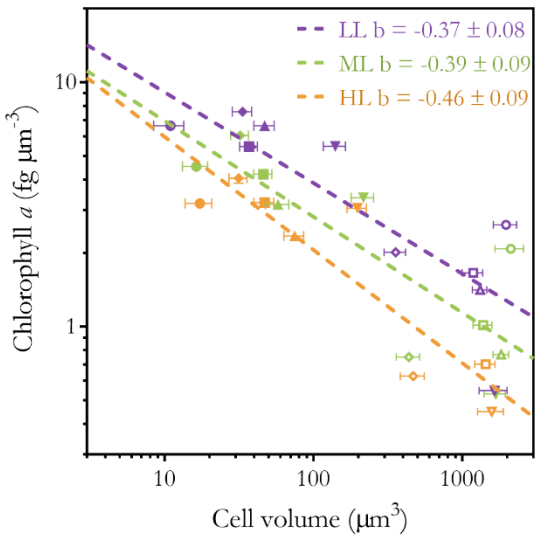


**Figure 3.4.** Size scaling of Chl *a* density for all 10 coccolithophore species, plotted on log-log axes. Data coloured according to growth irradiance as in Figure 3.2 (LL = purple, ML = green, HL = orange). Symbol shapes correspond to species as in Figure 3.2. For each growth irradiance, dashed lines show corresponding OLS linear regressions, and size scaling exponent 'b' (± SD).

The range of Chl *a* densities between species was large (Figure 3.4). Under LL, for example, there was a 14-fold difference between the most highly pigmented species (7.57 fg $\mu m^{-3}$, *E. huxleyi* 1N) and the least pigmented species (0.55 fg $\mu m^{-3}$, *S. pulchra*). A significant negative correlation between pigment density and cell volume was found under all growth irradiances (Figure 3.4, $p < 0.05$), meaning large strains had lower pigment densities than the small strains. Chl *a* density (fg $\mu m^{-3}$) scaled with an exponent of between -0.37 ± 0.08 under LL to -0.46 ± 0.09 under HL. The exponents are steeper than -0.33, the exponent predicted by a cost-

benefit pigment production analysis (Finkel, Irwin and Schofield, 2004), and as such can be interpreted as evidence that the increased package effects inherent to large cells constrains pigment densities.

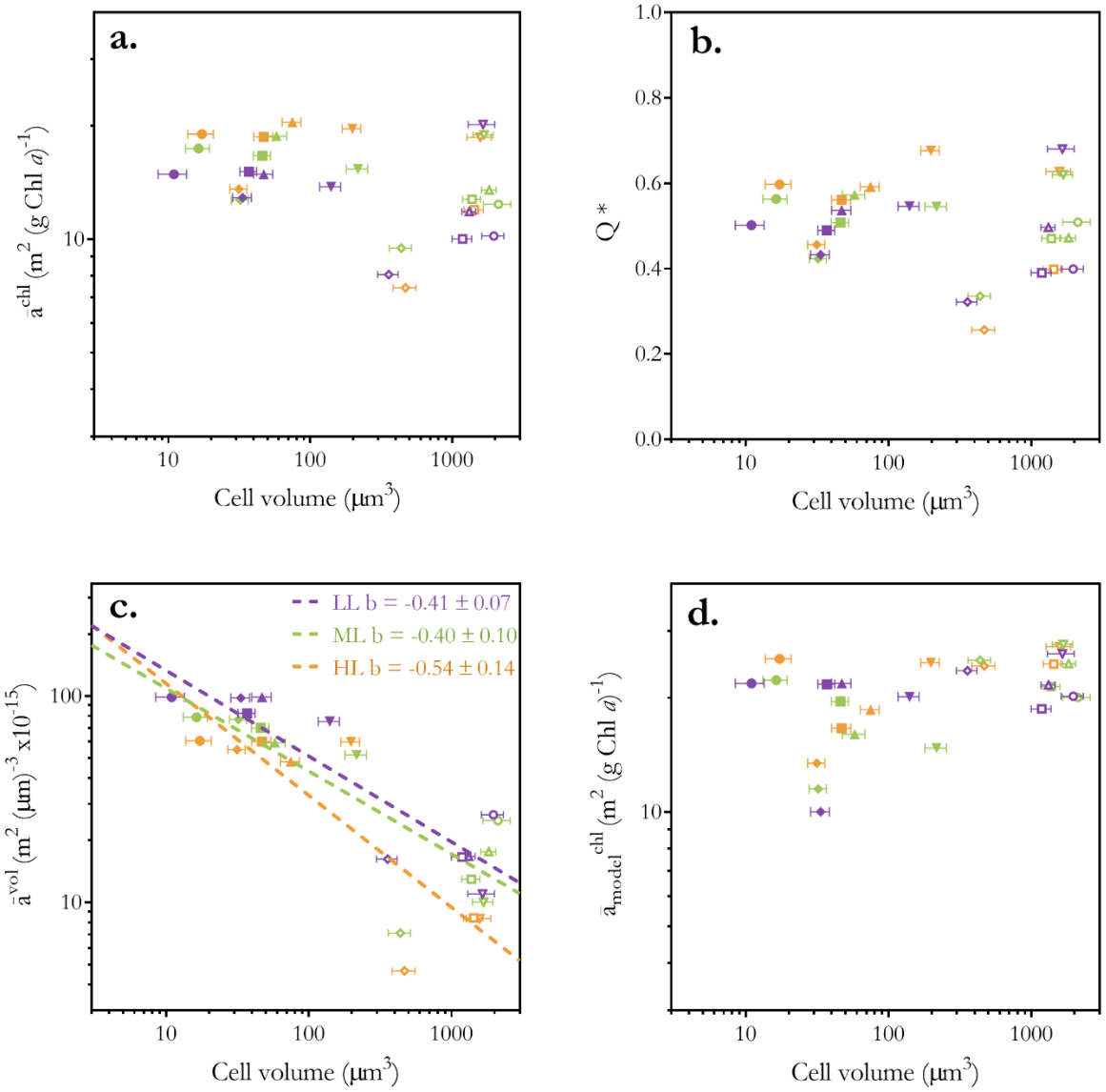


**Figure 3.5.** a) Spectrally averaged Chl *a*-specific absorption efficiency ($\bar{a}^{chl}$), b) Packaging factor Q*, c) spectrally averaged volume-specific absorption efficiencies ($\bar{a}^{vol}$) with corresponding OLS linear regressions (size scaling exponents 'b' ± SD indicated) and d) spectrally averaged model predicted absorption efficiencies ($\bar{a}_{model}^{chl}$) for all 10 coccolithophore species, plotted against cell volume, on log-log scales. Data coloured according to growth irradiance as in Figure 3.2 (LL = purple, ML = green, HL = orange). Symbol shapes correspond to species as in Figure 3.2.

The effects of packaging on the efficiency of light absorption were examined using spectrally averaged Chl *a*-specific absorption efficiency data ($\bar{a}^{chl}$). Intra-specifically, there was variation in $\bar{a}^{chl}$ between growth irradiances, with most, but not all, coccolithophore species having higher $\bar{a}^{chl}$ under high light conditions (Figure 3.5a). There was also variation in $\bar{a}^{chl}$ between species, though it was not related to cell size, as no correlation between $\bar{a}^{chl}$ and cell volume was seen (Figure 3.5a). The packaging factor, Q*, shows that Chl *a*-specific absorption efficiencies are between 32 % and 68 % of maximum absorption efficiency of the constituent pigments in solution (in *C. leptoporus* and *S. pulchra* respectively, under low light) (Figure 3.5b). Again, no correlation between Q* and cell volume was observed, meaning that overall, despite > 100-fold differences in cell volume between the species examined, pigments in large celled species were not absorbing light less efficiently than the small celled species.

Pigment-specific absorption efficiencies have been observed to scale negatively with cell size in other groups such as the diatoms and dinoflagellates (Finkel 2001; Suggett *et al.*, 2015), as packaging effects increase with cell size. However, pigmentation also has a strong influence on the degree of packaging (Kirk, 1976; Morel and Bricaud, 1981). Pigment density scales negatively with cell volume in the coccolithophores in this study (Figure 3.4), meaning decreases in $\bar{a}^{chl}$ due to pigmentation should be higher in small, more highly pigmented cells. Volume normalised absorption efficiencies ($\bar{a}^{vol}$) reveal the important role of pigment density on packaging in coccolithophores. A negative correlation between $\bar{a}^{vol}$ and size was found under all growth irradiances (Figure 3.5c) with exponents ranging from -0.40 ± 0.10 to -0.54 ± 0.14. The negative size scaling of $\bar{a}^{vol}$ is driven directly by the negative size scaling of pigment densities, and indicates that per unit of cell biovolume, large cells are less efficiently absorbing light. It is important to consider the change in currency from pigment to volume-specific absorption efficiency, as it is biovolume-specific absorption efficiencies that directly impact the biovolume-specific rates of light absorption that drives biovolume-specific photosynthesis.

The interactive effects of cell size and pigment density on packaging are revealed by model predicted absorption efficiencies, $\bar{a}_{model}^{chl}$ (Morel and Bricaud, 1981). No correlation between expected absorption efficiency ($\bar{a}_{model}^{chl}$) and cell size was identified, at any of the growth irradiances studied (Figure 3.5d), indicating that the size scaling of pigment densities in coccolithophores can somewhat counteract the influence of size-dependant package effects. The large celled coccolithophore species had restricted pigment density within their cells, which resulted in similar $\bar{a}^{chl}$ values to their smaller counterparts, under a range of growth irradiances. The model often overestimated absorption efficiency (Figure 3.5), probably due to assumptions made in the model that are not met by the cells. For example, the model assumes homogenous distribution of pigment throughout the total volume of the cell, whilst in reality,

pigment is packaged within discrete chloroplasts, increasing the potential for self-shading and package effects. Importantly for this work, there was no size-dependence in the difference between measured and model derived $\bar{a}^{chl}$, indicating that absorption efficiencies in these coccolithophores do not deviate from theoretical predictions in a size dependent fashion.

Negative size scaling of $\bar{a}^{chl}$ has been observed in some other phytoplankton groups, such as the diatoms and dinoflagellates (Finkel, 2001; Suggett *et al.*, 2015), with a relatively shallow reported exponent of ~ -0.08. Whilst the absence of significant size scaling of $\bar{a}^{chl}$ in the coccolithophores could be due to measurement error, or because the size range of coccolithophores is somewhat smaller than the size range within some other groups, it is more likely to be because of the steep size scaling of pigment densities, as previously discussed. Steeper size scaling of pigment densities in coccolithophores (exponent of -0.40 to -0.54) than in the diatoms or predicted by a cost-benefit model (exponent of -0.33, Finkel et al. 2004) is likely to contribute to smaller disparities in Chl *a*-specific absorption efficiencies between large and small coccolithophore cells.

Pigment density and absorption efficiency results indicate that in coccolithophores, the size-dependence of package effects result in restriction of pigment densities and volume-specific absorption efficiencies in large cells, entirely in keeping with mechanistic theory. There is, therefore, no evidence in this data set that coccolithophores have any unusual pigment or light absorption properties that could help mechanistically explain the unexpected increase in size scaling growth exponent under low light.

### 3.3.2 Hypothesis 2: Are biovolume-specific photosynthetic rates governed by light absorption rates?

Photosynthesis – irradiance curves from variable fluorescence data demonstrate rates of photosynthetic electron transport at PSII. Example curves from a small cell (*E. huxleyi*) and a large cell (*C. quadriperforatus*), both acclimated to the three growth irradiances, demonstrate the shapes and hyperbolic tangent curve fits of variable fluorescence light curve data (Figure 3.6a). Within species, growth irradiance affected the PSII-specific rates of electron transport in the higher irradiance portion of the curves (> 100 μmol photon $m^{-2}$ $s^{-1}$), and there was interspecific variation. The gradient of the early portion of the curve ($\alpha^{PSII}$) varied between strains from 1.87 (*C. braarudii*) to 4.18 (*G. muellerae*), revealing differences in the efficiency of utilisation of available light for photosynthetic electron transport at PSII (Figure 3.6b).

However, $\alpha^{PSII}$ did not correlate with cell volume, indicating that differences in the utilisation of light for electron transport at PSII did not scale with cell size (Figure 3.6b).

Pigment density (Figure 3.4) has important consequences for conversion of $ETR^{PSII}$ to a biovolume-specific currency. By definition, the number of RCIIs is directly related to pigment density, as pigments form part of the PSU surrounding the RCs. Converting the currency of photosynthesis to a biovolume-specific measure ($ETR^{vol}$) reveals greater differences between species than a PSII-specific currency (Figure 3.6c). For example, volume-specific rates of electron transport ($ETR^{vol}$) are consistently higher throughout the curve in the small species *E. huxleyi* than in the large species *C. quardriperforatus*, in cells acclimated to all three irradiances (Figure 3.6c). A significant negative correlation was found between $\alpha^{vol}$ and cell volume (Figure 3.6d), with size scaling exponents ranging from -0.45 ± 0.09 grown at LL to -0.56 ± 0.15 grown at HL, indicating that per unit of biovolume, small species were more efficient at using available light for electron transport than the large species. Lower pigment densities in large cells limits the volume-specific light absorption rate, which in turn directly results in lower volume-specific photosynthetic electron transport rates in large cells.

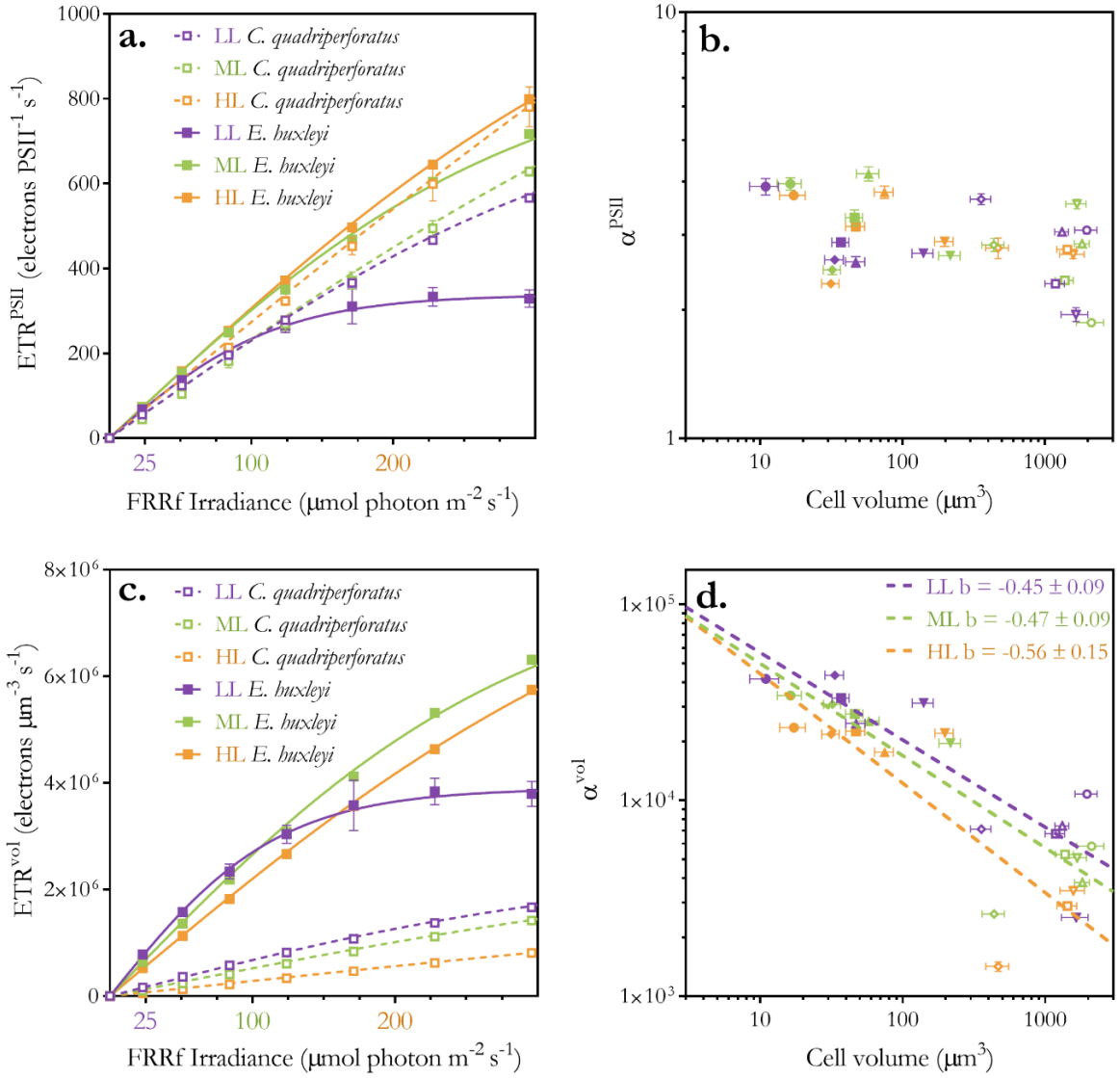


**Figure 3.6.** a) PSII-specific electron transport rates ($ETR^{PSII}$) calculated from variable fluorescence measurements (see methods) plotted against irradiance delivered by LEDs in the fluorometer, for *E. huxleyi* (filled squares) and *C. quadriperforatus* (unfilled squares). Hyperbolic tangent fits are shown. b) $\alpha^{PSII}$, the gradient of the early portion of $ETR^{PSII}$ curves for all 10 species, at each light level, plotted against cell volume, on a log-log scale. c) Volume-specific electron transport rates ($ETR^{vol}$, see methods) plotted against irradiance delivered by LEDs in the fluorometer for *E. huxleyi* (filled squares) and *C. quadriperforatus* (unfilled squares), with hyperbolic tangent fits. d) $\alpha^{vol}$, the gradient of the early portion of $ETR^{vol}$ curves for all 10 species, at each light level, plotted against cell volume, on a log-log scale, with corresponding OLS linear regressions (size scaling exponents 'b' ± SD indicated). All data coloured according to growth irradiance as in Figure 3.2 (LL = purple, ML = green, HL = orange). Symbol shapes correspond to species as in Figure 3.2.

Intra-specifically, photosynthetic photon absorption rates ($\bar{A}_{PS}^{vol}$) and electron transport rates at growth irradiance ($ETR_I^{vol}$) were always higher when growth irradiance was higher (Figure 3.7a), as both depend heavily on the amount of available irradiance in the growth incubator. There was large variation in $\bar{A}_{PS}^{vol}$ between species at any given irradiance, for example, ranging by a factor of 10 between *S. pulchra* and *E. huxleyi* 1N grown under LL ($9.20 \times 10^4$ to $92.06 \times 10^4$ photons $\mu m^{-3}$ $s^{-1}$, respectively). Negative size scaling correlations were identified in both $\bar{A}_{PS}^{vol}$ and $ETR_I^{vol}$, under all growth irradiances (Figure 3.7a & b). At a given light level, the size scaling of the rate of both $\bar{A}_{PS}^{vol}$ and $ETR_I^{vol}$ is influenced by the size scaling in pigment density (Figure 3.4), as there was no size-dependence of either pigment-specific absorption efficiency (Figure 3.5a) or PSII-specific photosynthetic efficiency (Figure 3.6b). Dividing electron transport rates ($ETR_I^{vol}$, Figure 3.7b) by absorption rates ($\bar{A}_{PS}^{vol}$, Figure 3.7a) estimates the quantum yield of electron transport ($\phi_{ETR}$), the electrons transported per photon absorbed by the photosynthetic pigments. There was some variation in $\phi_{ETR}$ between species, but no correlation with cell volume was found (Figure 3.7c), indicating that the efficiency with which photons absorbed by the photosynthetic pigments are used to drive photosynthesis is not size-dependent.

The absence of size-dependence in photosynthetic efficiencies, both relative to available photons ($\alpha^{PSII}$) and absorbed photons ($\phi_{ETR}$), show that whilst there is variation in photosynthetic efficiency between species of coccolithophore, there is no indication that size-dependent differences in photophysiology can explain the unexpected increase in the size scaling growth exponent under LL. Biovolume-specific electron transport rates were effectively governed by pigment densities, in keeping with the theoretical framework.

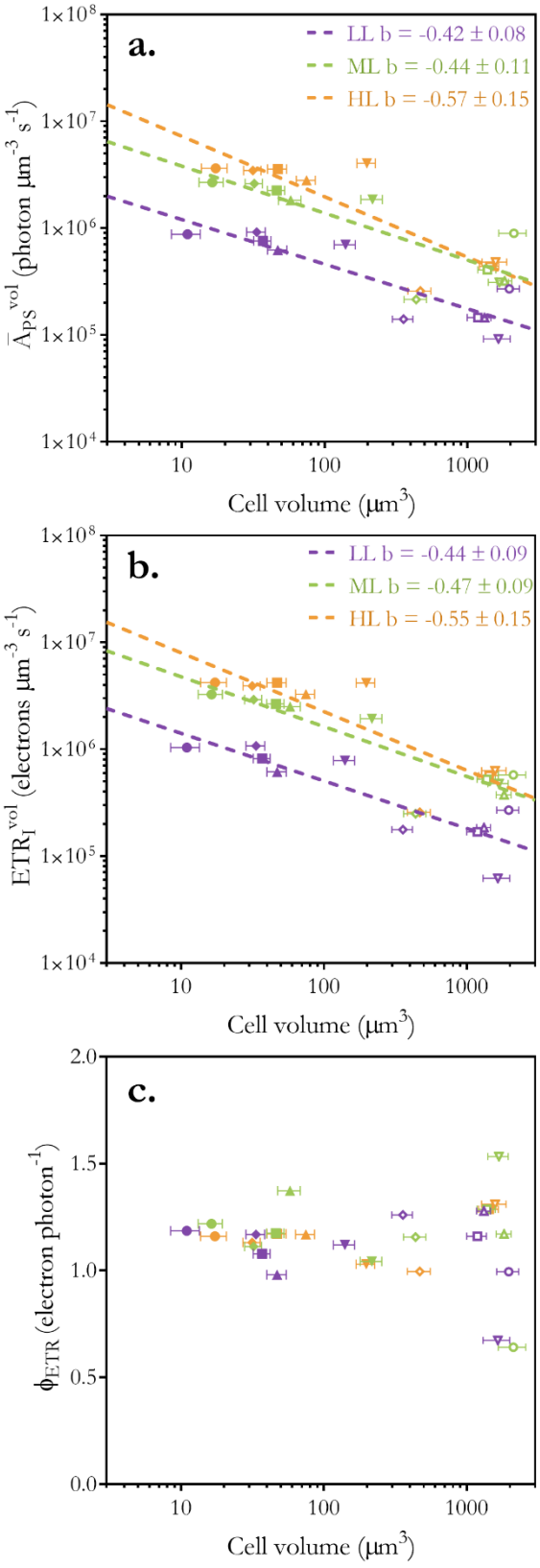


**Figure 3.7.** a) Volume-specific rate of light absorption by photosynthetic pigments ($\bar{A}_{PS}^{vol}$). b) Volume-specific electron transport rate ($ETR_I^{vol}$). c) Quantum yield of electron transport ($\phi_{ETR}$) for all 10 coccolithophore species (symbols as in Figure 3.2), at each growth irradiance (colours as in Figure 3.2). Where appropriate, corresponding OLS linear regressions (size scaling exponents 'b' ± SD) are indicated.

### 3.3.3 Hypothesis 3: Are growth rates governed by biovolume-specific photosynthesis rates?

The photosynthetic requirements of cells for reaching growth saturation were compared in order to examine if growth rate is directly governed by photosynthetic electron transport rate when light is limiting. Volume-specific electron transport rates ($ETR_I^{vol}$) when irradiance (I) equalled the growth saturation irradiance ($K_E$, Figure 3.3b) were negatively correlated with cell volume (Figure 3.8a). Negative size scaling exponents (-0.61 ± 0.06 under LL to -0.64 ± 0.17 under HL) indicate that growth rate begins to saturate at lower volume-specific electron transport rates in large cells rather than in small one (Figure 3.8a) and demonstrate that the required volume-specific ETR to reach maximum growth rate was lower in large cells.

The quantum yield of growth ($\phi_\mu$) indicates the efficiency with which electron transport drives biovolume production. A positive correlation was found between $\phi_\mu$ and cell volume under the low light treatment (Figure 3.8b), with higher $\phi_\mu$ in large cells. A positive size scaling exponent of $\phi_\mu$ (0.33 ± 0.08) indicates that large coccolithophores are more efficient at converting photosynthetic electron transport into biovolume production under LL. No significant correlation between $\phi_\mu$ and cell volume was found for ML or HL treatments.

The apparent size-dependent differences in growth efficiency under LL (negative size scaling of $ETR^{vol}$ when $I = K_E$ and the positive size scaling of $\phi_\mu$, Figure 3.8) were not predicted by the theoretical framework set out in Table 3.1. The assumption that under low light conditions, growth rate is directly governed by biovolume-specific electron transport rate (Hypothesis 3), does not prove valid for the coccolithophores. However, patterns are highly dependent on the currency used (i.e. the proxy of biomass used). Normalisation of parameters to other measures of biomass, such as dry weight or organic carbon content, would reveal different size scaling relationships if they themselves scale with cell size. The unexpected increase in size scaling growth exponent under LL could be reconciled with the current theoretical framework if carbon density in the coccolithophores were to scale negatively with cell volume, for example. Lower carbon densities in large cells would mean lower volume-specific carbon demand, and thus could explain the apparent lower volume-specific ETR requirement for achieving maximum growth rate (Figure 3.8a), and quantum yield of growth (Figure 3.8b) in the larger coccolithophores.

There is co-variation of cell size and taxonomy within the coccolithophores used in this study, as the five smallest coccolithophore strains all belong to the isochrysidale taxonomic order,

containing most of the typical bloom-forming species (e.g. *E. huxleyi*), whilst the larger cells belong to other orders. The coccolithophores as a group are often considered functionally homogenous, yet research in several areas continues to reveal species level differences between coccolithophore taxa. For example, differences in requirement for calcification (Walker *et al.*, 2018) and nutrient demands (Durak *et al.*, 2016), differences in inorganic carbon to organic carbon ratios, and apparent mixotrophy (Houdan *et al.*, 2006; Rokitta *et al.*, 2011), and motility in species such as *H. carteri* and *S. pulchra* in this study. These differences in life strategy could result in differential allocation of resources or energetic demands between the different species of coccolithophore, and could ultimately drive the unexpected resilience to growth rate limitation under LL in the large coccolithophores observed in this study. Further exploration of cellular composition and metabolic rates (carbon fixation, respiration and production of other metabolites) could reveal size or taxonomy-dependent differences in the physiological strategies of coccolithophores, and will be discussed further in Chapter 5.

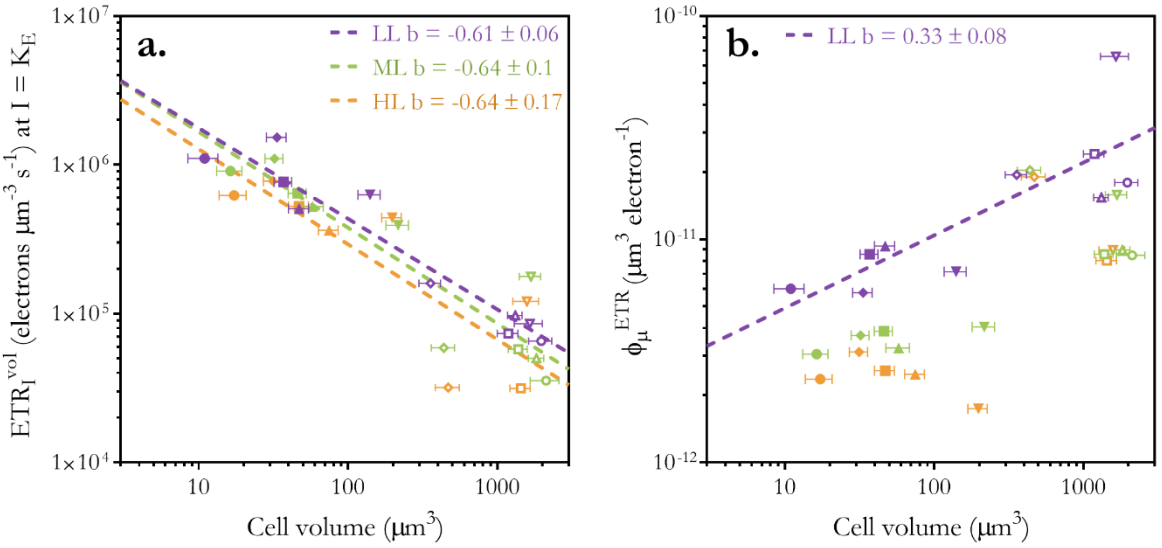


**Figure 3.8.** a) Volume-specific electron transport rates ($ETR_I^{vol}$) when irradiance equalled the growth saturation parameter ($K_E$). b) Quantum yield of growth ($\phi_\mu$) for all 10 coccolithophore species (symbols as in Figure 3.2), at each growth irradiance (colours as in Figure 3.2). Where appropriate, corresponding OLS linear regressions (size scaling exponents 'b' ± SD) are indicated.

## 3.4 Summary and Conclusion

Within the coccolithophores, the size scaling exponent of $\mu_{max}$ ($b = -0.22 \pm 0.04$) was not significantly different to the -0.25 predicted by metabolic theory (Figure 3.3c). However, LL growth rates ($\mu_{LL}$) scaled with cell volume with a higher exponent ($-0.12 \pm 0.03$, Figure 3.3d), than expected. This unexpected increase in size scaling exponent of growth rate under LL could not be explained by unusual pigment content or light absorption efficiencies (Figures 3.4 & 3.5), nor by differences in photosynthetic efficiency as probed by variable fluorescence (Figures 3.6 & 3.7), as trends in both were entirely in keeping with the theoretical framework developed (Table 3.4). Results show negative size scaling of pigment density (likely driven by the pressures of size-dependent packaging on the cells) with concomitant negative size scaling of volume-specific light absorption and electron transport rates. However, unexpected size-dependent differences in the efficiency with which the cells translated electron transport into growth were revealed (Figure 3.8), providing some insight into how the large coccolithophore cells maintain growth rates near maximal under LL, whilst small species suffered. The key to understanding the unexpectedly high size scaling exponent of growth rate under LL in coccolithophores is in primary production processes *downstream* of light absorption and electron transport.

**Table 3.4.** Summary of results in the context of the theoretical framework detailed in Table 3.1. Concurrence with, or deviation from, the theory is indicated.

| | Theory | | Result |
|---|---|---|---|
| **1** | Size-dependent package effects govern pigment densities in the cell |  | Pigment density scaled negatively with cell volume (Figures 3.4 & 3.5), probably due to the size-dependent pressures of package effects. |
| **2** | Biovolume-specific photosynthetic rates are governed by light absorption rates |  | Biovolume-specific photosynthetic electron transport rates were governed by negative scaling of biovolume-specific light absorption rates (Figures 3.6 & 3.7), as photosynthetic efficiency at PSII was not size-dependent (Figure 3.6), |
| **3** | Growth rates are governed by biovolume-specific photosynthesis rates |  | Large cells reached growth rate saturation at a lower biovolume-specific electron transport rate than small cells, and were more efficient at translating photosynthetic electron transfer into growth under LL (Figure 3.8). |

**Table 3.5.** Parameters found to scale significantly with cell volume (Pearson correlation coefficient, $p < 0.05$), and details of their respective correlation and regression statistics, including $p$-values, $R^2$ values and size scaling exponent 'b' ± SD calculated using OLS method (Ordinary Least Squares), and 'b' calculated using RMA method (Reduced Major Axis).

| Variable | Growth Irradiance | $p$ value | $R^2$ | Size scaling Exponent 'b' | |
|---|---|---|---|---|---|
| | | | | OLS ± SD | RMA |
| $\mu_{max}$ | N/A | 0.001 | 0.77 | -0.22 ± 0.04 | -0.25 |
| $\mu_{LL}$ | LL | 0.007 | 0.61 | -0.12 ± 0.03 | -0.15 |
| Chl *a* density | LL | 0.002 | 0.72 | -0.37 ± 0.08 | -0.44 |
| | ML | 0.002 | 0.70 | -0.39 ± 0.09 | -0.47 |
| | HL | 0.002 | 0.82 | -0.46 ± 0.09 | -0.51 |
| $\bar{a}^{vol}$ | LL | 0.000 | 0.82 | -0.41 ± 0.07 | -0.46 |
| | ML | 0.003 | 0.68 | -0.40 ± 0.1 | -0.49 |
| | HL | 0.008 | 0.72 | -0.54 ± 0.14 | -0.64 |
| $\alpha^{vol}$ | LL | 0.001 | 0.77 | -0.45 ± 0.09 | -0.51 |
| | ML | 0.001 | 0.79 | -0.47 ± 0.09 | -0.53 |
| | HL | 0.010 | 0.69 | -0.56 ± 0.15 | -0.67 |
| $\bar{A}_{PS}^{vol}$ | LL | 0.001 | 0.78 | -0.42 ± 0.08 | -0.47 |
| | ML | 0.003 | 0.68 | -0.44 ± 0.11 | -0.53 |
| | HL | 0.009 | 0.70 | -0.57 ± 0.15 | -0.67 |
| $ETR_I^{vol}$ | LL | 0.001 | 0.77 | -0.44 ± 0.09 | -0.51 |
| | ML | 0.001 | 0.78 | -0.47 ± 0.09 | -0.53 |
| | HL | 0.012 | 0.68 | -0.55 ± 0.15 | -0.67 |
| $ETR_{KE}^{vol}$ | LL | 0.000 | 0.92 | -0.61 ± 0.06 | -0.64 |
| | ML | 0.000 | 0.83 | -0.64 ± 0.1 | -0.70 |
| | HL | 0.009 | 0.71 | -0.64 ± 0.17 | -0.76 |
| $\phi_\mu$ | LL | 0.003 | 0.68 | 0.33 ± 0.08 | 0.39 |

# Chapter 4 Coccolithophore Community Distribution in Summer in a Shelf Sea (Celtic Sea)


## Abstract

Temperate shelf seas are regions of disproportionately high biological productivity, where coccolithophores can be an important seasonal component of the phytoplankton community. The vertical and horizontal patterns in diversity and abundance of the coccolithophore community in the Celtic Sea were investigated during summer 2015 when the water column was strongly stratified. On a cross shelf transect from the central shelf to the shelf-break, 35 coccolithophore species were identified, with *Emiliania huxleyi* the most numerically abundant species (64 % of the 10,436 cells identified). There were differences in the coccolithophore community between the strongly stratified shelf compared with the shelf-break (where there was evidence of increased mixing of the water column). Coccolithophore cell abundance and species diversity were higher at the shelf-break (up to 208 cells $mL^{-1}$, typically > 20 species) than on the shelf (< 120 cells $mL^{-1}$, < 5 species). Statistical differences in species composition (based on the Bray-Curtis dissimilarity matrix) were greater between shelf and shelf-break samples (ANOSIM R-stat 0.463, $p < 0.001$) than between samples grouped into depth categories (upper, lower and sub-euphotic zones); this indicates that horizontal differences in species composition were greater than vertical differentiation. High dissimilarity of species composition between communities at different points along an on shelf transect indicate that coccolithophore communities were patchily (non-homogenously) distributed across the shelf. Although the coccolithophores did not form the majority of the total phytoplankton community biomass, ancillary data suggests that the other phytoplankton groups (pico- and nano-eukaryotes) exhibit similar heterogeneous spatial patterns in abundance and diversity across the shelf. These results contrast with findings from open ocean coccolithophore communities, where vertical differentiation is strong and communities from depth horizons were statistically similar over large horizontal distances (hundreds of kilometres), and indicate the unique and dynamic nature of plankton community structure in shelf seas.

## 4.1 Introduction

### The Celtic Sea shelf environment

Shelf seas are the shallow regions (typically < 200 m deep) of the continental margins, extending out from the coast to the shelf-break, where the seabed then slopes steeply down to the abyssal plain. Whilst comprising only ~ 9 % of the area of global ocean, shelf seas are disproportionately productive regions, responsible for up to 30 % of total ocean primary production (Wollast, 1998; Muller-Karger *et al.*, 2005; Simpson and Sharples, 2012), and support an estimated 90 % of global fish catches (Pauly *et al.*, 2002).

The Celtic Sea, on the NW European shelf (see map Figure 4.1), is a temperate region where a seasonal cycle of thermal stratification influences the annual cycle of productivity (Pingree, Holligan and Mardell, 1978; Sharples and Holligan, 2006; Simpson and Sharples, 2012). The water column is well mixed during winter, and becomes stratified during spring as irradiance and surface water temperature increases, triggering development of a spring phytoplankton bloom. By summer, the water is thermally stratified, and nutrients have been drawn down to low levels (e.g. nitrate < 0.1 μmol $L^{-1}$) in the water column above the thermocline (known as the surface mixed layer; SML). Thus, summer phytoplankton productivity on the shelf is typically nutrient limited in the surface, and a chlorophyll maximum develops at the base of the SML, where there is both enough light to drive photosynthesis, and access to sufficient nutrients (Hickman *et al.*, 2009, 2012). The gradients in light and nutrient availability in the stratified water column typically result in vertical gradients of taxonomic composition of phytoplankton in shelf seas, with small picoplankton (e.g. *Synechococcus*) in the surface and large-celled phytoplankton such as diatoms and dinoflagellates in the chlorophyll maximum (Joint, Owens and Pomeroy, 2007; Hickman *et al.*, 2009; Barnett *et al.*, 2019). However, the physical and biological structure of the water column is not stable, as transient bursts of productivity in the SML are fuelled by wind or tidal turbulence-driven nutrient pulses (Simpson and Hunter, 1974; Williams *et al.*, 2013).

At the shelf-break the different regimes of shelf and the deep ocean meet, and important mixing, upwelling and vertical exchange processes occur (Holligan, 1981; Pingree and Mardell, 1981; Marra, Houghton and Garside, 1990; Garcia *et al.*, 2008). Enhanced mixing at the shelf-break in the Celtic Sea results in a band of cooler surface water along the shelf edge (Harlay *et al.*, 2010; Simpson and Sharples, 2012; Ruiz-Castillo *et al.*, 2018) where the thermocline and nutricline tend to be broader (Sharples *et al.*, 2007; Hickman *et al.*, 2012). Productivity is enhanced at the shelf-break (Joint *et al.*, 2001) and the phytoplankton community can be distinct when compared to the adjacent shelf and open Atlantic Ocean (Sharples *et al.*, 2007).

For example, in summer 2005, eukaryotes were typically more abundant at the shelf-break than in surface shelf waters, where small prokaryotic *Synechococcus* cells were more abundant. There is also evidence of differences in community composition within taxonomic groups (e.g. diatoms) between shelf and shelf-break regions (Sharples *et al.*, 2007; Poulton *et al.*, 2019). The transect in the present survey spanned over 400 km of the Celtic Sea shelf, including the area at the shelf-break, capturing hydrographic differences across this dynamic region.

**Coccolithophore communities in the Celtic Sea**

Coccolithophores are a diverse group of calcifying plankton that can form an important component of regional phytoplankton communities, including in temperate shelf seas where they can bloom in high cell concentrations (Holligan *et al.*, 1983; Garcia-soto *et al.*, 1995; Buitenhuis *et al.*, 1996; Iglesias-Rodriguez *et al.*, 2002; Rees *et al.*, 2002; Krueger-Hadfield *et al.*, 2014). Summer blooms of *E. huxleyi* are a recurring annual feature on the NW European shelf, where characteristic excessive shedding of coccoliths causes a high reflectance signature (Holligan *et al.*, 1983). Coccolithophore abundance typically peaks during spring and again later in the summer in shelf waters (Widdicombe *et al.*, 2010; Tarran and Bruun, 2015). Efforts to understand the conditions favouring growth of *E. huxleyi* have identified factors such as shallow mixed layers, high light and temperatures, and low nitrate to phosphate ratios as conductive to bloom formation (Iglesias-Rodriguez *et al.*, 2002; Tyrrell and Merico, 2004). However, there is an increasing appreciation that coccolithophores co-occur with other phytoplankton groups (De Souza *et al.*, 2012; Poulton *et al.*, 2014; Daniels *et al.*, 2015; Hopkins *et al.*, 2015), and that they can be an important component of the phytoplankton community in non-bloom conditions. For example, an analysis using marker pigments suggest that throughout the summer, prymnesiophytes (a group which includes the coccolithophores) are a dominant group of phytoplankton in the Celtic Sea (Joint *et al.*, 2001).

The coccolithophores are a diverse group comprising over 280 species (Young *et al.*, 2003). Detailed taxonomic data about the coccolithophore community is rarer than estimates of coccolithophore abundance based on reflectance signature, as identifying coccolithophores to species level requires special microscopy methods like Scanning Electron Microscopy (SEM) and taxonomic expertise. Such community composition data is valuable, however, as it ensures the rest of the coccolithophore community (other than *E. huxleyi*) is not overlooked. Additionally, differential depth distributions throughout the water column can be investigated, rather than the focus being on surface waters (< 5-10 m) only. Studies have revealed that different coccolithophore species have different environmental preferences and distributions, with both horizontal and vertical (depth) patterns in coccolithophore assemblage (McIntyre

and Bé, 1967; Winter and Siesser, 1994; Boeckel and Baumann, 2008; Charalampopoulou *et al.*, 2011). For example, in the stratified oceanic gyres, a vertical succession of different coccolithophore species is frequently observed (Hagino, Okada and Matsuoka, 2000; Haidar and Thierstein, 2001; Poulton *et al.*, 2017) with many species showing strong ecological preferences for particular photic zones (Upper Euphotic Zone, Lower Euphotic Zone, Sub-Euphotic Zone; Poulton *et al.*, 2017). In these stable stratified waters the vertical differentiation of the coccolithophore species composition is statistically stronger than horizontal (i.e. latitudinal) differences (Poulton *et al.*, 2017). Another study across the Atlantic found that an 'environmental distance', calculated using nutritional variables, explained more of the community differences between diatoms and coccolithophores than geographical distance (Cermeño *et al.*, 2010).

Communities on or near continental shelves have also been shown to have distinct depth zonation of species corresponding to the thermal structure of the water column. In the Arabian Sea, for example, distinct coccolithophore communities were found above, within and below the thermocline, and coccolithophore abundance was higher where the thermocline was deeper, compared to where the water column was more mixed (Andruleit *et al.*, 2003). However, species assemblages across these more dynamic regions (spanning shelf to off-shelf environments) are found to be more heterogeneous than in the mid-ocean gyres. Previous authors have also noted marked changes in species composition along transects from the continental shelf to deep waters (East China Sea shelf, Tanaka, 2003), and that coccolithophore communities in shelf environments were sporadic and less diverse, compared to higher diversity more uniform communities in open ocean environments (Okada and Honjo, 1975).

A high spatial and taxonomic resolution of the coccolithophore community in the Celtic Sea is lacking. Most studies in the region have either used methods which do not allow species level taxonomic resolution (flow cytometry (Tarran and Bruun, 2015), pigment analysis (Joint *et al.*, 2001; see Chapter 2, section 2.4.5) or reflectance (Garcia-soto *et al.*, 1995)), or lack vertical resolution because sampling was constrained to surface waters (van Oostende *et al.*, 2012) or the sediments (Houghton, 1988). However, some studies have used light microscopy to assess the species composition of the coccolithophore communities in more detail. For example, in June 2011 *Emiliania huxleyi* was the most abundant coccolithophore species in several sites around the NW European Shelf, with other species such as *Gephyrocapsa muellerae* and members of the *Syracosphaera* genus also present (Poulton *et al.*, 2014). During July 2015, a station in the central Celtic Sea showed vertical differences in the coccolithophore community (Mayers, 2018), with higher species richness deeper in the water column. The present study expands on

these previous findings with high-resolution depth profiles characterising the coccolithophore communities across a wide spatial transect from the shelf to the shelf-break, using SEM imaging to gain high taxonomic resolution (especially for lightly calcified cells). The findings presented augment current knowledge on coccolithophore community composition and biogeography in this region, and can help us to understand the environmental drivers of coccolithophores on the shelf and at the shelf-break. Additionally, information on the species composition of the coccolithophore community can be incorporated into assessments of pelagic $CaCO_3$ production in this region, as the various cell sizes and calcite content of different species mean they contribute differentially to calcite production (Daniels, Sheward and Poulton, 2014; Daniels *et al.*, 2016).

**Aims**

The aim of this study was to investigate the patterns in abundance and diversity of the coccolithophore community in summer in the Celtic Sea. Coccolithophore community data, along with ancillary environmental data, was used to address the following questions:

1) **How does coccolithophore species composition vary across a transect from on shelf to the shelf-break?**

2) **Is there vertical structuring of the coccolithophore community?**

3) **What factors might drive the patterns in species distribution?**

## 4.2 Methods

### 4.2.1 Site Description and Survey

The biodiversity and community composition of coccolithophores was investigated during the *RSS Discovery* expedition DY033 in summer 2015 in the Celtic Sea (UK), a temperate shelf sea. Sampling was carried out between 11th July to 2nd August 2015, several months after the main phytoplankton spring bloom in April (Mayers *et al.*, 2018). Twelve stations were sampled, following a NE-SW transect from on the shelf to the shelf-break (Figure 4.1). In subsequent descriptions, six stations nearest to shore are classified as 'shelf' (seafloor < 200 m) and six stations are classified as 'shelf-break' (seafloor > 200 m) where the continental slope rapidly steepens (seafloor 200 – 2500 m over 50 kms). In order to capture the steep environmental gradient at the shelf-break, sampling stations were placed spatially closer together than shelf stations.

Alongside coccolithophore community data, ancillary data collected and processed by other cruise participants is utilised in this study. See Table 4.1 for acknowledgement of the data originators.

**Table 4.1.** Details of the data sets used in this chapter contributed to by other scientists**.** Further details can be found in the *RRS Discovery* DY033 Cruise Report.

| Data set | Originator, and current affiliation |
|---|---|
| CTD Processing | Jo Hopkins, National Oceanography Centre, Liverpool |
| Chlorophyll *a* | Alex Poulton, Heriot Watt University, Edinburgh |
| Dissolved Nutrients | Malcolm Woodward, Plymouth Marine Laboratory, Plymouth |
| Phytoplankton Microscopy (Lugol's) | Claire Widdicombe, Plymouth Marine Laboratory, Plymouth |
| Phytoplankton (Flow Cytometry) | Glen Tarran, Plymouth Marine Laboratory, Plymouth |
| Light Attenuation, $K_d$ | Anna Hickman, University of Southampton, Southampton |

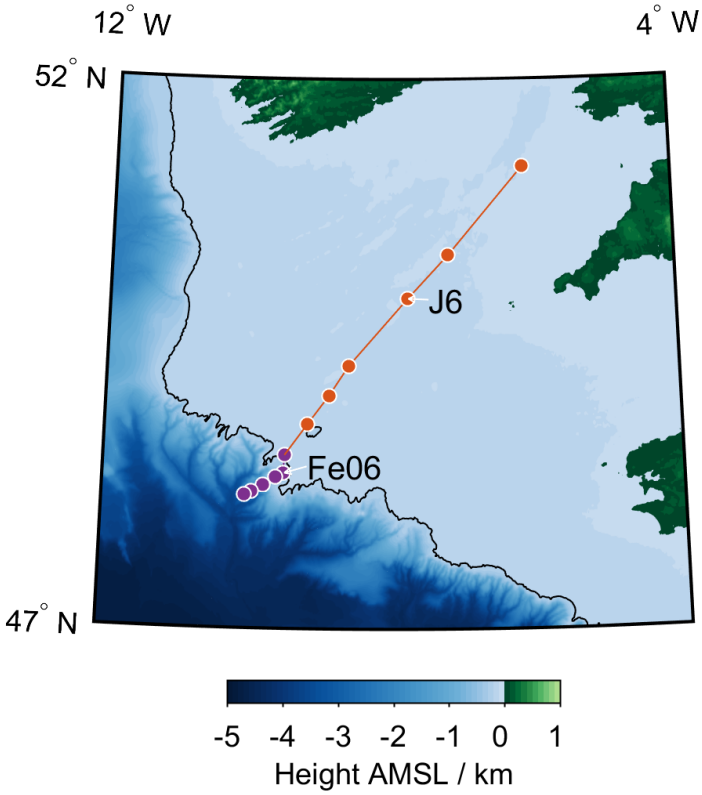


**Figure 4.1.** Location of sampling transect in the Celtic Sea (Northwest European shelf). Shelf stations (orange) and shelf-break stations (purple) are superimposed on bathymetry contours. Example stations J6 (shelf) and Fe06 (shelf-break) are indicated. The 200 m bathymetry contour, traditionally used to define the edge of the shelf, is also indicated. Topography data are from the GEBCO_2014 30 arc-second grid (version 20150318, http://www.gebco.net). AMSL = Above mean sea level.

### 4.2.2 Coccolithophore Community

Water samples were collected using a conductivity-temperature-depth (CTD) profiler fitted with 24 Niskin bottles (20 L capacity each). Between four and seven depths ranging from 5 – 60 m were sampled for analysis of the coccolithophore community at each station (see Table 4.2). Sampling depths varied between stations, as they were chosen in response to on site assessment of the features of the temperature and chlorophyll (fluorescence) structure from the downcast CTD profiles. At each station, at least one sample was taken at each of the following: near surface (5 – 10 m depth), in the thermocline / sub-surface chlorophyll maximum (SCM) where present, and below the SCM or base of the thermocline (see section 4.2.5 for details of how samples were depth classified with respect to the environmental parameters). Water samples (0.8 to 1.0 L) were collected and immediately filtered gently through 25 mm, 0.8 µm Whatman polycarbonate filters, with a Whatman GF/F backing filter to aid in equal distribution of the material. Filters were oven dried at 40 – 50 °C overnight, and stored in petri slides in the dark until analysis. Identification of coccolithophores to the

species level was done using SEM (scanning electron microscopy) methodology (Charalampopoulou *et al.*, 2011; Smith *et al.*, 2017). Briefly, the central portion of each filter was cut out and gold coated. A Leo 1450VP SEM (Carl Zeiss, Germany) was then used to take 225 photographs at a magnification of x 5000 (equivalent to ~ 1 $mm^2$). Whole coccolithophore cells (coccospheres) were identified (Young *et al.*, 2003), whilst detached coccoliths were ignored, as they are less likely to represent a living cell. Where a confident species level identification was not possible, cells were assigned to the level of genera (e.g., *Syracosphaera sp.*). ImageJ (v 1.49v) free software was used to enumerate each species identified. The abundance of each species was calculated following Equation 4.1:

$$\text{Cells mL}^{-1} = \frac{\left(\text{C} \times \frac{F}{A}\right)}{V} \quad (4.1)$$

where C is the total number of cells counted, A is the area investigated ($mm^2$), F is the total filter area ($mm^2$), and V is the volume filtered (mL).

**Table 4.2** Date, location of stations and sampling depths for coccolithophore community on Discovery cruise DY033, July 2015.

| Date | Station | Depths Sampled (m) | Latitude | Longitude | Shelf Location | Seafloor (m) |
|---|---|---|---|---|---|---|
| 26/07/15 | A | 5, 15, 25, 27, 35, 50 | 51.21 | -6.13 | Shelf | 107 |
| 28/07/15 | J4 | 5, 20, 35, 43, 45, 50 | 50.40 | -7.22 | Shelf | 111 |
| 28/07/15 | J6 | 5, 20, 35, 45, 50, 55 | 50.01 | -7.80 | Shelf | 113 |
| 14/07/15 | CCS | 10, 20, 40, 45, 48, 55 | 49.39 | -8.63 | Shelf | 145 |
| 23/07/15 | O2 | 10, 20, 30, 38, 42, 50 | 49.12 | -8.90 | Shelf | 153 |
| 23/07/15 | O4 | 5, 10, 20, 30, 42, 50 | 48.85 | -9.20 | Shelf | 165 |
| 19/07/15 | CS2 | 10, 20, 25, 35, 45, 50 | 48.57 | -9.51 | Shelf-break | 202 |
| 23/07/15 | Fe06 | 5, 10, 20, 30, 40, 50 | 48.41 | -9.53 | Shelf-break | 467 |
| 23/07/15 | Fe04 | 5, 10, 15, 20, 30, 40, 60 | 48.37 | -9.63 | Shelf-break | 991 |
| 23/07/15 | Fe15 | 5, 10, 20, 30, 40, 60 | 48.30 | -9.80 | Shelf-break | 1518 |
| 22/07/15 | Fe02 | 5, 10, 20, 30, 35, 40, 50 | 48.24 | -9.97 | Shelf-break | 1998 |
| 21/07/15 | Fe01 | 10, 20, 30, 40 | 48.21 | -10.05 | Shelf-break | 2489 |

### 4.2.3 Assessment of other Phytoplankton Taxa

Seawater samples were collected in clean 250 mL polycarbonate bottles from CTD casts and stored in a refrigerator. All samples were analysed within 1.5 hours of collection on high flow rate (approx. 170 μL $min^{-1}$) for 4 minutes, using a Becton Dickinson FACSort flow cytometer which characterised and enumerated *Synechococcus* sp. (cyanobacteria), and pico- and eukaryote phytoplankton, based on their light scattering and autofluorescence properties (Tarran, Heywood and Zubkov, 2006). Samples were also collected for enumeration of the microplankton community by light microscopy. Seawater samples were collected in 250 mL amber glass jars containing 5 mL Lugol's iodine solution as a preservative until analysis under an Olympus DMI4000B microscope (Widdicombe *et al.*, 2010). Further details on these sampling and analysis methods can be found in the *RRS Discovery* DY033 cruise report.

### 4.2.4 Physicochemical conditions

At all stations, water was sampled from the CTD for determination of the concentration of Chlorophyll *a* (Chl *a*) and nutrients (nitrate + nitrite, nitrite, phosphate, silicic acid and ammonia). For Chl *a* extraction, 0.2 – 0.25 L water samples were filtered through Whatman GF/F filters, extracted in 90 % acetone for 18 – 20 h at 4 °C, and measured on a Turner Designs Trilogy fluorometer calibrated using a pure Chlorophyll *a* standard, Sigma-Aldrich UK. Nutrient determination was carried out following the international GO-SHIP nutrient manual recommendations (Hydes *et al.*, 2010) where possible.

The attenuation coefficient ($K_d$) for each station was calculated using the Beer-Lambert Law equation:

$$E_d(z) = E_d(0).e^{-Kd.z} \quad (4.2)$$

Where $E_d(z)$ is the irradiance at depth z, $E_d(0)$ is surface irradiance, and $K_d$ is the PAR diffuse attenuation coefficient. The equation was fitted to data from the down-welling PAR sensors on the CTD, in the surface mixed layer. At the two stations sampled in darkness (O2 and Fe02) no suitable PAR data was available, so a linear relationship between average Chl *a* concentration and $K_d$ for the Celtic Sea region (Curran *et al.*, 2018) was used to infer $K_d$. Equation 4.2 was used to calculate light depths as a % of surface irradiance.

The depth of the SML at each station was calculated from the vertical density distribution, and defined as the depth where density changes by 0.02 kg $m^{-3}$ from the potential density at 10 m (or the nearest available measurement). As this SML depth criterion presents limitations in accurately identifying weakly versus strongly stratified water masses, an additional and more

robust index was used to measure stratification (Equation 4.3). A Stratification Index (SI) was calculated as the difference in density between the surface and 100 m (or deepest sampling depth (z) where total water depth was less than 100) divided by the respective difference in depth following (Fragoso *et al.*, 2016).

$$SI = \frac{\text{Density}_{surf} - \text{Density}_{z}}{\Delta z} \quad (4.3)$$

**Depth Categorization**

Rather than classify coccolithophore count samples into simple depth bins, samples were classified into three depth categories modified from those used in Poulton *et al.*, (2017) with respect to the vertical structure of important resources (i.e. light and nutrients) in the water column at each station. Upper euphotic zone (UEZ) was > 10 % surface irradiance (1 – 2 samples at each station), lower euphotic zone (LEZ) was < 10 % surface irradiance down to the depth where nitrate = 2.0 μmol $L^{-1}$ as an indicator of the nutricline/thermocline (1 to 6 samples at each station). The sub-euphotic zone (SEZ) were deep samples where nitrate > 2.0 μmol $L^{-1}$ (1 to 3 samples at each station). Categorizing the samples in this way allowed easier comparison between stations, where the physical structure of the water column is different.

### 4.2.5 Statistical Analysis

**Principal Component Analysis**

To simplify and visualise environmental variability, a principal component analysis (PCA) was used, which combines the more closely correlated variables and the relative influence of the environmental variables within the data (Clarke, 1993; Clarke and Warwick, 2001; Clarke and Gorley, 2006). Environmental data (nitrate, phosphate, temperature, salinity and SI) were normalized (mean of zero and a standard deviation of 1), and Euclidean distance was then used to determine spatial changes in these parameters, using PRIMER-6 (v6.1.15, (Clarke and Warwick, 2001)).

**Diversity Indices**

To investigate patterns in the coccolithophore community structure across a spatial gradient from the shelf to shelf-break, biodiversity was explored by calculating univariate diversity indices. Coccolithophore diversity was assessed as the total number of species (Species Richness), and Pielou's evenness index (J') which assesses how evenly the count data were distributed between the different species present:

$$J' = \frac{H'}{H'_{max}} \quad (4.4)$$

Where *H'* is Shannon's diversity Index:

$$H' = -\sum_i \rho_i \, log(\rho_i) \quad (4.5)$$

Where $\rho_i$ is the proportion of the total arising from the *i*th species, and $H'_{max}$ is the maximum value of H' (if every species were equally likely):

$$H'_{max} = -\sum_i \frac{1}{S} \, log\left(\frac{1}{S}\right) \quad (4.6)$$

Where *S* is the total number of species.

**Multivariate Analysis**

For statistical analysis, rare species (defined as consistently contributing < 5 % to total coccolithophore cell abundance, and being present in < 10 samples) were removed from the data set. In order to assess differences between the coccolithophore communities in different groups of samples, we applied a set of multivariate analyses. Coccolithophore count data was square root transformed (because data frequency was skewed to the left due to many species being present in low abundances) (Charalampopoulou *et al.*, 2011, 2016; Smith *et al.*, 2017). A dissimilarity distance matrix was constructed using the Bray-Curtis dissimilarity index and a dummy variable, to assess the (dis)similarity in species composition between samples, using PRIMER-6 (v6.1.15, (Clarke and Warwick, 2001)). The dissimilarity matrix was subsequently analysed with the Analysis of Similarity (ANOSIM), which is suitable for non-parametric data. Samples were grouped in two different ways, by shelf/shelf-break location (as described in section 2.1) and by depth category (as described in section 2.5), in order to test for significant differences between these groupings, and to obtain R values. The ANOSIM R value ranges between 0 and 1, with values closer to 0 indicating more statistical dissimilarity between samples from the same group than between groups, whilst values close to 1 indicate high dissimilarity between groupings, and that samples within groups are more similar to each other. The results were visualised using Nonmetric Multidimensional Scaling (NMDS) ordinations. In order to determine which species are primarily responsible for differences between groups of samples, SIMPER analysis was conducted. SIMPER analysis breaks down the Bray– Curtis similarity into individual species contributions, allowing for the statistical identification of which species are most important in contributing to community (dis)similarity.

## 4.3 Results

### 4.3.1 Environmental and Biological Context

#### Physical Setting

The water column in the Celtic Sea study site was stratified, with a strong density structure in the water column (Figure 4.2a), which was primarily temperature driven (Ruiz-Castillo *et al.*, 2018). Stratification was strongest on the shelf, with a sharp transition from low (< 1027 kg $m^{-3}$) to high (< 1027.5 kg $m^{-3}$) density waters at the thermocline (~ 40 – 50 m depth), whilst at shelf-break stations density isobars were spaced more widely, indicating that stratification was less strong at the shelf-break. A Stratification Index (estimated by the density differential with depth, see methods section 4.2.4) was highest at shelf stations (between 0.058 and 0.063), and lower at the shelf-break stations (between 0.041 and 0.056, Figure 4.2b). Similarly, the SML depth was shallower around the shelf-break region (between 12 and 21 m depth) than on the shelf (up to 39 m depth) (Figure 4.2b). These differences in physical structure and stratification strength suggest increased mixing processes were occurring at the shelf-break.

#### Nutrient and Light Availability

Nutrient concentrations were coupled with the physical structure of the water column, with depletion in the SML above the thermocline (< 0.1 μmol N $L^{-1}$), and elevated concentrations (> 7 μmol N $L^{-1}$) below the thermocline. In the upper 100 m of the water column, nitrate was closely coupled with phosphate concentrations (see Appendix A.i), and as such patterns in nitrate concentrations are discussed as representative of inorganic nitrogen and phosphorus availability generally. On the shelf, strong stratification was associated with a sharp increase in nitrate at the base of the thermocline, and nitrate increased from < 0.1 to 7.0 μmol $L^{-1}$ within ~10 metres (Figure 4.2c). At the shelf-break, where stratification was weaker, nitrate was mixed closer to the surface, and increased in concentration with depth more gently than on the shelf (over tens of metres, Figure 4.2c and Appendix A.ii). The light attenuation coefficient ($K_d$) varied across the transect from 0.06 to 0.13 $m^{-1}$, meaning that the 1 % light depth occurred between 15 to 33 m depth. At the shelf-break stations, the depth at which nitrate > 0.1 μmol $L^{-1}$ was close to or intersected the 1 % light depth (Figure 4.2c). As such, at the shelf-break nutrients were not drawn down to the low levels seen on the shelf in the relatively well-lit portion of the water column.

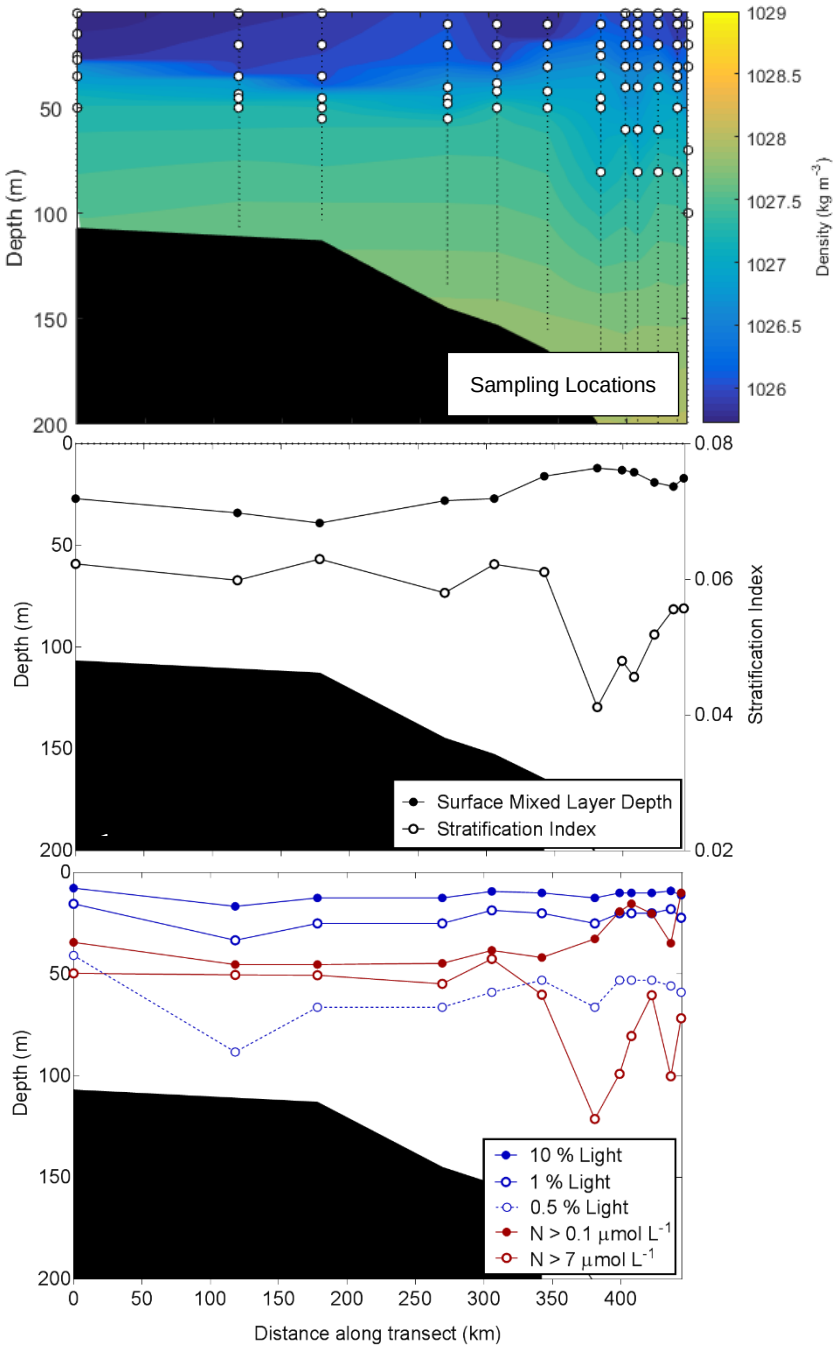


**Figure 4.2.** a) Seawater density (kg $m^{-3}$) contour plot along the sampling transect (from nearshore station on the left to furthest off-shelf station on the right). Overlaid in black lines are CTD cast stations, with depths at which the coccolithophore community was sampled in white circles. b) Stratification Index and SML depth (see methods section 4.2.4) along the sampling transect. c) The 10, 1 and 0.5 % light depths (relative to surface irradiance) indicated in blue, and the depth at which nitrate > 0.1 µmol $L^{-1}$, and > 7.0 µmol $L^{-1}$ indicated in red (solid and hollow respectively) along the sampling transect. Seafloor batthymetry patched out in black.

### Chlorophyll *a* and Other Phytoplankton

Patterns in Chl *a* concentration were coupled with the differences in the physical structure of the water column. At shelf stations with strong stratification, a well-defined sub-surface peak in Chl *a* (SCM) was evident (e.g. Figure 4.3a). The SCM at shelf stations contained up to 7 μg $L^{-1}$, and coincided approximately with the base of the thermocline. The less strongly stratified shelf-break stations had lower sub-surface peaks in Chl *a* (between 0.31 – 0.74 μg $L^{-1}$), but these were broader and less sharply defined than at shelf stations, and generally occurred closer to the surface (e.g. Figure 4.3b). Surface Chl *a* varied between 0.20 – 0.67 μg $L^{-1}$ across stations: with the exception of station A which had very high surface Chl *a* (1.5 μg $L^{-1}$, more than double that at any other station). There was increased surface Chl *a* in the stations around the shelf-break (CS2, Fe06 and Fe04) compared to most of the other stations (Figure 4.3c). Although SCM peaks in Chl *a* were higher in magnitude at the strongly stratified stations, depth integrated Chl *a* (to 100 m) was highest around the shelf-break region (Figure 4.3c), due to moderate Chl *a* concentrations over a broader depth range.

An overview of the trends in other phytoplankton groups in the surface waters across the transect helps to provide context for the findings within the coccolithophore community. Depth profiles from an example shelf station (J6, Figure 4.4a) and shelf-break station (Fe06, Figure 4.4b) demonstrate that nano-eukaryote (2-20 μm) abundance peaked around the SCM at shelf stations, but near the surface at the shelf-break. On the other hand, prokaryotic *Synechococcus* was consistently found in highest abundance in surface samples. Looking at surface waters across the shelf to shelf-break transect, small (<2 μm) prokaryotic cells of *Synechococcus* were found in higher abundance in surface waters at shelf stations than at shelf-break stations, whilst nano-eukaryotes (2-20 μm) and pico-eukaryotes (<2 μm) were generally found in higher abundance at shelf-break stations (Figure 4.4c). The increased Chl *a* at the shelf-break compared with the shelf is therefore likely to be due to higher abundances of eukaryotic phytoplankton.

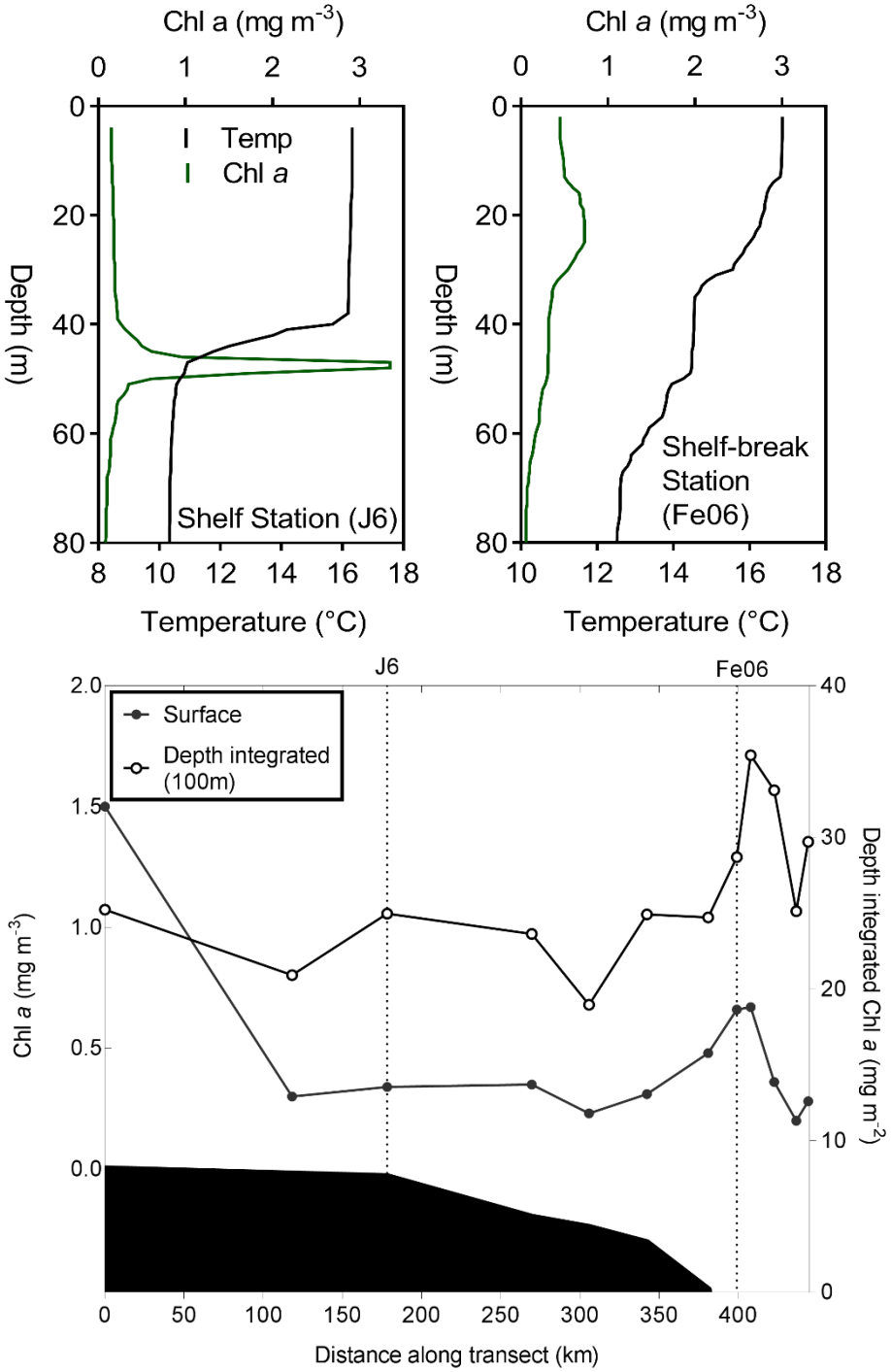


**Figure 4.3.** a) Chlorophyll *a* and temperature depth profiles (from downcast CTD profiles) from an example shelf station (J6) and an example shelf-break station (Fe06). b) Surface Chlorophyll *a* and depth-integrated Chlorophyll *a* along the sampling transect (left to right from nearshore station in the NE to furthest off shelf station in the SW). Seafloor batthymetry patched out in black.

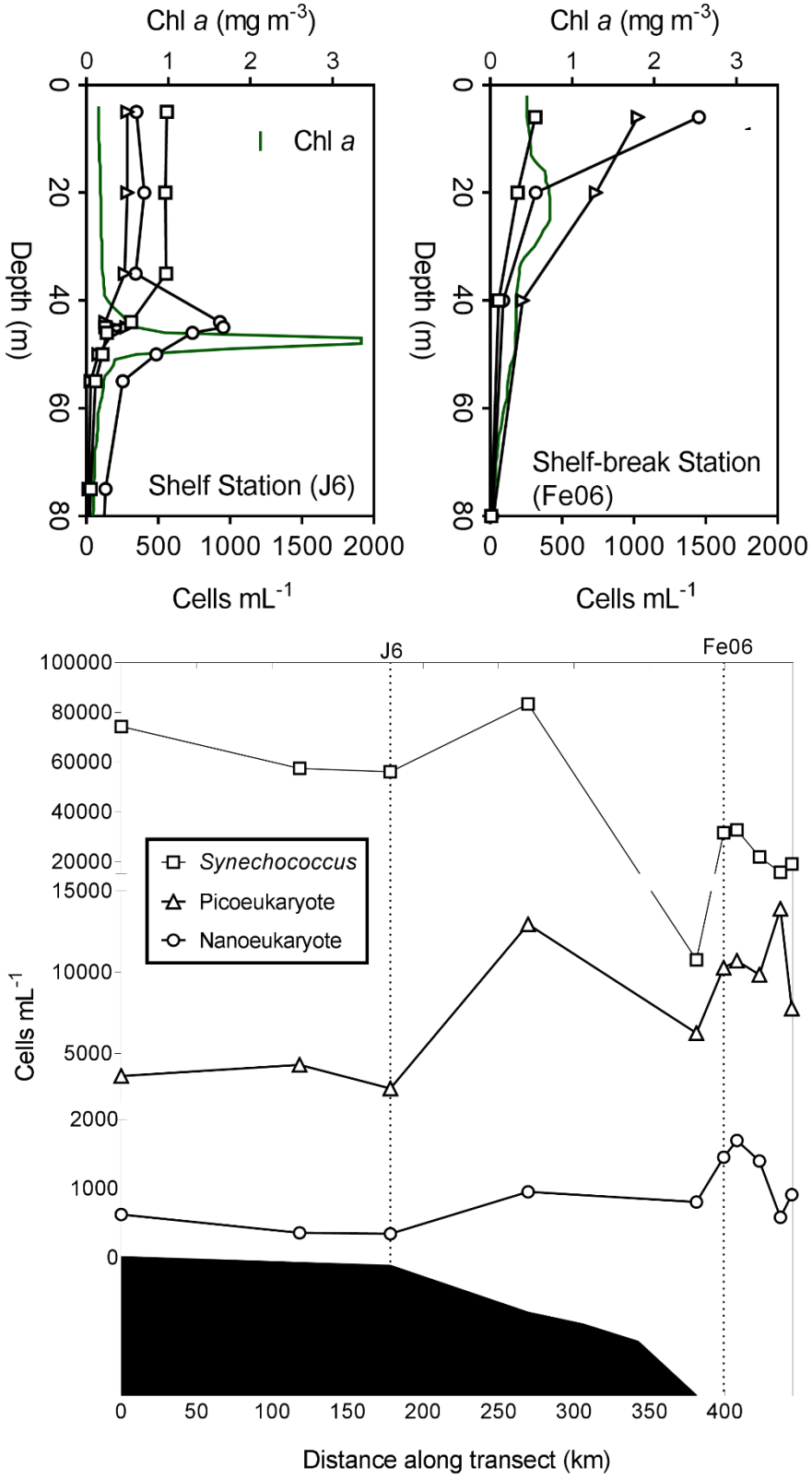


**Figure 4.4.** a) Depth profiles of the abundance of phytoplankton groups from flow cytometry (*Synechococcus* (x $10^3$ cells $mL^{-1}$) = square, picoeukaryotes (x $10^2$ cells $mL^{-1}$) = triangle, nanoeukaryotes = circles) at an example shelf station (J6) and an example shelf-break station (Fe06). b) Surface abundance of phytoplankton groups from flow cytometry. Seafloor batthymetry patched out in black.

### 4.3.2 Coccolithophore Community

#### General Description

Coccolithophore cells were identified at every station across the spatial transect, and at most depths sampled (coccolithophores were identified in 95 % of all samples). Over 10,000 coccolithophore cells were counted in total across all samples, with 35 different species identified (Table 4.3). The most abundant species was *Emiliania huxleyi* which accounted for 64 % of the total (10,000) coccolithophore cells identified, and was found at every station across the transect. Other commonly occurring species included *Gephyrocapsa muellerae* (10 % of all cells, present at 9 out of 12 stations), *Corisphaera gracilis* (5 %, present at all stations) and *Syracosphaera marginoporata* (4 %, present at 9 out of 12 stations). The other 31 species were less abundant, each accounting for less than 3 % of coccolithophore cells overall. However, some of these less common species had local importance, with 17 species contributing > 5 % to the community in individual samples, or being present in > 10 samples (highlighted in bold in Table 4.3). The genus *Syracosphaera* was represented by 9 different species (Table 4.3), including both heterococcolith and holococcolith forms (representing both stages of the life cycle, see Chapter 1, section 1.2). Individually, each of these species contributes only a small amount to the total community (typically < 5 %), but when summed together their contribution was substantial in some samples.

Patterns in cell abundances (Figure 4.5a) and species richness (Figure 4.5b) were similar. Highest total coccolithophore cell abundances and highest species richness were both found in the shelf-break region (Figure 4.5a & b), with depth-integrated species richness > 20 in four of the six shelf-break stations. Highest total coccolithophore cell abundance was found at shelf-break station Fe06 (208 cells $mL^{-1}$ at 20 m depth), and similarly, highest species diversity was found in samples at shelf-break stations Fe06 and Fe04. At shelf stations, coccolithophore cell abundance peaked in the thermocline (Figure 4.5a), approximately coincident with the SCM (see Appendix A.iii). An exception was at station A (nearest shore) at which peak coccolithophore cell numbers occurred in the surface (5 m). At shelf-break stations, greater cell abundances were found shallower in the water column (typically above the Chl *a* peak, in the upper 20 m). Across all the stations, cell abundance in the deepest samples was low (< 20 cells $mL^{-1}$).

Pielou's evenness index (J') of the community in shelf samples ranged widely between 0 (completely dominated by one species) and 1 (completely even spread) (Figure 4.5c). Evenness values were generally higher and more variable in shelf samples (mean 0.54 ± 0.35), than shelf-break samples (mean 0.49 ± 0.19). Evenness ranged between 0.25 and 0.55 in most samples

from the shelf-break, except in samples with low coccolithophore cell abundance (< 10 cells $mL^{-1}$, typically deep in the water column), where evenness was either high (> 0.6) or very low (0). Extreme evenness values (approaching 0 or 1) mostly occurred in samples where cell abundance was low (see Appendix A.iv), perhaps explaining why evenness was more variable in shelf samples, and samples in the sub-euphotic, many of which had cell abundances of < 10 cells $mL^{-1}$.

The most abundant species was *E. huxleyi* at eight of the twelve stations, including all of the shelf-break stations, where *E. huxleyi* largely dominated the community, contributing > 60 % of the community in most samples (Figure 4.5d). Evenness was generally lower (typically < 0.5) in samples where *E. huxleyi* formed a large majority of the coccolithophore community. For example, the shelf-break stations tended to have high species richness (> 20), yet low evenness (< 0.5), as they were dominated by *E. huxleyi*, and to a lesser extent *G. muellerae* (comprising between 7 - 15 % of the total cell abundance), whilst many other species were present in low abundances (each < 3 % of total cell abundance).

**Table 4.3.** Species presence (+) at each station across the sampling transect. Identification of the species at any depth is considered as species presence at that station. 'HOL' indicates that the cell identified possessed holococcoliths. Species in bold are considered 'common' while those not bolded are considered 'rare' and excluded from subsequent statistical analysis.

| Species | A | J4 | J6 | CCS | O2 | O4 | CS2 | Fe06 | Fe04 | Fe15 | Fe02 | Fe01 |
|---|---|---|---|---|---|---|---|---|---|---|---|---|
| *Acanthoica quattrospina* | | | | | + | | | + | + | | | + |
| *Alisphaera extenta* | | | | + | | | + | + | + | + | | + |
| ***Alisphaera unicornis*** | | + | | + | + | | | + | | | + | |
| ***Calciopappus caudatus*** | + | + | + | + | | | | | + | + | + | + |
| *Calyptrolithina divergens* | | | | | | | | | + | | | |
| ***Corisphaera gracilis*** | + | + | + | + | + | + | + | + | + | + | + | + |
| ***Cyrtosphaera aculeata*** | | | | + | + | + | + | + | + | + | + | + |
| ***Emiliania huxleyi*** | + | + | + | + | + | + | + | + | + | + | + | + |
| *Gephyrocapsa ericsonii* | | | | | | | | | + | + | | |
| ***Gephyrocapsa muellerae*** | | | + | | + | + | + | + | + | + | + | + |
| HOL *Calcidiscus sp* | | + | | | | + | | + | + | | | + |
| **HOL *Coccolithus pelagicus*** | | | | | | | | + | | | | |
| HOL *Corisphaera sp* | | | | | | | + | + | + | + | + | + |
| **HOL *Coronosphaera mediterranea*** | | | | | | | | | | | + | |
| HOL *Helicosphaera carteri* | | + | | | | | | | | | | |
| **HOL *Homozygosphaera sp*** | | | | + | | | | | | | | |
| **HOL *Syracosphaera ampliora*** | | | | | | | | + | + | + | + | |
| HOL *Syracosphaera pulchra* | + | + | | + | + | | + | + | + | + | + | + |
| ***Ophiaster formosus*** | | | | | | | | + | + | + | + | + |
| ***Palusphaera sp*** | | | | | | | | | + | + | + | + |
| ***Papposphaera sp*** | | | | | | | | | | | + | |
| *Picarola sp* | | | | | | | | | | | + | + |
| *Poricalyptra gaarderiae* | | | | | | | | + | | | | |
| *Reticulofenestra parvula* | | | | | | | | + | | | | + |
| *Rhabdosphaera clavigera* | + | + | + | + | + | + | | | | | + | |
| ***Syracospheara ampliora*** | | | + | | | + | | + | | + | | |
| ***Syracosphaera corolla*** | + | + | | | + | + | | + | + | + | + | + |
| ***Syracosphaera dilatata*** | | | | | | + | + | + | + | + | + | + |
| ***Syracosphaera halldalii*** | | | | | | | | + | + | | | + |
| ***Syracosphaera marginiporata*** | | + | | + | + | + | | + | + | + | + | + |
| ***Syracosphaera molischii*** | | | | | + | + | + | + | + | + | + | + |
| ***Syracosphaera nana*** | | | | + | + | | | | + | | | |
| ***Syracosphaera nodosa*** | | | | + | + | | | | + | | | |
| *Syracosphaera ossa* | + | | | | | | + | + | + | + | + | + |
| *Syracosphaera pulchra* | | | | | | | | + | | + | + | |

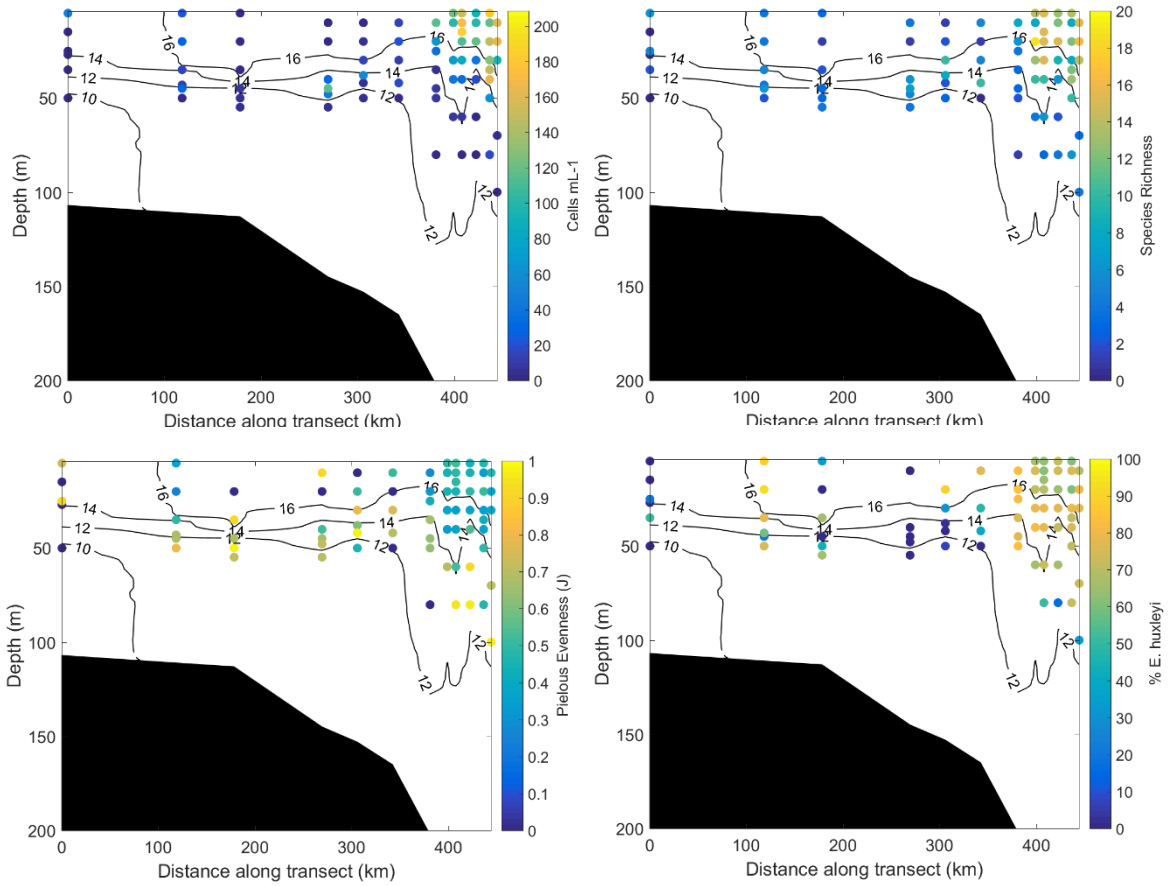


**Figure 4.5.** Cross-transect trends in the coccolithophore community, with sampling points coloured according to relative values of a) Total coccolithophore cell abundance (cells $mL^{-1}$). b) Species richness (number of species identified). c) Pielou's evenness (J', see methods 4.2.5). d) Relative abundance of *Emiliania huxleyi* cells, as a percentage of the total coccolithophore community. The temperature structure of the water column across the sampling transect is indicated by contours at 2 °C intervals in each figure for context

### Statistical Analysis

The variation in environmental variables across the transect was visualised by using a Principal Component Analysis ordination (PCA, Figure 4.6). The first principal component (PC1) accounted for 53.5 % of the variation in environmental variables, with the second principal component (PC2) accounting for an additional 34.0 % of environmental variation. PC1 describes the main depth dependent gradients (i.e. nutrient concentrations and temperature), and when factored according to depth category, the samples clearly fall out along the PC1 axis (Figure 4.6b). PC2 represented environmental variation which varied primarily horizontally across the shelf (salinity and stratification strength), and when factored according to shelf or shelf-break, the samples fall out along the PC2 axis (Figure 4.6a). The stations and coccolithophore samples are clearly differentiated by lower salinity and higher stratification strength on the shelf compared with at the shelf-break, and with vertical differences in nutrient availability and thermal structure.

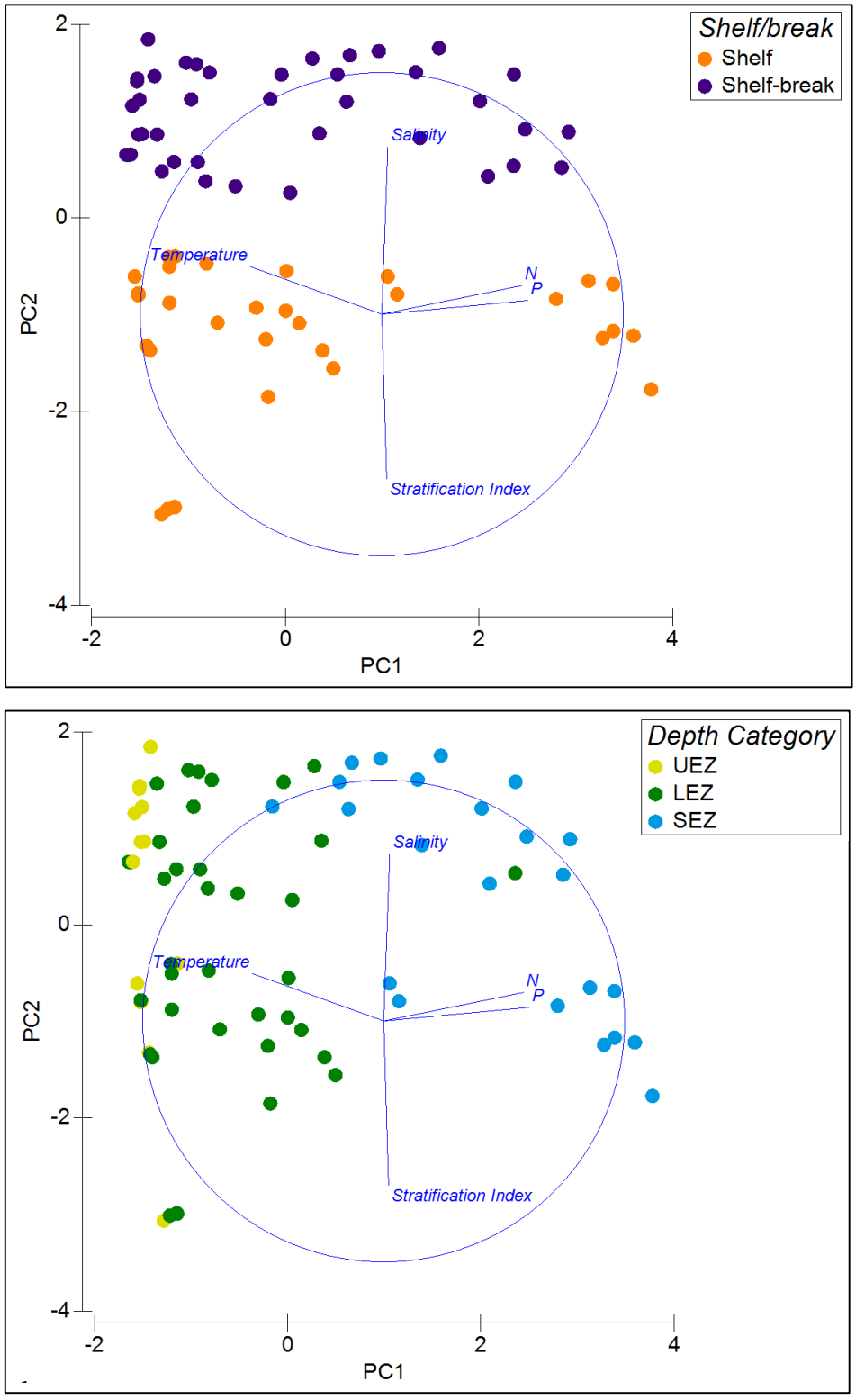


**Figure 4.6.** PCA ordinations of normalised environmental parameters for each sampling point (temperature, nitrate, phosphate, salinity and Stratification Index, see methods section 4.2.4 for details). Data points are coloured with respect to a) Shelf (water depth < 200 m, orange) or Shelf-break-break (water depth > 200 m, purple) and b) Depth category: UEZ = upper euphotic zone (yellow), LEZ = lower euphotic zone (green), SEZ = sub-euphotic zone (blue).

**Community Statistics**

To investigate patterns in community (dis)similarity between the samples, a multivariate statistical analysis of species composition was performed. Bray-Curtis similarity matrix was ordinated by non-metric Multi-Dimensional Scaling (NMDS), and coloured according to whether the sample was from a shelf or shelf-break location (Figure 4.7a) and depth category (Figure 4.7b). Relative distance between each sample indicates the relative (dis)similarity between the samples; clustered samples have statistically similar species composition, whilst statistical similarity is low between samples further away from each other.

Shelf-break samples clustered closely together in NMDS ordination (Figure 4.7a), and an ANOSIM found the community composition was significantly different between shelf and shelf-break sample groups ($p < 0.001$, R-stat = 0.463, Table 4.4). Shelf-break samples displayed higher similarity between each other (average Bray-Curtis similarity 47.8 %) than the communities from the shelf samples, which were spread more widely and showed higher variability between each other (average Bray-Curtis similarity 19.1 %). In contrast, when communities were identified according to depth group, there was no clear clustering in the NMDS ordination (Figure 4.7b). An ANOSIM factored according to depth category was non-significant ($p = 0.019$, R-stat = 0.084, Table 4.4), indicating high variability between samples from the same depth categories across the different stations.

SIMPER analysis revealed the average Bray-Curtis dissimilarity between shelf samples and shelf-break samples was high (81.6 %). A higher abundance of *E. huxleyi* and *G. muellerae* in shelf-break samples accounted for nearly half of the dissimilarity between the two groups. Higher abundance in shelf-break samples of *C. gracilis, O. formosus* and several *Syracosphaera* species (*S. marginiporata, S. dilatata, S. corolla* and *S. molischii*) also differentiated shelf-break from the shelf samples. The NMDS ordination presented as a bubble plot with respect to total coccolithophore cell abundance (Figure 4.7c) demonstrates further how overall abundance is important in driving the clustering patterns. However, differences in species assemblage were also important in differentiating shelf and shelf-break samples. For example, a few species (*S. ampliora, C. caudatus* and *A. unicornis*) were found in higher abundance in shelf samples, together contributing 10 % to the dissimilarity between the two groups. Additionally, an ANOSIM performed on presence/absence transformed data (to remove the weighting on abundance differences) also found a significant difference between the two groups ($p < 0.001$, R-stat 0.462). The NMDS ordination presented as a bubble plot with respect to species richness (Figure 4.7d) demonstrates how species diversity is also important in driving the clustering patterns.

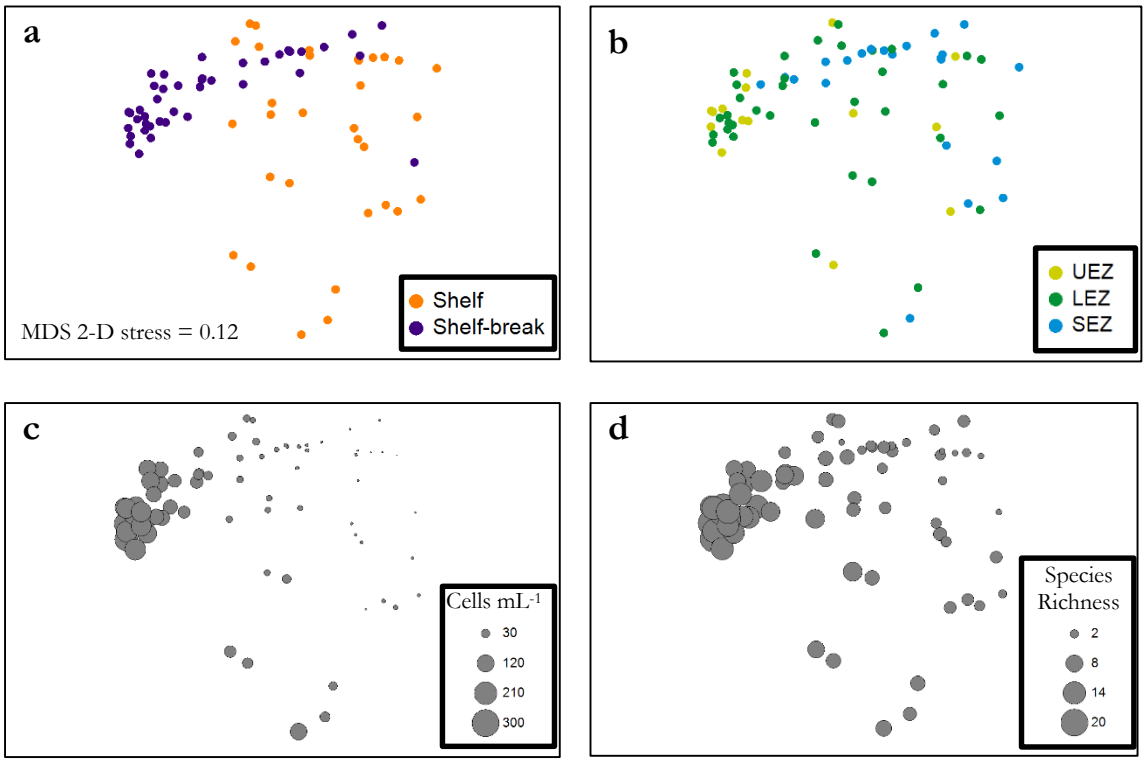


**Figure 4.7.** NMDS ordinations (See methods section 4.2.5) factored as in Figure 4.6 by: a) Location (shelf (orange) or shelf-break (purple)), b) depth category (UEZ = upper euphotic zone (yellow), LEZ = lower euphotic zone (green), SEZ = sub-euphotic zone (blue)), and by c) coccolithophore cell abundance (Cells $mL^{-1}$), and d) species richness (number of species).

**Table 4.4.** Multivariate statistical analyses of differences in coccolithophore composition for samples with respect to factors: shelf vs shelf-break, and depth category (UEZ = upper euphotic zone, LEZ = lower euphotic zone, SEZ = sub-euphotic zone). ANOSIM (one-way ANalysis Of SIMilarities) and SIMPER (one-way analysis of SIMilarity PERcentages of species contributions to the differences between groups) performed on square root transformed data.

| **Factors** | **ANOSIM R-stat** | ***p*-level** | **SIMPER Average Dissimilarity (%)** |
|---|---|---|---|
| Shelf vs Shelf-break | 0.463 | $p < 0.001$ | 81.58 |
| Depth Category | 0.084 | $p = 0.019$ | |
| Break samples: Depth Category | 0.339 | $p < 0.001$ | |
| UEZ vs LEZ | | | 34.68 |
| LEZ vs SEZ | | | 64.06 |
| SEZ vs UEZ | | | 69.73 |

**Depth profiles of community**

To determine whether the strong differences between the communities on the shelf and at the shelf-break could be obscuring statistical detection of vertical differentiation in the water column, samples from each location were considered separately in NMDS ordination (Figure 4.8). Amongst shelf samples, no significant vertical differentiation in communities was apparent (Figure 4.8a, non-significant ANOSIM, $p = 0.611$). Amongst shelf-break samples, however, there was some clustering of communities based on depth category (Figure 4.8b), and an ANOSIM found significant differences between samples from the different depth categories ($p < 0.001$, R-stat = 0.339, Table 4.4). At the shelf-break, there was a decrease in both coccolithophore cell abundance and species richness with depth (Figure 4.9), which were important in driving the dissimilarity between depth categories. At shelf stations on the other hand, depth profiles of species richness and abundance were far more variable between stations (Figure 4.9). As noted earlier, at several shelf stations peaks in abundance and species richness occurred around the depth of the thermocline, although this was not consistent across all the shelf stations.

The NMDS ordination presented as a bubble plot with respect to total coccolithophore cell abundance (Figure 4.8c & d) demonstrates how higher overall abundance in UEZ and LEZ samples is important in driving the clustering patterns amongst the shelf-break samples. SIMPER analysis revealed that the greatest dissimilarity was found between the upper euphotic zone and the sub-euphotic zone sample groups (UEZ vs SEZ average dissimilarity

69.7 %), driven largely by higher cell abundances of *E. huxleyi*, *G. muellerae, C. gracilis* and *S. nodosa* in the UEZ compared with the SEZ. There was less dissimilarity between the upper euphotic zone and the lower euphotic zone sample groups (UEZ vs LEZ average dissimilarity 34.68 %), and samples from these depth zones overlapped in the NMDS ordination (Figure 4.8). However, differences in species assemblages also contributed to vertical differentiation of the communities; several species were found in higher abundance in LEZ samples than UEZ (*O. formosus, S. marginoporata, S. corolla*), together contributing 16.0 % to the dissimilarity between the depth categories.

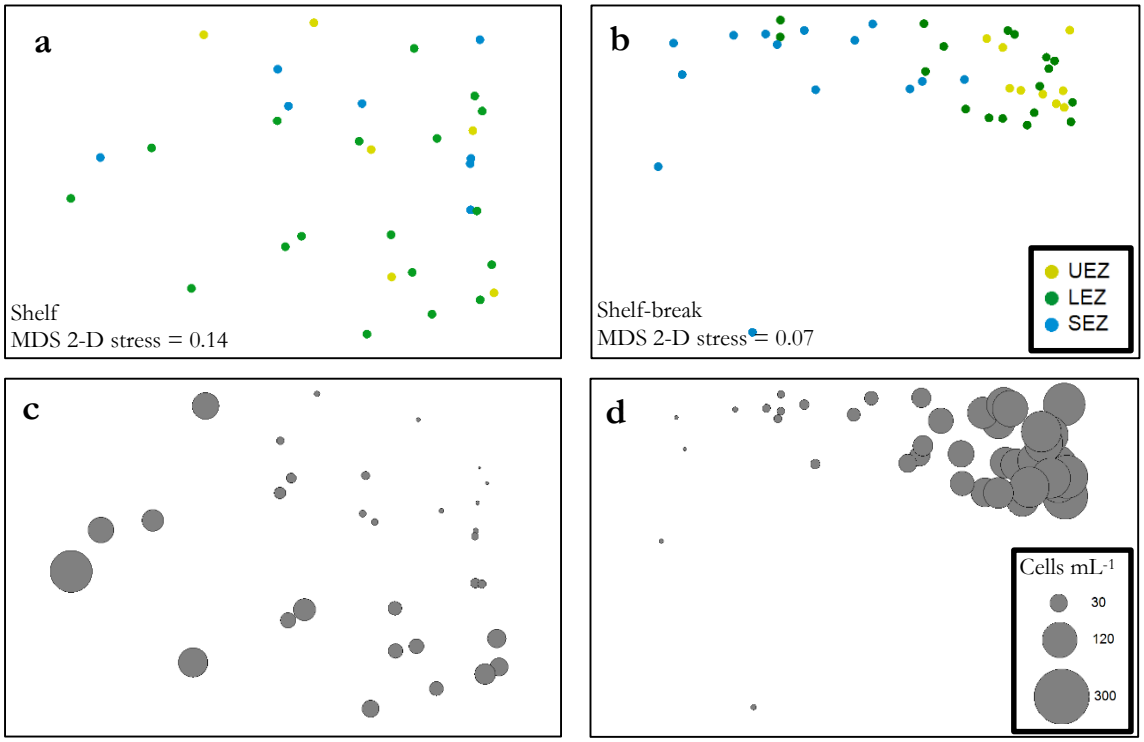


**Figure 4.8.** NMDS ordinations of shelf (a & c) and shelf-break (b & d) samples considered separately (see methods section 4.2.5). Factored by: a) & b) depth category (UEZ = upper euphotic zone (yellow), LEZ = lower euphotic zone (green), SEZ = sub-euphotic zone (blue)), and by c) & d) coccolithophore cell abundance (Cells $mL^{-1}$).

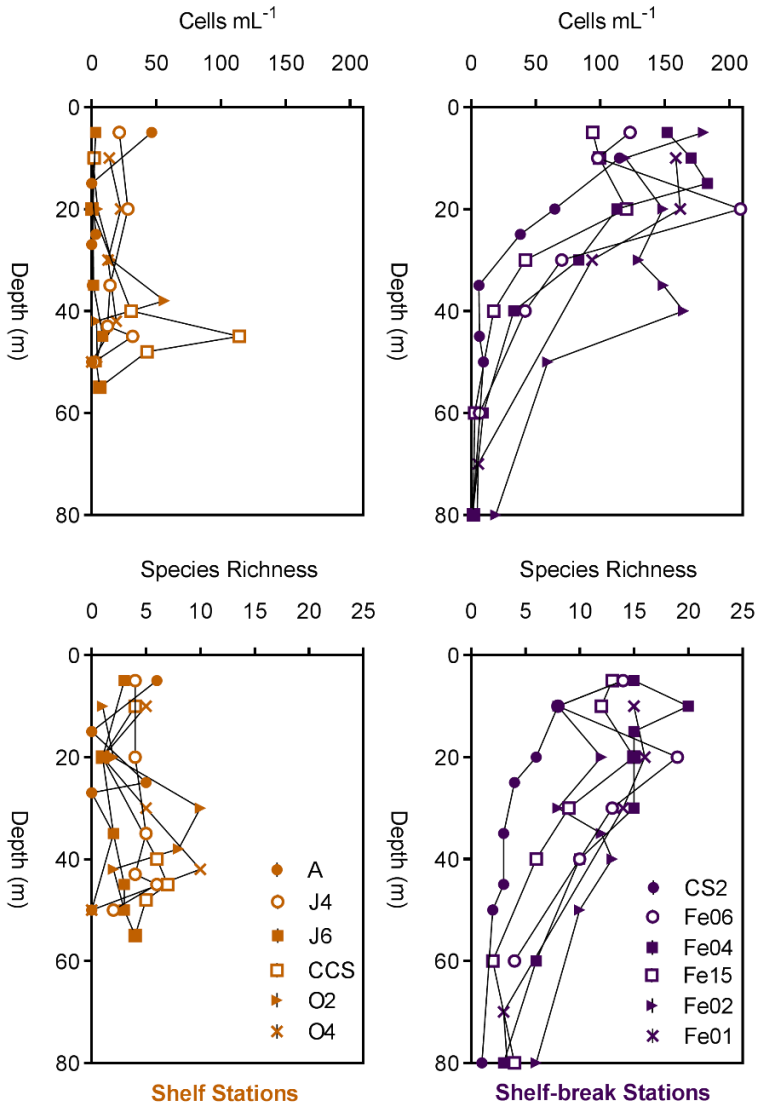


**Figure 4.9.** Depth profiles of coccolithophore cell abundance (cells $mL^{-1}$, a & b) and coccolithophore species richness (c & d), at shelf stations (a & c) and shelf-break stations (b & d).

## 4.4 Discussion

### 4.4.1 Differences between the Shelf and Shelf-break

The hydrography across the shelf transect from the mid-shelf to the shelf-break was consistent with patterns previously observed in the seasonally stratified Celtic Sea (Holligan, 1981; Harlay *et al.*, 2010; Simpson and Sharples, 2012), namely strong thermal stratification on the shelf, and evidence of increased mixing processes at the shelf-break. The coccolithophore counts across this shelf to shelf-break transect presented here provide a detailed picture of community distributions. Coccolithophore cells were identified at every station across the 400 km transect from the shelf to the shelf-break, with the most common species being *E. huxleyi,* consistent with previous findings in this region (van Oostende *et al.*, 2012; Young, Poulton and Tyrrell, 2014; Mayers *et al.*, 2018). Clear differences in abundance and community composition were also identified across the transect. The distinctly different hydrography at the shelf-break (relative to on the shelf, Figures 4.2, 4.3 and 4.6) was coupled with statistically distinct differences in the coccolithophore community. Coccolithophore cells were more abundant, and the community had a higher species richness at the shelf-break (Figure 4.5), where stratification was weaker, which is consistent with previous observations that off-shore coccolithophore species assemblages were more diverse than on shelf (Poulton *et al.*, 2014; Young, Poulton and Tyrrell, 2014).

Strength of stratification has been found to have a strong influence on summer phytoplankton community in several shelf seas, including the Celtic Sea (Jones and Gowen, 1990) the East China Shelf sea (Guo *et al.*, 2014; Jiang *et al.*, 2015) and the Patagonian shelf (Moreno *et al.*, 2012), as well as in the open ocean (Cermeno *et al.*, 2008). The close link between stratification and phytoplankton community composition is likely to be due to the close coupling of water column structure with the availability of nutrient and light resources. In particular, an increase in mixing such as that at the shelf-break can result in the intersection of relatively higher nutrients with well-lit waters (Figure 4.2c), which presents an opportunity for higher photosynthetic productivity and growth. Additionally, over the same time period (July 2015) mesozooplankton biomass was higher on the shelf than at the shelf-break (Giering *et al.*, 2018), meaning 'top-down' forces may also have contributed to a more favourable environment for phytoplankton productivity at the shelf-break.

Depth integrated (up to 100 m) Chl *a* concentrations were higher at the shelf-break stations (Figure 4.3), indicating that total phytoplankton biomass was greater here than on the shelf.

Interestingly, although coccolithophores are considered to be adapted to low nutrient, high light environments (Iglesias-Rodriguez *et al.*, 2002; Tyrrell and Merico, 2004, Chapters 2 and 3), they followed similar patterns in abundance as the total phytoplankton biomass (Figure 4.4), with higher abundance at the shelf-break (Figure 4.5 & 4.7c). Coccolithophores did not appear to be out-competed by other phytoplankton groups, such as diatoms which are adapted to higher nutrient environments, when higher levels of nutrients become available (Litchman, 2007). However, across open ocean gradients in nutrient availability, both the diatoms and the coccolithophores are observed to have similar patterns in abundance, with only the magnitude of abundance differences being greater in the diatoms (Cermeno *et al.*, 2008). As a result, coccolithophores may be proportionally more important in low nutrient, stratified areas, yet their greatest absolute abundance actually occurs where resource availability is higher. Future work aiming to identify, quantify and measure the growth rates amongst the entire plankton population across the shelf would help to unpick patterns in the relative contributions of the different phytoplankton groups to productivity in this shelf sea region.

High species richness was also important in distinguishing shelf-break communities from those of the shelf (Figure 4.7d). Species richness for some groups of large plankton (diatoms, dinoflagellates and ciliates) was examined at one shelf station (CCS) and one shelf-break station (CS2) (Figure 4.10). Depth integrated species richness of diatoms, dinoflagellates and ciliates were all higher at the shelf-break than in shelf waters, suggesting that the diversity trends identified within the coccolithophore community could be similar in other phytoplankton groups. Extension of the sampling transect beyond the shelf-break would help to inform whether species richness peaks in the shelf-break region, or whether species richness actually reaches maximum values in the open ocean (Poulton *et al.*, 2017), with the shelf-break region showing elevated diversity in comparison to the shelf due to an 'open ocean influence'. Notably, other measures of diversity, such as Pielou's evenness (J'), did not peak at the shelf-break, as *E. huxleyi* was more dominant in this region.

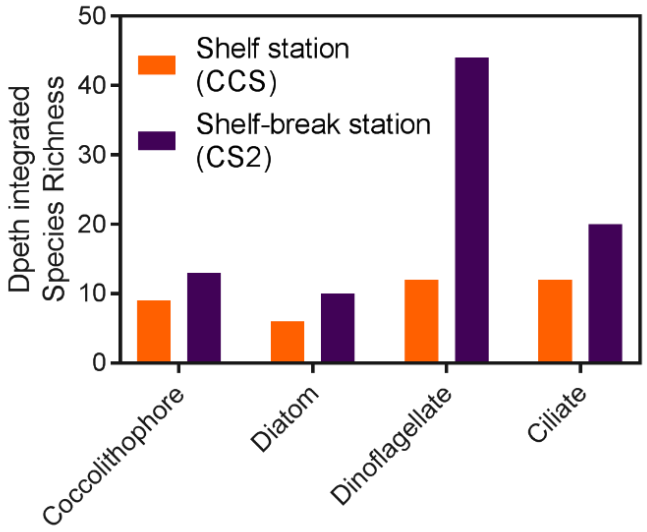


**Figure 4.10.** Depth-integrated species richness of diatoms, dinoflagellates and ciliates (determined from light microscopy counts), and of coccolithophores (determined by SEM counts), at a shelf station (CCS, orange) and a shelf-break station (CS2, purple).

### 4.4.2 Patchiness in the Shelf Environment

In addition to the dissimilarity between the shelf and shelf-break, there was also high dissimilarity between samples from different locations on the shelf (Figure 4.7). High dissimilarity between sampling locations indicates that the coccolithophore community was patchily distributed across the shelf. A survey sampling further north on the shelf also reported differences in the phytoplankton community between on and off-shelf waters, but also between different on shelf locations (Fehling *et al.*, 2012) and patchy distribution of the phytoplankton community has also been observed on the Patagonian shelf (De Souza *et al.*, 2012). As fairly stable thermal stratification persists throughout summer in the Celtic Sea (Simpson and Sharples, 2012) the drivers for this patchiness in shelf seas are not entirely understood, but physical processes causing stirring and mixing are known to have a strong role in generation of phytoplankton patchiness at different scales (Mackas, Denman and Abbott, 1985; Martin, 2003). The intermittent perturbations to stratification by wind and tide driven turbulence that can occur in the Celtic Sea region (Simpson and Hunter, 1974; Williams *et al.*, 2013) could therefore be responsible for transient changes to the water column structure, affecting the local biology.

Indeed, sampling the same location repeatedly over a time period reveals that the plankton community is temporally dynamic, changing in composition over a matter of days to weeks in the Celtic Sea (Giering *et al.*, 2018; Mayers, 2018) even during the relatively stable summer stratified period. Patchiness in the zooplankton populations (Giering *et al.*, 2018) could also

exert 'top-down' controls through a trophic cascade (i.e. grazing on the microzooplankton and subsequently onto the phytoplankton), influencing the patchiness of the coccolithophore community.

### 4.4.3 Vertical differentiation in the coccolithophore community

Vertical differentiation in the coccolithophore community was not as strong as the differences horizontally between shelf and shelf-edge waters. On the shelf especially, there was a lack of vertical structuring in the community despite strong stratification, and vertical position in the water column did not appear to have a strong impact on similarity of communities in between stations. Some species appeared to have some depth preferences, for example, on the shelf *Calciopappus caudatus* consistently peaked in abundance in the SCM, and *Ophiaster formosus* at the shelf-break peaked at or below the SCM. However, these two species formed only a small fraction of the overall coccolithophore community, in which most species did not show consistent depth preferences. In contrast, an analysis of coccolithophore communities with depth across the Atlantic Ocean (40 °N to 40 °S) found sharper gradients of statistical dissimilarity in species composition vertically over a few tens of metres than horizontally over hundreds of kilometres (Poulton *et al.*, 2017). Consistent vertical gradients in the overall phytoplankton community structure have been observed in the Celtic Sea (Hickman *et al.*, 2009), so it is noteworthy that there was a general lack of vertical differentiation within the coccolithophore community.

### 4.4.4 Conclusions

With respect to the aims set out in section 4.1, the main findings of this work are as follows:

1) **How does the coccolithophore community vary across a transect from shelf to the shelf-break?**

At most stations along the transect the most abundant coccolithophore species was *E. huxleyi*. However, statistical differences in the composition of the coccolithophore community were identified across the transect. Most notably both higher total coccolithophore cell abundance and species diversity were found at the shelf-break compared with on shelf samples.

2) **Is there vertical structuring of the coccolithophore community?**

Vertical differentiation in the coccolithophore community (mainly abundance driven) was identified at some shelf-break stations, but vertical differences were less strong than the differences horizontally.

3) **What factors might drive the patterns in coccolithophore community distributions?**

Differences between the shelf and shelf-break coccolithophore communities coincided with the different hydrographic regimes between these two sites, notably weaker stratification at the shelf-break indicative of increased mixing processes. However, samples from different stations along the strongly stratified shelf were highly dissimilar, indicating non-homogenous, patchy distributions, which cannot be entirely explained by the environmental data available.

# Chapter 5 Synthesis

## 5.1 Thesis Summary

This thesis set out to explore photophysiology in a range of coccolithophore species, to enhance our understanding of how coccolithophores use light for growth, and to identify patterns, similarities and differences within the group. The photophysiological laboratory experiments undertaken (Chapters 2 and 3) utilised a much greater diversity of species ($n$ = 10) than ever previously attempted in a single experimental setup. The results greatly expand the body of information on photosynthetic properties and responses amongst the coccolithophores, as existing literature about this important group of phytoplankton has overwhelmingly focussed on *Emiliania huxleyi* (e.g. Paasche, 2002; Suggett *et al.*, 2007; McKew, Davey, *et al.*, 2013; Aloisi, 2015).

In **Chapter 2**, the pigments, light absorption properties and photoacclimation strategies are compared across the 10 species. Similarities between all species were identified, namely all possessed the same types of pigments, and a high accessory pigment content was common to all species. Notable differences between the coccolithophore species were also revealed in, for example, the relative abundance of the coccolithophore 'biomarker pigment' (19'Hexanoyloxyfucoxanthin) varied widely between species, as did the mode of photoacclimation (expanded on further in section 5.3). The size range of the species cultured in the laboratory experiments allowed examination of interspecific size scaling with respect to light harvesting in the coccolithophores for the first time, in **Chapter 3.** Negative size scaling of maximum growth rate and pigment densities was found amongst the coccolithophores, consistent with previous findings in other phytoplankton groups such as the diatoms (Finkel, 2001). However, large coccolithophore cells (> 1000 $\mu m^3$, see Figure 3.2) did not experience a growth rate penalty under low light (25 μmol photons $m^{-2}$ $s^{-1}$) conditions due to size dependent packaging effects, which was an unexpected finding (expanded upon further in section 5.4). **Chapter 4** shifts focus to coccolithophore communities in the field, and found differences in the species composition between the contrasting hydrographic regimes of the stratified central shelf and mixed shelf-break of the Celtic Sea. Patchiness in the community on the stratified shelf, and a lack of vertical differentiation of the species present, underline the complexity of environmental drivers of coccolithophore distributions in the real world.

## 5.2 Synthesis Outline

This chapter synthesises the findings from Chapters 2 to 4, and integrates the results with respect to the implications for our understanding of the ecological niches of the coccolithophores. Photosynthetic characteristics that unite the coccolithophores (traits conserved amongst the species investigated) are summarised, as well as aspects in which there was considerable diversity identified between the 10 species studied. Particularly interesting areas for future research are also highlighted, and the suitability of the current model species *Emiliania huxleyi* as a representative for the entire group is considered.

## 5.3 Traits conserved amongst coccolithophore species

Results from the culture experiments undertaken reveal traits and characteristics that are relatively conserved amongst the 10 coccolithophore species examined. A very similar suite of pigments was identified in all species (Table 2.1, Figure 2.5, Chapter 2), and the ratio between Chl *a* and accessory pigments was remarkably conserved. Namely, all species had a stoichiometry between Chlorophyll *a* and Fucoxanthin-derived pigments (Fs) of ~ 1:1, regardless of growth irradiance (Figure 2.7, Chapter 2). This high abundance of accessory pigments sits in contrast to the diatoms, for example, which typically have higher Chl *a* to accessory ratios (e.g. Schlüter *et al.*, 2000). Indeed the diatom (*Thalassiosira weissflogii*) grown in parallel had a Chl *a* : Fs ratio of ~ 3:1 (Figure 2.7, Chapter 2).

Conserved pigment stoichiometry indicates that the structure of the light harvesting equipment is similar amongst the coccolithophores, but the functional significance of having equal amounts of accessory pigment and Chl *a* remains unclear. A possible hypothesis is that the putative energy dissipation capabilities of fucoxanthin derivatives could allow the photosynthetic units to have a large absorption cross-section (high probability of absorbing photons) whilst minimising the risk of photodamage. Future work to measure rates of photodamage (e.g. by quantifying repair rates of the D1 reaction centre protein; Bouchard, Campbell and Roy, 2005), and exploring the behaviour and function of the fucoxanthin-derived pigments in the pigment-protein complexes (e.g. quantifying excitation energy transfer kinetics; Papagiannakis *et al.*, 2005) will help to elucidate the benefits that a high abundance of accessory pigments affords the coccolithophores relative to other marine autotrophs.

High accessory pigment content in coccolithophores directly resulted in high light absorption in the 440 - 470 nm (blue) region, which made the shape of light absorption spectra of the coccolithophores clearly distinguishable from the diatom species (Figure 2.8, Chapter 2). An

interesting future avenue could be to explore if these spectral absorption properties may give the coccolithophores a competitive edge for light harvesting in the blue-water oligotrophic ocean, where coccolithophore diversity is high. Conserved pigment stoichiometry and unique spectral light absorption properties within the coccolithophores, including in a non-calcifying *E. huxleyi* strain, could also be harnessed to build on the current optical methods used to identify and quantify coccolithophores in mixed communities. For example, an average spectral shape for the coccolithophores (Figure 2.8, Chapter 2) could be used as a reference spectrum in hyper-spectral sensing methods (e.g. Bracher *et al.*, 2008; Sadeghi, Dinter, Vountas, B. Taylor, *et al.*, 2012), in conjunction with reflectance algorithms, with confidence that it is not biased towards calcifying *E. huxleyi*.

## 5.4 Notable diversity amongst coccolithophore species

Some characteristics or responses were not conserved amongst all the coccolithophore species examined. For example, the contribution of the coccolithophore 'biomarker pigment' 19'Hexanoyloxyfucoxanthin (Roy *et al.*, 2011) was highly variable between species (from 0.5 % of total pigment in *C. braarudii* to 38.4 % in *C. quadriperforatus*). This section will focus on a case study comparison between the common model species *E. huxleyi* and a representative of the highly diverse *Syracosphaera* genus (*S. pulchra*), to highlight some of the notable differences in photophysiology and ecology that have been revealed amongst the coccolithophores in this thesis.

Some of the key differences in physiology between *E. huxleyi* and *S. pulchra* are summarised in Figure 5.1. Firstly, note that there is a clear difference in size, with average cell volume 43 $\mu m^3$ and 1632 $\mu m^3$ in *E. huxleyi* and *S. pulchra* respectively. *S. pulchra* was substantially less pigmented than *E. huxleyi* under all irradiances (probably a consequence of size-dependent package effect, see Chapter 3). Photoacclimation strategy was markedly different between the two species (see Chapter 2, Figure 2.2 for background). When grown under low light (25 μmol photons $m^{-2}$ $s^{-1}$), *E. huxleyi* increased pigment density by > 70 % relative to when grown at high light (200 μmol photons $m^{-2}$ $s^{-1}$). Changes in absorption cross-section of PSII photochemistry ($\sigma_{PSII}$), the quantum yield of PSII photochemistry ($F_v/F_m$) and Chl *a*-specific absorption efficiency ($a^{chl}$) between growth irradiances were small (Figures 2.9 and 2.10, Chapter 2), indicating that *E. huxleyi* incorporated this extra amount of pigment by increasing the **number** of photosynthetic units (an 'n' strategy, see Figure 2.2, Chapter 2). In contrast, when grown under low light, *S. pulchra* increased pigment density by < 40 % relative to when grown at high light, and a significant increase in $\sigma_{PSII}$ (from 6.3 to 8.8 $nm^2$ $PSII^{-1}$) and a

decrease in $F_v/F_m$ (from 0.46 to 0.33) indicated that *S. pulchra* incorporated this extra pigment, at least partly, by increasing the **size** of photosynthetic units (a 'σ' strategy, see Figure 2.2., Chapter 2). These two contrasting photoacclimation strategies are likely to have different cost and benefit consequences for the cells. For example, the 'n' strategy of *E. huxleyi* is likely more expensive (in terms of nutrient resources) but could minimise the risk of over excitation of RCs and photodamage. The 'σ' strategy of *S. pulchra* probably requires less investment of nutrient resources, but could leave RCs more susceptible to photodamage. (Note that whilst the data suggests that *S. pulchra* increases the size of PSU's under low light, they are still estimated to be smaller than the PSU's of *E. huxleyi* in absolute terms (875 Chl *a* $RC^{-1}$ in *S. pulchra* compared with 1057 in *E. huxleyi*)). The high accessory pigment content could also minimise the risk of photodamage in both species, as discussed in Chapter 2. Notably, the changes in the non-photosynthetic to photosynthetic pigment ratios (an increase at high light compared to low) were similar in both *E. huxleyi* and *S. pulchra* (and indeed all the species examined) with a higher abundance of non-photosynthetic pigments under high light compared to low light conditions.

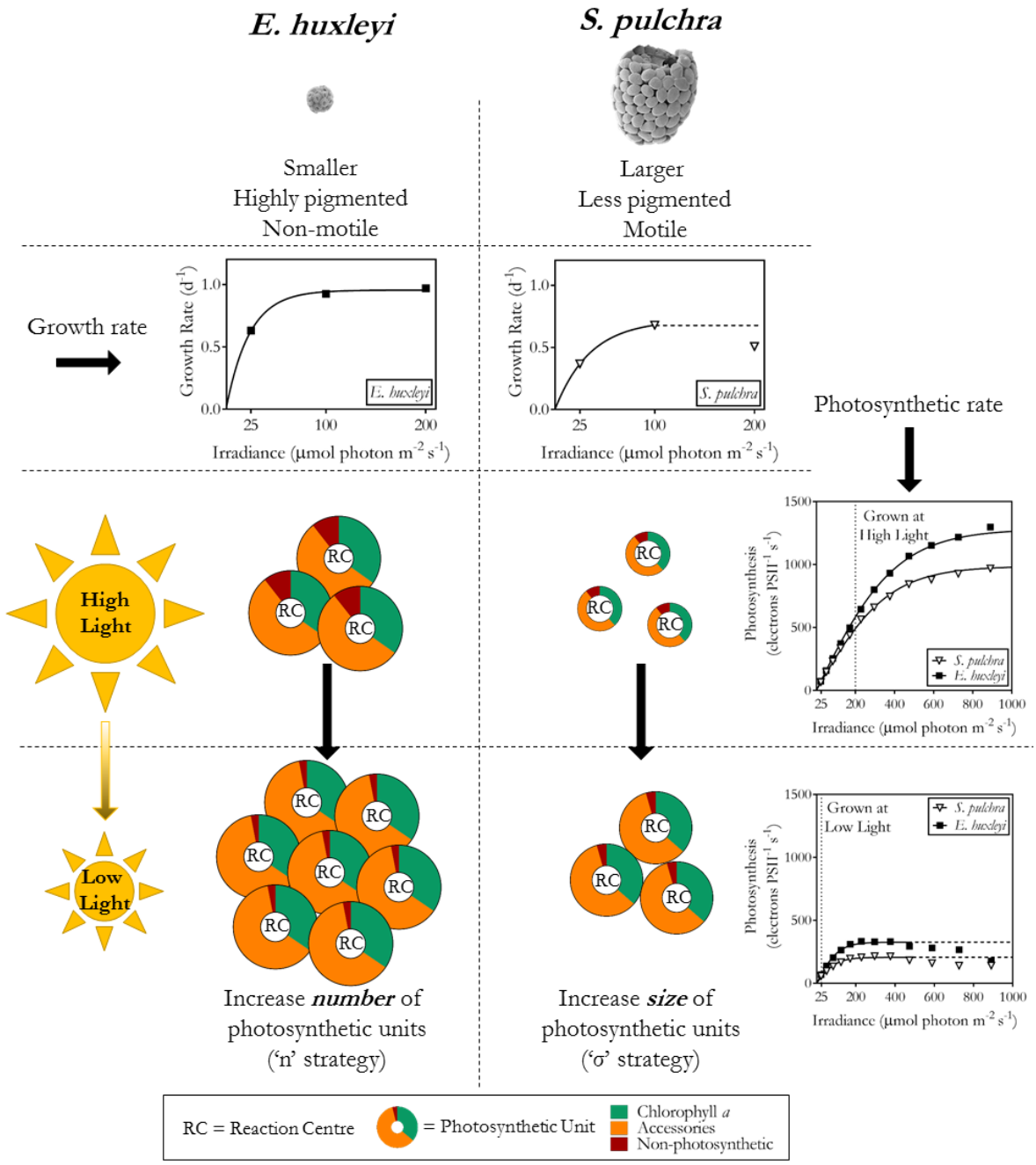


**Figure 5.1.** Schematic comparison of the photoacclimation of *Emiliania huxleyi* (filled squares) and *Syracosphaera pulchra* (unfilled triangles) between high light and low light (200 and 25 µmol photons $m^{-2}$ $s^{-1}$), including exponential growth rate – irradiance curves (top), and photosynthetic rate (PSII electron transport) – irradiance curves (right). Photosynthetic equipment is represented as circular photosynthetic units with a reaction centre (RC) at the centre surrounded by pigments (Chlorophyll *a* = green, Photosynthetic accessories = orange, Non-photosynthetic accessories = red). The size of the circles represents the size of the photosynthetic unit (amount of pigment associated with each RC).

The differences in photoacclimation strategy between *E. huxleyi* and *S. pulchra* highlighted in Figure 5.1 both result in similar acclimation of the photosynthesis-irradiance relationship (as probed by PSII fluorescence dynamics). Both species had a higher $P_{max}$ (maximum rate of electron transport) and $E_k$ (irradiance at which electron transport rate begins to saturate) when grown under high light (Figure 5.1), but PSII-specific electron transport rate was consistently higher in *E. huxleyi* than in *S. pulchra* under all irradiances. In turn, the photosynthesis – irradiance curves do not provide any obvious clues to the differences in the growth-rate irradiance relationship between the two species (Figure 5.1). Growth rate peaks at an intermediate irradiance in *S. pulchra,* and appears to be inhibited under higher irradiance (of 200 μmol photons $m^{-2}$ $s^{-1}$), yet electron transport rate shows no evidence of becoming inhibited in cells adapted to this irradiance (with electron transport rates still at a maximum at 1000 μmol photons $m^{-2}$ $s^{-1}$). Physiological acclimation to irradiance is complex amongst the different species of coccolithophore, and ultimately processes downstream of electron transport at PSII (e.g. carbon fixation rates and how this photosynthate is utilised by the cells) are important in dictating how acclimation of the light harvesting equipment translates into competitive advantages for the different species (e.g. growth rate response).

The differences in photophysiology between *E. huxleyi* and *S. pulchra* revealed in these laboratory studies can be contextualised with inferences about their relative ecologies made from biogeographical distributions. In the Celtic Sea transect (Chapter 4), *S. pulchra* was present but very rare (present in just 3 samples at < 1 cell $mL^{-1}$). Low *S. pulchra* abundance in this region is consistent with previous observations that *S. pulchra* is most abundant in sub-tropical waters, where it has a 'warm water, low productivity' preference (Ziveri *et al.*, 2004). Although it is sometimes present in high latitude waters (e.g. Findlay and Giraudeau, 2000), *S. pulchra* does not appear to grow well below 10 °C (Buitenhuis *et al.*, 2008). In a transect across the Atlantic tropics and sub tropics, *S. pulchra* had a preference for shallow waters (classified as an upper euphotic zone species, (Poulton *et al.*, 2017)) where it is likely to be exposed to high irradiance and low inorganic nutrients. *S. pulchra* is an abundant coccolithophore in the Mediterranean (Cros and Fortuno, 2002; Šupraha *et al.*, 2016) where it has a preference for warm summer stratified waters that are low in inorganic nitrogen. In summary, the biogeography of *S. pulchra* suggests that it prefers oligotrophic conditions, high in light and low in nutrients. Conversely, whilst *E. huxleyi* is widely distributed from the tropics to the poles, it blooms most extensively in temperate, (relatively) high productivity waters. Surprisingly, preference for high irradiance was not evident in the growth-irradiance response of *S. pulchra* (Figure 5.1), as it's growth rate at high light (200 μmol photons $m^{-2}$ $s^{-1}$) was below maximum (0.51 $d^{-1}$, compared to 0.68 $d^{-1}$ at an intermediate light level of 100 μmol photons $m^{-}$

$^{2}$ $s^{-1}$). However, there is a strong possibility that some of the motile coccolithophores, particularly the haploid forms such as the *S. pulchra* strain used in this study, could employ mixotrophy to meet their nutritional and energetic needs (Houdan *et al.*, 2006, Ian Probert, pers. comm.). Lower investment in light harvesting equipment in *S. pulchra* (e.g. lower pigment and PSU densities) compared to *E. huxleyi* and most of the other coccolithophores investigated in this work could indicate that *S. pulchra* has a survival strategy that does not depend entirely on autotrophy. Crucially, the laboratory experiments undertaken in this thesis were replete with inorganic nutrients. Therefore, competitive advantages in 'real' conditions where inorganic nutrients are limiting cannot be empirically assessed here. Exploring photosynthetic response amongst the coccolithophores in different nutrient conditions (e.g. 'oligotrophic' conditions with low inorganic nutrients, but with organic nitrogen and phosphorus in various dissolved and particulate forms) is a promising area for future work.

## 5.5 Carbon density scaling in the Coccolithophores

Results in Chapter 3 revealed size scaling of growth rates and pigment densities amongst the coccolithophores, in line with current theory regarding the limitations that size dependent packaging effects place on the light harvesting and photosynthetic rates of phytoplankton cells (Finkel, 2001; Finkel, Irwin and Schofield, 2004). However, an unexpected result was revealed under low light (25 μmol photons $m^{-2}$ $s^{-1}$) conditions, wherein large cells (> 1000 $\mu m^3$) did not experience greater growth rate limitation than the small cells (Figure 3.3, Chapter 3), and were able to maintain their growth rates near maximum. The growth rate differential between large and small coccolithophore cells was less under low light conditions than in high light conditions, in contrast to an expectation that small cells (experiencing less package effects) would have a relative competitive advantage under low light conditions. This unusual result could have consequences for our understanding of coccolithophore ecology, as light availability in natural systems may therefore drive the size distribution of coccolithophores in unexpected ways. For example, small coccolithophores could be more successful (relative to large cells) in high light environments, whilst large cells could be relatively more successful in low light environments.

It is interesting to consider how large (> 1000 $\mu m^3$) coccolithophore cells might physiologically achieve the maintenance of growth rate near maximal under low irradiance. The discussion in Chapter 3 touches on how scaling of carbon density with cell volume could reconcile this unexpected increase in the size scaling growth exponent under low light with the current theoretical framework. Namely, if carbon density in coccolithophores were to scale negatively with cell volume (as has been noted for some other phytoplankton groups

(Menden-Deuer and Lessard, 2000)), larger cells could have a lower volume-specific carbon demand, and a correspondingly lower volume-specific photosynthetic requirement for achieving maximum growth rate. The consequences of different carbon size scaling scenarios on the photosynthetic requirements of cells are now explored in a small cell (*E. huxleyi*) and a large cell (*C. quadriperforatus*). These "back of the envelope" calculations demonstrate theoretically how small cells could potentially become light limited at a greater irradiance than large cells, when the carbon demands of large cells are lower.

Carbon density for a small cell (*E. huxleyi*) was estimated following Menden-Deuer and Lessard (2000) (Table 5.1). Carbon density of the large cell (*C. quadriperforatus*) was then scaled according to three different exponents (Table 5.1) (exponents = 1, 0.8 and 0.7). A scaling exponent of 1 represents isometric scaling (or no size scaling, as carbon content is directly proportional to cell volume), whilst exponents < 1 represents a lower carbon density in large cells. Volume-specific photosynthetic requirements for achieving maximum growth rate (pg C $\mu m^{-3}$ $d^{-1}$) were then estimated by multiplying the maximum exponential growth rate ($d^{-1}$) with the estimated carbon density (pg C $\mu m^{-3}$), which in *C. quadriperforatus* varied with the size scaling factor. These hypothetical carbon requirement scenarios (indicated by a dashed lines in Figure 5.2), were applied to the photosynthesis-irradiance curves generated for *E. huxleyi* and *C. quadriperforatus* when grown under low irradiance (25 μmol photons $m^{-2}$ $s^{-1}$).

**Table 5.1.** Maximum growth rate ($d^{-1}$), estimated carbon density (pg C $\mu m^{-3}$) and estimated carbon requirement for maximum growth rate ( pg C $\mu m^{-3}$ $d^{-1}$) for *E. huxleyi* and *C. quadriperforatus* using three different carbon scaling exponents (1, 0.8 and 0.7).

| | **Species** | **Max Growth Rate ($d^{-1}$)** | **Carbon Density (pg C $\mu m^{-3}$)** | **Carbon Requirement (pg C $\mu m^{-3}$ $d^{-1}$)** |
|---|---|---|---|---|
| | *E. huxleyi* | 0.95 | 0.173 | 0.166 |
| **Size-Scaling Exponent** | | | | |
| 1 | *C. quadriperforatus* | 0.40 | 0.173 | 0.070 |
| 0.8 | | | 0.087 | 0.035 |
| 0.7 | | | 0.061 | 0.025 |

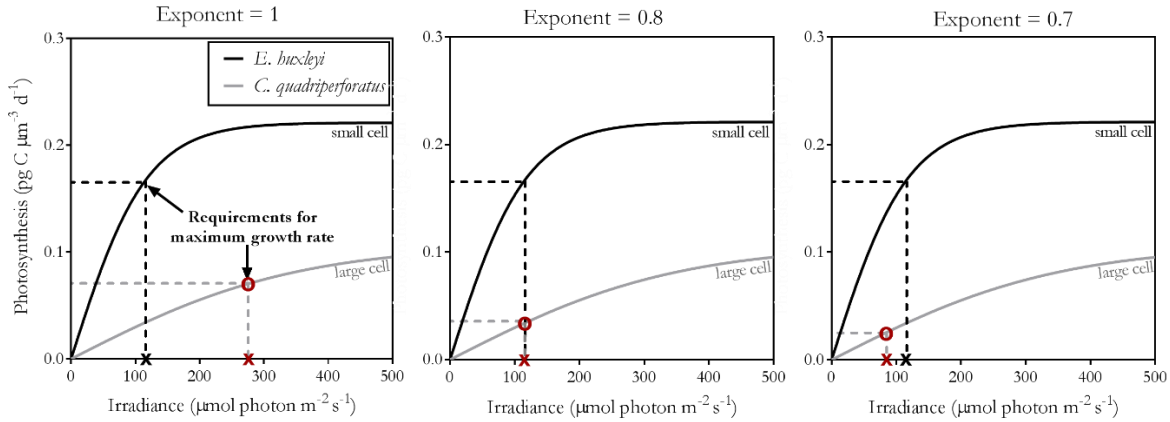


**Figure 5.2.** Photosynthesis-irradiance curves for large species *C. quadriperforatus* and small species *E. huxleyi*. Volume-specific photosynthesis (P) was estimated by converting volume-specific electron transport at PSII (electrons $\mu m^{-3}$ $d^{-1}$) to carbon fixation (pg C $\mu m^{-3}$ $d^{-1}$) using a quantum yield of 0.1 mol C (mol electrons)$^{-1}$. Note that the volume-specific photosynthetic rate is lower in the large cell, due to the lower density of pigments and PSII (see Chapter 3). Photosynthetic carbon requirement for maximum growth rate (dashed lines) calculated by scaling carbon density with cell volume with an exponent of 1 (a), 0.8 (b) and 0.7 (c). The irradiance required for attaining photosynthetic carbon requirement is marked by 'x' in black for *E. huxleyi* and red for *C. quadriperforatus*. Note how the point on the *C. quadriperforatus* curve (red 'o') shifts to lower values with the different carbon scaling exponents.

In the isometric scaling scenario (a, exponent = 1), the difference in photosynthetic carbon requirement between the two species is proportional to the difference in maximum growth rate. The irradiance required for the cell to achieve the photosynthetic requirement for maximum growth rate is higher in the large cell than in the small. When carbon density scaled with an exponent of 0.8 (similar to the carbon density scaling pattern amongst the diatoms; Menden-Deuer and Lessard, 2000), the photosynthetic requirement for the large cell is reduced, and the two species required a similar irradiance to meet their photosynthetic demands (b). When carbon density was assumed to decrease with cell volume even more steeply (e.g. c, exponent = 0.7) the photosynthetic requirement for the large cell is reduced such that the irradiance the large cell requires to meet this photosynthetic requirement is actually *lower* than for the small cell.

These examples show that size scaling of carbon density (and volume-specific carbon demand) could be important in allowing large coccolithophore cells to maintain growth rates near maximum under low light conditions. Although this thesis does not provide empirical data to support scaling of carbon density amongst the coccolithophores, the negative size

scaling of pigment density amongst the coccolithophores studied (Chapters 2 and 3) also suggests a lower density of organic matter generally in the large cells. Additionally, scaling of carbon density is common in many phytoplankton groups, including an exponent of 0.89 in the prymnesiophytes (Menden-Deuer and Lessard, 2000). However, *E. huxleyi* is commonly the only coccolithophore species considered in such analyses, and exploring the organic composition and cell stoichiometry amongst coccolithophore of various sizes presents a promising area of future research.

## 5.6 Concluding Remarks

In this thesis, the detailed analysis of physiology in a wide range of coccolithophore species, under carefully controlled experimental conditions, has provided a wealth of insights into the physiological ecology of the coccolithophores. The results presented reveal characteristics which unite the coccolithophores as a group, but have also identified notable diversity amongst the group. Some of the species-specific differences can be understood in the context of cell size, but other differences were entirely unexpected, and indicate substantial differences in ecological strategy amongst the coccolithophores. Together, the evidence presented in this thesis advocates continuing to expand the use of a higher diversity of coccolithophore species in experimental work. Physiological studies using a variety of coccolithophore species can build on the solid foundation of pre-existing research on *E. huxleyi*, and advance our understanding of the coccolithophore algae.

# Appendix A Supplementary Data for Chapters 2 & 3

**Appendix A.i**. Exponential growth rate ($d^{-1}$, see methods section 2.2.2) for culture replicates (A and B) of each coccolithophore species under low, medium and high light conditions (25, 100 and 200 μmol photons $m^{-2}$ $s^{-1}$, respectively).

| | Exponential Growth Rate ($d^{-1}$) | | | | | |
|---|---|---|---|---|---|---|
| **Species** | **Low Light** (25 μmol photons $m^{-2}$ $s^{-1}$) | | **Medium Light** (100 μmol photons $m^{-2}$ $s^{-1}$) | | **High Light** (200 μmol photons $m^{-2}$ $s^{-1}$) | |
| | **A** | **B** | **A** | **B** | **A** | **B** |
| *Reticulofenestra parvula* | 0.56 | 0.56 | 0.91 | 0.89 | 0.88 | 0.91 |
| *Gephyrocapsa muellerae* | 0.51 | 0.52 | 0.74 | 0.72 | 0.72 | 0.74 |
| *Gephyrocapsa oceanica* | 0.50 | 0.50 | 0.71 | 0.70 | 0.65 | 0.66 |
| *Emiliania huxleyi* (1N) | 0.56 | 0.56 | 0.97 | 0.97 | 1.12 | 1.08 |
| *Emiliania huxleyi* | 0.62 | 0.64 | 0.90 | 0.95 | 0.97 | 0.97 |
| *Calcidiscus leptoporus* | 0.30 | 0.32 | 0.47 | 0.44 | 0.42 | 0.46 |
| *Calcidiscus quadriperforatus* | 0.34 | 0.39 | 0.40 | 0.41 | 0.40 | 0.42 |
| *Helicosphaera carteri* | 0.25 | 0.26 | 0.30 | 0.30 | | |
| *Syracosphaera pulchra* | 0.38 | 0.36 | 0.57 | 0.65 | 0.49 | 0.52 |
| *Coccolithus braarudii* | 0.45 | 0.42 | 0.47 | 0.41 | | |

**Appendix A.ii**. Average cell volume ($\mu m^3$) (n = 50, ± SD, see methods section 2.2.3) for cultures of each coccolithophore species under low, medium and high light conditions (25, 100 and 200 μmol photons $m^{-2}$ $s^{-1}$, respectively)

| | Cell Volume ($\mu m^{-3}$) ± SD | | |
|---|---|---|---|
| **Species** | **Low Light** (25 μmol photons $m^{-2}$ $s^{-1}$) | **Medium Light** (100 μmol photons $m^{-2}$ $s^{-1}$) | **High Light** (200 μmol photons $m^{-2}$ $s^{-1}$) |
| *Reticulofenestra parvula* | 10.95 ± 4.99 | 16.31 ± 6.28 | 17.24 ± 7.03 |
| *Gephyrocapsa muellerae* | 47.07 ± 14.52 | 57.85 ± 20.89 | 74.71 ± 22.72 |
| *Gephyrocapsa oceanica* | 140.10 ± 47.33 | 216.70 ± 74.98 | 197.50 ± 58.22 |
| *Emiliania huxleyi* (1N) | 33.43 ± 9.92 | 32.19 ± 8.82 | 31.48 ± 8.72 |
| *Emiliania huxleyi* | 36.95 ± 10.03 | 46.10 ± 12.75 | 47.02 ± 14.37 |
| *Calcidiscus leptoporus* | 356.90 ± 117.50 | 438.40 ± 157.30 | 468.80 ± 170.70 |
| *Calcidiscus quadriperforatus* | 1184.00 ± 371.60 | 1381.00 ± 399.90 | 1434.00 ± 447.70 |
| *Helicosphaera carteri* | 1317.00 ± 295.00 | 1823.00 ± 434.20 | |
| *Syracosphaera pulchra* | 1648.00 ± 702.50 | 1675.00 ± 544.90 | 1574.00 ± 613.40 |
| *Coccolithus braarudii* | 1964.00 ± 689.50 | 2120.00 ± 915.60 | |

**Appendix A.iii.** Pigment Concentration (pg cell$^{-1}$, see methods in section 2.2.4) in coccolithophore cultures grown under low light conditions (25 µmol photons m$^{-2}$ s$^{-1}$). Chl $c_3$ = Chlorophyll *c*3, Chl $c_2$ = Chlorophyll *c*2, Chl $c_1$ = Chlorophyll *c*1, BF = 19'Butanoyloxy-fucoxanthin, F = Fucoxanthin, HKF= 19'Hexanoyloxy-4-ketofucoxanthin, HF = 19'Hexanoyloxy-fucoxanthin, Dd = Diadinoxanthin, Dt = Diatoxanthin, Chl $c_2$ M = Chlorophyll c2-monogalactosyl-diacylglyceride-ester, Chl *a* = Chlorophyll *a*, Other = Gyroxanthin dodecanoate ethanoate and magnesium-2,4-divinylpheoporphyrin-a5-monomethyl-ester

| **Low Light** (25 µmol photons m$^{-2}$ s$^{-1}$) | **Average Pigment Concentration (pg cell$^{-1}$)** | | | | | | | | | | | | |
|---|---|---|---|---|---|---|---|---|---|---|---|---|---|
| **Species** | **Chl $c_3$** | **Chl $c_2$** | **Chl $c_1$** | **BF** | **F** | **HKF** | **HF** | **Dd** | **Dt** | **Chl $c_2$-M** | **Chl *a*** | **Chl $c_3$** | **Other** |
| *Reticulofenestra parvula* | 0.019 | 0.014 | | | 0.005 | 0.008 | 0.063 | 0.006 | 0.012 | 0.073 | 0.002 | 0.001 | 0.019 |
| *Gephyrocapsa muellerae* | 0.049 | 0.040 | | 0.001 | 0.007 | 0.002 | 0.205 | 0.017 | 0.034 | 0.215 | 0.007 | 0.003 | 0.049 |
| *Gephyrocapsa oceanica* | 0.172 | 0.131 | | | 0.459 | 0.120 | 0.159 | 0.089 | 0.126 | 0.765 | 0.026 | | 0.172 |
| *Emiliania huxleyi* (1N) | 0.053 | 0.060 | | | 0.118 | 0.036 | 0.110 | 0.014 | 0.044 | 0.253 | 0.007 | 0.001 | 0.053 |
| *Emiliania huxleyi* | 0.059 | 0.040 | | 0.001 | 0.058 | 0.025 | 0.140 | 0.011 | 0.038 | 0.201 | 0.006 | 0.003 | 0.059 |
| *Calcidiscus leptoporus* | 0.112 | 0.111 | | 0.027 | | | 0.630 | 0.062 | 0.043 | 0.718 | 0.022 | 0.019 | 0.112 |
| *Calcidiscus quadriperforatus* | 0.376 | 0.312 | | 0.019 | | | 1.909 | 0.178 | 0.092 | 1.963 | 0.071 | 0.049 | 0.376 |
| *Helicosphaera carteri* | 0.297 | 0.294 | | | 0.009 | | 1.496 | 0.123 | 0.129 | 1.860 | 0.072 | 0.054 | 0.297 |
| *Syracosphaera pulchra* | 0.252 | 0.098 | | | | | 0.914 | 0.079 | 0.162 | 0.900 | 0.030 | 0.038 | 0.252 |
| *Coccolithus braarudii* | 1.069 | 0.582 | 0.240 | 0.112 | 4.282 | 0.381 | 0.066 | 0.428 | 0.477 | 5.117 | 0.153 | 0.086 | 1.069 |

**Appendix A.iii. continued**. Pigment concentrations in coccolithophore cultures grown under high light conditions (200 μmol photons $m^{-2}$ $s^{-1}$).

| **Medium Light** (100 μmol photons $m^{-2}$ $s^{-1}$) | **Average Pigment Concentration (pg $cell^{-1}$)** | | | | | | | | | | | | |
|---|---|---|---|---|---|---|---|---|---|---|---|---|---|
| **Species** | **Chl *c*$_3$** | **Chl *c*$_2$** | **Chl *c*$_1$** | **BF** | **F** | **HKF** | **HF** | **Dd** | **Dt** | **Chl *c*$_2$-M** | **Chl *a*** | **Chl *c*$_3$** | **Other** |
| *Reticulofenestra parvula* | 0.016 | 0.016 | | | 0.007 | 0.006 | 0.062 | 0.008 | 0.012 | 0.074 | 0.002 | 0.002 | 0.016 |
| *Gephyrocapsa muellerae* | 0.042 | 0.035 | | | 0.005 | | 0.176 | 0.043 | 0.029 | 0.183 | 0.005 | 0.002 | 0.042 |
| *Gephyrocapsa oceanica* | 0.144 | 0.137 | | 0.003 | 0.301 | 0.105 | 0.254 | 0.087 | 0.121 | 0.729 | 0.024 | 0.009 | 0.144 |
| *Emiliania huxleyi* (1N) | 0.033 | 0.047 | | 0.001 | 0.041 | 0.014 | 0.133 | 0.029 | 0.033 | 0.195 | 0.006 | 0.002 | 0.033 |
| *Emiliania huxleyi* | 0.042 | 0.045 | | 0.001 | 0.021 | 0.013 | 0.175 | 0.042 | 0.030 | 0.194 | 0.006 | 0.003 | 0.042 |
| *Calcidiscus leptoporus* | 0.035 | 0.064 | | 0.010 | | | 0.284 | 0.040 | 0.018 | 0.329 | 0.010 | 0.010 | 0.035 |
| *Calcidiscus quadriperforatus* | 0.194 | 0.254 | | 0.019 | 0.019 | | 1.242 | 0.242 | 0.067 | 1.400 | 0.056 | 0.055 | 0.194 |
| *Helicosphaera carteri* | 0.215 | 0.313 | | | 0.015 | | 1.318 | 0.208 | | 1.400 | 0.053 | 0.062 | 0.215 |
| *Syracosphaera pulchra* | 0.209 | 0.108 | | 0.008 | 0.009 | | 0.788 | 0.091 | 0.157 | 0.889 | 0.029 | 0.040 | 0.209 |
| *Coccolithus braarudii* | 0.791 | 0.594 | 0.268 | 0.050 | 3.793 | 0.371 | 0.149 | 0.854 | 0.466 | 4.411 | 0.113 | 0.075 | 0.791 |

**Appendix A.iii. continued**. Pigment concentrations in coccolithophore cultures grown under high light conditions (200 μmol photons $m^{-2}$ $s^{-1}$).

| **High Light** (200 μmol photons $m^{-2}$ $s^{-1}$) | **Average Pigment Concentration (pg $cell^{-1}$)** | | | | | | | | | | | | |
|---|---|---|---|---|---|---|---|---|---|---|---|---|---|
| **Species** | **Chl *c*$_3$** | **Chl *c*$_2$** | **Chl *c*$_1$** | **BF** | **F** | **HKF** | **HF** | **Dd** | **Dt** | **Chl *c*$_2$-M** | **Chl *a*** | **Chl *c*$_3$** | **Other** |
| *Reticulofenestra parvula* | 0.011 | 0.011 | | | 0.005 | 0.004 | 0.045 | 0.015 | 0.008 | 0.055 | 0.002 | 0.001 | 0.011 |
| *Gephyrocapsa muellerae* | 0.033 | 0.036 | | | 0.005 | | 0.165 | 0.059 | 0.026 | 0.176 | 0.005 | 0.002 | 0.033 |
| *Gephyrocapsa oceanica* | 0.115 | 0.113 | | 0.002 | 0.205 | 0.083 | 0.262 | 0.120 | 0.093 | 0.602 | 0.019 | 0.006 | 0.115 |
| *Emiliania huxleyi* (1N) | 0.017 | 0.026 | | 0.001 | 0.018 | 0.006 | 0.097 | 0.032 | 0.019 | 0.127 | 0.003 | 0.002 | 0.017 |
| *Emiliania huxleyi* | 0.027 | 0.034 | | 0.000 | 0.012 | 0.006 | 0.133 | 0.041 | 0.022 | 0.151 | 0.005 | 0.003 | 0.027 |
| *Calcidiscus leptoporus* | 0.027 | 0.057 | | 0.008 | | | 0.244 | 0.068 | 0.009 | 0.294 | 0.010 | 0.010 | 0.027 |
| *Calcidiscus quadriperforatus* | 0.127 | 0.167 | | 0.011 | 0.019 | | 0.830 | 0.371 | 0.036 | 1.007 | 0.048 | 0.034 | 0.127 |
| *Syracosphaera pulchra* | 0.138 | 0.079 | | 0.004 | 0.009 | | 0.583 | 0.168 | 0.104 | 0.705 | 0.028 | 0.028 | 0.138 |

**Appendix A.iv.** Chlorophyll a specific light absorption efficiency ($m^2$ $g^{-1}$ Chl *a,* ± SD, see methods in section 2.2.5) at select wavelengths (440 nm and 675 nm) for cultures of each coccolithophore species under low, medium and high light conditions (25, 100 and 200 μmol photons $m^{-2}$ $s^{-1}$, respectively).

| | **Chl *a* specific light absorption efficiency ($m^2$ $g^{-1}$ Chl *a*) ± SD** | | | | | |
|---|---|---|---|---|---|---|
| **Species** | **Low Light** (25 μmol photons $m^{-2}$ $s^{-1}$) | | **Medium Light** (100 μmol photons $m^{-2}$ $s^{-1}$) | | **High Light** (200 μmol photons $m^{-2}$ $s^{-1}$) | |
| | **440 nm** | **675 nm** | **440 nm** | **675 nm** | **440 nm** | **675 nm** |
| *Reticulofenestra parvula* | 33.43 ± 3.28 | 14.63 ± 1.15 | 41.52 ± 1.93 | 15.59 ± 0.71 | 46.65 ± 4.96 | 15.93 ± 1.64 |
| *Gephyrocapsa muellerae* | 36.22 ± 1.90 | 16.04 ± 0.95 | 45.78 ± 1.72 | 17.26 ± 0.57 | 52.28 ± 6.36 | 18.22 ± 2.13 |
| *Gephyrocapsa oceanica* | 28.63 ± 5.14 | 14.89 ± 2.84 | 33.51 ± 3.95 | 16.70 ± 1.72 | 43.93 ± 9.04 | 20.62 ± 4.88 |
| *Emiliania huxleyi* (1N) | 27.63 ± 2.06 | 13.66 ± 0.94 | 28.70 ± 2.61 | 13.37 ± 1.12 | 31.85 ± 1.66 | 13.91 ± 0.69 |
| *Emiliania huxleyi* | 33.75 ± 3.11 | 15.41 ± 1.27 | 39.91 ± 5.17 | 16.32 ± 1.80 | 46.90 ± 1.88 | 17.16 ± 0.56 |
| *Calcidiscus leptoporus* | 18.23 ± 1.30 | 8.66 ± 0.73 | 24.11 ± 2.48 | 10.38 ± 1.02 | 19.64 ± 3.45 | 7.75 ± 1.48 |
| *Calcidiscus quadriperforatus* | 21.79 ± 2.00 | 11.17 ± 1.46 | 30.07 ± 5.18 | 13.76 ± 2.50 | 30.15 ± 3.36 | 12.24 ± 1.20 |
| *Helicosphaera carteri* | 25.35 ± 4.59 | 14.06 ± 3.36 | 32.20 ± 7.18 | 13.10 ± 3.37 | | |
| *Syracosphaera pulchra* | 46.19 ± 6.47 | 17.76 ± 2.71 | 45.42 ± 1.14 | 18.23 ± 0.70 | 45.03 ± 7.62 | 15.84 ± 3.02 |
| *Coccolithus braarudii* | 19.45 ± 5.70 | 11.88 ± 3.74 | 25.78 ± 2.68 | 13.50 ± 1.50 | | |

**Appendix A.v**. Parameters derived from Fast repetition rate fluorometry (FRRf, both single turnover measurements, and from fluorescence light curve protocols, see methods in section 2.2.6 and 3.2.3) in cultures of each coccolithophore species under low, medium and high light conditions (25, 100 and 200 μmol photons $m^{-2}$ $s^{-1}$, respectively). $F_v/F_m$ = Maximum quantum yield of PSII, $\sigma_{PSII}$ = Absorption cross-section of PSII photochemistry ($nm^2$ $PSII^{-1}$), $\alpha_{PSII}$ = Initial slope of fluorescence light curve, $E_k$ = Saturation parameter of the fluorescence light curve (μmol photons $m^{-2}$ $s^{-1}$).

| Species | **Low Light** (25 μmol photons $m^{-2}$ $s^{-1}$) | | | | **Medium Light** (100 μmol photons $m^{-2}$ $s^{-1}$) | | | | **High Light** (200 μmol photons $m^{-2}$ $s^{-1}$) | | | |
|---|---|---|---|---|---|---|---|---|---|---|---|---|
| | **$F_v/F_m$** | **$\sigma_{PSII}$** | **$\alpha_{PSII}$** | **$E_K$** | **$F_v/F_m$** | **$\sigma_{PSII}$** | **$\alpha_{PSII}$** | **$E_K$** | **$F_v/F_m$** | **$\sigma_{PSII}$** | **$\alpha_{PSII}$** | **$E_K$** |
| *Reticulofenestra parvula* | 0.42 | 9.50 | 3.90 | 204.98 | 0.42 | 9.79 | 3.96 | 263.46 | 0.41 | 9.57 | 3.72 | 343.20 |
| *Gephyrocapsa muellerae* | 0.41 | 7.76 | 2.60 | 169.06 | 0.35 | 9.80 | 4.18 | 426.35 | 0.34 | 10.35 | 3.78 | 409.74 |
| *Gephyrocapsa oceanica* | 0.51 | 5.99 | 2.72 | 448.62 | 0.41 | 6.82 | 2.68 | 524.45 | 0.39 | 6.91 | 2.89 | 394.26 |
| *Emiliania huxleyi* (1N) | 0.42 | 5.81 | 2.62 | 132.72 | 0.41 | 5.90 | 2.48 | 209.38 | 0.43 | 5.60 | 2.31 | 342.78 |
| *Emiliania huxleyi* | 0.47 | 7.34 | 2.88 | 117.32 | 0.42 | 8.21 | 3.29 | 258.31 | 0.40 | 8.49 | 3.14 | 410.64 |
| *Calcidiscus leptoporus* | 0.42 | 8.41 | 3.64 | 181.35 | 0.36 | 8.34 | 2.84 | 240.52 | 0.34 | 9.57 | 2.80 | 353.81 |
| *Calcidiscus quadriperforatus* | 0.43 | 5.44 | 2.31 | 375.76 | 0.39 | 5.65 | 2.35 | 551.77 | 0.35 | 7.45 | 2.78 | 833.51 |
| *Helicosphaera carteri* | 0.48 | 6.31 | 3.05 | 425.76 | 0.48 | 7.87 | 3.70 | 345.30 | | | | |
| *Syracosphaera pulchra* | 0.33 | 8.77 | 1.95 | 109.64 | 0.49 | 7.15 | 3.55 | 201.41 | 0.46 | 6.36 | 2.70 | 364.70 |
| *Coccolithus braarudii* | 0.44 | 6.56 | 3.08 | 379.79 | 0.28 | 7.22 | 1.87 | 477.73 | | | | |

Appendix A

# Appendix B Supplementary Data for Chapter 4

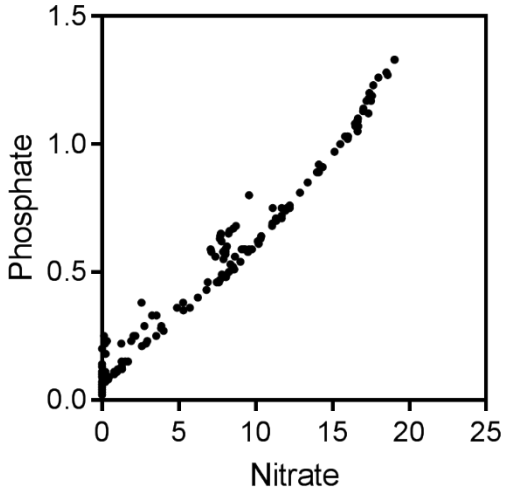


**Figure B.i.** Nitrate concentration (μmol $L^{-1}$) plotted against phosphate concentration (μmol $L^{-1}$) at all sampling depths across the Celtic Sea transect described in Chapter 4 (Figure 4.1, Table 4.2)

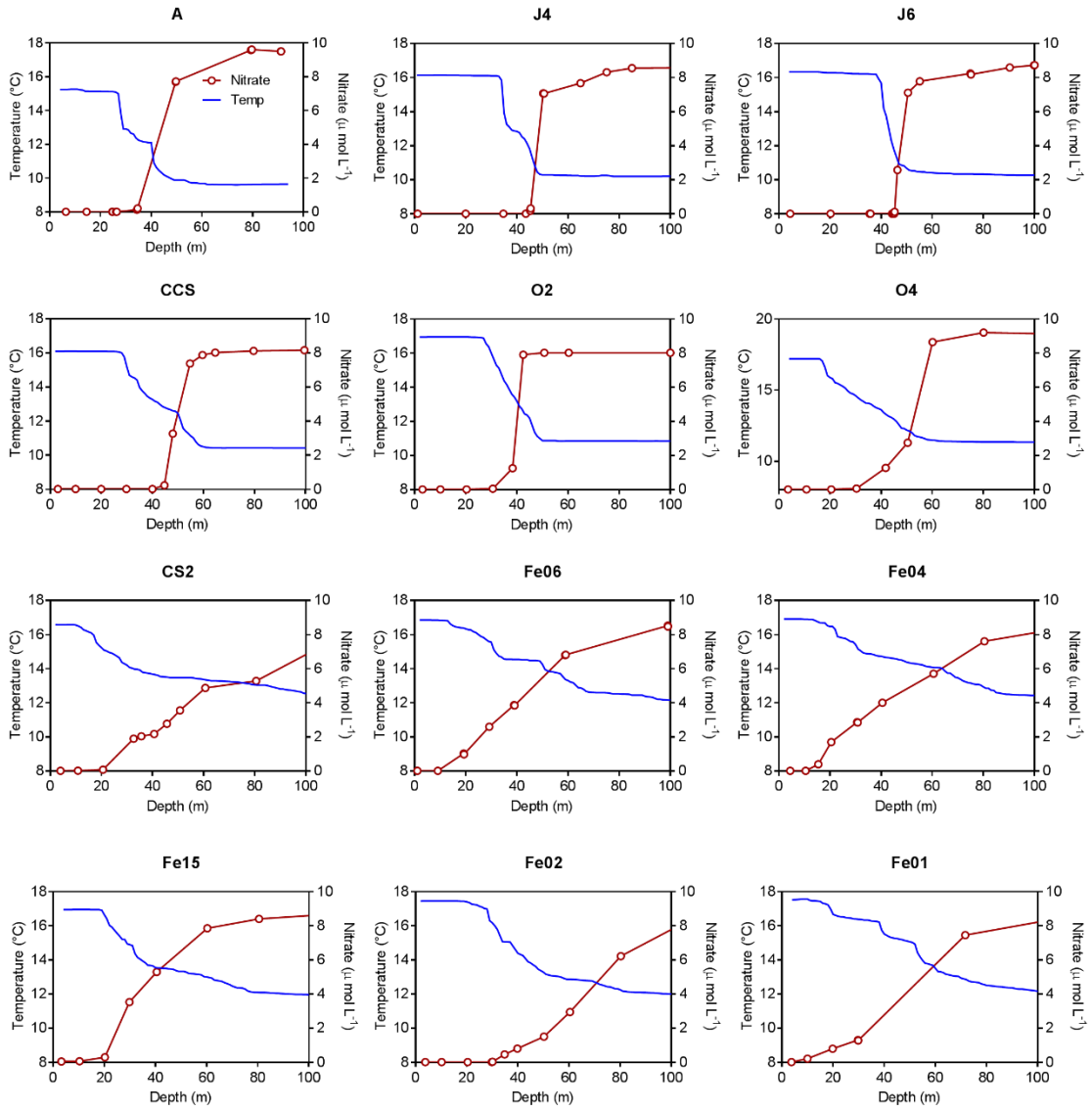


**Figure B.ii.**. Temperature (blue), and nitrate (red) depth profiles for each station on the Celtic Sea transect described in Chapter 4 (Figure 4.1, Table 4.2). Top left is the nearshore end of the transect, to bottom right is the furthest off shelf station.

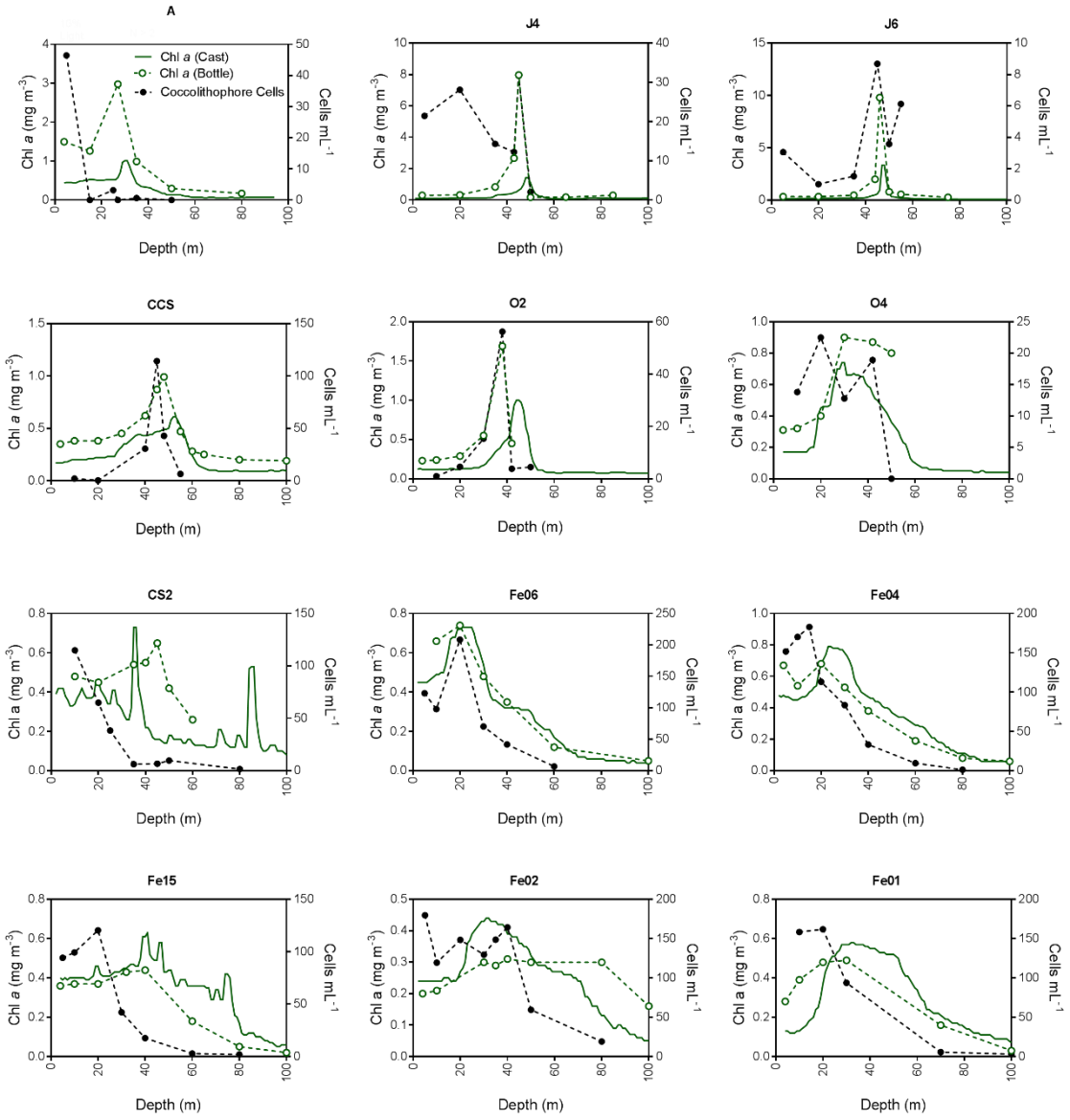


**Figure B.iii.** Depth profiles of Chl *a* (CTD fluorometer green solid line, discrete sampling from CTD bottles dashed green line) and coccolithophore cell abundance (black) for each station on the Celtic Sea transect described in Chapter 4 (Figure 4.1, Table 4.2). Top left is the nearshore end of the transect, to bottom right is the furthest off shelf station .

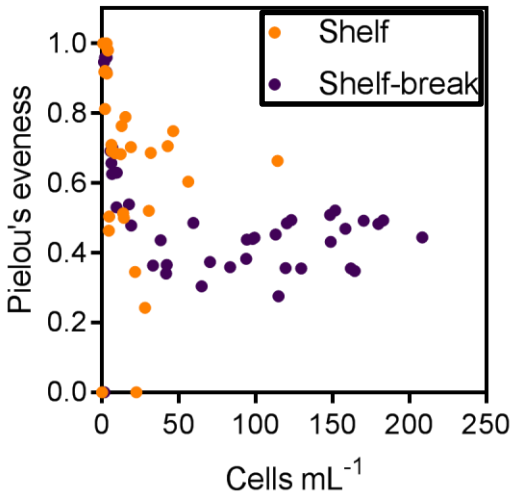


**Figure B.iv.**. Pielou's evenness index (J', see methods 4.2.5) plotted against total coccolithophore cell abundance (Cells $mL^{-1}$) for all depth samples across the Celtic Sea transect described in Chapter 4 (Figure 4.1, Table 4.2). Samples from shelf stations are coloured orange whilst shelf-break samples are coloured purple.

# References

Aiken, J. *et al.* (2009) 'Phytoplankton pigments and functional types in the Atlantic Ocean: A decadal assessment, 1995-2005', *Deep-Sea Research Part II: Topical Studies in Oceanography*, 56, pp. 899–917. doi: 10.1016/j.dsr2.2008.09.017.

Alami, M., Lazar, D. and Green, B. R. (2012) 'The harmful alga Aureococcus anophagefferens utilizes 19'butanoyloxyfucoxanthin as well as xanthophyll cycle carotenoids in acclimating to higher light intensities', *Biochimica et Biophysica Acta - Bioenergetics*. Elsevier B.V., 1817(9), pp. 1557–1564. doi: 10.1016/j.bbabio.2012.05.006.

Aloisi, G. (2015) 'Co-variation of metabolic rates and cell-size in coccolithophores', *Biogeosciences Discussions*, 12, pp. 6215–6284. doi: 10.5194/bgd-12-6215-2015.

Andruleit, H. *et al.* (2003) 'Living coccolithophores in the northern Arabian Sea: Ecological tolerances and environmental control', *Marine Micropaleontology*, 49, pp. 157–181. doi: 10.1016/S0377-8398(03)00049-5.

Armstrong, R. a. *et al.* (2002) 'A new, mechanistic model for organic carbon fluxes in the ocean based on the quantitative association of POC with ballast minerals', *Deep-Sea Research Part II: Topical Studies in Oceanography*, 49(1–3), pp. 219–236. doi: 10.1016/S0967-0645(01)00101-1.

Balch, W. M. (2004) 'Re-evaluation of the physiological ecology of coccolithophores', *Coccolithophores: From Molecular Processes to Global Impact*, (1978), pp. 165–190.

Balch, W. M. *et al.* (2005) 'Calcium carbonate measurements in the surface global ocean based on Moderate-Resolution Imaging Spectroradiometer data', *Journal of Geophysical Research C: Oceans*, 110(7), pp. 1–21. doi: 10.1029/2004JC002560.

Balch, W. M. *et al.* (2016) 'Factors regulating the Great Calcite Belt in the Southern Ocean and its biogeochemical significance', *Global Biogeochemical Cycles*, 30(8), pp. 1124–1144. doi: 10.1002/2016GB005414.

Balch, W. M. (2018) 'The Ecology, Biogeochemistry, and Optical Properties of Coccolithophores', *Annual Review of Marine Science*, 10(1), pp. 71–98. doi: 10.1146/annurev-marine-121916-063319.

Balch, W. M., Holligan, P. M. and Kilpatrick, K. A. (1992) 'Calcification, photosynthesis and growth of the bloom-forming coccolithophore, Emiliania huxleyi', *Continental Shelf Research*,

12(12), pp. 1353–1374.

Banavar, J. R. *et al.* (2002) 'Supply-demand balance and metabolic scaling.', *Proceedings of the National Academy of Sciences of the United States of America*, 99(14), pp. 10506–10509. doi: 10.1073/pnas.162216899.

Barber, J. and Andersson, B. (1992) 'Too much of a good thing - light can be bad for photosynthesis', *Trends in Biochemical Sciences*, 17(2), pp. 61–66.

Barlow, R. G. *et al.* (2002) 'Phytoplankton pigment and absorption characteristics along meridional transects in the Atlantic Ocean', *Deep-Sea Research Part I: Oceanographic Research Papers*, 49, pp. 637–660. doi: 10.1016/S0967-0637(01)00081-4.

Barnett, M. L. *et al.* (2019) 'Shelf sea subsurface chlorophyll maximum thin layers have a distinct phytoplankton community structure', *Continental Shelf Research*. Elsevier Ltd, 174(June 2018), pp. 140–157. doi: 10.1016/j.csr.2018.12.007.

Baumann, K. H., Andruleit, H. A. and Samtleben, C. (2000) 'Coccolithophores in the Nordic Seas: comparison of living communities with surface sediment assemblages', *Deep Sea Research Part II: Topical Studies in Oceanography*, 47, pp. 1743–1772. doi: 10.1002/bltj.20093.

Baumann, K. H., Boeckel, B. and Frenz, M. (2004) 'Coccolith contribution to South Atlantic carbonate sedimentation'. doi: 10.1007/978-3-662-06278-4_14.

Bec, B. *et al.* (2008) 'cell size in marine Growth rate peaks at intermediate picoeukaryotes photosynthetic', *Limnology and Oceanography*, 53(2), pp. 863–867.

Behrenfeld, M. J. *et al.* (2002) 'Photoacclimation and nutrient-based model of light-saturated photosynthesis for quantifying oceanic primary production', *Marine Ecology Progress Series*, 228, pp. 103–117. doi: 10.3354/meps228103.

Bendif, E. M. *et al.* (2015) 'Morphological and Phylogenetic Characterization of New Gephyrocapsa Isolates Suggests Introgressive Hybridization in the Emiliania/Gephyrocapsa Complex (Haptophyta)', *Protist*. Elsevier GmbH., 166(3), pp. 323–336. doi: 10.1016/j.protis.2015.05.003.

Berelson, W. M. *et al.* (2007) 'Relating estimates of CaCO3 production, export, and dissolution in the water column to measurements of CaCO3 rain into sediment traps and dissolution on the sea floor: A revised global carbonate budget', *Global Biogeochemical Cycles*, 21(1), p. GB1024. doi: 10.1029/2006GB002803.

Bidigare, R., Marra, J., *et al.* (1990) 'Evidence for phytoplankton succession and chromatic adaptation in the Sargasso Sea during spring 1985', *Marine Ecology Progress Series*, 60, pp. 113–122. doi: 10.3354/meps060113.

Bidigare, R., Ondrusek, M. E., *et al.* (1990) 'In-vivo absorption properties of algal pigments', *Proceedings of the Society of Photo-Optical Instrumentation Engineers. Ocean Optics X*, 1302, pp. 290–302. doi: 10.1117/12.21451.

Blankenship, R. E. (2014) *Molecular Mechanisms of Photosynthesis*. 2nd edn. Wiley Blackwell.

Boeckel, B. and Baumann, K.-H. (2008) 'Vertical and lateral variations in coccolithophore community structure across the subtropical frontal zone in the South Atlantic Ocean', *Marine Micropaleontology*, 67, pp. 255–273. doi: 10.1016/j.marmicro.2008.01.014.

Bouchard, J. N., Campbell, D. A. and Roy, S. (2005) 'Effects of UV-B radiation on the D1 protein repair cycle of natural phytoplankton communities from three latitudes (Canada, Brazil, and Argentina)', *Journal of Phycology*, 41(2), pp. 273–286. doi: 10.1111/j.1529-8817.2005.04126.x.

Bouman, H. A. *et al.* (2003) 'Temperature as indicator of optical properties and community structure of marine phytoplankton: implications for remote sensing', *Marine Ecology Progress Series*, 258(19–30).

Bown, P., Lees, J. and Young (2004) 'Calcareous nannoplankton evolution and diversity through time'. doi: 10.1007/978-3-662-06278-4_18.

Braarud, T. and Nordli, E. (1952) 'Coccoliths of Coccolithus huxleyi seen in an electon microscope.', *Nature*, 170, pp. 361–362.

Bracher, A. *et al.* (2008) 'Quantitative observation of cyanobacteria and diatoms from space using PhytoDOAS on SCIAMACHY data', *Biogeosciences Discussions*, 5, pp. 4559–4590. doi: 10.5194/bgd-5-4559-2008.

Brewin, R. J. W. *et al.* (2010) 'A three-component model of phytoplankton size class for the Atlantic Ocean', *Ecological Modelling*, 221(11), pp. 1472–1483. doi: http://dx.doi.org/10.1016/j.ecolmodel.2010.02.014.

Bricaud, A. *et al.* (2004) 'Natural variability of phytoplanktonic absorption in oceanic waters: Influence of the size structure of algal populations', *Journal of Geophysical Research*, 109(440), p. C11010. doi: 10.1029/2004JC002419.

References

Bricaud, A. and Stramski, D. (1990) 'Spectral absorption coefficients of living phytoplankton and nonalgal biogenous matter: A comparison between the Peru upwelling areaand the Sargasso Sea', *Limnology and Oceanography*, 35(3), pp. 562–582. doi: 10.4319/lo.1990.35.3.0562.

Broecker, W. and Clark, E. (2009) 'Ratio of coccolith CaCO3 to foraminifera CaCO3 in late Holocene deep sea sediments', *Paleoceanography*, 24(3), pp. 1–11. doi: 10.1029/2009PA001731.

Brown, J. H. (1995) *Macroecology*. University of Chicago Press, Chicago.

Buitenhuis, E. *et al.* (1996) 'Trends in inorganic and organic carbon in a bloom of Emiliania huxleyi in the North Sea', *Marine Ecology Progress Series*, 143(1–3), pp. 271–282. doi: 10.3354/meps143271.

Buitenhuis, E. T. *et al.* (2008) 'Growth rates of six coccolithophorid strains as a function of temperature.', 53(3), pp. 1181–1185. doi: 10.4319/lo.2008.53.3.1181.

Cermeno, P. *et al.* (2008) 'The role of nutricline depth in regulating the ocean carbon cycle', *Proceedings of the National Academy of Sciences*, 105(51), pp. 20344–20349.

Cermeño, P. *et al.* (2010) 'Phytoplankton biogeography and community stability in the ocean', *PLoS ONE*, 5(4). doi: 10.1371/journal.pone.0010037.

Charalampopoulou, A. *et al.* (2011) 'Irradiance and pH affect coccolithophore community composition on a transect between the North Sea and the Arctic Ocean', *Marine Ecology Progress Series*, 431(Zondervan 2007), pp. 25–43. doi: 10.3354/meps09140.

Charalampopoulou, A. *et al.* (2016) 'Environmental drivers of coccolithophore abundance and calcification across Drake Passage (Southern Ocean)', *Biogeosciences*, 13(21), pp. 5917–5935. doi: 10.5194/bg-13-5917-2016.

Chisholm, S. W. *et al.* (1988) 'A novel free-living prochlorophyte abundant in the oceanic euphotic zone', *Nature*, 334, pp. 340–343.

Clarke, K. R. and Warwick, R. M. (2001) *PRIMER-E Change in Marine Communities: An Approach to Statistical Analysis and Interpretation*. PRIMER-E Ltd.

Cortés, M. Y., Bollmann, J. and Thierstein, H. R. (2001) 'Coccolithophore ecology at the HOT station ALOHA, Hawaii', *Deep-Sea Research Part II: Topical Studies in Oceanography*, 48, pp. 1957–1981. doi: 10.1016/S0967-0645(00)00165-X.

Croce, R. and van Amerongen, H. (2014) 'Natural strategies for photosynthetic light harvesting', *Nature Chemical Biology*. Nature Publishing Group, 10(7), pp. 492–501. doi:

10.1038/nchembio.1555.

Cros, L. and Fortuno, J.-M. (2002) 'Atlas of Northwestern Mediterranean Coccolithophores', *Scientia Marina*, 66, pp. 7–182. doi: 10.1007/978-3-319-02804-0_4.

Cullen, J. J. *et al.* (1993) 'Toward a general description of phytoplankton growth for biogeochemical models', *Towards a Model of Ocean Biogeochemical Processes*, pp. 153–67. doi: 10.1007/978-3-642-84602-1_7.

Curran, K. *et al.* (2018) 'Estimation of size-fractionated primary production from satellite ocean colour in UK shelf seas', *Remote Sensing*, 10(9). doi: 10.3390/rs10091389.

Daniels, C. J. *et al.* (2015) 'Phytoplankton dynamics in contrasting early stage North Atlantic spring blooms: Composition, succession, and potential drivers', *Biogeosciences*, 12(8), pp. 2395–2409. doi: 10.5194/bg-12-2395-2015.

Daniels, C. J. *et al.* (2016) 'Species-specific calcite production reveals Coccolithus pelagicus as the key calcifier in the Arctic Ocean', *Marine Ecology Progress Series*, 555, pp. 29–47. doi: 10.3354/meps11820.

Daniels, C. J. *et al.* (2018) 'A global compilation of coccolithophore calcification rates', *Earth System Science Data*, 10(4), pp. 1859–1876. doi: 10.5194/essd-10-1859-2018.

Daniels, C. J., Sheward, R. M. and Poulton, a J. (2014) 'Biogeochemical implications of comparative growth rates of Emiliania huxleyi and Coccolithus species', pp. 6915–6925. doi: 10.5194/bg-11-6915-2014.

von Dassow, P. *et al.* (2014) 'Life-cycle modification in open oceans accounts for genome variability in a cosmopolitan phytoplankton', *The ISME Journal*, pp. 1–13. doi: 10.1038/ismej.2014.221.

Dubinsky, Z., Falkowski, P. G. and Wyman, K. (1986) 'Light harvesting and utilization by phytoplankton.pdf', *Plant and cell physiology*, 27(7), pp. 1335–1349.

Durak, G. M. *et al.* (2016) 'A role for diatom-like silicon transporters in calcifying coccolithophores', *Nature Communications*, 7. doi: 10.1038/ncomms10543.

Duysens, L. N. M. (1956) 'The flattening of the absorption spectrum of suspensions, as compared to that of solutions.', *Biochimica et biophysica acta*, 19, pp. 1–12. doi: 10.1016/0006-3002(56)90380-8.

Falkowski, P. G. and Raven, J. A. (2007) *Aquatic photosynthesis*. Princeton University Press.

References

Falkowski, P. G. and La Roche, J. (1991) 'Acclimation to spectral irradiance in algae', *Journal of Phycology*, 27, pp. 8–14.

Fehling, J. *et al.* (2012) 'The relationship between phytoplankton distribution and water column characteristics in north west european shelf sea waters', *PLoS ONE*, 7(3). doi: 10.1371/journal.pone.0034098.

Fell, F. and Fischer, J. (2001) 'Numerical simulation of the light field in the atmosphere-ocean system using the matrix-operator method', *Journal of Quantitative Spectroscopy and Radiative Transfer*, 69(3), pp. 351–388. doi: 10.1016/S0022-4073(00)00089-3.

Ferrari, G. M. and Tassan, S. (1999) 'A method using chemical oxidation to remove light absorption by phytoplankton pigments', *Journal of Phycology*, 35(5), pp. 1090–1098. doi: 10.1046/j.1529-8817.1999.3551090.x.

Field, C. B. *et al.* (1998) 'Primary Production of the Biosphere : Integrating Terrestrial and Oceanic Components', *Science*, 281, pp. 237–240. doi: 10.1126/science.281.5374.237.

Findlay, C. S. and Giraudeau, J. (2000) 'Extant calcareous nannoplankton in the Australian Sector of the Southern Ocean (austral summers 1994 and 1995)', *Marine Micropaleontology*, 40(4), pp. 417–439. doi: 10.1016/S0377-8398(00)00046-3.

Finkel, Z. V. (2001) 'Light absorption and size scaling of light-limited metabolism in marine diatoms', *Limnology and Oceanography*, 46(1), pp. 86–94. doi: 10.4319/lo.2001.46.1.0086.

Finkel, Z. V. and Irwin, A. J. (2000) 'Modeling size-dependent photosynthesis: Light absorption and the allometric rule', *Journal of Theoretical Biology*, 204(3), pp. 361–369. doi: 10.1006/jtbi.2000.2020.

Finkel, Z. V, Irwin, A. J. and Schofield, O. (2004) 'Resource limitation alters the 3/4 size scaling of metabolic rates in phytoplankton', *Marine Ecology Progress Series*, 273, pp. 269–279. doi: 10.3354/meps273269.

Frada, M. J. *et al.* (2018) 'The private life of coccolithophores', *Perspectives in Phycology*, (August), pp. 1–20. doi: 10.1127/pip/2018/0083.

Fragoso, G. M. *et al.* (2016) 'Biogeographical patterns and environmental controls of phytoplankton communities from contrasting hydrographical zones of the Labrador Sea', *Progress in Oceanography*. Elsevier Ltd, 141, pp. 212–226. doi: 10.1016/j.pocean.2015.12.007.

Fujiki, T. and Taguchi, S. (2002) 'Variability in chlorophyll a specific absorption coefficient in

marine phytoplankton as a function of cell size and irradiance', *Journal of Plankton Research*, 24(9), pp. 859–874. doi: 10.1093/plankt/24.9.859.

Gao, K. *et al.* (2009) 'Ocean acidification exacerbates the effect of UV radiation on the calcifying phytoplankter Emiliania huxleyi', *Limnology and Oceanography*, 54(6), pp. 1855–1862. doi: 10.4319/lo.2009.54.6.1855.

Garcia-soto, C. *et al.* (1995) 'Evolution and structure of a shelf coccolithophore bloom in the Western English Channel', *Journal of Plankton Research*, 17(11), pp. 2011–2036.

Garcia, V. M. T. *et al.* (2008) 'Environmental factors controlling the phytoplankton blooms at the Patagonia shelf-break in spring', *Deep-Sea Research Part I: Oceanographic Research Papers*, 55(9), pp. 1150–1166. doi: 10.1016/j.dsr.2008.04.011.

Garrido, J. L., Brunet, C. and Rodríguez, F. (2016) 'Pigment variations in Emiliania huxleyi (CCMP370) as a response to changes in light intensity or quality', *Environmental Microbiology*, 18, pp. 4412–4425. doi: 10.1111/1462-2920.

Geider, R. J., MacIntyre, H. L. and Kana, T. M. (1997) 'Dynamic model of phytoplankton growth and acclimation: Responses of the balanced growth rate and the chlorophyll a:carbon ratio to light, nutrient-limitation and temperature', *Marine Ecology Progress Series*, 148, pp. 187–200. doi: 10.3354/meps148187.

Gibbs, S. J. *et al.* (2013) 'Species-specific growth response of coccolithophores to Palaeocene–Eocene environmental change', *Nature Geoscience*. Nature Publishing Group, 6(3), pp. 218–222. doi: 10.1038/ngeo1719.

Giering, S. L. C. *et al.* (2018) 'Seasonal variation of zooplankton community structure and trophic position in the Celtic Sea: A stable isotope and biovolume spectrum approach', *Progress in Oceanography*. doi: 10.1016/j.pocean.2018.03.012.

Gillooly, J. F. *et al.* (2001) 'Effects of Size and Temperature on Metabolic Rate', *Science*, 293(5538), pp. 2248–2251.

Gilmore, A. M. and Yamamoto, H. Y. (1991) 'Zeaxanthin Formation and Energy-Dependent Fluorescence Quenching in Pea Chloroplasts under Artificially Mediated Linear and Cyclic Electron Transport', *Plant Physiology*, 96(2), pp. 635–643. doi: 10.1104/pp.96.2.635.

Gordon, H. R. *et al.* (2009) 'Light scattering by coccoliths detached from Emiliania huxleyi.', *Applied optics*, 48(31), pp. 6059–6073. doi: 10.1364/AO.48.006059.

References

Graff, J. *et al.* (2016) 'Photoacclimation of natural phytoplankton communities', *Marine Ecology Progress Series*, 542, pp. 51–62. doi: 10.3354/meps11539.

Green, J. C., Course, P. A. and Tarran, G. A. (1996) 'The life-cycle of Emiliania huxleyi: A brief review and a study of relative ploidy levels analysed by flow cytometry', *Journal of Marine Systems*, 9(1–2), pp. 33–44. doi: 10.1016/0924-7963(96)00014-0.

Guan, W. C. and Gao, K. S. (2010) 'Enhanced calcification ameliorates the negative effects of UV radiation on photosynthesis in the calcifying phytoplankter Emiliania huxleyi', *Chinese Science Bulletin*, 55(7), pp. 588–593. doi: 10.1007/s11434-010-0042-5.

Guiry, M. D. (2012) 'How many species of algae are there?', *Journal of Phycology*, 48(5), pp. 1057–1063. doi: 10.1111/j.1529-8817.2012.01222.x.

Guo, S. *et al.* (2014) 'Seasonal variation in the phytoplankton community of a continental-shelf sea: The East China Sea', *Marine Ecology Progress Series*, 516, pp. 103–126. doi: 10.3354/meps10952.

Hagino, K., Okada, H. and Matsuoka, H. (2000) 'Spatial dynamics of coccolithophore assemblages in the Equatorial Western-Central Pacific Ocean', *Marine Micropaleontology*, 39, pp. 53–72. doi: 10.1016/S0377-8398(00)00014-1.

Haidar, A. T. and Thierstein, H. R. (2001) 'Coccolithophore dynamics off Bermuda (N. Atlantic)', *Deep-Sea Research Part II: Topical Studies in Oceanography*, 48, pp. 1925–1956. doi: 10.1016/S0967-0645(00)00169-7.

Harlay, J. *et al.* (2010) 'Biogeochemical study of a coccolithophore bloom in the northern Bay of Biscay (NE Atlantic Ocean) in June 2004', *Progress in Oceanography*. Elsevier Ltd, 86(3–4), pp. 317–336. doi: 10.1016/j.pocean.2010.04.029.

Harris, G. N., Scanlan, D. J. and Geider, R. J. (2005) 'Acclimation of Emiliania huxleyi (Prymnesiophyceae) to photon flux density', *Journal of Phycology*, 41(4), pp. 851–862. doi: 10.1111/j.1529-8817.2005.00109.x.

Henderiks, J. and Pagani, M. (2007) 'Refining ancient carbon dioxide estimates: Significance of coccolithophore cell size for alkenone-based p CO 2 records', *Paleoceanography*, 22, pp. 1–12. doi: 10.1029/2006PA001399.

Herrmann, R. G. (1999) 'Biogenesis and Evolution of Photosynthetic (Thylakoid) Membranes', *Bioscience Reports*, 19(5), pp. 355–365. doi: 10.1023/A:1020251903707.

Hickman, A. E. *et al.* (2009) 'Distribution and chromatic adaptation of phytoplankton within a shelf sea thermocline', *Limnology and Oceanography*, 54(2), p. 525. doi: https://doi.org/10.4319/lo.2009.54.2.0525.

Hickman, A. E. *et al.* (2010) 'Modelling the effects of chromatic adaptation on phytoplankton community structure in the oligotrophic ocean', *Mar. Ecol. Prog. Ser*, 406, pp. 1–17.

Hickman, A. E. *et al.* (2012) 'Primary production and nitrate uptake within the seasonal thermocline of a stratified shelf sea', *Marine Ecology Progress Series*, 463, pp. 39–57. doi: 10.3354/meps09836.

Hoffmann, R. *et al.* (2015) 'Insight into Emiliania huxleyi coccospheres by focused ion beam sectioning', *Biogeosciences*, 12(3), pp. 825–834. doi: 10.5194/bg-12-825-2015.

Holligan, P. M. (1981) 'Biological implications of fronts on the northwest European continental shelf', *Phil. Trans. R. Soc. Lond.*, 302, pp. 547–562.

Holligan, P. M. *et al.* (1983) 'Satellite and ship studies of coccolithophore production along a continental shelf edge', *Nature*, 304, pp. 339–342.

Holligan, P. M. *et al.* (1993) 'A biogeochemical study of the coccolithophore, Emiliania huxleyi, in the north Atlantic', *Global Biogeochemical Cycles*, 7(4), pp. 879–900.

Hopkins, J. *et al.* (2015) 'Phenological characteristics of global coccolithophore blooms', *Global Biogeochemical Cycles*, pp. 239–253. doi: 10.1002/2014GB004919.

Houdan, A. *et al.* (2005) 'Comparison of photosynthetic responses in diploid and haploid life-cycle phases of Emiliania huxleyi ( Prymnesiophyceae )', *Marine Ecology Progress Series*, 292, pp. 139–146. doi: 10.3354/meps292139.

Houdan, A. *et al.* (2006) 'Ecology of oceanic coccolithophores. I. Nutritional preferences of the two stages in the life cycle of Coccolithus braarudii and Calcidiscus leptoporus', *Aquatic Microbial Ecology*, 44, pp. 291–301. doi: 10.3354/ame044291.

Houghton, S. D. (1988) 'Thermocline control on coccolith diversity and abundance in Recent sediments from the Celtic Sea and English Channel', *Marine Geology*, 83(1–4), pp. 313–319. doi: 10.1016/0025-3227(88)90065-5.

Hydes, D. J. *et al.* (2010) 'Determination of dissolved nutrients (N, P, Si) in seawater with high precision and inter-comparability using gas-segmented continuous flow analysers', *The GO-SHIP Repeart Hydrography Manual: A Collection of Expert Reports and Guidelines*, pp. 1–87.

Available at: http://archimer.ifremer.fr/doc/00020/13141/.

Iglesias-Rodriguez, M. D. *et al.* (2002) 'Representing key phytoplankton functional groups in ocean carbon cycle models: Coccolithophorids', *Global Biogeochemical Cycles*, 16(4), pp. 1–20. doi: 10.1029/2001GB001454.

Jassby, A. D. and Platt, T. (1976) 'Mathematical formulation of the relationship between photosynthesis and light for phytoplankton', *Limnology and Oceanography*, 21(4), pp. 540–547. doi: 10.4319/lo.1976.21.4.0540.

Jaya, B. N. *et al.* (2016) 'Coccospheres confer mechanical protection : New evidence for an old hypothesis', *Acta Biomaterialia*. Acta Materialia Inc. doi: 10.1016/j.actbio.2016.07.036.

Jeffrey, S. W. *et al.* (2011) 'Part I: Chlorophylls and Carotenoids', in Roy, S. et al. (eds) *Phytoplankton Pigments. Characterization, Chemotaxonomy and Applications in Oceanography*. Cambridge University Press, pp. 3–161.

Jeffrey, S. W., Mantoura, R. F. C. and Wright, S. W. (1997) *Phytoplankton pigments in oceanography: guidelines to modern methods*. UNESCO Press.

Jeffrey, S., Wright, S. and Zapata, M. (2011) 'Microalgal classes and their signature pigments', in Roy, S. et al. (eds) *Phytoplankton pigments: Characterization, Chemotaxonomy and Applications in Oceanography*. Cambridge University Press. doi: 10.1017/CBO9780511732263.

Jiang, Z. *et al.* (2015) 'Controlling factors of summer phytoplankton community in the Changjiang (Yangtze River) Estuary and adjacent East China Sea shelf', *Continental Shelf Research*. Elsevier Ltd, 101, pp. 71–84. doi: 10.1016/j.csr.2015.04.009.

Johnson, Z. I. *et al.* (2006) 'Niche partitioning among Prochlorococcus ecotypes along ocean-scale environmental gradients.', *Science*, 311, pp. 1737–1740. doi: 10.1126/science.1118052.

Joint, I. *et al.* (2001) 'Pelagic production at the Celtic Sea shelf break', *Deep-Sea Research Part II: Topical Studies in Oceanography*, 48(14–15), pp. 3049–3081. doi: 10.1016/S0967-0645(01)00032-7.

Joint, I., Owens, N. and Pomeroy, A. (2007) 'Seasonal production of photosynthetic picoplankton and nanoplankton in the Celtic Sea', *Marine Ecology Progress Series*, 28, pp. 251–258. doi: 10.3354/meps028251.

Jones, K. J. and Gowen, R. J. (1990) 'Influence of stratification and irradiance regime on summer phytoplankton composition in coastal and shelf seas of the British Isles', *Estuarine, Coastal and Shelf Science*, 30(6), pp. 557–567. doi: 10.1016/0272-7714(90)90092-6.

Kawachi, M. *et al.* (1991) 'The haptonema as a food-capturing device: observations on Chrysochromulina hirta (Prymnesiophyceae)', *Phycologia*, 30(6), pp. 563–573. doi: 10.2216/i0031-8884-30-6-563.1.

Keller, M. D. *et al.* (2007) 'Media for the culture of oceanic ultraphytoplankton', *Journal of Phycology*, 23(4), pp. 633–638. doi: 10.1111/j.1529-8817.1987.tb04217.x.

Key, T. *et al.* (2010) 'Cell size trade-offs govern light exploitation strategies in marine phytoplankton', *Environmental Microbiology*, 12, pp. 95–104. doi: 10.1111/j.1462-2920.2009.02046.x.

Kilmer, J. T. and Rodríguez, R. L. (2017) 'Ordinary least squares regression is indicated for studies of allometry', *Journal of Evolutionary Biology*, 30(1), pp. 4–12. doi: 10.1111/jeb.12986.

Kinkel, H., Baumann, K. H. and Cepek, M. (2000) 'Coccolithophores in the equatorial Atlantic Ocean: Response to seasonal and Late Quaternary surface water variability', *Marine Micropaleontology*, 39, pp. 87–112. doi: 10.1016/S0377-8398(00)00016-5.

Kirk, J. T. O. (1976) 'A theoretical analysis of the contribution of algal cells to the attenuation of light within natural waters', *New Phytologist*, 77, pp. 341–358.

Kirk, J. T. O. (2011) *Light and Photosynthesis in Aquatic Ecosystems*. Cambridge: Cambridge University Press.

Klaveness, D. (1972) '(Lohm.) Kamptn II. The flagellate cell, aberrant cell types, vegetative propagation and life cycles', *British Phycological Journal*, 7(3), pp. 309–318. doi: 10.1080/00071617200650321.

Kolber, Z. S., Prášil, O. and Falkowski, P. G. (1998) 'Measurements of variable chlorophyll fluorescence using fast repetition rate techniques: Defining methodology and experimental protocols', *Biochimica et Biophysica Acta - Bioenergetics*, 1367, pp. 88–106. doi: 10.1016/S0005-2728(98)00135-2.

Krueger-Hadfield, S. A. *et al.* (2014) 'Genotyping an Emiliania huxleyi (prymnesiophyceae) bloom event in the North Sea reveals evidence of asexual reproduction', *Biogeosciences*, 11(18), pp. 5215–5234. doi: 10.5194/bg-11-5215-2014.

Langer, G. *et al.* (2006) 'Species-specific responses of calcifying algae to changing seawater carbonate chemistry', *Geochemistry, Geophysics, Geosystems*, 7, p. Q09006. doi: 10.1029/2005GC001227.

References

Langer, G. *et al.* (2009) 'Strain-specific responses of Emiliania huxleyi to changing seawater carbonate chemistry', *Biogeosciences*, 6, pp. 2637–2646.

Lavaud, J. *et al.* (2002) 'Influence of the Diadinoxanthin Pool Size on Photoprotection in the Marine Planktonic Diatom Phaeodactylum tricornutum 1', *Plant physiology*, 129, pp. 1398–1406. doi: 10.1104/pp.002014.dissipation.

Leeuwe, M. A. Van, Visser, R. J. W. and Stefels, J. (2014) 'The pigment composition of Phaeocystis antarctica (Haptophyceae) under various conditions of light, temperature, salinity, and iron', *Journal of Phycology*, 1080, pp. 1070–1080. doi: 10.1111/jpy.12238.

Lefebvre, S. C. *et al.* (2010) 'Characterization and expression analysis of the LHCF gene family in emiliania huxleyi (haptophyta) reveals differential responses to light and co2', *Journal of Phycology*, 46, pp. 123–134. doi: 10.1111/j.1529-8817.2009.00793.x.

Legendre, P. and Legendre, L. (2012) *Numerical Ecology*. 3rd edn. Elsevier.

van Lenning, K. *et al.* (2004) 'Pigment diversity of coccolithophores in relation to taxonomy , phylogeny and ecological preferences', in *Coccolithophores: from molecular processes to global impact*, pp. 51–73.

Leonardos, N. and Harris, G. N. (2006) 'Comparative effects of light on pigments of two strains of Emiliania huxleyi (Haptophyta)', *Journal of Phycology*, 42(6), pp. 1217–1224. doi: 10.1111/j.1529-8817.2006.00289.x.

Lepetit, B. *et al.* (2012) 'Molecular dynamics of the diatom thylakoid membrane under different light conditions', *Photosynthesis Research*, 111(1–2), pp. 245–257. doi: 10.1007/s11120-011-9633-5.

Letelier, R. M. *et al.* (1993) 'Temporal variability of phytoplankton community structure based on pigment analysis', *Limnology & Oceanography*, 38(7), pp. 1420–1437.

Litchman, E. (2007) 'Resource Competition and the Ecological Success of Phytoplankton', in *Evolution of Primary Producers in the Sea*, pp. 351–376.

Liu, Z. *et al.* (2004) 'Crystal structure of spinach major light-harvesting complex at 2.72 Å resolution', *Nature*, 428(6980), pp. 287–292. doi: 10.1038/nature02373.

Llewellyn, C. a. and Gibb, S. W. (2000) 'Intra-class variability in the carbon , pigment and biomineral content of prymnesiophytes and diatoms', *Marine Ecology Progress Series*, 193, pp. 33–44.

Lohmann, H. (1913) 'Über Coccolithophoriden', *Verhandlungen der Deutschen Zoologischen Gesellschaft*, 23, pp. 143–164.

MacIntyre, H. L. *et al.* (2002) 'Photoacclimation of photosynthesis irradiance response curves and photosynthetic pigments in microalgae and cyanobacteria', *Journal of Phycology*, 38(July 2000), pp. 17–38. doi: 10.1046/j.1529-8817.2002.00094.x.

Mackas, D. L., Denman, K. L. and Abbott, M. R. (1985) 'Plankton patchiness: biology in the physical vernacular.', *Bulletin of Marine Science*, 37(2), pp. 653–674.

Mackey, M. D. *et al.* (1996) 'CHEMTAX - a program for estimating class abundances from chemical markers: application to HPLC measurements of phytoplankton', *Marine Ecology Progress Series*, 144, pp. 265–283. doi: 10.3354/meps144265.

Malerba, M. E. *et al.* (2018) 'Cell size, photosynthesis and the package effect: an artificial selection approach', *New Phytologist*. doi: 10.1111/nph.15163.

Maranon, E. *et al.* (2013) 'Unimodal size scaling of phytoplankton growth and the size dependence of nutrient uptake and use', *Ecology Letters*, 16, pp. 371–379. doi: 10.1111/ele.12052.

Marañón, E. (2015) 'Cell Size as a Key Determinant of Phytoplankton Metabolism and Community Structure.', *Annual Review of Marine Science*, 7, pp. 241–64. doi: 10.1146/annurev-marine-010814-015955.

Marchant, H. J. and Thomsen, H. (1994) 'Haptophytes in polar waters', in Green, J. C. and Leadbeater, B. (eds) *The Haptophyte Algae*. Clarendon Press, Oxford, pp. 209–228.

Marra, J. *et al.* (2000) 'Pigment absorption and quantum yields in the Arabian Sea', *Deep-Sea Research Part II: Topical Studies in Oceanography*, 47(7–8), pp. 1279–1299. doi: 10.1016/S0967-0645(99)00144-7.

Marra, J., Houghton, R. W. and Garside, C. (1990) 'Phytoplankton growth at the shelf-break front in the Middle Atlantic Bight', *Journal of Marine Research*, 48(4), pp. 851–868. doi: 10.1357/002224090784988665.

Marsh, M. E. (2003) 'Regulation of CaCO3 formation in coccolithophores', *Comparative Biochemistry and Physiology - B Biochemistry and Molecular Biology*, 136(4), pp. 743–754. doi: 10.1016/S1096-4959(03)00180-5.

Martin, A. P. (2003) 'Phytoplankton patchiness: the role of lateral stirring and mixing', *Progress*

*in Oceanography*, 57(2), pp. 125–174. doi: 10.1016/s0079-6611(03)00085-5.

Mayers, K. M. J. *et al.* (2018) 'Growth and mortality of coccolithophores during spring in a temperate Shelf Sea (Celtic Sea, April 2015)', *Progress in Oceanography*. Elsevier. doi: 10.1016/j.pocean.2018.02.024.

Mayers, K. M. J. (2018) *Probing rates of growth and mortality in natural coccolithophore populations*, *Thesis*. doi: 10.1016/j.jsv.2010.04.020.

McArdle, B. . (1988) 'The structural relationship: regression in biology', *Canadian Journal of Zoology*, 66(11), pp. 2329–2339.

McFadden, G. I. (2001) 'Primary and secondary endosymbiosis and the origin of plastids', *Journal of Phycology*, 37, pp. 951–959. doi: 10.1046/j.1529-8817.2001.01126.x.

McIntyre, A. and Bé, A. W. H. (1967) 'Modern coccolithophoridae of the atlantic ocean—I. Placoliths and cyrtoliths', *Deep Sea Research and Oceanographic Abstracts*, 14(5), pp. 561–597. doi: 10.1016/0011-7471(67)90065-4.

McKew, B. a., Lefebvre, S. C., *et al.* (2013) 'Plasticity in the proteome of Emiliania huxleyi CCMP 1516 to extremes of light is highly targeted', *New Phytologist*, 200, pp. 61–73. doi: 10.1111/nph.12352.

McKew, B. a., Davey, P., *et al.* (2013) 'The trade-off between the light-harvesting and photoprotective functions of fucoxanthin-chlorophyll proteins dominates light acclimation in Emiliania huxleyi (clone CCMP 1516)', *New Phytologist*, 200(1), pp. 74–85. doi: 10.1111/nph.12373.

Menden-Deuer, S. and Lessard, E. J. (2000) 'Carbon to volume relationships for dinoflagellates, diatoms, and other protist plankton', *Limnology and Oceanography*, pp. 569–579. doi: 10.4319/lo.2000.45.3.0569.

Millie, D. F., Kirkpatrick, G. J. and Vinyard, B. T. (1995) 'Relating photosynthetic pigments and in vivo optical density spectra to irradiance for the Florida red-tide dinoflagellate Gymnodinium breve', *Marine Ecology Progress Series*, 120(1–3), pp. 65–76. doi: 10.3354/meps120065.

Milliman, J. D. (1993) 'Production and accumulation of calcium carbonate in the ocean: Budget of a nonsteady state', *Global Biogeochemical Cycles*, 7(4), pp. 927–957. doi: 10.1029/93GB02524.

Monteiro, F. M. *et al.* (2016) 'Why marine phytoplankton calcify', *Science Advances*, 2(7). doi: 10.1126/sciadv.1501822.

Moore, C. M. *et al.* (2005) 'Basin-scale variability of phytoplankton bio-optical characteristics in relation to bloom state and community structure in the Northeast Atlantic', *Deep-Sea Research Part I: Oceanographic Research Papers*, 52(3), pp. 401–419. doi: 10.1016/j.dsr.2004.09.003.

Moore, C. M. *et al.* (2006) 'Phytoplankton photoacclimation and photoadaptation in response to environmental gradients in a shelf sea', *Limnology and Oceanography*, 51(2), pp. 936–949. doi: https://doi.org/10.4319/lo.2006.51.2.0936.

Moore, C. M. *et al.* (2013) 'Processes and patterns of oceanic nutrient limitation', *Nature Geoscience*. Nature Publishing Group, 6(9), pp. 701–710. doi: 10.1038/ngeo1765.

Morel, A. and Bricaud, A. (1981) 'Theoretical results concerning light absorption in a discrete medium, and application to specific absorption of phytoplankton', *Deep Sea Research*, 28A(11), pp. 1375–1393. doi: https://doi.org/10.1016/0198-0149(81)90039-X.

Moreno, D. V. *et al.* (2012) 'Phytoplankton functional community structure in Argentinian continental shelf determined by HPLC pigment signatures', *Estuarine, Coastal and Shelf Science*. Elsevier Ltd, 100, pp. 72–81. doi: 10.1016/j.ecss.2012.01.007.

Muller-Karger, F. E. *et al.* (2005) 'The importance of continental margins in the global carbon cycle', *Geophysical Research Letters*, 32(1), pp. 1–4. doi: 10.1029/2004GL021346.

Nanninga, H. J. and Tyrrell, T. (1996) 'Importance of light for the formation of algal blooms by Emiliania huxleyi', *Marine Ecology Progress Series*, 136, pp. 195–203. doi: 10.3354/meps136195.

Neilson, J. A. D. and Durnford, D. G. (2010) 'Structural and functional diversification of the light-harvesting complexes in photosynthetic eukaryotes', *Photosynthesis Research*, 106(1–2), pp. 57–71. doi: 10.1007/s11120-010-9576-2.

Nelson, N. and Ben-Shem, A. (2004) 'The complex architecture of oxygenic photosynthesis', *Nature Reviews Molecular Cell Biology*, 5(12), pp. 971–982. doi: 10.1038/nrm1525.

Nelson, N. and Junge, W. (2015) 'Structure and Energy Transfer in Photosystems of Oxygenic Photosynthesis', *Annual Review of Biochemistry*, 84(1), pp. 659–683. doi: 10.1146/annurev-biochem-092914-041942.

O'Brien, C. J. *et al.* (2013) 'Global marine plankton functional type biomass distributions:

Coccolithophores', *Earth System Science Data*, 5, pp. 259–276. doi: 10.5194/essd-5-259-2013.

O'Brien, C. J., Vogt, M. and Gruber, N. (2016) 'Global coccolithophore diversity: Drivers and future change', *Progress in Oceanography*. Elsevier Ltd, 140, pp. 27–42. doi: 10.1016/j.pocean.2015.10.003.

Okada, H. and Honjo, S. (1975) 'Distribution of Coccolithophores in Marginal Seas along the Western Pacific Ocean and in the Red Sea *', *Marine Biology*, 31, pp. 271–285.

van Oostende, N. *et al.* (2012) 'Phytoplankton community dynamics during late spring coccolithophore blooms at the continental margin of the Celtic Sea (North East Atlantic, 2006-2008)', *Progress in Oceanography*. Elsevier Ltd, 104, pp. 1–16. doi: 10.1016/j.pocean.2012.04.016.

Oxborough, K. (2015) *Act2Run software and Act2 system Handbook*. Chelsea Technologies Group Ltd.

Paasche, E. (2002) 'A reveiw of the coccolithophorid Emiliania huxleyi (Prymnesiophyceae), with particular reference to growth, formation, and calcification-photosynthesis interactions', *Phycologia*, 40(6), pp. 503–529. doi: https://doi.org/10.2216/i0031-8884-40-6-503.1.

Papagiannakis, E. *et al.* (2005) 'Spectroscopic characterization of the excitation energy transfer in the fucoxanthin-chlorophyll protein of diatoms', *Photosynthesis Research*, 86(1–2), pp. 241–250. doi: 10.1007/s11120-005-1003-8.

Parke, M. and Adams, I. (1960) 'The motile (Crystallolithus hyalinus) and non-motile phases in the life history of Coccolithus pelagicus', *Journal of the Marine Biological Association of the UK*. southampton oceangrap, 39, pp. 263–274.

Partensky, F., Hess, W. R. and Vaulot, D. (1999) 'Prochlorococcus, a marine photosynthetic prokaryote of global significance.', *Microbiology and molecular biology reviews : MMBR*, 63(1), pp. 106–127. doi: doi:1092-2172/99/$04.00.

Pauly, D. *et al.* (2002) 'Towards sustainability in world fisheries', *Nature*, 418(August), pp. 689–695. doi: 10.1038/nature01017.

Peters, R. H. (1983) *The ecological implications of body size*. Cambridge University Press.

Pingree, R. D., Holligan, P. M. and Mardell, G. T. (1978) 'The effects of vertical stability on phytoplankton distributions in the summer on the northwest European Shelf', *Deep-Sea Research*, 25(11). doi: 10.1016/0146-6291(78)90584-2.

Pingree, R. and Mardell, G. (1981) 'Slope turbulence, internal waves and phytoplankton growth at the Celtic Sea shelf-break', *Philos. Trans. R. Soc. Lond.*, 302(1472), pp. 663–682. doi: DOI: 10.1098/rsta.1981.0191.

Polívka, T. and Frank, H. A. (2010) 'Moleular Factors Controlling Photosynthetic Light Harvesting by Carotenoids', *Accounts of Chemical Research*, 43(8), pp. 1125–1134. doi: 10.1021/ar100030m.

Poulton, A. . J. *et al.* (2017) 'Coccolithophore ecology in the tropical and subtropical Atlantic Ocean: New perspectives from the Atlantic meridional transect (AMT) programme', *Progress in Oceanography*. The Authors, 158, pp. 150–170. doi: 10.1016/j.pocean.2017.01.003.

Poulton, A. J. *et al.* (2006) 'Phytoplankton mineralization in the tropical and subtropical Atlantic Ocean', *Global Biogeochemical Cycles*, 20(4), pp. 1–10. doi: 10.1029/2006GB002712.

Poulton, A. J. *et al.* (2007) 'Relating coccolithophore calcification rates to phytoplankton community dynamics: Regional differences and implications for carbon export', *Deep Sea Research Part II: Topical Studies in Oceanography*, 54(5–7), pp. 538–557. doi: http://dx.doi.org/10.1016/j.dsr2.2006.12.003.

Poulton, A. J. *et al.* (2010) 'Coccolithophore dynamics in non-bloom conditions during late summer in the central Iceland Basin (July-August 2007)', *Limnology and Oceanography*, 55(4), pp. 1601–1613. doi: 10.4319/lo.2010.55.4.1601.

Poulton, A. J. *et al.* (2013) 'The 2008 Emiliania huxleyi bloom along the Patagonian Shelf: Ecology, biogeochemistry, and cellular calcification', *Global Biogeochemical Cycles*, 27(4), pp. 1023–1033. doi: 10.1002/2013GB004641.

Poulton, A. J. *et al.* (2014) 'Coccolithophores on the north-west European shelf : calcification rates and environmental controls', *Biogeosciences*, (11), pp. 3919–3940. doi: 10.5194/bg-11-3919-2014.

Poulton, A. J. *et al.* (2019) 'Dissolution dominates silica-cycling in a shelf sea autumn bloom', *Geophysical Research Letters*, p. 2019GL083558. doi: 10.1029/2019GL083558.

Premvardhan, L. *et al.* (2010) 'Pigment organization in fucoxanthin chlorophyll a/c2proteins (FCP) based on resonance Raman spectroscopy and sequence analysis', *Biochimica et Biophysica Acta - Bioenergetics*. Elsevier B.V., 1797(9), pp. 1647–1656. doi: 10.1016/j.bbabio.2010.05.002.

Probert, I. and Houdan, A. (2004) 'The laboratory culture of coccolithophores', in Thierstein, H. R. and Young, J. R. (eds) *Coccolithophores: From Molecular Processes to Global Impact*. Springer,

pp. 217–249.

Le Quere, C. *et al.* (2005) 'Ecosystem dynamics based on plankton functional types for global ocean biogeochemistry models\rdoi:10.1111/j.1365-2486.2005.1004.x', *Global Change Biology*, 11(11), pp. 2016–2040. doi: 10.1111/j.1365-2486.2005.01004.x.

Rees, A. P. *et al.* (2002) 'Size-fractionated nitrogen uptake and carbon fixation during a developing coccolithophore bloom in the North Sea during June 1999', *Deep-Sea Research Part II: Topical Studies in Oceanography*, 49(15), pp. 2905–2927. doi: 10.1016/S0967-0645(02)00063-2.

Renger, T., May, V. and Kühn, O. (2001) 'Ultrafast excitation energy transfer dynamics in photosynthetic pigment-protein complexes', *Physics Reports*, 343(3), pp. 137–254. doi: 10.1016/S0370-1573(00)00078-8.

Rokitta, S. D. *et al.* (2011) 'Transcriptome analyses reveal differential gene expression patterns between the life-cycle stages of emiliania huxleyi (haptophyta) and reflect specialization to different ecological niches', *Journal of Phycology*, 47(4), pp. 829–838. doi: 10.1111/j.1529-8817.2011.01014.x.

Roy, S. *et al.* (2011) *Phytoplankton Pigments Characterization, Chemotaxonomy and Applications in Oceanography*. Cambridge University Press.

Ruiz-Castillo, E. *et al.* (2018) 'Seasonality in the cross-shelf physical structure of a temperate shelf sea and the implications for nitrate supply', *Progress in Oceanography*. Elsevier, pp. 0–1. doi: 10.1016/j.pocean.2018.07.006.

Saavedra-Pellitero, M. *et al.* (2014) 'Biogeographic distribution of living coccolithophores in the pacific sector of the southern ocean', *Marine Micropaleontology*. Elsevier B.V., 109, pp. 1–20. doi: 10.1016/j.marmicro.2014.03.003.

Sadeghi, A., Dinter, T., Vountas, M., Taylor, B. B., *et al.* (2012) 'Improvement to the PhytoDOAS method for identification of coccolithophores using hyper-spectral satellite data', *Ocean Science*, 8(6), pp. 1055–1070. doi: 10.5194/os-8-1055-2012.

Sadeghi, A., Dinter, T., Vountas, M., Taylor, B., *et al.* (2012) 'Remote sensing of coccolithophore blooms in selected oceanic regions using the PhytoDOAS method applied to hyper-spectral satellite data', *Biogeosciences*, 9(6), pp. 2127–2143. doi: 10.5194/bg-9-2127-2012.

Sanders, R. *et al.* (2014) 'The Biological Carbon Pump in the North Atlantic', *Progress in Oceanography*. Elsevier Ltd, 129(PB), pp. 200–218. doi: 10.1016/j.pocean.2014.05.005.

Sandmann, G., Kuhn, M. and Böger, P. (1993) 'Carotenoids in photosynthesis: Protection of D1 degradation in the light', *Photosynthesis Research*, 35(2), pp. 185–190. doi: 10.1007/BF00014749.

Schlüter, L. *et al.* (2000) 'The use of phytoplankton pigments for identifying and quantifying phytoplankton groups in coastal areas: Testing the influence of light and nutrients on pigment/chlorophyll a ratios', *Marine Ecology Progress Series*, 192, pp. 49–63. doi: 10.3354/meps192049.

Schofield, O., Bidigare, R. and Prézelin, B. (1990) 'Spectral photosynthesis, quantum yield and blue-green light enhancement of productivity rates in the diatom Chaetoceros gracile and the prymnesiophyte Emiliania huxleyi', *Marine Ecology Progress Series*, 64, pp. 175–186. doi: 10.3354/meps064175.

Seoane, S., Zapata, M. and Orive, E. (2009) 'Growth rates and pigment patterns of haptophytes isolated from estuarine waters', *Journal of Sea Research*. Elsevier B.V., 62(4), pp. 286–294. doi: 10.1016/j.seares.2009.07.008.

Sharples, J. *et al.* (2007) 'Spring-neap modulation of internal tide mixing and vertical nitrate fluxes at a shelf edge in summer', *Limnology and Oceanography*, 52(5), pp. 1735–1747. doi: 10.4319/lo.2007.52.5.1735.

Sharples, J. and Holligan, P. (2006) 'Interdisciplinary studies in the Celtic Seas', in Robinson, A. R. and Brink, K. (eds) *The sea. Vol 14B: the global coastal ocean: interdisciplinary regional studies and synthesis*. Cambridge University Press, pp. 1003–1031.

Sheward, R. M. *et al.* (2017) 'Physiology regulates the relationship between coccosphere geometry and growth phase in coccolithophores', *Biogeosciences*, 14(6), pp. 1493–1509. doi: 10.5194/bg-14-1493-2017.

Sikes, C. S. and Wilbur, K. . (1982) 'Function of coccolith formation', *Limnology and Oceanography*, 27(l), pp. 18–26.

Silva, A. *et al.* (2013) 'Coccolithophore species as indicators of surface oceanographic conditions in the vicinity of Azores islands', *Estuarine, Coastal and Shelf Science*, 118, pp. 50–59. doi: 10.1016/j.ecss.2012.12.010.

Simpson, J. H. and Hunter, J. R. (1974) 'Fronts in the Irish Sea', *Nature*, 250(5465), pp. 404–406. doi: 10.1038/250404a0.

Simpson, J. and Sharples, J. (2012) *Introduction to the physical and biological oceanography of shelf seas*

*Introduction to the physical and biological oceanography of shelf seas*. Cambridge University Press.

Six, C. *et al.* (2008) 'Contrasting photoacclimation costs in ecotypes of the marine eukaryotic picoplankter Ostreococcus', 53(1), pp. 255–265.

Smith, H. E. K. *et al.* (2017) 'The influence of environmental variability on the biogeography of coccolithophores and diatoms in the Great Calcite Belt', *Biogeosciences*, 14(21), pp. 4905–4925. doi: 10.5194/bg-14-4905-2017.

Sommer, U. (1989) 'Maximal growth rates of Antarctic phytoplankton: Only weak dependence on cell size', *Limnology and Oceanography*, 34(6), pp. 1109–1112. doi: 10.4319/lo.1989.34.6.1109.

De Souza, M. S. *et al.* (2012) 'Phytoplankton community during a coccolithophorid bloom in the Patagonian Shelf: Microscopic and high-performance liquid chromatography pigment analyses', *Journal of the Marine Biological Association of the United Kingdom*, 92(1), pp. 13–27. doi: 10.1017/S0025315411000439.

Steele, D. J. *et al.* (2015) 'Abundance of a chlorophyll a precursor and the oxidation product hydroxychlorophyll a during seasonal phytoplankton community progression in the Western English Channel', *Progress in Oceanography*, 137(October), pp. 434–445. doi: 10.1016/j.pocean.2015.04.021.

Stolte, W. *et al.* (2000) 'Genetic and physiological variation in pigment composition of Emiliania huxleyi (Prymnesiophyceae) and the potential use of its pigment ratios as a quantitative physiological marker', *Journal of Phycology*. Blackwell Science Inc, 36(3), pp. 529–539. doi: 10.1046/j.1529-8817.2000.99158.x.

Suggett, D. J. *et al.* (2006) 'Fast Repetition Rate (FRR) Chlorophyll a Fluorescence Induction Measurements', *Chelsea Technologies Group, West Molesey*, pp. 1–53. Available at: http://www.psi.cz/ftp/publications/kautsky/FRRFmethodsManual.pdf%5Cnpapers://64c875cb-35e9-49cc-86a7-69f7bda703f6/Paper/p289.

Suggett, D. J. *et al.* (2007) 'Different strategies of photoacclimation by two strains of Emiliania huxleyi (Haptophyta)', *Journal of Phycology*, 43, pp. 1209–1222. doi: 10.1111/j.1529-8817.2007.00406.x.

Suggett, D. J. *et al.* (2015) 'Functional diversity of photobiological traits within the genus Symbiodinium appears to be governed by the interaction of cell size with cladal designation', *New Phytologist*. doi: 10.1111/nph.13483.

Suggett, D. J., MacIntyre, H. L. and Geider, R. J. (2004) 'Evaluation of biophysical and optical

determinations of light absorption by photosystem II in phytoplankton', *Limnology and Oceanography: Methods*, 2, pp. 316–332. doi: 10.4319/lom.2004.2.316.

Sun, J. and Liu, D. (2003) 'Geometric models for calculating cell biovolume and surface area for phytoplankton', *Journal of Plankton Research*, 25(11), pp. 1331–1346. doi: 10.1093/plankt/fbg096.

Šupraha, L. *et al.* (2016) 'Coccolithophore life-cycle dynamics in a coastal Mediterranean ecosystem: seasonality and species-specific patterns', *Journal of Plankton Research*, 38(5), pp. 1178–1193. doi: 10.1093/PLANKT/FBW061.

Tanaka, Y. (2003) 'Coccolith fluxes and species assemblages at the shelf edge and in the Okinawa Trough of the East China Sea', *Deep-Sea Research Part II: Topical Studies in Oceanography*, 50(2), pp. 503–511. doi: 10.1016/S0967-0645(02)00467-8.

Tarran, G. A. and Bruun, J. T. (2015) 'Nanoplankton and picoplankton in the Western English Channel : abundance and seasonality from 2007 – 2013', *Progress in Oceanography*. Elsevier Ltd, 137, pp. 446–455. doi: 10.1016/j.pocean.2015.04.024.

Tarran, G. A., Heywood, J. L. and Zubkov, M. V. (2006) 'Latitudinal changes in the standing stocks of nano- and picoeukaryotic phytoplankton in the Atlantic Ocean', *Deep-Sea Research Part II: Topical Studies in Oceanography*, 53(14–16), pp. 1516–1529. doi: 10.1016/j.dsr2.2006.05.004.

Tassan, S. and Ferrari, G. M. (1995a) 'An alternative approach to absorption measurements of aquatic particles retained on filters', *Limnology and Oceanography*, 40(8), pp. 1358–1368. doi: 10.4319/lo.1995.40.8.1358.

Tassan, S. and Ferrari, G. M. (1995b) 'An alternative approach to absorption measurements of aquatic particles retained on filters', *Limnology and Oceanography*, 40(8), pp. 1358–1368. doi: 10.4319/lo.1995.40.8.1358.

Taylor, A. R. *et al.* (2007) 'Dynamics of formation and secretion of heterococcoliths by Coccolithus pelagicus ssp braarudii', *European Journal of Phycology*, 42(2), pp. 125–136. doi: 10.1080/09670260601159346.

Taylor, A. R., Brownlee, C. and Wheeler, G. (2017) 'Coccolithophore Cell Biology: Chalking Up Progress', *Annual Review of Marine Science*, 9(1), pp. 283–310. doi: 10.1146/annurev-marine-122414-034032.

Thierstein, H. R. and Young, J. R. (2004) *Coccolithophores: From molecular processes to global impact*.

Edited by H. R. Thierstein and J. R. Young. Springer, Berlin, Germany.

Tillmann, U. (1998) 'Phagotrophy by a plastidic haptophyte, Prymnesium patelliferum', *Aquatic Microbial Ecology*, 14(2), pp. 155–160. doi: 10.3354/ame014155.

Tréguer, P. *et al.* (2018) 'Influence of diatom diversity on the ocean biological carbon pump', *Nature Geoscience*. Springer US, 11(1), pp. 27–37. doi: 10.1038/s41561-017-0028-x.

Tyrrell, T. and Merico, A. (2004) 'Emiliania huxleyi: bloom observation and the conditions that induce them', *Coccolithophores: From Molecular Processes to Global Impact*, pp. 585–604. Available at: files/160/Tyrrell_Merico.pdf.

de Vargas, C. *et al.* (2007) 'Origin and Evolution of Coccolithophores. From Coastal Hunters to Oceanic Farmers.', *Evolution of Primary Producers in the Sea*, pp. 251–285. doi: 10.1016/B978-012370518-1/50013-8.

Walker, C. E. *et al.* (2018) 'The requirement for calcification differs between ecologically important coccolithophore species', *New Phytologist*. doi: 10.1111/nph.15272.

Ward, B. A. *et al.* (2012) 'A size-structured food-web model for the global ocean', *Limnology and Oceanography*, 57(6), pp. 1877–1891. doi: 10.4319/lo.2012.57.6.1877.

Ward, B. A. *et al.* (2017) 'The Size Dependence of Phytoplankton Growth Rates : A Trade-Off between Nutrient Uptake and Metabolism', *The American Naturalist*, 189(2). doi: 10.1086/689992.

West, G. B. (1997) 'A General Model for the Origin of Allometric Scaling Laws in Biology', *Science*, 276(5309), pp. 122–126. doi: 10.1126/science.276.5309.122.

Westberry, T. *et al.* (2008) 'Carbon-based primary productivity modeling with vertically resolved photoacclimation', *Global Biogeochemical Cycles*, 22(2), pp. 1–18. doi: 10.1029/2007GB003078.

Widdicombe, C. E. *et al.* (2010) 'Long-term phytoplankton community dynamics in the Western English Channel', *Journal of Plankton Research*, 32(5), pp. 643–655. doi: 10.1093/plankt/fbp127.

Wientjes, E., Van Amerongen, H. and Croce, R. (2013) 'Quantum yield of charge separation in photosystem II: Functional effect of changes in the antenna size upon light acclimation', *Journal of Physical Chemistry B*, 117(38), pp. 11200–11208. doi: 10.1021/jp401663w.

Williams, C. *et al.* (2013) 'Wind-driven nutrient pulses to the subsurface chlorophyll maximum

in seasonally stratified shelf seas', *Geophysical Research Letters*, 40(20), pp. 5467–5472. doi: 10.1002/2013GL058171.

Winter, A. and Siesser, W. . (1994) *Coccolithophores*. Cambridge University Press.

Wollast, R. (1998) 'Evaluation and comparison of the global carbon cycle in the coastal zone and in the open ocean', in Brink, K. H. and Robinson, A. R. (eds) *The Sea, Vol.10*. John Wiley, New York., pp. 213–252.

Xu, J. *et al.* (2016) 'The role of coccoliths in protecting Emiliania huxleyi against stressful light and UV radiation', *Biogeosciences*, 13, pp. 4637–4643. doi: 10.5194/bg-2016-129.

Young, J. R. (1994) 'Functions of coccoliths.', in Winter, A. and Siesser, G. . (eds) *Coccolithophores*. Cambridge University Press, pp. 63–82.

Young, J. R. *et al.* (2003) 'A guide to extant coccolithophore taxonomy ', *Journal of Nannoplankton Research*, (Special Issue 1), p. 125.

Young, J. R., Henriksen, K. and Probert, I. (2004) 'Structure and morphogenesis of the coccoliths of the CODENET species', *Coccolithophores: from molecular process to global impact*, (2), pp. 191–216.

Young, J. R., Poulton, A. J. and Tyrrell, T. (2014) 'Morphology of Emiliania huxleyi coccoliths on the northwestern European shelf – is there an influence of carbonate chemistry ?', 2, pp. 4771–4782. doi: 10.5194/bg-11-4771-2014.

Zapata, M. *et al.* (2004) 'Photosynthetic pigments in 37 species (65 strains) of Haptophyta: Implications for oceanography and chemotaxonomy', *Marine Ecology Progress Series*, 270, pp. 83–102. doi: 10.3354/meps270083.

Zapata, M., Rodríguez, F. and Garrido, J. L. (2000) 'Separation of chlorophylls and carotenoids from marine phytoplankton: A new HPLC method using a reversed phase C8 column and pyridine-containing mobile phases', *Marine Ecology Progress Series*, 195, pp. 29–45. doi: 10.3354/meps195029.

Ziveri, P. *et al.* (2004) 'Biogeography of selected Holocene coccoliths in the Atlantic Ocean', in *Coccolithophores: from molecular process to global impact*. Springer, Berlin, Germany, pp. 403–428.